Naval Surface Warfare Center
Carderock Division
West Bethesda, MD 20817-5700

NSWCCD-50-TR-2011/065 **December 2011**
Hydromechanics Department Report

Development of Second Generation Intact Stability Criteria

by
Vadim Belenky
Christopher C. Bassler
Konstantinos J. Spyrou

NSWCCD-50-TR-2011/065 Development of Second Generation Intact Stability Criteria

REPORT DOCUMENTATION PAGE

Form Approved
OMB No. 0704-0188

1. REPORT DATE (DD-MM-YYYY)	2. REPORT TYPE	3. DATES COVERED (From-To)
06-12-2011	Final	May 2010 – Oct 2010

4. TITLE AND SUBTITLE
Development of Second Generation Intact Stability Criteria

5a. CONTRACT NUMBER
HSCG-23-10-X--MSR-105

5b. GRANT NUMBER

5c. PROGRAM ELEMENT NUMBER

6. AUTHOR(S)
Vadim Belenky
Christopher C. Bassler
Konstantinos J. Spyrou

5d. PROJECT NUMBER

5e. TAKS NUMBER

5f. WORK UNIT NUMBER
10-1-5500-737

7. PERFORMING ORGANIZATION NAME(S) AND ADDRESS(ES)
NAVAL SURFACE WARFARE CENTER CARDEROCK DIVISION
9500 MACARTHUR BLVD
WEST BETHESDA, MD 20817-5700

8. PREFORMING ORGANIZATION REPORT NUMBER
NSWCCD-50-TR-2011/065

9. SPONSORING / MONITORING AGENCY NAME(S) AND ADDRESS(ES)
UNITED STATES COAST GUARD
OFFICE OF DESIGN AND ENGINEERING STANDARDS
NAVAL ARCHITECTURE DIVISION
2100 SECOND ST SW, M/S 7126
WASHINGTON DC 20593-7126

10. SPONSOR/MONITOR'S ACROYNM(S)
CG-521

11. SPONSOR/MONITOR'S REPORT NUMBER(S)

12. DISTRIBUTION / AVAILABILITY STATEMENT
Approved for public release; distribution unlimited.

20120516016

13. SUPPLEMENTARY NOTES

14. ABSTRACT

Significant changes in the design and operation of commercial ships have occurred over the last several decades. These changes, and their impact on the intact stability performance of ships, have motivated the development of the second generation intact stability criteria by the IMO Subcommittee on Stability and Load Lines and on Fishing Vessels Safety (SLF). Parametric roll resonance, pure loss of stability, and broaching-to are among the primary modes of stability failures which are being addressed. The second generation intact stability criteria are planned to have a multi-tiered structure. As the direct assessment of dynamic stability may he not necessary for all ships covered by IMO instruments, the first two tiers consists of level 1 and 2 vulnerability criteria that are used as a preliminary design process check of dynamic stability failure risk. This report describes the U.S. contribution to this development, including the three modes of stability failure listed above. It also contains a justification of the U.S. position at SLF on dead ship condition criteria, as well as an overview of possible methods for direct stability assessment procedures.

15. SUBJECT TERMS
IMO, Intact Stability, Criteria, Parametric Roll, Pure Loss of Stability, Surf-riding, Broaching-to, Dead Ship Conditions, Direct Stability Assessment

16. SECURITY CLASSIFICATION OF:			17. LIMITATION OF ABSTRACT	18. NUMBER OF PAGES	19a. NAME OF RESPONSIBLE PERSON
a. REPORT	b. ABSTRACT	c. THIS PAGE	UNCLASSIFIED	174	Vadim Belenky
UNCLASSIFIED	UNCLASSIFIED	UNCLASSIFIED			19b. TELEPHONE NUMBER (include area code) (301) 227-1720

Contents

Figures

Tables

This page is intentionally left blank

Abstract

Significant changes in the design and operation of commercial ships have occurred over the last several decades. These changes, and their impact on the intact stability performance of ships, have motivated the development of the second generation intact stability criteria by the IMO Subcommittee on Stability and Load Lines and on Fishing Vessels Safety (SLF). Parametric roll resonance, pure loss of stability, and broaching-to are among the primary modes of stability failures which are being addressed. The second generation intact stability criteria are planned to have a multi-tiered structure. As the direct assessment of dynamic stability may not be necessary for all ships covered by IMO instruments, the first two tiers consists of level 1 and 2 vulnerability criteria that are used as a preliminary design process check of dynamic stability failure risk. This report describes the U.S. contribution to this development, including the three modes of stability failure listed above. It also contains a justification of the U.S. position at SLF on dead ship condition criteria, as well as an overview of possible methods for direct stability assessment procedures.

Administrative Information

The work described in this report was performed by the Seakeeping Division (Code 55) of the Hydromechanics Department at the Naval Surface Warfare Center, Carderock Division (NSWCCD). The work was funded by the U.S. Coast Guard Headquarters, Office of Design and Engineering Standards (CG-521), Naval Architecture Division, in FY 2010, under work unit 10-1-5500-737.

Acknowledgements

The developments in the procedures described in this report were based on the results of research funded by the Office of Naval Research (ONR), under the ongoing research project, "A Probabilistic Procedure for Evaluating the Dynamic Stability and Capsizing of Naval Vessels" under the direction of Dr. L. Patrick Purtell. Another major project, with results that contributed to this work, was funded by Naval Sea Systems Command (NAVSEA 05D1), under the direction of Mr. James Webster.

Technical discussions regarding the content of this report from Dr. Arthur Reed, Mr. Martin Dipper, Jr. (NSWCCD) and Prof. N. Umeda (Osaka University) are greatly appreciated. The authors also would like to recognize fruitful discussions with A. Francescutto and G. Bulian (University of Trieste), B. Altmayer, O. Hympendahl, R. Pereira, and V. Shigunov (Germanischer Lloyd), A. Rozen and M. Palmquist (Seaware, Sweden), Y. Kim (Scoul National University) and H. Son (Korean Register of Shipping).

This page is intentionally left blank

1 Introduction

1.1 The Context of the Work

Sufficient intact stability is one of the most fundamental requirements for any type of vessel. While different stability criteria have been developed since the 1930s, including national stability standards and classification society rules, the first international stability regulations were formulated in the 2008 Intact Stability (IS) Code, which came into force in July 2010, adopted through resolution MSC.267(85) of the Maritime Safety Committee (MSC) of the International Maritime Organization (IMO)

The origin of the first-generation intact stability criteria, which are the foundation of the 2008 IS code, can be traced to the pioneering work of Rahola (1939), as well as the early versions of the weather criterion developed in the 1950s. The history of development and the background of these criteria are described by Kobylinski and Kastner (2003).

The development of the second generation of intact stability criteria started in 2002 with the re-establishment of the intact stability working group by the IMO Subcommittee on Stability and Load Lines and on Fishing Vessels Safety (SLF) – see Francescutto (2004, 2007). However, due to other priorities, the actual work on the second generation of intact stability criteria did not start until the 48th session of the SLF, in September 2005. The working group decided that the second generation of intact stability criteria should be performance-based and address three fundamental modes of stability failures (SLF 48/21, paragraph 4.18):

- Restoring arm variation problems, such as parametric excitation and pure loss of stability;
- Stability under dead ship condition, defined by SOLAS regulation II-1/3-8; and
- Maneuvering related problems in waves such as broaching-to.

A similar formulation was included in the preamble of the 2008 IS Code, as a direction for long-term development. However, the restoring arm variation problem was considered as two modes of parametric roll and pure loss of stability; hence, four stability failure modes were considered.

The first steps in the development of the criteria have shown that the development is a formidable task. Among the first proposals for these criteria was that which was contained in SLF 49/5/2 and with supporting information presented in SLF 49/INF.3. This proposal suffered from multiple theoretical shortcomings and was rejected by the working group at 49th session of SLF (July 2006). The development of second generation of the intact stability criteria clearly required a new approach.

A significant part of that consideration was general agreement that the second generation criteria should be based on physics of the phenomena leading to intact stability failure. Design and modes of operations of new ships take on characteristics that cannot, with confidence, rely solely on the statistics of failures and regression-based techniques. Also, there was general agreement of the desirability of relating the new criteria to probability, or some other measures of the likelihood of stability failures, as

methods of risk analysis have gained greater acceptance and become standard tools in other industries.

These considerations lead to the formulation of the framework for the second generation of intact stability criteria, as described in SLF 50/4/4 and discussed at the 50th session of SLF (May 2007). The key elements of this framework were the distinction between performance-based and parametric criteria, and between probabilistic and deterministic criteria. Special attention was paid to probabilistic criteria; the existence of the problem of rarity was recognized for the first time and a definition was offered. Also, due to the rarity of stability failures, the brute-force approach for the evaluation of probability with numerical tools was recognized to present a significant challenge.

By that time (2007), there was already some experience in the maritime industry on how to handle issues related to dynamic stability. Following a parametric roll accident with *APL China* (France, *et al.*, 2003), the American Bureau of Shipping (ABS) issued a guide on assessment of parametric roll for containerships (ABS, 2004). The guide offered an optional class notation by following a multi-tiered assessment procedure. The first level, susceptibility criteria, was formulated upon changing GM in a regular waves and the Mathieu equation. If a ship was found susceptible to parametric roll, then a more complex criterion, severity criterion, was applied. This "severity" criterion involved the calculation of the full GZ curve in waves and the numerical integration of the roll equation. If the roll response was "severe enough" (based on some specified level), then advanced numerical simulations were applied and ship-specific operational guidance was developed.

Although conservative, the susceptibility and severity criteria were still capable of distinguishing ships for which the occurrence of parametric roll was not possible. Shin, *et al.* (2004) describes the application of the susceptibility criteria to a tanker, which is not known to have any problems due to parametric roll. Both susceptibility and severity criteria have shown that parametric roll is not a problem for a tanker.

Application of the ABS guide to two series of ships has shown that the multi-tier approach has significant practical benefits. Because numerical simulations are expensive, the susceptibility and severity check provide a formal justification for such expenditures, ensuring that this work is done only for ships that may suffer from parametric roll.

In addition to the efforts of the classification societies, significant progress was achieved in developing training programs in order to enable crews to be fully aware of parametric roll phenomenon. An instructional video produced by Herbert Engineering Corporation is one successful example of this activity[1].

Analysis of this experience lead to an understanding that the multi-tiered approach should be applied for the development of the second generation intact stability criteria, as a way to avoid unnecessary work; the idea of vulnerability criteria was first formulated in the paper by Belenky, *et al.* (2008), see Figure 1.1. This paper also gave a broad review of the physics background of the dynamic stability failures under consideration. This paper, in a sense, played a role of "explanatory notes" to SLF 50/4/4 and was further submitted for information to the 51st session of SLF (SLF 51/INF.4).

[1] Trailer available at http://www.herbert.com/videos/ParametricRoll/

Figure 1.1 describes the current view of the multi-tiered approach for intact stability criteria (SLF 53/WP.4). In this process, the criteria contain in section 2.2 and then that of Section 2.3 of Part A of the 2008 IS Code is applied for all ships covered under IMO instruments. Each ship is also checked for vulnerability to pure loss of stability, parametric roll, and broaching and surf-riding phenomena using level I vulnerability criteria (L1). If a possible vulnerability is detected, then the level 2 criteria (L2) are used, followed by direct stability assessment (DA), if necessary. If the direct stability assessment shows an elevated level of risk for the respective mode of stability failure, then ship specific operational guidance (OG) may be developed, which is subject to the requirements of the flag administration (ADM). If vulnerability to each mode of stability failure was not detected, or the risk of stability failure is not considered excessive, then no additional requirements must to be satisfied. The process is repeated for all three stability failure modes. Dead ship conditions currently are excluded from consideration– which is discussed further in section 5.

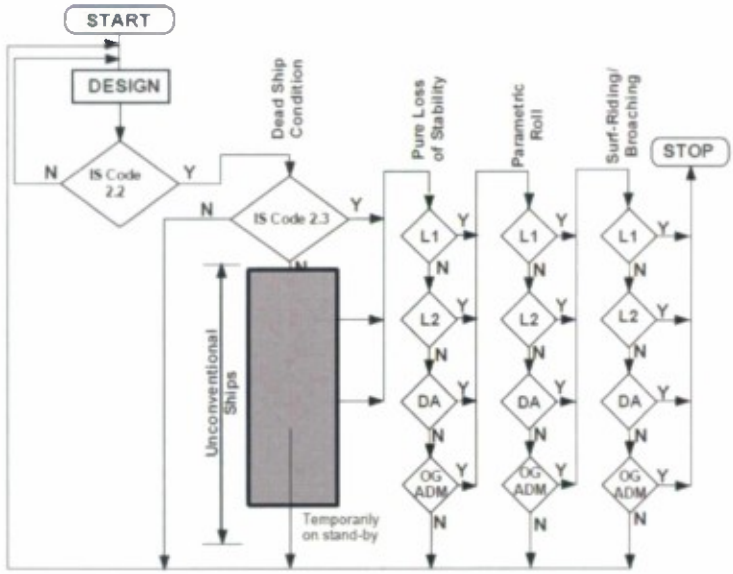

Figure 1.1 Multi-tiered Approach for the Second Generation of Intact Stability Criteria

Meanwhile, the intersessional correspondence group established by the 50th session of SLF was tasked to further develop the framework and create the draft terminology for the second generation of intact stability (SLF 50/WP.2 Annex 6). The draft framework developed by the intersessional group (SLF 51/4/1 Annex 2) was the next step after SLF 50/4/4, as it represented the common understanding of the correspondence group. In particular, the document made a clear distinction between a criterion and a standard– the former being "an instrument of judging" and the latter is a boundary "between a good and bad" outcome. The terminology list is included as Annex 4 of SLF 51/4/1. Both the framework and the terminology list are considered as working documents.

After the discussion of these documents at the 51st session of SLF (July 2008), the intact stability working group agreed on the framework of the second generation intact stability criteria (Annex 1 SLF 51/WP.2) and commissioned the intersessional

correspondence group to develop preliminary specifications of the second generation intact stability criteria, and to collect information relevant to development of vulnerability criteria and sample ship data to test these criteria (SLF 51/WP.2).

During the discussions of the working group there was expressed a notion that, in general, it is bad practice to submit completely new technologies to SLF. It should be first published in a technical journal, preferably also being presented and discussed at technical conferences. In particular, the international conferences on stability of ships and ocean vehicles (also known as STAB) and international ship stability workshops (ISSW) are very appropriate venues to discuss these advances. Such presentations, while being unofficial from the IMO perspective, are very important as they allow discussion of the technical background of new proposals among experts and therefore, improve the quality of the future submissions. The 10th STAB conference included a number of papers presented on vulnerability criteria and direct assessment: Kobylinski (2009), Bassler, *et al.* (2009), Belenky, *et al.* (2009a), Umeda, *et al.* (2009), Shigunov, *et al.* (2009) and others. These discussions were also continued at the 1st International Workshop on Dynamic Stability Consideration in Ship Design (DSCSD), see Kobylinski (2009a).

The Japan Society of Naval Architects and Ocean Engineers (JASNAOE) established a Strategic Research Committee on Estimation Methods of Capsizing Risk for the IMO New Generation Stability Criteria (SCAPE Committee) in 2005. Outcome of this program was reported in five sessions of JASNAOE; some other results were also reported in English at the Osaka Colloquium (Ikeda, et al., 2008). An overview of this work is available from SLF 51/INF.6. In the meantime, certain developments in the field were affected by the increasing consideration and practical formulation of the so-called "critical wave groups" approach. This was used for probabilistic intact stability assessment during the European SAFEDOR project (e.g. Themelis & Spyrou, 2007), which allowed for a practical interfacing between the deterministic and probabilistic viewpoints. SNAME established a Dynamic Stability Task Group whose purpose is to provide a detailed review of developments in the field of dynamic stability (SLF 53/3/3). SNAME has also funded research on the next generation of stability criteria for small fishing boats (Womack and Johnson, 2005).

These and other discussions held in the professional community were one of the factors why the intersessional correspondence group was able to succeed in gathering a very large amount of information (SLF 52/INF.3) and formulating several options for preliminary specifications of vulnerability criteria (SLF 52/3/1).

Following the IS Code coming into force, and reflecting the importance of the development of the second generation of intact stability criteria, the 52nd session of SLF (January 2010) has changed the title of the agenda item from "Revision of Intact Stability Code" to "Development of New Generation of Intact Stability Criteria."[2] The intact stability working group agreed on the preliminary specification for the second generation intact stability criteria, adopting the principle of increasing complexity within the multi-tiered approach (Annex 2 SLF 52/WP.1). The intersessional correspondence group was tasked to collect additional methodologies and refine proposals on the vulnerability criteria level 1 and 2 for all the modes of stability failures.

[2] The term "New generation of intact stability criteria was replaced by the second generation intact stability criteria at the 53rd session of SLF, following the proposal from Poland (SLF 53/3/5)

1.2 The Contents of the Work

This report describes the work that was commissioned by the Naval Architecture Division of the Office of Design and Engineering Standards of the United States Coast Guard (CG 521) to the Naval Warfare Center Carderock Division (NSWCCD – David Taylor Model Basin, Seakeeping Division, Code 55) to provide technical support services in FY 10, which covered a significant part of the intersessional period between the 52nd and 53rd session of SLF (the 52/53 intersessional period). The objective of this R&D work is to support U.S. participation in the work of the intersessional correspondence group. In particular, the development and testing of the level 1 and 2 vulnerability criteria for all modes of stability failures is the top priority of this work, as they were expected to be the main focus of the working group at the 53rd session of SLF. Other objectives included relevant development towards the direct stability assessment methods. The work also included the development of documents to be submitted to intersessional correspondence group and to SLF directly.

Based on the work described in this report, the U.S. contribution to the intersessional correspondence group was developed and submitted (Annex 5 SLF 53/INF.10).

Proposals for level 1 and level 2 vulnerability criteria were developed for parametric roll (Section 2), pure loss of stability (Section 3) and maneuvering related problems in waves (Section 4). All of the criteria were tested on a sample population of 17 vessels (described in Section 7). It was shown that all of the developed criteria successfully identified ships with a higher risk of particular modes of intact stability failure.

At the 52nd session of SLF, the intact stability working group decided to use the modified weather criterion as the level 1 vulnerability criterion for the dead ship condition (SLF 53/3). Therefore, the development was focused on the weather criterion as a possible candidate for vulnerability criteria. However, additional analysis has shown that it is not likely this will be possible (Section 5). The same position was taken by the Poland (SLF 53/3/6). Supported by the results of the analysis in Section 5 of this report, the U.S. delegation supported the Polish position. This position turned out to be an acceptable approach to the problem as the working group also supported these positions; there was also a problem related with integration of the vulnerability check in the dead ship condition with 2008 IS code. As a result, the working group has recommended postponing the development related to dead ship condition, focusing instead on another additional mode of stability failure – excessive accelerations (SLF 53/WP.4).

While the focus of the 52/53 intersessional period was the vulnerability criteria, fueled by SLF priorities, work has also started on the direct stability assessment methods. Section 6 of the report presents a comprehensive review of the methods available for solution of the problem of rarity. This part of the work also underwent extensive discussion in meetings of the technical community (Belenky, *et al.*, 2010a, 2010b).

The 52/53 intersession period was characterized by very intensive discussions in the professional community concerning vulnerability criteria. It was a prominent subject at the 11th ISSW in Wageningen, the Netherlands. Some of the work included in this report was also presented and discussed there as well (Peters, *et al.*, 2010).

Understanding that these discussions hold a vital element for success, the 2nd International Workshop on Dynamic Stability Consideration in Ship Design (DSCSD) was organized by the U.S. Coast Guard and sponsored by Japan Ship Technology Research Association. The workshop was held in Windsor, UK in September 2010. The discussion among the experts revealed the tendency of vulnerability criteria proposals to converge, indicating a good chance for agreement and harmonization during the 53rd session of SLF.

Therefore, the additional work after the workshop was mostly focused on facilitating possible agreement at SLF 53. Following this, a joint proposal with Japan was developed for the maneuvering related problems in waves (SLF 53/3/8). Lengthy discussions with Prof. N. Umeda (Osaka University, Japan) were instrumental in reaching the agreement on surf-riding and broaching-to issues.

Another individual whose contribution was instrumental for this work was Prof. K. Spyrou (National Technical University of Athens, Greece). He proposed an alternative to the level 1 vulnerability criteria on parametric roll. This alternative contained elements of the common background between several proposals which were used for the development of the document (SLF 53/3/7). He also collaborated with V. Belenky and C. Bassler on vulnerability criteria level 1 and 2 for surf-riding. Recognizing Prof. K. Spyrou's significant contribution to the work described within this report, he was invited to be one of the authors of this report.

The criteria development described in this report was based on the results of research funded by the Office of Naval Research (ONR), under the ongoing research project, "A Probabilistic Procedure for Evaluating the Dynamic Stability and Capsizing of Naval Vessels" under the direction of Dr. L. Patrick Purtell. Major works developed under this project and used in this report are Belenky and Weems (2008, 2008a), Belenky, *et al.* (2008a, 2009, 2010), Bassler, *et al.* (2008; 2009). Another major project, with results that were used for this work, was funded by NAVSEA, under the direction of Mr. James Webster (Bassler, *et al.*, 2010; 2010a, Belenky and Bassler 2010, Minnick, *et al.*, 2010; 2011; 2011a). Technical discussions regarding the content of this report from Dr. Arthur Reed, Mr. Martin Dipper, Jr. (NSWCCD) and Prof. N. Umeda (Osaka University) is greatly appreciated. The authors also would like to recognize fruitful discussions with A. Francescutto and G. Bulian (University of Trieste), B. Altmayer, O. Hympendahl, R. Pereira, and V. Shigunov (Germanischer Lloyd), A. Rozen and M. Palmquist (Seaware, Sweden), and Y. Kim (Seoul National University) and H. Son (Korean Register of Shipping).

As the development of the second generation intact stability criteria gains momentum, additional people with different technical backgrounds are becoming involved. Clear communication of the motivations, objectives, and approaches of this development becomes paramount for the success of this enterprise. To facilitate this communication, this report consists of a three-tiered structure in its main part (Sections: 2, 3, 4 and 5). The first subsection of each of these sections is an executive level, graphic-based brief explanation of the physical background of each of the phenomena. The second subsection in each of these sections describes the main mathematical model that is used to develop the criteria; the second subsection is intended to primarily for regulators and class society engineers who would like to gain deeper understanding of the ongoing development. The rest of the sections describe the technical details of the methods.

2 Vulnerability Criteria for Parametric Roll

This section describes the development of vulnerability criteria for parametric roll, including some general background information on the physics of parametric roll phenomenon, the basic mathematical model used for detecting susceptibility to parametric roll, and proposals and testing of levels 1 and 2 vulnerability criteria. Sample calculations were performed using the characteristics of 17 ships.

2.1 Physical Background

2.1.1 Changing Stability in Waves

When a ship is sailing through waves, the submerged part of the hull changes. These changes may become especially significant if the length of the wave is comparable to the length of the ship.

As a first example, one may observe the changes that occur when the trough of a wave is located amidships (see Figure 2.1). For most ships, the upper part of the bow section is usually wide, due to bow flare. Bow flare provides protection from spray and green water shipping, and also allows additional cargo to be stored on deck. As a result, the bow flare makes the waterplane larger, if the upper part of the bow section becomes partially submerged.

The upper part of the aft section of the hull is typically even larger. Apart from cargo stowage considerations, this section must also provide room for steering machinery. Therefore, the after part of the waterplane also increases, once the upper part of the aft section becomes submerged.

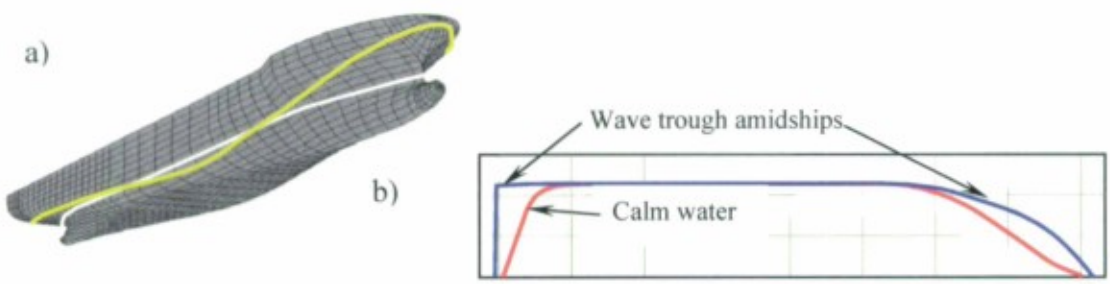

Figure 2.1 Changes in Hull Geometry when a Wave Trough is Amidships (a) 3D View (b) Waterplane

Unlike the bow and aft sections, the midship section of most ships is almost nearly wall-sided. This means that very little change occurs in the waterplane width with variations in draft. When the wave trough is amidships, the draft at the midship section is low, but as the hull is wall-sided in this region, there is little waterplane change. As a result, when the wave trough is located around the midship section, the overall waterplane area is increased (see Figure 2.1b).

When the wave crest is located near amidships, the situation changes dramatically (Figure 2.2). The underwater part of the bow section is usually quite narrow, especially around the waterline. Even for a bulbous bow, it is still narrower than for the section with bow flare. The reason for this is the consideration of resistance. The faster the ship is, the narrower its underwater bow section must be. If the wave crest is amidships and the wave has a length similar to a ship length, the wave trough is located around the bow section. This makes the draft at the bow quite shallow. As a result, the waterplane become becomes very narrow in this region.

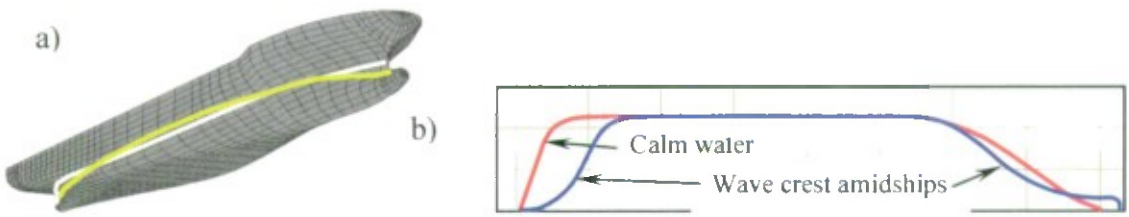

Figure 2.2 Changes in Hull Geometry when a Wave Crest is Amidships (a) 3D View (b) Waterplane

The underwater part of the aft section is also very narrow. The main design consideration is to provide the propulsor with enough inflow for the speed and power of the ship. Consideration of energy efficiency impels a designer towards a buttock flow stern design. When the wave crest is located amidships, another wave trough is located near the aft section. The draft at the stern becomes shallow, which makes the waterplane very narrow in the aft part. This also is exaggerated with increased ship speed, as more power must be handled by the propeller.

As mentioned previously, the midship section is typically more wall-sided, so it does not significantly affect the waterplane. Figure 2.2b shows the effect of the wave crest amidships, where the overall waterplane is reduced in area.

As it is well known from ship hydrostatics, the waterplane area has a significant effect on ship stability. If the waterplane area is reduced, then so is the GZ curve (see Figure 2.3).

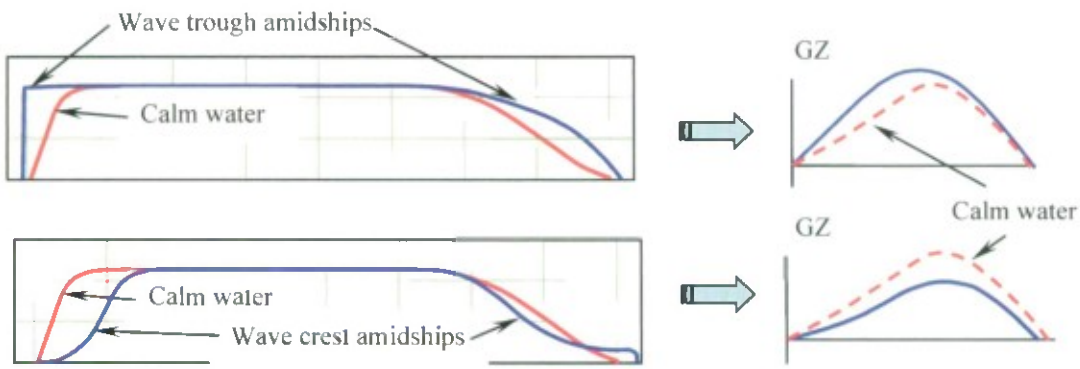

Figure 2.3 Stability Corresponding to Waterplane Changes on the Wave Trough (Top) and the Wave Crest (Bottom)

2.1.2 Development of Parametric Roll

The development of the occurrence of parametric roll is caused by periodic stability changes occurring with a certain frequency – about twice per roll period, see Figure 2.4.

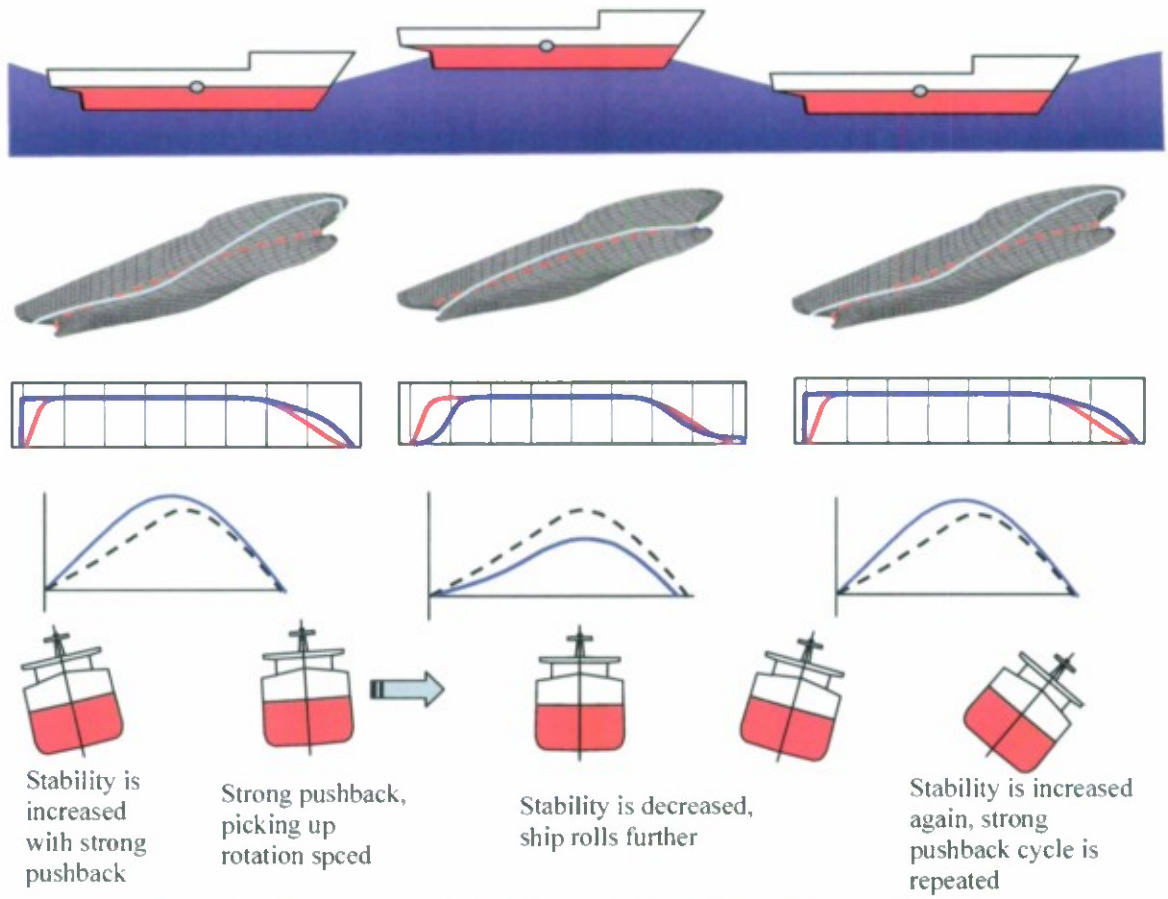

Figure 2.4 Development of Parametrie Roll Resonanee (Parametric Roll)

If the ship is rolled while on thc wave trough, inereased stability provides stronger pushbaek, or restoring moment. As the ship returns to the upright position, its roll rate is greater, since there was an additional pushbaek from the increased stability. If at that time, the ship has the wave erest at midship, the stability is dcereased and the ship will roll further to the opposite side because of the greater spced of rolling and less resistance to heeling. Then, if the wave trough reaehes the midship section when the ship reaches its maximum amplitude roll, stability inereases again and the cycle starts again.

Note that there was one half of the roll cycle associated with the passing of an entire wave. So, there are two waves that pass during eaeh roll period. That means the roll period is about twice that of the wave period (see Figure 2.5).

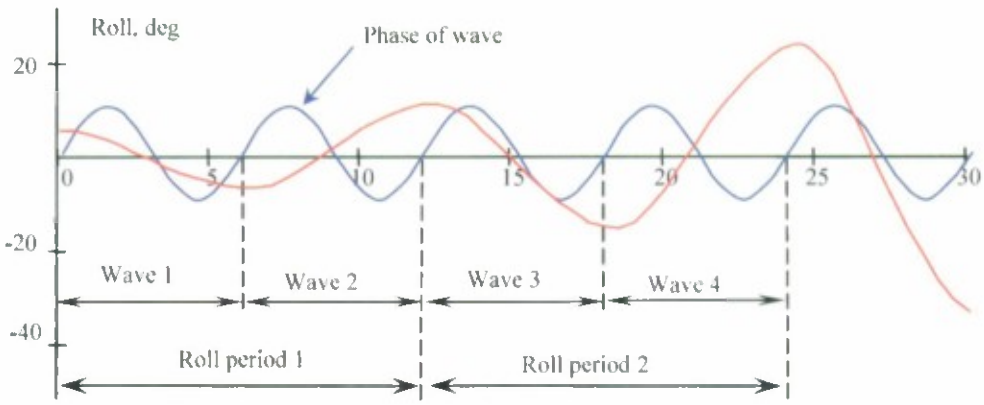

Figure 2.5 Development of Parametric Roll

2.1.3 Frequency Characteristics of Parametric Roll

Parametric roll is a resonance phenomenon and similar to roll resonance in beam waves (Figure 2.6a), parametric roll has a limited frequency range (Figure 2.6b).

The principal difference between the two phenomena is that the span of the frequency range for parametric roll depends on the magnitude of stability change, while the frequency range for roll resonance depends on wave height (Figure 2.6c). Also, if the beam waves are far from the resonance frequency, the ship only rolls with very small amplitude. Parametric roll does not exist (the amplitude is equal to zero) outside of the frequency range.

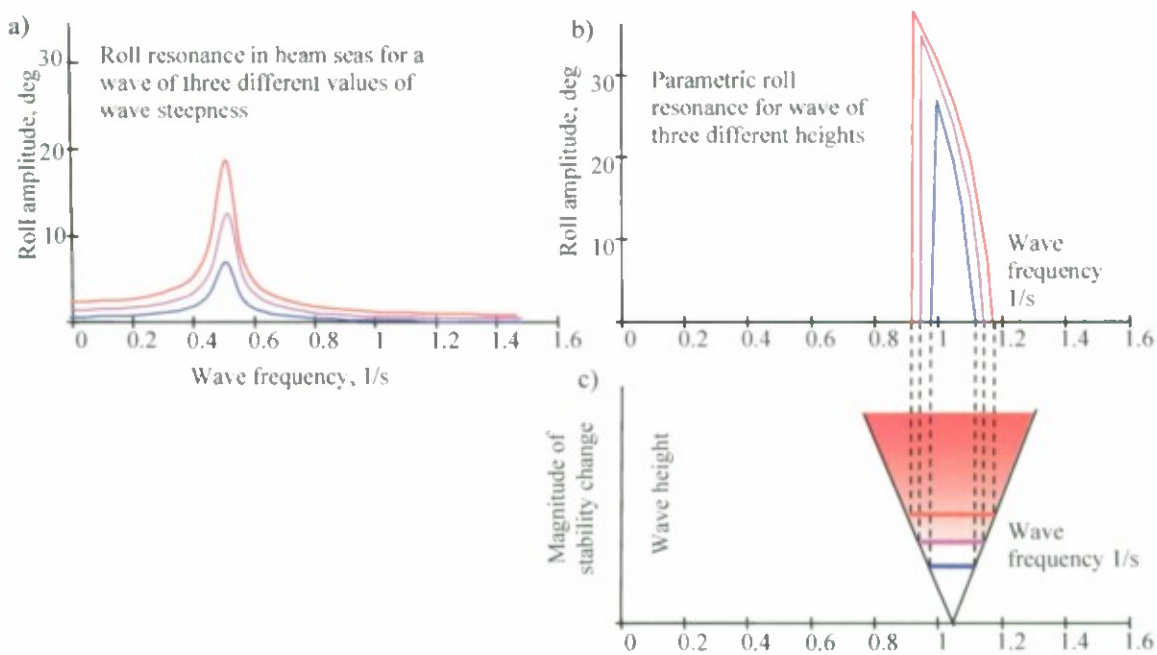

Figure 2.6 (a) Roll Resonance in Beam Waves (b) Parametric Roll Resonance (c) Frequency Range of Parametric Roll Resonance

2.1.4 Influence of Speed and Wave Direction

The frequency of encounter with waves changes when a ship is in motion. When a ship is sailing in following or stern-quartering seas, the direction of waves and the ship heading are similar (Figure 2.7a). As a result, the relative speed is small and a ship encounters fewer waves during the same time period (compared to a zero speed case). The encounter period is increased (and the encounter frequency is decreased) in following or stern-quartering waves.

When a ship is sailing in head or bow-quartering seas, the direction of waves and the ship heading are opposite (Figure 2.7b). As a result, the relative speed is large and a ship encounters more waves during the same time (compared with the zero speed case). The encounter period is decreased (and the encounter frequency is increased) in head or bow-quartering waves.

a) Following and stern-quartering seas: the encounter period is longer that the wave period

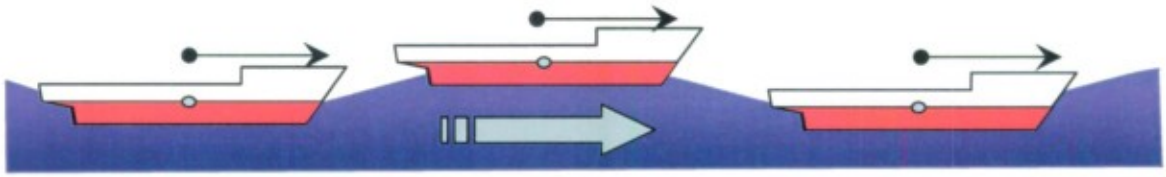

b) Head and bow-quartering seas: the encounter period is shorter that the wave period

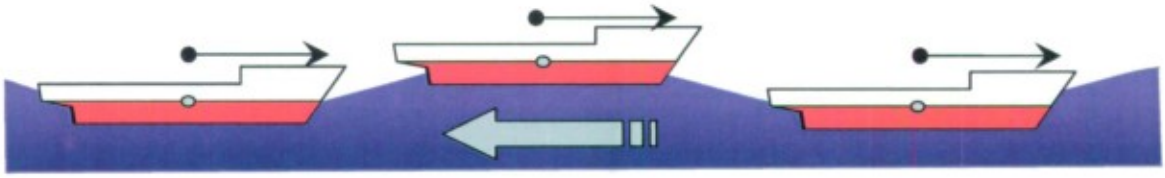

Figure 2.7 Influence of Speed and Wave Direction

The inception of parametric roll depends on the frequency of encounter being in the frequency range where the parametric roll is possible (Figure 2.6c). Therefore, the development of parametric roll depends on speed and heading.

2.2 Mathematical Description of Parametric Roll

2.2.1 Derivation of Mathieu-Type Equation

The Mathieu equation is the simplest mathematieal model of parametrie roll and it has been extensively used to analyze this phenomenon. As this model is instrumental in the development of vulnerability eriteria, it makes sense to repeat its derivation and describe its properties. It is done mostly following Shin, *et al.* (2004).

Consider a ship sailing in longitudinal seas (following or head), so there is no wave heeling moment:

$$(I_x + A_{44})\ddot{\phi} + B_{44}\dot{\phi} + \Delta \cdot GM(t)\phi = 0 \tag{2.1}$$

Here, B_{44} is the linear (or linearized) damping coefficient, Δ is the weight displacement of a ship, I_x is the transverse moment of inertia, and A_{44} is the added mass in roll.

The variation of GM with time is the key physieal feature to model for parametrie roll. As this variation experienees periodie ehanges onee waves pass through, its dependenee on time is simulated with sine or eosine funetion:

$$GM(t) = GM_m + GM_a \cos(\omega_e t) \tag{2.2}$$

Here, ω_e is the wave frequeney of eneounter while GM_m is a mean value of the GM. GM_a is the amplitude of the GM changes in waves

$$GM_a = 0.5(GM_{\max} - GM_{\min}) \tag{2.3}$$

$$GM_m = 0.5(GM_{\max} + GM_{\min}) \tag{2.4}$$

Here, $GM_{\max}$ and $GM_{\min}$ are maximal and minimal instantaneous values of GM for a number of wave erest positions along the ship hull.

Using the eosine funetion to describe GM ehanges in time is just an approximation to express the periodie eharaeter of the ehanges during the wave pass. Figure 2.8 shows the ealeulated GM in waves eompared to a eosine funetion approximation, as a function of the position of the wave erest along the length of the hull. As can be seen from this figure, the minimum of the ealeulated GM is shallower, while the maximum is sharper in eomparison with the cosine approximation in (2.2). The calculated curve is also slightly shifted.

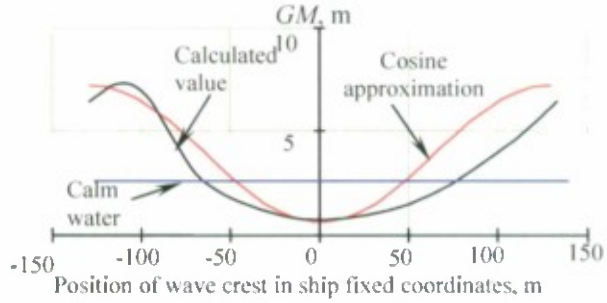

Figure 2.8 *GM* Values in Waves vs. Cosine Approximation for a Post Panamax Containership

Substitution of the definition of (2.2) into the roll equation (2.1) and its division by the inertial eoeffieient yields the following equation for roll motion:

$$\ddot{\phi} + 2\delta\dot{\phi} + \left(\omega_m^2 + \omega_a^2 \cos(\omega_e t)\right)\cdot\phi = 0 \tag{2.5}$$

Here:

$$\omega_m = \sqrt{\frac{\Delta \cdot GM_m}{I_x + A_{44}}}\ ; \quad \omega_a = \sqrt{\frac{\Delta \cdot GM_a}{I_x + A_{44}}}\ ; \quad \delta = \frac{1}{2}\frac{B_{44}}{I_x + A_{44}} \tag{2.6}$$

In order to transform (2.5) into the standard form of the Mathieu equation, a dimensionless time (in terms of encounter period) is introduced:

$$\tau = \omega_e t \quad \Rightarrow \quad t = \frac{\tau}{\omega_e} \tag{2.7}$$

Substitution (2.7) into the roll equation (2.5) turns it into a dimensionless form:

$$\frac{d^2\phi}{d\tau^2} + 2\mu\frac{d\phi}{d\tau} + \left(\overline{\omega}_m^2 + \overline{\omega}_a^2 \cos(\tau)\right)\cdot\phi = 0 \tag{2.8}$$

Here, the eoefficients of equation (2.8) are the dimensionless quantities:

$$\mu = \frac{\delta}{\omega_e}; \quad \overline{\omega}_m = \frac{\omega_m}{\omega_e}; \quad \overline{\omega}_a = \frac{\omega_a}{\omega_e} \tag{2.9}$$

The next substitution eliminates damping by introdueing new variable x:

$$\phi(\tau) = x(\tau)\cdot\exp(-\mu\tau) \tag{2.10}$$

This finally expresses roll in the form of the Mathieu equation by substitution equation (2.10) into (2.8):

$$\frac{d^2x}{d\tau^2} + \left(p + q\cos(\tau)\right)\cdot x = 0 \tag{2.11}$$

Here:

$$p = \left(\overline{\omega}_m^2 - \mu^2\right); \quad q = \overline{\omega}_a^2 \tag{2.12}$$

2.2.2 Solution of the Mathieu Equation and Its Properties

The Mathieu equation is a linear differential equation with variable coefficients. It solution cannot be expressed in elementary functions. Therefore, as the Mathieu equation is widely used in mathematics, physics, and engineering, its solution is considered to be a specialized function, known as the Mathieu function. It is tabulated and included in advanced mathematical software packages.

As is known, the Mathieu equation (2.11) may have two types of solutions (Mathieu functions): bounded, or "stable," (Figure 2.9) and unbounded, commonly referred as "unstable" (Figure 2.10).

Whether a solution is bounded or unbounded depends on the combination of coefficients, p and q. The combinations of p and q values that correspond to a bounded or unbounded solution can be graphed in a figure that is known as the Ince-Strutt diagram (shown in Figure 2.11). The blank areas correspond to the bounded solution, while the shaded areas correspond to the unbounded solution.

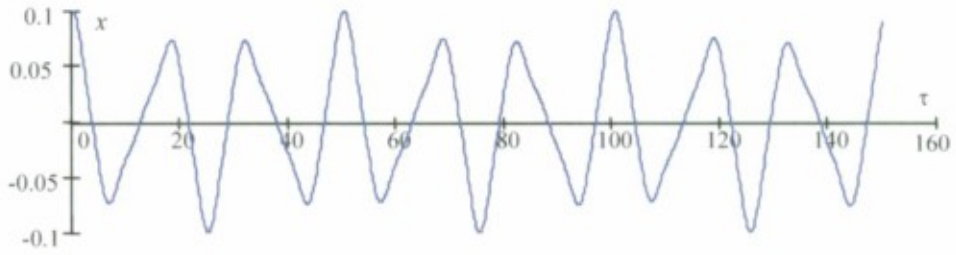

Figure 2.9 Bounded Solution of the Mathieu Equation p=0.1; q=0.2

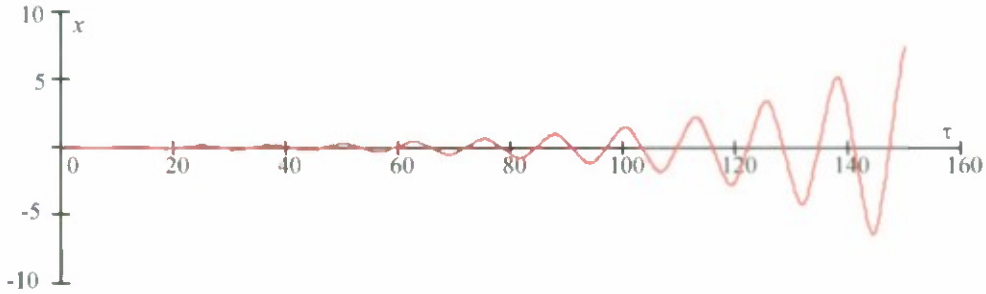

Figure 2.10 Unbounded Solution of the Mathieu Equation p=0.15; q=0.2

The shaded areas, identified with Roman numerals in Figure 2.11, correspond to the unbounded solution and have shapes of curved triangles. Each such triangle touches the p-axis and, with an increase of q, becomes wider. The areas with the smaller p-intercept grow in width faster; it can be seen at the level $q = 2$, the first shaded area is the widest.

The parameter p is seen, in equations (2.9) and (2.12), to be equal to a difference of the square of the ratio of natural and excitation frequencies and the square of the ratio of the damping and the excitation frequencies.

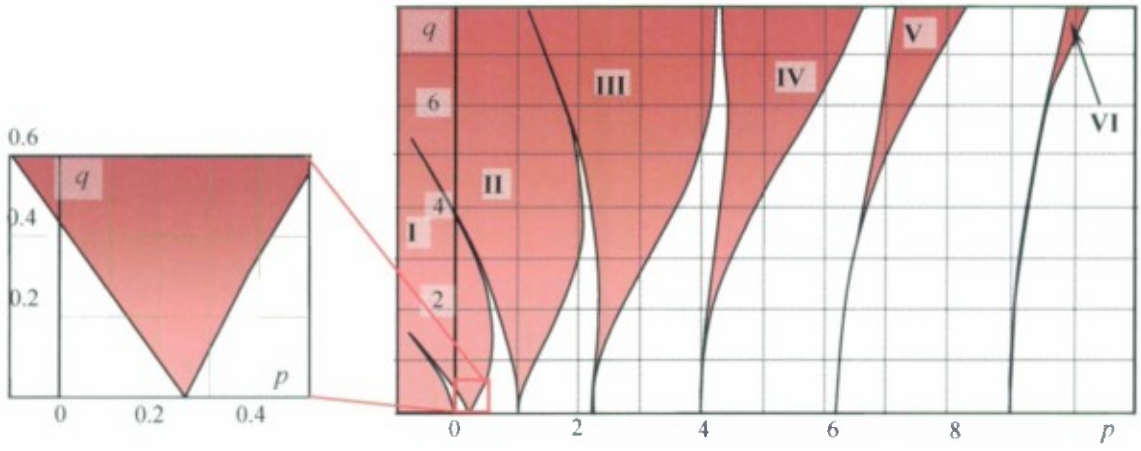

Figure 2.11 Ince-Strutt Diagram

The parameter q reflects the level of GM change in waves, expressed as the square of the frequency ratio, as can be seen in equations (2.3), (2.9) and (2.12). Therefore, the parameter q plays the role of the amplitude of parametric excitation. As a result, the entire Ince-Strutt diagram can be considered in terms of the amplitude of parametric excitation vs. the square of non-dimensional frequency.

The first instability zone intersects the axis exactly at $p = 0.25$, which corresponds to the frequency ratio of 2, so the excitation frequency is twice the natural roll frequency at this point. The unbounded motion belonging to this zone is commonly referred to as the principal parametric resonance. The zoomed-in view of this zone is shown in the insert of Figure 2.11.

The second instability zone intersects the axis at $p = 1.0$, where the excitation frequency is equal to the natural roll frequency. Unbounded solutions belonging to this zone are defined as the fundamental parametric resonance.

2.2.3 Influence of Damping and Nonlinearity

The Mathieu equation (2.11) has a periodic bounded solution since the damping was excluded by the substitution (2.10). This means that the corresponding roll, $\phi(\tau)$, decays with the damping decrement, μ, if $x(\tau)$ is a periodical solution of the Mathieu equation, as shown Figure 2.9.

An unbounded solution of the Mathieu equation, $x(\tau)$ (as in Figure 2.10), does not necessarily mean that rolling will be unbounded because the exponential term $\exp(-\mu\tau)$ might undo the effect of boundlessness by damping the solution back to a decaying form.

It also means that there is a threshold value for roll damping for each pair of Mathieu parameters, p and q. If roll damping is less than the threshold value, roll will be unbounded as the solution of the Mathieu equation. If the roll damping is larger than the threshold, roll is still bounded, even if the Mathieu equation is unbounded. The increment of the Mathieu solution is not enough to overcome the decrement of roll damping. In addition, it is also means that with linear damping, the instability zone is narrower and requires some finite value of GM variations even at p=1/4; i.e., it does not touch the axis (see Figure 2.12).

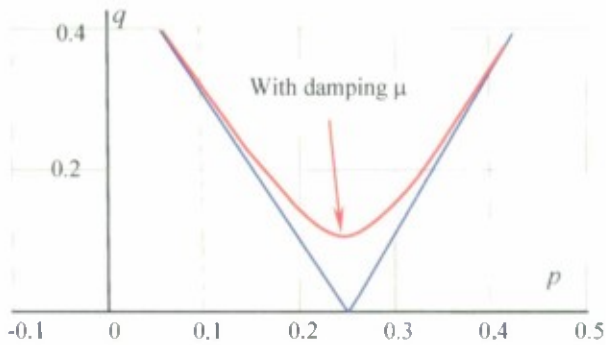

Figure 2.12 Influence of Damping on Parametric Roll

The Mathieu equation, however, is only capable of indicating parametric roll starts or not. Once it starts, the amplitude grows exponentially and the solution goes into infinity. In order make a model to stabilize with certain amplitude, the nonlinearity of stiffness (*GZ* curve) needs to be introduced. The one of the simplest expressions is a cubic parabola:

$$GZ(\phi) = GM \cdot \phi\left(1 - \phi^2\right) \tag{2.13}$$

Such cubic parabola models a *GZ* curve with an angle of vanishing stability of 1 rad ≈ 57.3 deg, an angle of maximum about $3^{-0.5}$ rad ≈33 deg, while the maximum of the *GZ* curve is about 0.385 *GM*. This model, of course, cannot simulate all the regulated properties of the real *GZ* curve. However, it still may be used as the first expansion to study parametric roll behavior of a ship-like oscillator.

The simplest model of changing *GZ* curve in waves can be expressed by combining (2.2) and (2.13), using the definitions in (2.6):

$$GZ(\phi,t) = GM_m \cdot \phi \cdot \left(1 - \phi^2\right) \cdot \left(\omega_m^2 + \omega_a^2 \cos(\omega_e t)\right) \tag{2.14}$$

Figure 2.13 shows the modeled *GZ* curve as it changes during a one wave pass. Substitution of the model of the GZ curve (2.14) into the linear equation (2.5) makes it nonlinear and capable for stabilization in the mode of parametric roll:

$$\ddot{\phi} + 2\delta\dot{\phi} + \left(\omega_m^2 + \omega_a^2 \cos(\omega_e t)\right) \cdot \phi \cdot \left(1 - \phi^2\right) = 0 \tag{2.15}$$

Figure 2.14 shows the difference between nonlinear roll response with stabilization of roll amplitude just below 30 degrees compared to linear roll response (solution of equation (2.5)) with unbounded growth of amplitude.

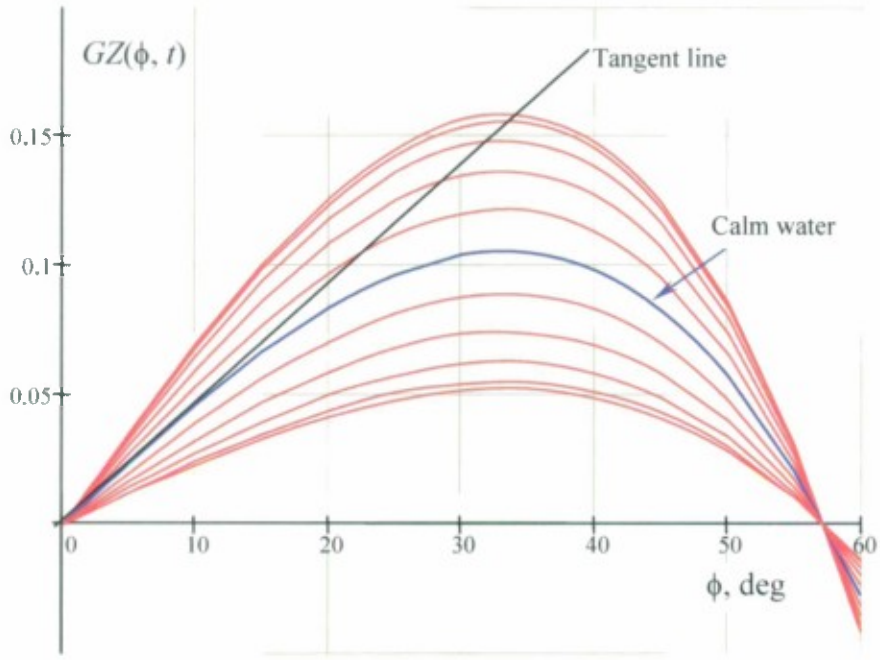

Figure 2.13 Periodically Changed Cubic GZ Curve

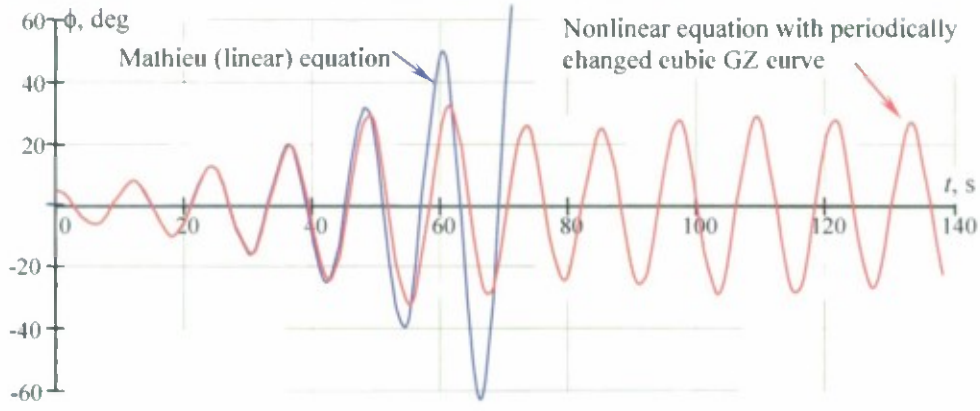

Figure 2.14 Modeling of Parametric Roll with Mathieu Equation (Blue) and Nonlinear Equation (Red)

It can be noted from Figure 2.14, that in the beginning, both linear and nonlinear roll response are identical (this is natural, as the *GM* formula works well for small angles). However, once the amplitude exceeds 10-15 degrees, the difference between the linear and nonlinear roll response becomes apparent. This is also clear from Figure 2.13, as the difference between the *GZ* curve and its initial tangent becomes noticeable starting about 10-15 degrees.

The difference between the actual *GZ* curve and its tangent (expressed through *GM*) is a key to explaining the stabilization of parametric roll. The roll amplitudes keep increasing, while energy is supplied by parametric excitation. A periodic change of parameters is a parametric excitation. It can cause parametric resonance if it meets the frequency conditions. If the oscillator is linear, its natural frequency does not change and

the energy continues to be incorporated. For a ship, the instantaneous GM changes with roll angle, so the instantaneous natural frequency also changes. This means that sooner or later the frequency condition of parametric roll will not be satisfied and the supply of energy from parametric roll will stop. Once the amount of energy from parametric excitation is limited, the oscillator reaches a certain balance and parametric roll is stabilized with certain roll amplitude.

There are other important consequences of the nonlinearity of the GZ curve. Since the instantaneous GM changes, parametric roll may become possible for the frequencies where it is not considered possible, if judged only using the initial GM. This requires, however, fairly large amplitude rolling, or very significant nonlinearity in the initial part of the GZ curve.

2.3 Level 1 Vulnerability Criteria

In order to give rise to parametric roll, the parametric excitation (change of stability in waves) must satisfy two conditions: its frequency (the encounter frequency) must be within the range and its magnitude must be above the threshold (resulting from damping). The Mathieu equation (and Ince-Strutt diagram) is the simplest mathematical model that can be used to check if these conditions are satisfied. ABS Susceptibility Criteria are based on this approach (ABS 2004, Shin *et al*, 2004).

K. Spyrou proposed a more advanced and practical version of the criteria based on the Mathieu equation (Spyrou, 2005). This idea was further used as a background for SLF 53/3/7 and is explained further below.

2.3.1 Frequency Condition

Boundaries of the 1st instability zone of at Ince-Strutt diagram have a known approximation:

$$p_{B1,B2} = \frac{1}{4} \pm \frac{q}{2} \tag{2.16}$$

Here p and q are parameters of the Mathieu equation (2.11) given by formula (2.12).
The encounter frequency is related with speed and heading as:

$$\omega_e = \omega - \frac{\omega^2}{g} V \cos\beta \tag{2.17}$$

Here V is the forward speed in m/s, β is heading angle relative waves (0 is following waves), g is acceleration of gravity, and ω is true frequency of a wave.

Assuming $q = 1$ (this is a conservative assumption as most container ships have q = 0.25~0.4). Spyrou (2005) formulated the criterion in terms of speed range (in knots):

$$V_{S1} = \frac{\sqrt{gL}}{0.5144}\left(\frac{1}{\sqrt{2\pi}} - \frac{\sqrt{2 \cdot L}}{T_\phi \sqrt{g}}\right) \quad ; \quad V_{S2} = \frac{\sqrt{gL}}{0.5144}\left(\frac{1}{\sqrt{2\pi}} - \frac{\sqrt{6 \cdot L}}{T_\phi \sqrt{g}}\right) \tag{2.18}$$

Here L is length of a ship, and T_ϕ is the natural period of roll.

This criterion was used in SLF 53/3/7 as a preliminary condition. If the service speed of a ship does not fall into the range defined by equations (2.18), it is not susceptible to parametric roll and a further vulnerability check is unnecessary. This preliminary condition makes the criteria easier to use, as the calculation of stability in waves is not required if the ship speed is outside of the range (2.18).

2.3.2 Magnitude of Stability Change

The second condition requires the results of the calculation of the stability in waves, as it is based on the magnitude of parametric excitation. The idea is to see how much the roll motions could grow, after a certain number of "dangerous" waves are encountered.

Consider the roll equation (2.5), re-writing it as:

$$\ddot{\phi} + 2\delta\dot{\phi} + \omega_m^2\left(1 + h\cos(\omega_e t)\right)\cdot\phi = 0 \tag{2.19}$$

Here h is another form of non-dimensional magnitude of parametric excitation:

$$h = \frac{\omega_a^2}{\omega_m^2} \tag{2.20}$$

As was mentioned earlier, the equation (2.19) does not have a solution that can be exactly expressed as an elementary function. Spyrou (2005) used the approximate solution according to Hayashi (1985):

$$\phi(t) = e^{-\delta t}\left(C_1 e^{\kappa\omega_m t}\sin\left(\omega_m t - \varepsilon\right) + C_2 e^{\kappa\omega_m t}\sin\left(\omega_m t + \varepsilon\right)\right) \tag{2.21}$$

Here C_1 and C_2 are arbitrary constants determined through initial conditions, and κ is a parameter controlling the growth or decay of oscillations. It is expressed as:

$$\kappa = \frac{1}{4}\sqrt{a^2h^2 - 4(a-1)^2} \tag{2.22}$$

Here a is another variable expressing frequency ratio:

$$a = 4\frac{\omega_m^2}{\omega_e^2} \tag{2.23}$$

Obviously $a = 1$ when $\omega_e = 2\,\omega_m$, and this is exactly the middle of the first instability zone of the Ince-Strutt diagram (the occurrence of principal parametric resonance).

The phase ε is determined from the following expression:

$$\cos(2\varepsilon) = \frac{2(a-1)}{a \cdot h}\ ; \quad -\frac{\pi}{2} \le \varepsilon \le 0 \tag{2.24}$$

For the sake of being conservative, the encounter frequency of a "dangerous" wave is considered to correspond exactly to the principal parametric resonance:

$$a = 1\ ; \quad \kappa = -\frac{h}{4}\ ; \quad \varepsilon = -\frac{\pi}{4}\ ; \tag{2.25}$$

Assuming zero for the initial roll rate and the cosine function for parametric excitation, the arbitrary constants were found equal to

$$C_1 = -C_2 = \frac{\sqrt{2}}{2}\phi_0\ ; \quad \dot{\phi}_0 = 0 \tag{2.26}$$

Substitution of (2.25) and (2.26) into (2.21) yields:

$$\phi(t) = \frac{\sqrt{2}}{2}\phi_0 e^{-\delta t}\left(e^{-0.25h\omega_m t}\sin\left(\omega_m t + \frac{\pi}{4}\right) - e^{0.25h\omega_m t}\sin\left(\omega_m t - \frac{\pi}{4}\right)\right) \tag{2.27}$$

This formula allows for the calculation of the amplification factor, f, after n oscillations (note that in the considered case, the response has a frequency, ω_m, and there were $2n$ "dangerous" waves):

$$f = \frac{1}{\phi_0}\phi\left(\frac{2\pi n}{\omega_m}\right) \tag{2.28}$$

Note that after one or two cycles of oscillation, the term with the negative exponent in the equation (2.27) will become small, compared to the exponentially growing term, and could be neglected. Then the substitution (2.27) into (2.28) yields:

$$f = -\frac{\sqrt{2}}{2}\exp\left(\frac{\pi n h}{2} - \frac{2\delta\pi n}{\omega_m}\right)\sin\left(2\pi n - \frac{\pi}{4}\right) \tag{2.29}$$

Expressing h from equation (2.29) leads to

$$h = 2\frac{\ln f + \ln 2}{\pi n} + \frac{4\delta}{\omega_m} \tag{2.30}$$

Given a factor of amplification and a number of oscillations, the following criterion is deduced:

$$h \geq 2\frac{\ln f + \ln 2}{\pi n} + \frac{4\delta}{\omega_m} \tag{2.31}$$

Substitution of the constants and moving the damping to the left hand side of the inequality produces the criterion in its final form (Spyrou 2005):

$$h - \frac{4\delta}{\omega_m} \geq \frac{0.693 + \ln f}{1.571 n} \tag{2.32}$$

Formula (2.6) allows rewriting the criterion in (2.31) in terms of GM in waves:

$$\frac{GM_a}{GM_m} \geq 2\frac{\ln f + \ln 2}{\pi n} + \frac{4\delta}{\omega_m} \tag{2.33}$$

If stability changes in waves can be assumed symmetric, the calm water values for GM and roll frequency can be used instead of the mean values in waves:

$$\frac{GM_a}{GM_0} \geq 2\frac{\ln f + \ln 2}{\pi n} + \frac{4\delta}{\omega_0} \tag{2.34}$$

To complete this consideration, the parameters in (2.34) have to be chosen. If no other data is available, ABS (2004) recommends, as a conservative estimate:

$$\frac{\delta}{\omega_0} = 0.03 \tag{2.35}$$

The number of cycles and the factor of amplification are obviously related. A larger amplification of initial roll may be expected for more cycles. These parameters are very important for the tuning of the criterion and need to be addressed during the later stage of development. As a preliminary guess, $f = 5$ while $n = 4$ leads to:

$$\frac{GM_a}{GM_0} \geq 0.49 \tag{2.36}$$

This is very close to the standard proposed in Annex 2 of SLF 53/INF.10 – the value of 0.51 was used there for a standard, while the general form of a criterion is similar to (2.36).

2.3.3 Parameters of the Wave

To carry out the calculation of stability in waves, the parameters of the wave need to be assigned. Assuming the wave length is equal to the ship's length seems to be logical, as this maximizes the stability changes. ABS susceptibility criteria are based on this assumption. The height of the wave is defined by a table depending on length (ABS, 2004).

K. Spyrou proposed to relate the wave height with wave length by using the principle of equal probability in order to establish a fair basis for the safety assessment of ships of all sizes. This entails a steepness decrease for a longer ship, thus taking care of the fact that a high value of wave steepness is less probable to occur for long waves. It is noteworthy that a similar approach to steepness was implicitly used in the formulation of the weather criterion.

Parametric roll is excited by a consecutive action of a series of waves. Therefore, it is logical to evaluate probability for the encounter of a group rather than for a single wave. This can be done using wave group representations described in Themelis and Spyrou, (2007; 2008) and Themelis (2008).

Sequential wave heights are presented with a Markov chain. This means that the wave height is assumed to be dependent only on the height of the previous wave, but is independent of the waves prior to the previous wave. This assumption seems to be quite logical, since the wave envelope (a curve that contains all the heights) has an autocorrelation function with relatively fast decay; so the correlation is practically zero after two wave periods.

Because a joint distribution of wave heights and wave lengths is known, this approach allows for the calculation of the probability of encountering a number of waves of a given length (actually the length within a given range) and height. K. Spyrou

ealculated how the steepness depends on wave length, keeping the probability of eneounter of a group of four waves constant ($P = 6.3 \times 10^{-6}$). The caleulations were earried out for a significant wave height of 5 m and modal period of 12 s. There were two series of ealculations using different ranges for wave length. The results of the ealeulations are shown in Figure 2.15.

This analysis, although preliminary, still allows eapturing of the dependence of steepness on length, and avoiding penalizing large ships.

Based on these ealeulations, a sample formula for wave height is proposed:

$$H = \begin{cases} 0.05L & if \quad L < 100 \\ \frac{L}{3}(0.2 - 0.0005L) & if \quad 100 \le L < 300 \\ 0.01667L & \quad L \ge 300 \end{cases} \tag{2.37}$$

Results of the applieation of these eriteria to the population of the sample ships are shown in Table 1. Further details of the sample ships are given in Seetion 7.

Table 1 Sample Results for Vulnerability Criteria Level 1 Based on Parametric Excitation

Ship	GM	Vs, kts	Equation (2.18): boundaries for dangerous speeds		Stability variation check needed?	Stability variation equation (2.34)	Vulnerability detected?
			V_{s1}	V_{s2}			
Fishing Vessel 2	0.73	15.00	1.74	-5.24	Yes	0.09	No
Fishing Vessel 1 (ITTC A2)	1.70	18.00	-6.08	-20.98	Yes	0.16	No
General Cargo 1(S60)	0.27	18.00	14.40	5.29	Yes	1.03	Yes
RoPax	1.79	18.00	-2.65	-25.41	Yes	0.82	Yes
Bulk Carrier 2	0.56	15.00	12.96	1.02	Yes	0.40	No
Naval Combatant 2 (ONRTH)	3.03	30.00	-17.99	-52.94	Yes	0.26	No
Naval Combatant 1 (ONRFL)	1.04	30.00	1.73	-18.79	Yes	0.58	Yes
General Cargo 2 (C4)	0.90	16.00	7.85	-8.99	Yes	0.57	Yes
Containership 5 (C11)	2.00	25.00	7.45	-15.89	Yes	0.77	Yes
LNG Carrier	3.42	18.00	-1.16	-31.11	Yes	0.18	No
Bulk Carrier	3.46	15.00	2.90	-24.48	Yes	0.09	No
Passenger Ship	3.75	25.00	-16.75	-58.59	Yes	0.57	Yes
Containership 4	1.15	25.00	8.43	-15.33	Yes	0.75	Yes
Tanker	9.95	14.00	-16.36	-60.16	No	0.03	No
Containership 1	1.27	25.00	16.22	-3.85	Yes	1.42	Yes
Containership 3	1.85	25.00	10.31	-14.45	Yes	0.58	Yes
Containership 2	1.79	25.00	17.05	-4.95	Yes	0.90	Yes

The eheek on dangerous ship speeds shows the need for the stability variation eheek for all the sample vessels, exeept for the tanker. The stability variation eheck indieates possible vulnerability for all eontainerships, RoPax, Naval Combatant 1, passenger ship and the general eargo ship 1. These results are less conservative

compared with the geometry-based criterion (Peters, *et al.*, 2010), which is expected, as these criteria are more complex.

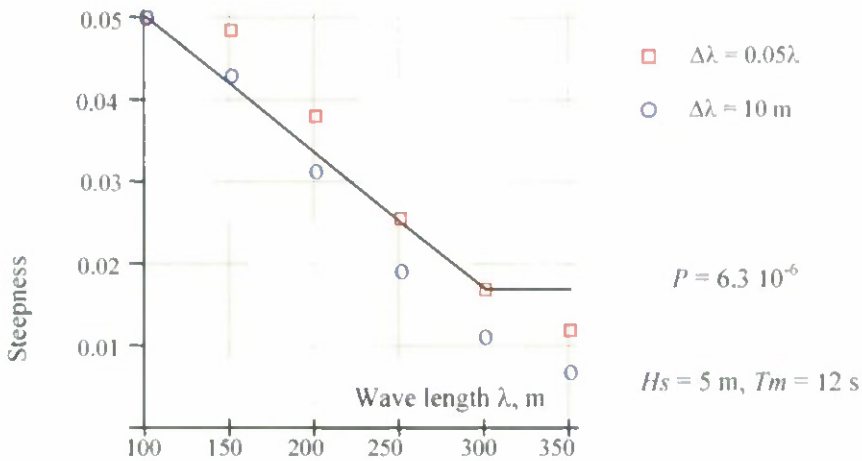

Figure 2.15 Dependence of Wave Steepness on Length, Based on Equal Probability of Encountering a Group of Four Waves

2.4 Level 2 Vulnerability Criteria

2.4.1 Mathematical Model of Wave Environment

Excessive conservatism may be a problem for the second level of the vulnerability criteria; it may incur unnecessary cost, because a ship not susceptible to parametric roll will be subjected to expensive direct analysis procedures. In order to avoid excessive conservatism, without compromising safety, mathematical models of higher fidelity are used for the second level vulnerability check.

Therefore, consideration of the vulnerability of a ship to parametric roll in irregular waves is preferable, not only because it is consistent with the probabilistic approach discussed above, but also because the use of regular waves may be too conservative. Regular waves are essentially a wave group of infinite length; therefore, the time to develop large amplitude is also infinite (SLF 48/4/12). In a real seaway, parametric roll development is the response to a particular wave group, of finite duration, which contains waves capable of generating parametric resonance. Not all wave groups possess such characteristics, and this is the reason why parametric roll can start and stop.

The fidelity of the mathematical model used for the second level vulnerability criteria can be improved by considering the response to a group of large waves with some "typical" characteristics. The length of this wave group can be found from the sea state conditions (Themelis and Spyrou, 2007; 2008, Themelis 2008). However, at this stage of study, it is suggested to keep this as a tunable parameter. Further work to justify its choice will be discussed in a future study. At this stage, the length of a wave group is proposed to be 5~9 waves. The numerical example discussed below used 7 waves.

The "typical" wave group, shown in Figure 2.16, is assumed to consist of a number of waves of the same length and period which corresponds to the spectral mean period. Justification of this assumption is considered later, in the next subsection:

$$\zeta(t) = A(t)\cos(\omega_1 t) \tag{2.38}$$

where ω_1 is the mean frequency, $A(t)$ is an amplitude of the group; it is defined with a sine function envelope:

$$A(t) = A_{\min} + 0.5(A_{\max} - A_{\min})\sin(\omega_A t - 0.5\pi) \tag{2.39}$$

$A_{\min}$ and $A_{\max}$ are the minimum and maximum amplitude of the group, respectively. ω_A is an envelope frequency defined as:

$$\omega_A = \frac{2\pi}{T_G} \tag{2.40}$$

T_G is a time interval for a group to pass a fixed point, and depends on number of waves in a group and the mean period:

$$T_G = N_G T_1 \tag{2.41}$$

where N_G is assumed number of waves in a group. The amplitude of the group is considered as a function of time only; its spatial change is not modeled.

For simplicity, consideration of the wave direction is limited to only head or following seas. This is expected to be appropriate, as parametric roll will likely be most severe in these conditions. Encounter frequency is expressed as:

$$\omega_e = \omega_1 + k_{dir} k_1 V_S \tag{2.42}$$

where V_S is forward speed, k_1 is the wave number corresponding to the mean period, T_1, and k_{dir} is a wave direction coefficient; it equals 1 for head seas and -1 for following seas.

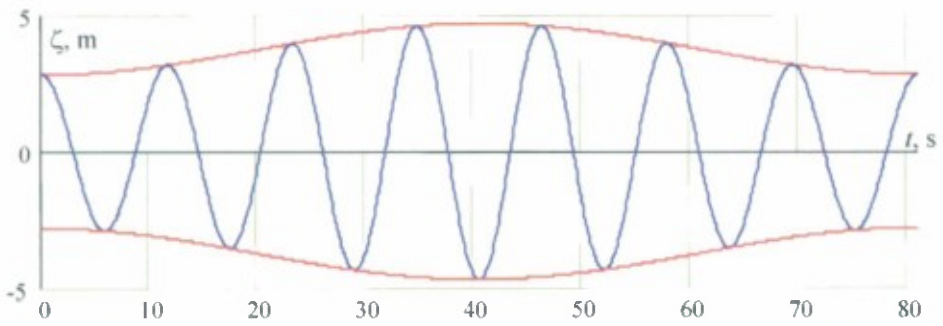

Figure 2.16 Time history of a wave group passing fixed point in space, Sea State 7

The time while the group passes a point at the midship section is expressed as:

$$T_{Ge} = \frac{N_G \lambda_1}{c + k_{dir} Vs} \tag{2.43}$$

where λ_1 is the wave length corresponding to the mean period, and c is the wave celerity. The relation between period, length, and wave celerity is:

$$T_1 = \frac{\lambda_1}{c} \tag{2.44}$$

The deep-water dispersion relation is used to relate the mean frequency to the wave length (through the wave number):

$$\lambda_1 = \frac{2\pi}{k_1}; \qquad k_1 = \frac{\omega_1^2}{g} \tag{2.45}$$

The duration of time that the wave group passes the midship section affects the formula for the amplitude envelope:

$$A_e(t) = A_{\min} + 0.5(A_{\max} - A_{\min})\sin(\omega_{Ae} t - 0.5\pi); \quad \omega_{Ae} = \frac{2\pi}{T_{Ge}} \tag{2.46}$$

This leads to a re-formulation of the wave group description in terms of the frequency of encounter:

$$\zeta_e(t) = A_e(t)\cos(\omega_e t) \tag{2.47}$$

2.4.2 Parameters of a Wave Group

All the waves in the group are assumed to have the same frequency which equal to the mean frequency of the spectrum. The justification of this assumption comes from the envelope theory, which was used by Longuett-Higgins to derive the joint distribution of wave heights and periods. The theory of envelope was originally developed by Rice (1944; 1945) and considered a stochastic process (in this case, wave elevations) in the form:

$$\zeta(t) = A(t)\cos(\Phi(t)) \tag{2.48}$$

Here one stochastic process is presented as a function of two other stochastic processes: the wave elevation envelope $A(t)$ and the phase $\Phi(t)$. If the spectrum of process, $\zeta(t)$, is narrow banded (or at least has an articulated peak), the processes of the envelope and the phase are slowly changing in comparison with process $\zeta(t)$. The process is conveniently presented as:

$$\zeta(t) = A(t)\cos\left(\dot{\Phi}(t)t + \Delta\Phi(t)\right) \tag{2.49}$$

The derivative of the phase is related to frequency:

$$\dot{\Phi}(t) = |\omega(t)| \tag{2.50}$$

The frequency is a positive value, by the definition. The phase shift process, $\Delta\Phi(t)$, is "responsible" for the "randomness" of the process $\zeta(t)$. In particular, this helps to keep its autocorrelation function of the presentation (3.50) equal to the autocorrelation of the original process (Autocorrelation function of a stochastic process is a measure of its "memory"; it shows the correlation of the value at present instant of time with the value in the past).

The autocorrelation function of waves does not have to be modeled for vulnerability criteria (it makes the mathematical model too complex). Therefore, the term $\Delta\Phi(t)$ can be neglected:

$$\zeta(t) = A(t)\cos\left(\omega(t)t\right) \tag{2.51}$$

One of the results of the envelope theory (Rice 1944; 1945) is the joint distribution of the envelope and the derivatives of the phases:

$$f(A,\dot{\Phi}) = \frac{A^2}{\sigma_\zeta^3\sqrt{2\pi}\sqrt{\omega_2^2-\omega_1^2}}\exp\left(-A^2\cdot\frac{\omega_2^2-2\omega_1\dot{\Phi}+\dot{\Phi}^2}{2\sigma_\zeta^2(\omega_2^2-\omega_1^2)}\right) \tag{2.52}$$

Here σ_ζ is the standard deviation of wave elevations, ω_1 is the mean frequency, and ω_2 is the average width of a spectrum:

$$\omega_1 = \int_0^\infty s(\omega)\omega d\omega \tag{2.53}$$

$$\omega_2 = \frac{1}{\sigma_\zeta}\sqrt{\int_0^\infty s(\omega)\omega^2 d\omega} \tag{2.54}$$

For the envelope presentation, the amplitude follows the Rayleigh distribution, and the conditional probability density function (PDF) can be expressed as:

$$f(\dot{\Phi} \mid A) = \frac{f(A,\dot{\Phi})}{f(A)} = \frac{A}{\sigma_\zeta \sqrt{2\pi}\sqrt{\omega_2^2 - \omega_1^2}} \exp\left(- A^2 \cdot \frac{\left(\dot{\Phi} - \omega_1\right)^2}{2\sigma_\zeta^2(\omega_2^2 - \omega_1^2)} \right); \qquad (2.55)$$

The mean value and the variance are expressed as:

$$\begin{aligned} m &= \int_{-\infty}^{\infty} f(\dot{\Phi} \mid A)\dot{\Phi} d\dot{\Phi} = \omega_1 \\ V(\dot{\Phi} \mid A) &= \int_{-\infty}^{\infty} f(\dot{\Phi} \mid A)(\dot{\Phi} - m(\dot{\Phi} \mid A))^2 d\dot{\Phi} = \frac{\sigma_\zeta^2\left(\omega_2^2 - \omega_1^2\right)}{A^2} \end{aligned} \qquad (2.56)$$

Then, it becomes not difficult to see that the conditional distribution of the derivative of phase is, in fact, normal. Taking into account (2.50), the PDF for frequency can be expressed as:

$$f(\omega \mid A) = f(\dot{\Phi} = -\omega \mid A) + f(\dot{\Phi} = \omega \mid A) \qquad (2.57)$$

Figure 2.17 shows this PDF computed for three different amplitudes. The mean value and variance of the frequency can be computed using this PDF:

$$\begin{aligned} m(\omega \mid A) &= \int_{-\infty}^{\infty} f(\omega \mid A)\omega \, d\omega \\ V(\omega \mid A) &= \int_{-\infty}^{\infty} f(\omega \mid A)(\omega - m(\omega \mid A))^2 d\omega \end{aligned} \qquad (2.58)$$

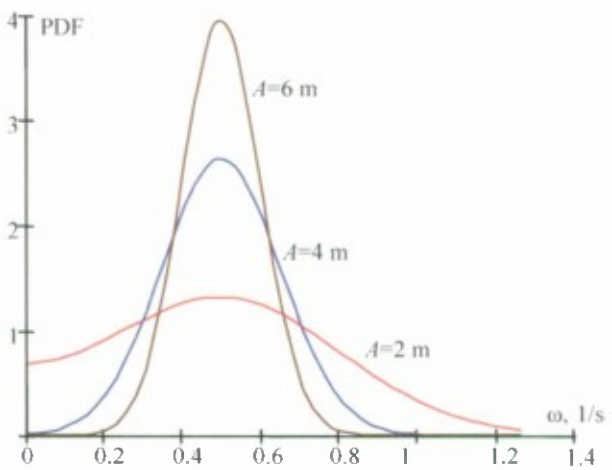

Figure 2.17 Conditional Distribution of Frequency for Three Different Amplitudes

The dependence of conditional mean value and variance on amplitude is shown in Figure 2.18.

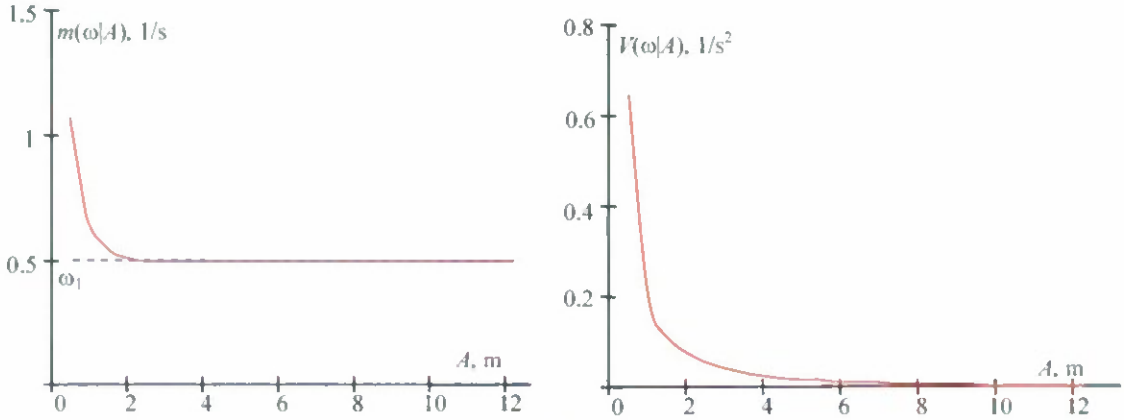

Figure 2.18 Conditional Mean Value and Amplitude of Frequency as a Function of Amplitude

Figure 2.18 shows that, with increase of the amplitude, the mean value of the frequency quickly approaches the spectral mean frequency, ω_1, while variance is reduced dramatically. This means that once to the wave becomes larger, their frequency is very likely to be close to the mean frequency, with little deviation. As the wave group is meant to consist of large waves, this justifies the choice of the frequency for the wave group.

Three more parameters remain to be defined: the number of waves in a group, and the initial and maximum amplitudes. A robust choice of these parameters can be made based on wave statistics, either measured or simulated. For the purposes of testing the proposed criteria, the following values of these parameters were chosen:

$$N_G = 7; \quad A_{\min} = 0.5H_S; \quad A_{\max} = 1.5A_{\min} \tag{2.59}$$

Here H_S is significant wave height.

2.4.3 Roll Response of a Group

As was mentioned previously, the level two vulnerability criteria should be based on a higher fidelity mathematical model, in order to prevent excessive conservatism. Consideration of irregular waves was one step towards this objective. Another step is to better account for the instantaneous attitude of a ship on the wave, while computing stability in waves. As it was demonstrated in Shin, *et al*, (2004), neglecting heave and pitch increases the magnitude of instantaneous stability variations in waves.

The attitude of a ship is calculated based on the heave and pitch response to a wave group:

$$\begin{cases} (M + A_{33})\ddot{\xi}_G + B_{33}\dot{\xi}_G + F_\xi(\zeta_G, \theta, t) = 0 \\ (I_Y + A_{55})\ddot{\theta} + B_{55}\dot{\theta} + M_\theta(\zeta_G, \theta, t) = 0 \end{cases} \tag{2.60}$$

where M is mass of the ship, I_Y is mass moment of inertia relative to the transversal axes, A_{33} and A_{55} are heave added mass and pitch moment of inertia (assumed to be equal to the corresponding mass and moment of inertia), respectively; and B_{33} and B_{55} are damping coefficients for heave and pitch. Functions F_ξ and M_θ are the difference between Froude-Krylov and hydrostatic forces and moments, respectively, at the instant of time, t. These values are expressed as follows:

$$F_\xi(\zeta_G, \theta, t) = \rho g \left(V_0 - \int_{-0.5L}^{0.5L} \Omega(x, z(\zeta_G, \theta, t))dx \right) \tag{2.61}$$

$$M_\theta(\zeta_G, \theta, t) = \rho g \left(V_0 \cdot LCB_0 - \int_{-0.5L}^{0.5L} M_\Omega(x, z(\zeta_G, \theta, t))dx \right) \tag{2.62}$$

where ρ is mass density of water, V_0 volumetric displacement in calm water, LCB_0 is the longitudinal position of center of buoyancy in calm water. Functions Ω and M_Ω calculate an area and a static moment relative to the y-axis of a station located at a longitudinal position along the hull, x. The second argument of this function shows the submergence of this position along the hull, as expressed by the function of instantaneous waterline $z(\zeta_G,\theta,t)$, see Figure 2.19

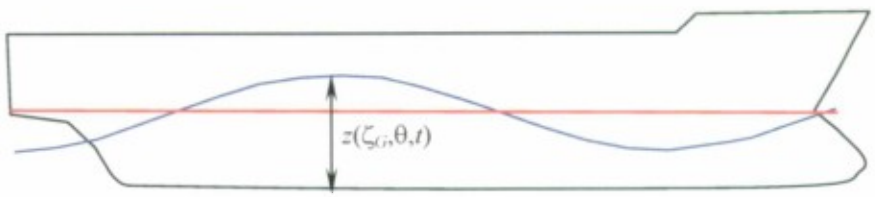

Figure 2.19 Sample Instantaneous Waterlines Evaluated from Heave and Pitch Response on a Group

Once the Froude-Krylov terms are defined, a system of differential equations (2.60) can be integrated with a standard Runge-Kutta solver. Initial conditions are chosen in order to avoid unrealistically large initial transients. To find such initial conditions, let the system (2.60) begin with regular waves of the same frequency, but with the initial group amplitude. Steady state conditions for heave and pitch, corresponding to the initial phase of the group, can be used to calculate the heave and pitch response on the group (see Figure 2.20).

Each point of the time histories of heave and pitch, shown in Figure 2.20, correspond to a waterline, three of which are shown in Figure 2.21. These waterlines allow for the evaluation of the GM response to the wave group (shown in Figure 2.22).

Nonlinearity of the instantaneous GZ curve is one additional factor that may be taken into account, in order to avoid excessive conservatism by improving fidelity of the mathematical model. However, before using a fully nonlinear model, it makes sense to evaluate the roll response using a linear model. This will also help to see if the frequency conditions are chosen correctly. Also comparing the linear and nonlinear response enables examination of the influence of nonlinearity.

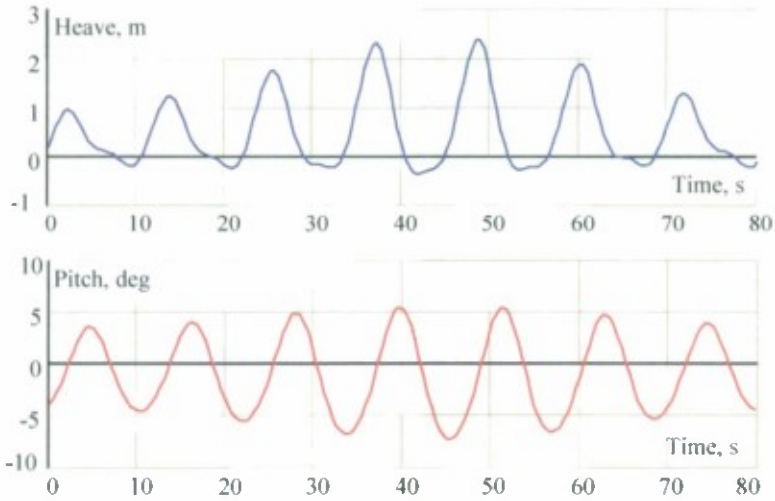

Figure 2.20 Heave and Pitch Response on a Group

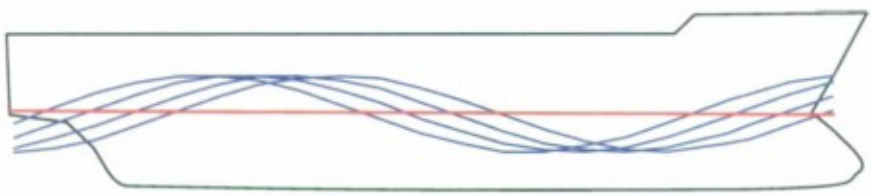

Figure 2.21 Sample Waterlines Evaluated from Pitch and Heave Time History

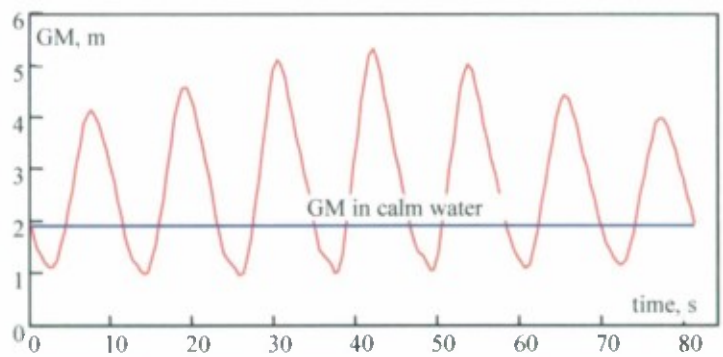

Figure 2.22 GM Response on "Typical" Wave Group, with the GM Value in Calm Water Shown in Blue

The *GM* response to a "typical" wave group first should be approximated using a cosine function with time-dependent amplitude (see Figure 2.23):

$$f_L(\phi,t) = \frac{GM_m + GM_a(t)\cos(\omega_e t + \varphi)}{GM} \tag{2.63}$$

where ω_e is the encounter frequency,

$$\omega_e = \omega_1 + k_1 V_S \tag{2.64}$$

and where ω_1 and k_1 are the wave frequency and wave number corresponding to the mean spectral period. V_S is ship forward speed, which is chosen to satisfy the frequency condition for principal parametric resonance, while keeping the value within the achievable range for the given vessel, in the considered sea state.

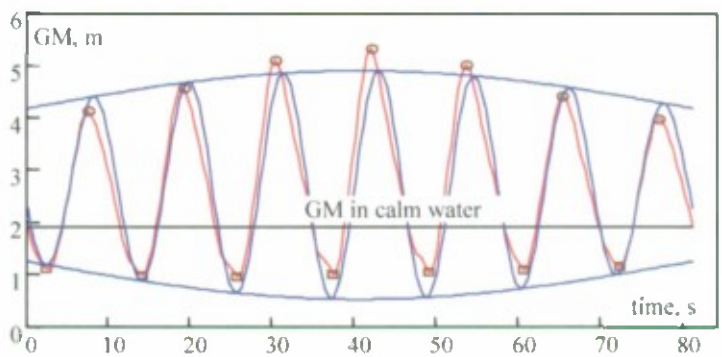

Figure 2.23 Approximation of GM Response on "Typical" Wave Group with Cosine Function

Roll response is evaluated by the numerical solution of the roll equation with stiffness (2.63) and assumed roll damping. The initial conditions for the numerical solution of roll motion can be chosen as 5-10 degrees for the initial roll angle and zero roll rate.

$$\ddot{\phi} + 2\delta_\phi \dot{\phi} + \omega_0^2 f_L(\phi,t) = 0 \tag{2.65}$$

Equation (2.65) is essentially the Mathieu equation (see Equation (2.11)). If the amplification of roll oscillations is observed, then parametric excitation is large enough, taking into account speed limitations. The largest absolute value of the roll angle observed during the wave group pass can be used as a criterion:

$$CrL = \max(|\phi|) \quad for \quad f = f_L \tag{2.66}$$

The next step is taking into aeeount the nonlinearity of the *GZ* eurve. Due to signifieant nonlinearity of the *GZ* eurve, the development of parametrie resonanee may be reversed, as the ehange in instantaneous *GM* with roll angle may take the system out of the Mathieu instability region (Spyrou 2004).

To model this nonlinearity, the *GZ* eurve in waves ean be evaluated direetly using instantaneous draft and trim available from pitch and heave ealculations. There are several software paekages available for this type of ealculations. Alternatively the following approximation may be used in lieu of the aetual instantaneous *GZ* eurve (other approximations ean be formulated too):

$$GZ_W(\phi,t) = \frac{GM_w(t)}{GM_0} GZ_0(\phi) \tag{2.67}$$

Here the index "0" refers to calm water conditions. Equation (2.67) ean be used in the roll equation with nonlinear stiffness:

$$f_N(\phi,t) = \frac{GZ_W(\phi,t)}{GM} \tag{2.68}$$

$$\ddot{\phi} + 2\delta_\phi \dot{\phi} + \omega_0^2 f_N(\phi,t) = 0 \tag{2.69}$$

Equation (2.69) is a variation of Hill's equation. However, it may be neeessary to extend (2.68) up to 180 degrees, to avoid numerieal issues while solving equation (2.69), see Figure 2.24.

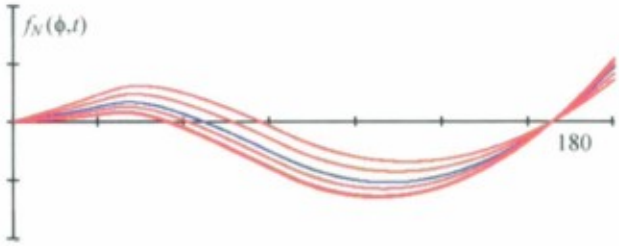

Figure 2.24 GZ Curve Modeled for Response to a "Typical" Wave Group

Based on the solution of (2.69) shown in Figure 2.25, a seeond eriterion, *CrN*, is formulated

$$CrN = \max(|\phi|) \quad for \quad f = f_N \tag{2.70}$$

Due to the nonlinearity of the time-dependent stiffness, it is not known in advanee what eneounter frequeney range may lead to parametrie resonanee. This implies that ealeulation has to be repeated for several speeds.

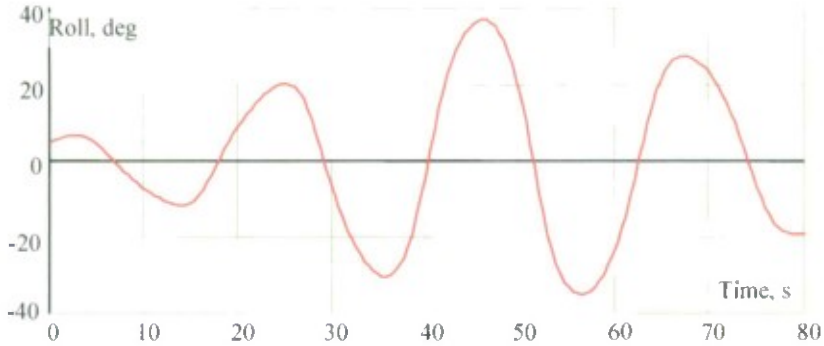

Figure 2.25 Nonlinear Roll Response to a "Typieal" Wave Group

2.4.4 Results of Sample Calculations

Results are shown for the two criteria (*CrL* and *CrN*) for the sample ships (see Figure 2.26). The values used for the evaluation for each ship are given in Table 2. For the ships considered, a common damping ratio was chosen, typieal for these types of ships. For the two naval combatants, which typieally have larger bilge keels, a larger damping ratio was speeified. The *GM* condition used was a typical operational loading condition for each of the sample ships, GM_{OP}. Sea States 5-8 were evaluated, but only the lowest sea state where parametric roll was observed and the given speed condition to satisfy the frequency ratio conditions are presented.

Modern containerships, partieularly the C11-class containership, are known for their vulnerability to parametric roll (e.g. France, *et al.*, 2003). The proposed criteria shows large roll angles for all five containerships, as well as the notional RoPax vessel and the passenger ship, encountering representative wave groups in Sea States 6, 7, and 8. As expeeted, Series 60, which is representative of a conventional ship type, the tanker, and bulk carriers did not show any vulnerability for the considered loading and operational conditions.

Both ONR Topside configurations (flared and tumblehome) have relatively large bilge keels. The damping ratio used was meant to model the fully appended hulls. While the ONR Tumblehome Topside did not show any parametric roll for the analyzed loading condition, parametric roll was predicted for ONR Flared Topside, using the linear formulation. However, parametric roll was not observed from earlier experimental and numerical investigations (based on nonlinear formulations) for these hull forms with bilge keels (e.g. Bassler, 2008; Olivieri, *et al.*, 2008; Hashimoto & Matsuda, 2009), including for the flared topside eonfiguration with roll damping eoeffieients corresponding to the fully appended hull. Furthermore, when the instantaneous *GZ* curve is used instead of the approximation, parametric roll was not indicated, which corresponded to previous findings.

The indication of parametrie roll is consistent with the earlier findings of Peters, *et al.* (2010) for a smaller population of sample ships. However, the linear eriterion also provides large values for the two fishing vessels, in addition to Naval Combatant 1. The case with two fishing vessels deserves more attention, as these ships were found not to be

susceptible to parametric roll by the level 1 vulnerability criteria based on magnitude of stability variations (see Table 1).

The reason for this inconsistency becomes clear when plotting *GM* response from the wave group. Figure 2.27 shows *GM* response on the "typical" wave group for a fishing vessel calculated for Sea State 6. As can be seen from this figure, the approximation is not applicable, and as a result the linear criterion (2.66) cannot be used. At the same time, the nonlinear criterion (2.70) yields results that are consistent with the level 1 criteria, based on magnitude of stability changes.

The reason for this inconsistency is use of the linear approximation beyond the applicability of a linear model. The level 1 criterion uses a wave with the same length that the ship length, while the wave height is calculated from a prescribed steepness. For the Fishing Vessel 2, this means that the wave length was 22 m, while the wave height was about 1.1 m. A linear model may be valid in these conditions. The level 2 criterion used a "typical" group for Sea State 6. The wave length was 143 m, and the wave height varied from 5 to 7.5 m. Figure 2.27 demonstrates that the linear approximation is clearly not appropriate of a stretch for these conditions.

The nonlinear model nevertheless yielded reasonable results, stating the absence of parametric roll in these conditions. To verify this conclusion, Large Amplitude Motion Program (*LAMP*) simulations were carried out for a regular wave of 143 m long, with wave height of 5 m. The Fishing Vessel 1 was made to sail in head seas with a forward speed of 10 knots. The initial roll angle was 10 degrees. The results are shown in Figure 2.28. As it could be expected, after a short initial transient, the ship is simply countering the waves and roll motions are simply decaying.

The nonlinear criterion, given in (2.70), provides correct evaluation of the outcome: no parametric roll.

Another case which requires more detailed consideration is for Naval Combatant 1. The linear criterion indicated parametric roll. In this case, the linear result is consistent between the levels 1 and 2. However, this ship is not known for parametric roll, and *LAMP* simulations did not indicate parametric roll (see Figure 2.29).

These simulations were carried out for conditions where the largest wave (height 7.5 m) in a "typical" wave group corresponded to Sea State 6 (length 143 m, wave height from 5 to 7.5 m). As can be clearly seen from Figure 2.29, pitch and heave motions are not small, while the roll motions decays. At the same time, the application of the *GZ* curve approximation (2.67), based on the *GM* response to a "typical" wave group, leads to parametric roll (see Figure 2.30). Use of the actual instantaneous *GZ* curve in waves (calculated for conditions where the largest wave in the group had a height of 7.5 m) showed correctly no parametric roll (see Figure 2.31).

This example demonstrates that use of the actual *GZ* curve in waves is preferable, as the approximation (2.67) seems to be too conservative.

In conclusion, the nonlinear criterion provides a clearer separation between the sample ships with increased vulnerability and those which are not known to be vulnerable (Figure 2.32).

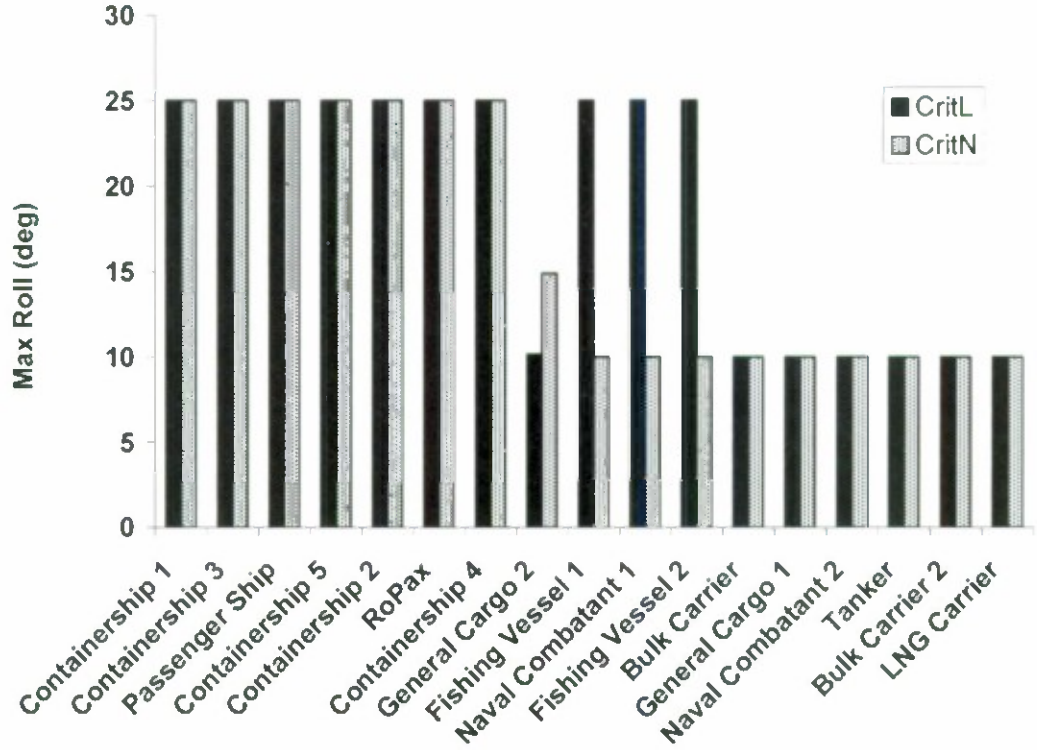

Figure 2.26 Calculation Results for the Two Level 2 Vulnerability Criteria for Parametric Roll for the Sample Ships, Linear and Nonlinear Criteria

Table 2 Calculation Results for the Two Level 2 Vulnerability Criteria for Parametric Roll for the Sample Ships

Type	SS	GM_{OP} (m)	Roll Damping	Speed (kts)	CrL	CrN
Containership 1	7	1.118	0.05	10	25	25
Containership 3	8	1.644	0.05	1	25	25
Passenger Ship	7	3.695	0.05	20	25	25
Containership 5 (C11)	7	1.905	0.05	0.01008	25	25
Containership 2	7	1.84	0.05	2	25	25
RoPax	6	1.773	0.05	25	25	25
Containership 4	7	1.064	0.05	10	25	25
General Cargo 2 (C4)	6	1.099	0.05	5.144	10.16	14.9
Fishing Vessel 1 (ITTC A2)	6	1.69	0.05	10	25	10
Naval Combatant 1 (ONR FL)	6	1.028	0.15	15	25	10
Fishing Vessel 2	6	0.7271	0.05	10	25	10
Bulk Carrier	7	9.405	0.05	10	10	10
General Cargo 1	6	0.2449	0.05	9.261	10	10
Naval Combatant 2 (ONR TH)	6	3.013	0.15	25	10	10
Tanker	7	9.763	0.05	10	10	10
Bulk Carrier 2	6	0.5293	0.05	6.904	10	10
LNG Carrier	6	3.398	0.05	1.799	10	10

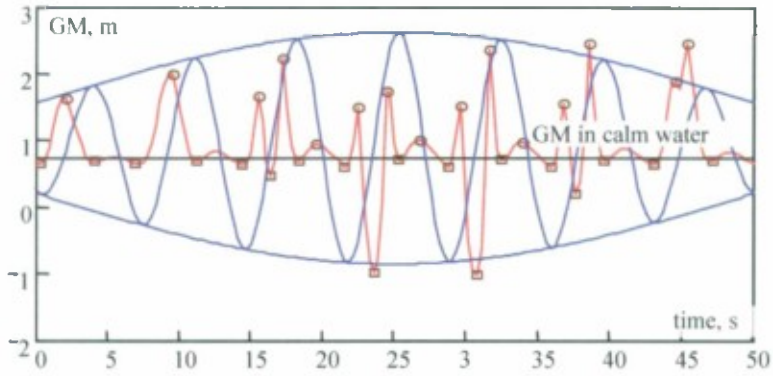

Figure 2.27 Approximation of GM Response on "Typical" Wave Group for Fishing Vessel 2, in Sea State 6.

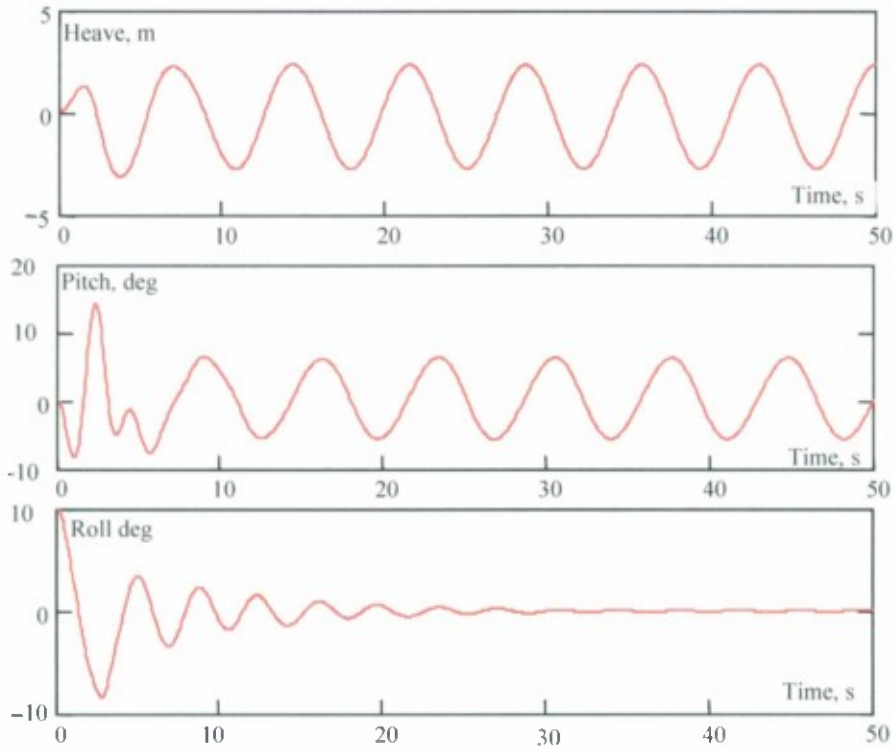

Figure 2.28 Results of *LAMP* Simulation of Fishing Vessel 1

The level 2 eriteria were independently implemented in Germany (Annex 9 of SLF 53/INF.10) and in Sweden (SLF 53/INF.8 and Annex 10 SLF 53/INF.10). Caleulations presented in Annex 9 (SLF 53/INF.10) were performed for 26 ships ineluding eontainer earriers, bulk carriers, eruise vessels, tankers, multi-purpose vessels (MPVs) and tugs. The eonsisteney between the level 1 (geometry–based formulation) and level 2 was analyzed. An inconsistency was deteeted in the ease of the MPVs, as the level 1 eriteria did not indieate vulnerability, while the level 2 did. However, based on the available information, a suggested hypothesis for this difference is not currently possible and additional analysis needs to be performed.

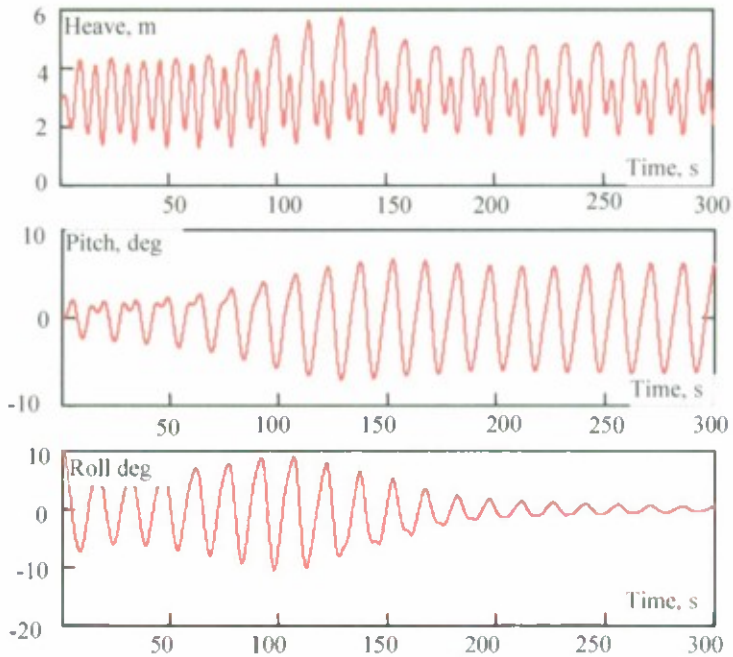

Figure 2.29 Results of *LAMP* Simulation for Naval Combatant 1

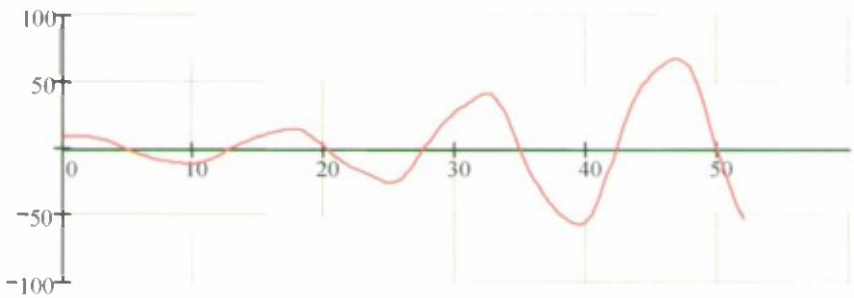

Figure 2.30 Roll Response to a Typical Wave Group– Approximate GZ

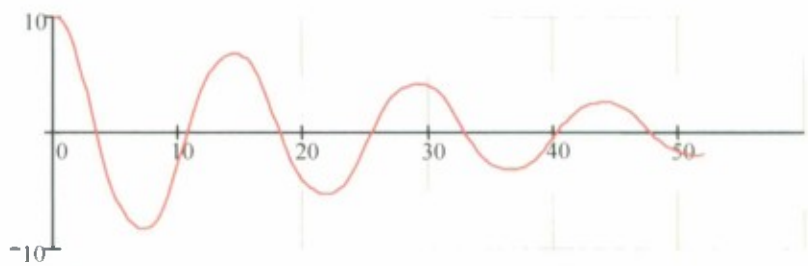

Figure 2.31 Roll Response to the Largest Wave in the Group– Actual Instantaneous GZ Curve in Waves

Documents SLF 53/INF.8 and Annex 10 of SLF 53/INF.10 reported calculations made for 25 ships including container carriers, bulk carriers, tankers, Ro-Ro ships and military. Comparisons were also performed with the ABS severity criteria. No inconsistency has been reported. However, it was noted that the modulation of wave amplitude in a group does not change the conclusion on vulnerability.

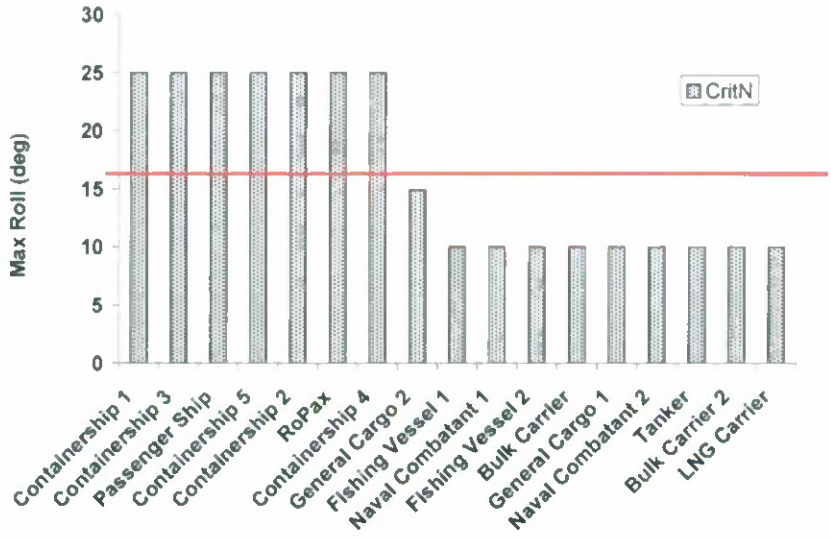

Figure 2.32 Calculation Results for the Two Level 2 Vulnerability Criteria for Parametric Roll for the Sample Ships, Using the Nonlinear Criterion

2.5 Summary

This section describes the development of vulnerability criteria for parametric roll. The subsection 2.1 provides some general background information on the physics of the parametric roll phenomenon. It is shown how parametric roll develops and how it is related to stability variations in waves. The influence of speed and wave direction is also considered.

Subsection 2.2 describes the basic mathematical model used for detecting susceptibility to parametric roll. It is a linear differential equation with a periodic coefficient, also known as the Mathieu equation. This equation may have a growing solution, corresponding to the inception of parametric roll. The influence of damping leads to the appearance of a threshold for parametric excitation (stability variation in waves); below this threshold, parametric roll is impossible. The nonlinearity of the GZ curve leads to stabilization of parametric roll at a certain amplitude.

Subsection 2.3 describes level 1 vulnerability criteria. The proposal criteria consider two different conditions. The first condition examines if a ship is capable of achieving speeds that provide dangerous frequencies of encounter, while the second condition examines if the magnitude of stability change may result in a given increase in roll angle during a certain number of cycles.

Subsection 2.4 describes level 2 vulnerability criteria. The mathematical model used is more sophisticated, in order to avoid possible excessive conservatism. The method accounts for irregular waves, by limiting the number of waves (a typical wave group with properties of a sea state), the influence of heave and pitch (through attitude of the wave), and the nonlinearity of the GZ curve.

Sample calculations were performed using 17 ships.

This page is intentionally left blank

3 Vulnerability Criteria to Pure Loss of Stability

This section describes the development of vulnerability criteria for pure loss of stability, including the physical background for this mode of stability failure, a review of the basics of probability theory used for further development of vulnerability criteria, and a derivation of this joint distribution, based on envelope theory. A proposal for level 1 vulnerability criterion is considered, based on the geometric characteristics of the hull, and two level 2 vulnerability criteria are also presented and tested. Sample calculations were performed using 17 ships.

3.1 Physical Background

Change of stability in waves, as examined in subsection 2.1.1, is also the physical basis for another mode of stability failure: pure loss of stability. The dynamics of pure loss of stability are different from parametric roll, but are also closely related to the severity and duration of waterplane changes. A possible scenario for the development of a stability failure caused by pure loss of stability is shown in Figure 3.1.

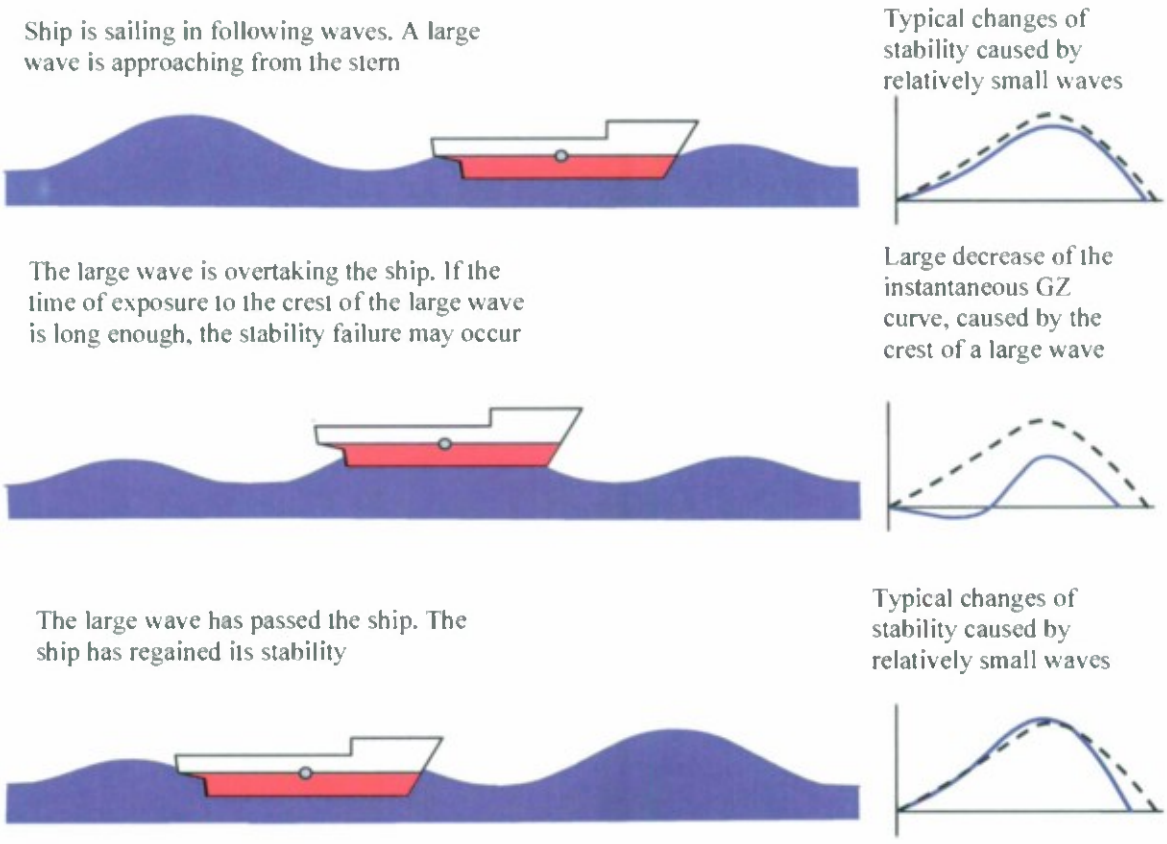

Figure 3.1 Possible Scenario for the Development of Pure Loss of Stability

A large wave is approaching from the stern, while the ship is sailing with relatively high speed in following seas. If the celerity (speed) of the large wave is just slightly above the ship speed, the time duration for the large wave to pass the ship may be long. Once the crest of the large wave is near the midship section of the ship, its stability may be significantly decreased. Because the wave celerity is just slightly more than ship speed, the condition of decreased stability may exist long enough for the ship to develop a large heel angle, or even capsize. Once the large wave has passed the ship, its stability is regained and the ship will eventually return to the upright position, if she did not already heel too far.

3.2 Mathematical Tools for Development of Criteria

3.2.1 Role of Probability

There are two factors determining the risk of stability failure caused by pure loss of stability. The first one is how large the stability changes on the wave. If stability changes are small because the hull is wall-sided (a pontoon barge is an extreme example), then this mode of stability failure is impossible.

The second factor is the likelihood of encountering a large and steep wave, which can cause a decrease of stability for a sufficiently long time so a large heel will develop. There are several contributors to this likelihood:

- Length of the ship; for a large ship, a longer wave is needed to cause significant changes of stability. The likelihood of encounter of the ship with a large and steep wave is low.
- Length of the ship also has an influence on the time of exposure, as the longer waves are faster (e.g., a wave with a length of 250 meters has a celerity of 38 knots in deep water).
- Speed of the ship; this has an influence on the time of exposure. Large waves are usually faster than typical ship speed. However, faster ships may potentially have longer durations of exposure.
- Spectral characteristics of the wave environment can increase or decrease the likelihood of encountering long and steep waves.

A brief review of these contributors makes it clear that the stability failure caused by pure loss of stability has a probabilistic nature. An attempt to develop criteria based on deterministic background, say wave length equal to ship length, may lead to excessive penalizing of large vessels and introduce excessive conservatism (Annex 5 SLF 52/INF.2), which is not desirable.

Also, fundamentally, pure loss of stability is a single-wave event; once the large wave has passed by the ship, its stability is regained. Therefore, the risk of pure loss of stability for a particular ship can be completely determined by the probability of encountering a large wave, which causes enough exposure time to permit a failure. Therefore, mathematical tools to evaluate the probability of a large wave are needed.

These tools should also be capable of determining the probabilistic characteristics of the related exposure time.

Wave elevation is a three-dimensional stochastic process. It changes in time at a given point. It changes in two spatial dimensions, for a given instant of time. So there are one temporal and two spatial dimensions to consider. This three-dimensional stochastic process is a source of information for finding the probability of encountering a wave of certain characteristics. While this may sound complicated, this problem is considered to be solved with reasonable accuracy required for engineering practice (Longuett-Higgins, 1957; 1976; 1984)

Prior to the use of these tools, a brief review of the basic probabilistic concepts used for these models may be useful. This review comprises the remainder of the contents of this subsection.

There are three types of mathematical objects relevant for the current development of vulnerability criteria:

- Random event: an event that may or may not occur in a given set of conditions (example: tossing a coin results in "tails")
- Random variable: a number that appears as the result of a random event (a number given by throwing dice)
- Stochastic process: a set of random numbers depending on each other.

3.2.2 Random Events

Probabilistic independence/dependence is a very important concept. Two random events A and B are independent, if the probability that event A will happen does not affect in any way the probability of event B. The probability that both events A and B will occur simultaneously is just the product of these probabilities, if the events are independent:

$$P(A \cap B) = P(A)P(B) \tag{3.1}$$

If random events A and B are dependent, then the probability of occurrence of A is affected by the probability of occurrence of event B. Mathematically, this is expressed through the probability that event A will occur, if it is known for sure that the event B happened. This probability is known as the conditional probability and is defined as:

$$P(A \mid B) = \frac{P(A \cap B)}{P(B)} \tag{3.2}$$

Formula (3.2) allows for examination of the difference between independent and dependent events, in terms of the probability of their simultaneous occurrence:

$$P(A \cap B) = P(A)P(A \mid B) \tag{3.3}$$

3.2.3 Random Variables

Random variables are charaeterized by probability distribution funetions, used in two forms: eumulative distribution funetion (CDF) and probability density funetion (PDF). The former is defined as the probability that a random variable will not exeeed the argument of the CDF:

$$F(x) = P(X \leq x) \tag{3.4}$$

Per the definition that the probability is a number between zero and one, the limits of the CDF are:

$$\lim_{x \to -\infty} F(x) = 0; \quad \lim_{x \to \infty} F(x) = 1 \tag{3.5}$$

The probability that a random variable will take a value in the interval from a to b is expressed through the CDF in a following way:

$$P(a \leq x \leq b) = F(b) - F(a) \tag{3.6}$$

The probability density funetion is defined as a derivative of the CDF:

$$f(x) = \frac{dF(x)}{dx} \tag{3.7}$$

As a result, the probability that a random variable will take a value in the interval from a to b is expressed through the PDF in a following way:

$$P(a \leq x \leq b) = \int_a^b f(x)dx \tag{3.8}$$

As a eonsequenee of (3.5), the area under the PDF must be unity – this is known as a "normalization eondition":

$$\int_{-\infty}^{\infty} f(x)dx = 1 \tag{3.9}$$

Besides the functions of distribution, random variables are also characterized by the moments of the distribution (or just, the moments). There are two types of moments: initial and central. The initial moment of order n is defined as:

$$\alpha_n = \int_{-\infty}^{\infty} f(x)x^n dx \tag{3.10}$$

The most important initial moment is the mean value (a.k.a the mathematical expectance, the average). It has an order n=1:

$$m_x = \alpha_{n=1} = \int_{-\infty}^{\infty} f(x)x dx \tag{3.11}$$

The central moment on the order n is defined as:

$$\mu_n = \int_{-\infty}^{\infty} f(x)(x - m_x)^n dx \tag{3.12}$$

The most important central moment is the variance. It is the measure of variation of the random number around the mean value. It is the central moment of the second order n=2:

$$V_x = \mu_{n-2} = \int_{-\infty}^{\infty} f(x)(x - m_x)^2 dx \tag{3.13}$$

The variance has a dimension of square of the units of the random variable. Sometimes it is more convenient to operate with a characteristic of the same dimension. Therefore, the standard deviation is defined as:

$$\sigma_x = \sqrt{V_x} \tag{3.14}$$

There are many distributions derived to describe behavior of different random variable appearing as a result of different circumstances. However, one distribution is more important than others, as it is a "limit case" in a certain sense. It is the normal, or Gaussian, distribution:

$$f(x) = \frac{1}{\sqrt{2\pi V_x}} \exp\left(-\frac{(x - m_x)^2}{2V_x}\right) \tag{3.15}$$

Formally, the normal distribution is derived as a distribution of a sum of an infinite number of random variables; each variable may have any distribution, but if their contribution is about the same, the sum of these variables have a normal distribution. The practical importance of normal distribution is that if there are many random factors of the same level of influence, the result will have a normal distribution. This is why errors of the measurement usually are assumed to be normal. This statement is known as the "Central Limit Theorem".

Two independent random events produce two independent random numbers (e.g. throwing two dice). The joint distribution of two variables is characterized by the CDF and PDF that are functions of two arguments. However, if two random variables are independent, their joint distribution is just a product of the one-dimensional (marginal) distributions):

$$f(x,y) = f(x)f(y) \tag{3.16}$$

Equation (3.16) is, in a sense, similar to the equation (3.1). If the random variables x and y are dependent, their dependence is fully characterized with the conditional distribution of x, if y took a certain value (say $y = b$):

$$f(x \mid y = b) = \frac{f(x, y = b)}{f(y = b)} \tag{3.17}$$

Another characteristic of dependence is a correlation moment. It is defined as:

$$M_{xy} = \int_{-\infty}^{\infty}\int_{-\infty}^{\infty} f(x,y)(x - m_x)(y - m_y)dxdy \tag{3.18}$$

It is convenient to use a non-dimensional expression of the correlation moment, namely the correlation coefficient

$$r_{xy} = \frac{M_{xy}}{\sqrt{V_x V_y}} = \frac{M_{xy}}{\sigma_x \sigma_y} \tag{3.19}$$

The correlation coefficient varies from -1 to 1. If it is zero, the variables x and y are not correlated. Strictly speaking, absence of correlation does not prove independence in the general case. Only normally distributed variables are independent if they are not correlated. However, in most practical cases, absence of correlation is a strong indication of independence. The opposite is always correct, independent variables are not correlated.

If the correlation coefficient is close to positive or negative unity, the correlation is very strong. In case of unity (positive or negative), there is a deterministic relation between two random variables.

Two random variables may be related with a deterministic function, like a linear function, square, and eventually any type of function:

$$y = \varphi(x) \tag{3.20}$$

Knowing what this function is allows determination of all the characteristics of the random variable y, if similar characteristics are known for the random variable x. For example, the mean value of y can be found as:

$$m_y = m(\varphi(x)) = \varphi(m_x) \tag{3.21}$$

Other characteristics, like variance and distribution also can be found.

3.2.4 Stochastic Processes

Finally, the stochastic process is a set of interdependent random variables. Wave elevation at a point is a very good example of one-dimensional stochastic process. Here, probabilistic dependence describes the fact that water is a heavy fluid, so its level cannot change instantaneously.

Similar to the random variable, the stochastic process is characterized by the CDF, PDF, mean value, variance and other moments of the distribution. However, in the most general case, these figures may be dependent on time. For example, significant wave height (which is related to the variance of wave elevation) changes with time when the change of wind speed and direction leads to a change in waves.

If the probability distribution of a process does not change in time, such a process is defined as a stationary. Naturally, mean value, variance, and other moments are also constant. A stationary process is a good model of wave elevations during a relatively short time (<4 hours), while the change of waves normally may be considered insignificant.

The autocorrelation function is the measure of dependence within a process. It is defined as a correlation moment calculated between two values of the process, taken at the time instant t_1 and time instant t_2

$$R(t_1, t_2) = \int_{-\infty}^{\infty}\int_{-\infty}^{\infty} f(x(t_1), x(t_2))(x(t_1) - m_x(t_1))(x(t_2) - m_x(t_2))dxdx \tag{3.22}$$

The autocorrelation function shows how quickly dependence decays in time. The current wave elevation at a point cannot really depend on what happened a half-hour ago, as memory of the wave surface does not last that long. If the process is stationary, the autocorrelation function only depends on the interval:

$$R(\tau) = \int_{-\infty}^{\infty}\int_{-\infty}^{\infty} f(x(t), x(t+\tau))(x(t) - m_x)(x(t+\tau) - m_x)dxdx \tag{3.23}$$

The autocorrelation function can also be calculated from the spectral density, s(ω):

$$R(\tau) = \int_{0}^{\infty} s(\omega)\cos(\omega\tau)d\omega \tag{3.24}$$

This brief review of available probabilistic tools helps with formulating the steps for the development of a probabilistic vulnerability criterion for the second level. Remaining considerations include:

- Specify an appropriate distribution of wave lengths and wave heights;
- Formulate criteria for a regular wave;
- Consider these criteria as a deterministic function of random arguments wave height and wave length;
- Use the distributions of wave length and wave height to find the mean values of the criteria.

These steps allow consideration of specific features of the sea state, through the distributions wave lengths and wave heights, while also maintaining the simplicity of the regular wave approach.

3.3 Joint Distribution of Wave Number and Wave Heights

3.3.1 Envelope of Wave Elevations

This section is focused on the derivation of the joint distribution of wave lengths and wave heights, as this is the key element of the model used for the wave environment. This model is based on the work of Longuett-Higgins (1957; 1976; 1984).

Strictly speaking, the wave surface is a random field, or three-dimensional stochastic process. However, for the development of probabilistic vulnerability criteria for pure loss of stability, several significant simplifications can be made.

Because the objective is the determination of vulnerability, the model can be limited to long-crested seas. Changes of stability in long-crested seas are expected to be more dramatic than in short-crested seas, as there is no angular spread of wave energy.

Because the objective is wave height and length only, changes of the wave profile, while the wave passes the ship, can be neglected.

These two simplifications allow for consideration of only one dimension: the x-coordinate. The stochastic process of wave elevation in space can be presented as:

$$z(x) = \sum_{i=1}^{N_w} r_{Wi} \cos(k_i x + \varphi_i) \tag{3.25}$$

Here, k_i is set of wave numbers (spatial frequencies) used for discretization of the given spectral density, r_{Wi} is amplitude of the i-th component and φ_i is the phase shift for the i^{th} component. The wave numbers are related with frequencies through the deep-water dispersion formula:

$$k_i = \frac{\omega_i^2}{g} \tag{3.26}$$

Here g is the gravity acceleration.

To obtain joint distributions, following of Longuett-Higgins (1957; 1976; 1984), consider the envelope presentation of the wave along the x-axis:

$$z(x) = a(x)\cos\big(\Phi(x)\big) \tag{3.27}$$

Here the process $z(x)$ is presented through two other stochastic processes: amplitude, or envelope, $a(x)$, and phase $\Phi(x)$. Originally, the envelope presentation was developed for a stationary normal process by Rice (1944; 1945), so it is fully applicable for wave elevations. The envelope, $a(x)$, is defined through a complimentary process, $y(x)$, which is the result of the Hilbert transformation of the process $z(x)$:

$$y(x) = H\big(z(x)\big) = \sum_{i=1}^{N_w} r_{Wi} \sin(k_i x + \varphi_i) = a(x)\sin\big(\Phi(x)\big) \tag{3.28}$$

The envelope is defined as:

$$a(x) = \sqrt{z^2 + y^2} \tag{3.29}$$

Obviously, the variance of the complimentary process is identical to the variance of wave elevations:

$$V_z = V_y = \frac{1}{2}\sum_{i=1}^{N_m} r_{Wi}^2 = V \tag{3.30}$$

The dependency of two processes can be expressed through the cross-correlation function (similar that autocorrelation function, but defined for two different stochastic processes taken at different points).

$$C_{zy}(x_1, x_2) = \int_{-\infty-\infty}^{\infty\ \infty} f(z(x_1), y(x_2))(z(x_1) - m_z(x_1))(y(x_2) - m_y(x_2))dydz \tag{3.31}$$

Since both the processes z(x) and $y(x)$ are stationary, the cross correlation function depends only on the difference in x-coordinates:

$$C_{zy}(\Delta x) = \int_{-\infty-\infty}^{\infty\ \infty} f(z(x), y(x + (\Delta x)))(z(x) - m_z)(y(x + \Delta x) - m_y)dydz \tag{3.32}$$

The cross-correlation function (as well as autocorrelation function) can also be expressed by averaging along the x-axis.

$$C(\Delta x) = E(z(x), y(x + \Delta x)) \tag{3.33}$$

Here $E(..)$ is an averaging operator along the axis x:

$$E(..) = \lim_{X\to\infty}\left(\frac{1}{X}\int_0^X (..)dx\right) \tag{3.34}$$

Similarly, the autocorrelation function can be expressed as:

$$R(\Delta x) = E(z(x), z(x + \Delta x)) \tag{3.35}$$

Substitution in the presentation of (3.25) and (3.28) allows re-writing both the autocorrelation of the process z and cross- correlation of processes z and y as:

$$R(\Delta x) = \frac{1}{2}\sum_{i=1}^{N_m} r_{Wi}^2 \cos(\Delta x) \tag{3.36}$$

$$C(\Delta x) = \frac{1}{2}\sum_{i=1}^{N_m} r_{Wi}^2 \sin(\Delta x) \tag{3.37}$$

The stochastic processes $z(x)$ and $y(x)$ are not correlated if the x-coordinate is fixed, since the phases were shifted 90 degrees.

$$C(0) = 0 \tag{3.38}$$

Since both the processes $x(t)$ and $y(t)$ are normal, they are also independent at the fixed point. However, the values of the processes may be correlated, if they are taken at different points on the x-axis

Similar to autocorrelation function, the cross-correlation function is related with spectrum through the sine Fourier transform in time and in space

$$C(\tau) = \int_0^\infty s(\omega)\sin(\omega\tau)d\omega \tag{3.39}$$

$$C(\Delta x) = \int_0^\infty S(k)\sin(k\Delta x)dk \tag{3.40}$$

Here $S(k)$ is spatial spectral density

3.3.2 Joint Distribution of Envelope and Phase

Consider the probability that the envelope takes a particular value. Taking into account (3.29) , it can be expressed in a form of the following inequality

$$a \le \sqrt{z^2 + y^2} < a + da \tag{3.41}$$

The probability of satisfying the inequality (3.41) is directly related with the PDF of the envelope, $f(a)$:

$$P\left(a \le \sqrt{z^2 + y^2} < a + da\right) = f(a)da \tag{3.42}$$

The probability (3.42) can be evaluated if the joint distribution of z and y is known:

$$f(a)da = P\left(a \le \sqrt{z^2 + y^2} < a + da\right) = \iint_{a \le \sqrt{z^2+y^2} < a+da} f(z, y)dzdy \tag{3.43}$$

Here $f(z,y)$ is a joint distribution of the original process z and its complimentary process y. Since both these processes have normal distribution; their joint distribution is also normal:

$$f(z,y)=\frac{1}{2\pi\sqrt{V_z V_y\left(1-c_{zy}^2\right)}}\exp\left(-\frac{1}{2\left(1-c_{zy}^2\right)}\left(\frac{z^2}{V_z}-\frac{2c_{zy}zy}{\sqrt{V_z V_y}}+\frac{y^2}{V_z}\right)\right) \tag{3.44}$$

Here c_{zy} is a correlation coefficient.

$$c_{zy}=\frac{C_{zy}(0)}{\sqrt{V_z V_y}}=0 \tag{3.45}$$

Taking also into account that the variances of the original process z and its complimentary process y are identical (3.30):

$$f(z,y)=\frac{1}{2\pi V}\exp\left(-\frac{1}{2}\left(\frac{z^2+y^2}{V}\right)\right) \tag{3.46}$$

An substitution of the distribution (3.46) into Equation (3.43) together with a transition to polar coordinates yields:

$$\begin{aligned}
&f(a)da=\iint\limits_{a\le\sqrt{z^2+y^2}<a+da} f(z,y)dzdy=\\
&=\frac{1}{2\pi V}\iint\limits_{a\le\sqrt{z^2+y^2}<a+da}\exp\left(-\frac{1}{2}\left(\frac{z^2+y^2}{V_x}\right)\right)dzdy=\\
&=\left|\begin{array}{ll} a=\sqrt{z^2+y^2} & x=a\cos(\Phi)\\ \Phi=\arctan\left(\dfrac{y}{z}\right) & y=a\sin(\Phi)\end{array}\right|=\\
&=\frac{1}{2\pi V}\int_a^{a+da}\int_0^{2\pi} a\exp\left(-\frac{1}{2}\left(\frac{a^2}{V}\right)\right)d\Phi\,da
\end{aligned} \tag{3.47}$$

Marginal distribution is defined as:

$$f(a)=\int_0^{2\pi} f(a,\Phi)d\Phi \tag{3.48}$$

Then, eonsider f(a) as a marginal distribution of the joint distribution $f(a,\Phi)$.

$$f(a)da = \int_{a}^{a+da} \int_{0}^{2\pi} f(a,\Phi)\, d\Phi\, da \tag{3.49}$$

This joint distribution $f(a,\Phi)$, then is expressed as:

$$f(a,\Phi) = \frac{a}{2\pi V} \exp\left(-\frac{1}{2}\left(\frac{a^2}{V}\right)\right) \tag{3.50}$$

The right-hand side does not eontain the phase variable Φ. This means that the variables a and Φ are independent. The PDF of a can be found by the integration of (3.50) by Φ from 0 to 2π.

$$f(a) = \int_{0}^{2\pi} f(a,\Phi)\, d\Phi = \frac{a}{V} \exp\left(-\frac{1}{2}\left(\frac{a^2}{V}\right)\right) \tag{3.51}$$

This distribution is known as the Rayleigh distribution.

The distribution of the phase ean be found from the formula (3.50) using the established faet of independenee of envelope and phase:

$$f(\Phi) = \frac{f(a,\Phi)}{f(a)} = \frac{1}{2\pi}; \quad 0 \le \Phi < 2\pi \tag{3.52}$$

The phase in the envelope presentation follows a uniform distribution from 0 to 2π. This eoneludes eonsideration of PDFs of the envelope and the phase.

3.3.3 Joint Distribution of Envelope and Phase in Two Points

Consider the four-dimensional distribution of values z and y of x and of $x+\Delta x$. It ean be presented as a system of four random variables:

$$\vec{U} = \left(z(x)\,,\, z(x+\Delta x)\,,\, y(x)\,,\, y(x+\Delta x)\right) \tag{3.53}$$

Since the processes z and y are normal, all four variables have a normal distribution. Then the distribution of the vector U is completely defined by a covariance matrix.

The variables $z(x)$ and $y(z)$ are not correlated, and the variables $z(x+\Delta x)$ and $y(x+\Delta x)$ are not either. However, the $z(x)$ and $y(x+\Delta x)$ are correlated with the correlation coefficient

$$\frac{1}{V}M\left(z(x), y(x+\Delta x)\right)=\frac{1}{V}C(\Delta x)=\frac{1}{2V}\sum_{i=1}^{N_w} r_{Wi}^2 \sin(\Delta x)=c(\Delta x) \tag{3.54}$$

A similar formula can be written for another "cross-pair" of the random variables $z(x+\Delta x)$ and $y(x)$.

$$\frac{1}{V}M\left(z(x+\Delta x), y(x)\right)=\frac{1}{V}C(-\Delta x)=\frac{1}{2V}\sum_{i=1}^{N_w} r_{Wi}^2 \sin(-\Delta x)=-c(\Delta x) \tag{3.55}$$

Note that the correlation between $z(x)$ and $z(x+\Delta x)$ is expressed through the autocorrelation function:

$$\frac{1}{V}M\left(z(x), z(x+\Delta x)\right)=\frac{1}{V}R(\Delta x)=\frac{1}{2V}\sum_{i=1}^{N_w} r_{Wi}^2 \cos(\Delta x)=r(\Delta x) \tag{3.56}$$

The same can be written for the correlation between $y(x)$ and $y(x+\Delta x)$:

$$\frac{1}{V}M\left(y(x), y(x+\Delta x)\right)=\frac{1}{V}R(\Delta x)=\frac{1}{2V}\sum_{i=1}^{N_w} r_{Wi}^2 \cos(\Delta x)=r(\Delta x) \tag{3.57}$$

The covariance matrix can be written as:

$$K(\Delta x)=V\begin{pmatrix} 1 & r(\Delta x) & 0 & c(\Delta x) \\ r(\Delta x) & 1 & -c(\Delta x) & 0 \\ 0 & -c(\Delta x) & 1 & r(\Delta x) \\ c(\Delta x) & 0 & r(\Delta x) & 1 \end{pmatrix} \tag{3.58}$$

The four-dimensional normal distribution is expressed as:

$$f(U) = \frac{1}{(2\pi)^2\sqrt{\det(K)}}\exp\left(-\frac{1}{2}U^T K^{-1}U\right) = \\ = \frac{1}{(2\pi)^2\sqrt{\det(K)}}\exp\left(-\frac{1}{2}\sum_{i=1}^{4}\sum_{j=1}^{4}K_{ij}^{-1}U_i U_j\right) \tag{3.59}$$

Here the superscript T stands for the transpose operation. It converts a vector-column into a vector-row. K^{-1} is an inverse covariance matrix. It is expressed as:

$$K^{-1}(\Delta x) = \frac{1}{V\cdot(p(\Delta x))^2}\begin{pmatrix} 1 & -r(\Delta x) & 0 & -c(\Delta x) \\ -r(\Delta x) & 1 & c(\Delta x) & 0 \\ 0 & c(\Delta x) & 1 & -r(\Delta x) \\ -c(\Delta x) & 0 & -r(\Delta x) & 1 \end{pmatrix} \tag{3.60}$$

Here

$$p(\Delta x) = \sqrt{1 - r(\Delta x)^2 - c(\Delta x)^2} \tag{3.61}$$

The determinant of the covariance matrix is:

$$\det(K(\Delta x)) = V^4\left(1 - r(\Delta x)^2 - c(\Delta x)^2\right)^2 = (V\,p(\Delta x))^4 \tag{3.62}$$

Substitution of (3.62) and (3.60) into (3.59) yields the following expression for the four-dimensional distribution:

$$f(U) = \frac{1}{(2\pi V)^2 p^2}\exp\left(-\frac{1}{2Vp^2}\left(z_1^2 + y_1^2 + z_2^2 + y_2^2 \right.\right. \\ \left.\left.\left(-2r(x_1x_2 + y_1y_2) - 2c(x_1y_2 + y_1x_2)\right)\right)\right) \tag{3.63}$$

To avoid a bulky formula, the following nomenclature was used in formula (3.63):

$$z_1 = z(x)\ ;\quad z_2 = z(x+\Delta x)\ ;\quad r = r(\Delta x)\ ;\quad p = p(\Delta x) \\ y_1 = y(x)\ ;\quad y_2 = y(x+\Delta x)\ ;\quad c = r(\Delta x) \tag{3.64}$$

Formula (3.63) describes probability density in the four-dimensional space with coordinates: z_1, z_2, y_1, y_2. The next step is to re-write it in polar coordinates, which is defined as follows:

$$a = \sqrt{z^2 + y^2} \qquad z = a\cos(\Phi)$$
$$\Phi = \operatorname{aretan}\left(\frac{y}{z}\right) \qquad y = a\sin(\Phi) \tag{3.65}$$

The new coordinates are:

$$a_1 = a(x) \;\; ; \;\; a_2 = a(x + \Delta x)$$
$$\Phi_1 = \Phi(x) \;\; ; \;\; \Phi_2 = \Phi(x + \Delta x) \tag{3.66}$$

To complete the transition, two pairs of rectangular coordinates (z_1, y_1) and (z_2, y_2) are substituted with (a_1, Φ_1) and (a_2, Φ_2). Then the expression needs to be multiplied by $a_1\, a_2$ as the element of the area in the polar coordinates $a\, d\Phi\, da$.

$$f(a_1, a_2, \Phi_1, \Phi_2) = \frac{a_1 a_2}{(2\pi V)^2 p^2} \exp\left(-\frac{1}{2Vp^2}\left(a_1^2 + a_2^2 - \right.\right.$$
$$\left.\left. - 2ra_1 a_2 \cos(\Phi_2 - \Phi_1) - 2ca_1 a_2 \sin(\Phi_2 - \Phi_1)\right)\right) \tag{3.67}$$

The expression (3.67) can be further simplified by the substitution:

$$\gamma(\Delta x) = \operatorname{aretan}\left(\frac{c(\Delta x)}{r(\Delta x)}\right) \tag{3.68}$$

$$f(a_1, a_2, \Phi_1, \Phi_2) = \frac{a_1 a_2}{(2\pi V)^2 p^2} \exp\left(-\frac{1}{2Vp^2}\left(a_1^2 + a_2^2 - \right.\right.$$
$$\left.\left. - 2a_1 a_2 \sqrt{1 - p^2}\cos(\Phi_2 - \Phi_1 - \gamma)\right)\right) \tag{3.69}$$

3.3.4 Distribution of Phase and Its Derivative

The joint distribution of phases in two points can be obtained by integration of the distribution (3.69) by the value of envelope a_1 and a_2

$$f(\Phi_1, \Phi_2) = \int_0^\infty \int_0^\infty f(a_1, a_2, \Phi_1, \Phi_2)\, da_1 da_2$$
$$= \frac{p^2}{4\pi^2}\left(\frac{1}{1 - \kappa^2} + \frac{\kappa}{\sqrt{(1 - \kappa^2)^3}}\left(\frac{\pi}{2} + \operatorname{aresin}(\kappa)\right)\right) \tag{3.70}$$

Where

$$\kappa = \sqrt{1-p^2}\cos(\Phi_2 - \Phi_1 - \gamma) \tag{3.71}$$

The joint distribution of the phase and its derivative can be derived from the joint distribution (3.70). This problem can be classified as multivariate probability transformation, when the distribution of one random vector is derived from the distribution of the other random vector. It also implies that these random vectors are related to the deterministic vector valued function.

$$\begin{pmatrix} \Phi_1 \\ \Phi_1' \end{pmatrix} = \vec{\Xi}\begin{pmatrix} \Phi_1 \\ \Phi_2 \end{pmatrix} \tag{3.72}$$

The derivative is defined as a limit:

$$\Phi_1' = \lim_{\Delta x \to 0} \frac{\Phi_2 - \Phi_1}{\Delta x} \tag{3.73}$$

Formula (3.73) represents a component of a vector-valued deterministic function of a random vector; the other component is:

$$\vec{\Xi}\begin{pmatrix} \Phi_1 \\ \Phi_2 \end{pmatrix} = \begin{pmatrix} \Phi_1 \\ \lim\limits_{\Delta x \to 0} \dfrac{\Phi_2 - \Phi_1}{\Delta x} \end{pmatrix} \tag{3.74}$$

Since the first component of the function (3.74) maps Φ_1 into itself and does not depend on Δx, the symbol of limit can be applied to the entire function:

$$\vec{\Xi}\begin{pmatrix} \Phi_1 \\ \Phi_2 \end{pmatrix} = \lim_{\Delta x \to 0}\begin{pmatrix} \Phi_1 \\ \dfrac{\Phi_2 - \Phi_1}{\Delta x} \end{pmatrix} \tag{3.75}$$

Assuming Δx being small:

$$\vec{\Xi}\begin{pmatrix}\Phi_1\\ \Phi_2\end{pmatrix} \approx \vec{\Xi}^*\begin{pmatrix}\Phi_1\\ \Phi_2\end{pmatrix} = \begin{pmatrix}\Phi_1\\ \dfrac{\Phi_2-\Phi_1}{\Delta x}\end{pmatrix} \tag{3.76}$$

The formulation of the problem of multivariate probability transformation is completed. Its solution is well-known from the general theory of probability (see, for example, Goodman 1985):

$$f^*(\Phi_1,\Phi_1') = |J(\vec{\Psi}^*)|\, f\left(\Psi_1^*(\Phi_1,\Phi_2),\Psi_2^*(\Phi_1,\Phi_2)\right) \tag{3.77}$$

Here vector valued function Ψ^* is an inverse to the vector valued function Ξ^* and J stands for the determinant of Jacobean matrix.

$$\begin{pmatrix}\Phi_1\\ \Phi_2\end{pmatrix} = \vec{\Psi}^*\begin{pmatrix}\Phi_1\\ \Phi_1'\end{pmatrix} = \begin{pmatrix}\Phi_1\\ \Phi_1+\Phi_1'\Delta x\end{pmatrix} \tag{3.78}$$

The determinant of the Jacobean matrix of the inverse function is expressed as:

$$J(\Psi^*) = \det\begin{pmatrix}\dfrac{\partial\Psi_1^*(\Phi_1,\Phi_1')}{\partial\Phi_1} & \dfrac{\partial\Psi_1^*(\Phi_1,\Phi_1')}{\partial\Phi_1'}\\ \dfrac{\partial\Psi_2^*(\Phi_1,\Phi_1')}{\partial\Phi_1} & \dfrac{\partial\Psi_2^*(\Phi_1,\Phi_1')}{\partial\Phi_1'}\end{pmatrix} = \det\begin{pmatrix}1 & 0\\ 1 & \Delta x\end{pmatrix} = \Delta x \tag{3.79}$$

Substitution of (3.79) and (3.78) into (3.77) to the following expression for the approximate joint distribution:

$$f^*(\Phi_1,\Phi_1') = \Delta x\cdot f(\Phi_1,\Phi_1+\Phi_1'\Delta x) \tag{3.80}$$

The exact distribution of the envelope and its derivative is actually a limit of (3.80), when Δx tends to zero:

$$\begin{aligned} f(\Phi_1,\Phi_1') &= \lim_{\Delta x\to 0}\left(\Delta x\cdot f(\Phi_1,\Phi_1+\Phi_1'\Delta x)\right)\\ &= \lim_{\Delta x\to 0}\frac{p^2\Delta x}{4\pi^2}\left(\frac{1}{1-\varepsilon^2}+\frac{\varepsilon}{\sqrt{(1-\varepsilon^2)^3}}\left(\frac{\pi}{2}+\arcsin(\varepsilon)\right)\right) \end{aligned} \tag{3.81}$$

Where ε is defined as:

$$\varepsilon = \sqrt{1-p^2}\cos\left(\Phi_1'\Delta x - \gamma(\Delta x)\right) \tag{3.82}$$

Taking that into account, in accordance with equation (3.68)

$$\lim_{\Delta x\to 0}\gamma(\Delta x) = \lim_{\Delta x\to 0}\arctan\left(\frac{c(\Delta x)}{r(\Delta x)}\right) = \arctan\left(\frac{0}{1}\right) = 0 \tag{3.83}$$

The value of correlation and cross-correlation at zero

$$r(0) = 1 \;;\; c(0) = 0 \tag{3.84}$$

While in accordance with equation (3.61)

$$\lim_{\Delta x\to 0} p(\Delta x) = \lim_{\Delta x\to 0}\sqrt{1-r(\Delta x)^2 - c(\Delta x)^2} = 0 \tag{3.85}$$

The limit of ε can be evaluated as

$$\lim_{\Delta x\to 0}\varepsilon(\Delta x) = 1 \tag{3.86}$$

This leads to uncertainty 0/0, if a limit in (3.81) is attempted. To overcome this uncertainty, the quantities depending on Δx may be expanded into Taylor series about the zero point (the Maclaurin series)

$$p(\Delta x)^2 = p(0)^2 + \frac{1}{1!}p'(0)^2\Delta x + \frac{1}{2!}p''(0)^2\Delta x^2 + \ldots \tag{3.87}$$

Consider the derivatives in (3.87):

$$\begin{aligned} p'(0)^2 &= \frac{d}{d\Delta x}\left(1 - r(\Delta x)^2 - c(\Delta x)^2\right)\Big|_{\Delta x=0} \\ &= -2\left(r(\Delta x)r'(\Delta x) + c(\Delta x)c'(\Delta x)\right)\Big|_{\Delta x=0} \end{aligned} \tag{3.88}$$

$$p''(0)^2 = \frac{d}{d\Delta x}\left(-2r(\Delta x)r'(\Delta x) - 2c(\Delta x)c'(\Delta x)\right)\Big|_{\tau=0} = \\ = -2\left(r(\Delta x)r''(\Delta x) + r'(\Delta x)^2 + c(\Delta x)c''(\Delta x) + c'(\Delta x)^2\right)\Big|_{\tau=0} \tag{3.89}$$

The derivatives of the auto- and eross-eorrelation funetions are:

$$r'(\Delta x) = \frac{1}{V}\int_0^\infty S(k)k\sin(k\Delta x)dk \tag{3.90}$$

$$r''(\Delta x) = -\frac{1}{V}\int_0^\infty S(k)k^2\cos(k\Delta x)dk \tag{3.91}$$

$$c'(\Delta x) = -\frac{1}{V}\int_0^\infty S(k)k\cos(k\Delta x)dk \tag{3.92}$$

$$c''(\Delta x) = -\frac{1}{V}\int_0^\infty S(k)k^2\sin(k\Delta x)dk \tag{3.93}$$

The values of these derivatives at $\Delta x = 0$ are expressed as:

$$r'(0) = -\frac{1}{V}\int_0^\infty S(k)k\sin(k\Delta x = 0)dk = 0 \tag{3.94}$$

$$r''(0) = -\frac{1}{V}\int_0^\infty S(k)k^2\cos(k\Delta x = 0)dk = \frac{1}{V}\int_0^\infty S(k)k^2dk = -k_2^2 \tag{3.95}$$

$$c'(0) = \frac{1}{V}\int_0^\infty S(k)k\cos(k\Delta x = 0)dk = \frac{1}{V}\int_0^\infty S(k)k\,dk = k_1 \tag{3.96}$$

$$c''(0) = -\frac{1}{V}\int_0^\infty S(k)k^2\sin(k\Delta x = 0)dk = 0 \tag{3.97}$$

The value $-c'(0)$ is the mean wave k_1 as determined from the speetral density, while the quantity $-r''(0)$ has a meaning of the seeond moment of the speetral area, normalized by the varianee and expressed in term of wave number. Its usual nomenelature is k_2^2. As a result, the equation (3.87) ean be re-written as:

$$p(\Delta x)^2 = p(0)^2 + \frac{1}{1!}p'(0)^2\Delta x + \frac{1}{2!}p''(0)^2\Delta x^2 + \ldots \approx \left(k_2^2 - k_1^2\right)\Delta x^2 \tag{3.98}$$

Similar formulae can be derived for other functions:

$$\varepsilon(\Delta x)^2 \approx 1-\left(\left(\Phi'-c'(0)\right)^2-\left(r''(0)+c'(0)^2\right)\right)\Delta x^2 = \\ =1-\left(\left(\Phi'-k_1\right)^2+\left(k_2^2-k_1^2\right)\right)\Delta x^2 \tag{3.99}$$

$$1-\varepsilon(\Delta x)^2 \approx \left(\left(\Phi'-c'(0)\right)^2-\left(r''(0)+c'(0)^2\right)\right)\Delta x^2 = \\ =\left(\left(\Phi'-k_1\right)^2+\left(k_2^2-k_1^2\right)\right)\Delta x^2 \tag{3.100}$$

Substitution of equations (3.98) through (3.100) into (3.81) removes uncertainty and reveals the final result:

$$f\left(\Phi,\Phi'\right)=\frac{1}{2\pi}\cdot\frac{k_2^2-k_1^2}{2\sqrt{\left(\left(\Phi'-k_1\right)^2+\left(k_2^2-k_1^2\right)\right)^3}} \tag{3.101}$$

Note that equation (3.101) does not contain phase, Φ, only its derivative. This means phase and its derivatives are independent.

3.3.5 Distribution of Envelope and Derivative of Phase

The procedure described in subsection 3.3.4 can be applied in order to derive the four-dimensional joint distribution of envelope, phases, and their derivatives. This is still a multivariate probability transformation, applied to the distribution (3.69) using the following vector valued function:

$$\begin{pmatrix} a_1 \\ a_1' \\ \Phi_1 \\ \Phi_1' \end{pmatrix} = \vec{\Xi}\begin{pmatrix} a_1 \\ a_2 \\ \Phi_1 \\ \Phi_2 \end{pmatrix} = \begin{pmatrix} a_1 \\ \lim\limits_{\Delta x\to 0}\dfrac{a_2-a_1}{\Delta x} \\ \Phi_1 \\ \lim\limits_{\Delta x\to 0}\dfrac{\Phi_2-\Phi_1}{\Delta x} \end{pmatrix} \approx \vec{\Xi}\cdot\begin{pmatrix} a_1 \\ a_2 \\ \Phi_1 \\ \Phi_2 \end{pmatrix} = \begin{pmatrix} a_1 \\ \dfrac{a_2-a_1}{\Delta x} \\ \Phi_1 \\ \dfrac{\Phi_2-\Phi_1}{\Delta x} \end{pmatrix} \tag{3.102}$$

The approximate inverse function is

$$\begin{pmatrix} a_1 \\ a_2 \\ \Phi_1 \\ \Phi_2 \end{pmatrix} = \vec{\Psi}^* \begin{pmatrix} a_1 \\ a_1' \\ \Phi_1 \\ \Phi_1' \end{pmatrix} = \begin{pmatrix} a_1 \\ a_1 + a_1'\Delta x \\ \Phi_1 \\ \Phi_1 + \Phi_1'\Delta x \end{pmatrix} \tag{3.103}$$

The Jacobean is expressed as:

$$J(\Psi^*) = \det \begin{pmatrix} 1 & 0 & 0 & 0 \\ 1 & \Delta x & 0 & 0 \\ 0 & 0 & 1 & 0 \\ 0 & 0 & 1 & \Delta x \end{pmatrix} = \Delta x^2 \tag{3.104}$$

To derive the four-dimensional distribution, the Jacobean and the approximate inverse function (3.103) are used with the original distribution (3.69):

$$f(a_1, a_1', \Phi_1, \Phi_1') = \lim_{\Delta x \to 0} \left(\Delta x^2 \cdot f(a_1, a_1 + a'\Delta x_1, \Phi_1, \Phi_1 + \Phi_1'\Delta x) \right) \tag{3.105}$$

After the substitution and evaluation of the limit, the final result is expressed as:

$$f(a, a', \Phi, \Phi') = \frac{a^2}{4\pi^2 (k_2^2 - k_1^2) V^2} \exp\left(- \frac{a'^2 + a^2 (\Phi'^2 - 2k_1\Phi' + k_2^2)}{2V(k_2^2 - k_1^2)} \right) \tag{3.106}$$

The joint distribution of the envelope and derivative of phase can be derived by the integration of (3.106):

$$\begin{aligned} f(a, \Phi') &= \int_0^{2\pi} \int_0^{\infty} f(a, a', \Phi, \Phi') da'\, d\Phi = \\ &\int_0^{\infty} \frac{a^2}{4\pi^2 (k_2^2 - k_1^2) V^2} \exp\left(- \frac{a'^2 + a^2 (\Phi'^2 - 2k_1\Phi' + k_2^2)}{2V(k_2^2 - k_1^2)} \right) da' \int_0^{2\pi} d\Phi = \\ &= \frac{a^2}{2\pi V \sqrt{2\pi V} \sqrt{(k_2^2 - k_1^2)}} \exp\left(- \frac{a^2 (\Phi'^2 - 2k_1\Phi' + k_2^2)}{2V(k_2^2 - k_1^2)} \right) \times \\ &\int_0^{\infty} \frac{1}{\sqrt{2\pi (k_2^2 - k_1^2) V}} \exp\left(- \frac{a'^2}{2V(k_2^2 - k_1^2)} \right) da' \int_0^{2\pi} d\Phi \end{aligned} \tag{3.107}$$

This integration does not create any difficulties, the first integral equals unity while the second integral equal 2π:

$$f(a,\Phi') = \frac{a^2}{\sqrt{2\pi\left(k_2^2 - k_1^2\right)}\sqrt{V^3}} \exp\left(- \frac{a^2\left(\Phi'^2 - 2k_1\Phi' + k_2^2\right)}{2V\left(k_2^2 - k_1^2\right)} \right) \tag{3.108}$$

3.3.6 Joint Distribution of Wave Amplitude and Wave Number

As a speetrum of wind-driven waves usually has a peak, whieh eontains a signifieant part of the wave energy, the phase in the equation (3.27) may be presented as

$$\Phi(x) = \Phi'(x)x + \psi^*(x) = k(x)x + \psi(x) \tag{3.109}$$

Here $k(x)$ is a relatively slowly changing wave number assoeiated with the absolute value of the spatial derivative of the phase Φ'. The rest of the phase is presented as a stoehastie proeess, $\psi^*(x)$, or $\psi(x)$. These figures are not essential here: their role is to model the spatial autoeorrelation funetion, where only a single wave event is addressed.

$$k(x) = |\Phi'(x)| \tag{3.110}$$

To derive the joint distribution of wave number and wave amplitudes, the derivative of the phase in (3.108) needs to be substituted by its absolute value. The absolute value of the derivative of the phase, Φ', can be eonsidered as a deterministie funetion of a random variable. This is again the problem of multivariate probability transformation. Beeause only one variable is involved in the transformation, the problem can be solved as one-dimensional using conditional distribution.

Consider the eonditional distribution of the derivative of the phase, taking into aeeount that the distribution of amplitude (envelope) follows Rayleigh (3.51)

$$f(\Phi' \mid a) = \frac{f(a,\Phi')}{f(a)} = \frac{a}{\sqrt{k_2^2 - k_1^2}\sqrt{2\pi V}} \exp\left(- \frac{a^2}{2V} \frac{(\Phi' - k_1)^2}{(k_2^2 - k_1^2)} \right) \tag{3.111}$$

The function of the absolute value is:

$$k = u(\Phi') = \begin{cases} \Phi' & if \quad \Phi' > 0 \\ -\Phi' & otherwise \end{cases} \tag{3.112}$$

This function is not monotonic, but it has two monotonie sub-domains. Therefore, its distribution contains two eomponents:

$$f(k) = f(v_1(k))\,|\,v_1'(k)\,| + f(v_2(k))\,|\,v_2'(k)\,| \tag{3.113}$$

Here $v(k)$ is a function inverse to (3.112) and v' is its derivative. Because the function u is not monotonic, its inverse expression is not single-valued, so two values exist at the same time for all k, and its derivative is also dual-valued:

$$v(k) = \begin{cases} v_1 = \Phi' \\ v_2 = -\Phi' \end{cases} \qquad v'(k) = \begin{cases} v_1' = 1 \\ v_2' = -1 \end{cases} \tag{3.114}$$

Therefore,

$$f(k) = f(k)\,|-1| + f(-k)\,|1| = f(k) + f(-k) \tag{3.115}$$

The application of (3.115) for (3.113) yields the conditional distribution of wave number:

$$f(k \mid a) = f(k \mid a) + f(-k \mid a) = \frac{a}{\sqrt{k_2^2 - k_1^2}\sqrt{2\pi V}}\left(\exp\left(-\frac{a^2}{2V}\frac{(k-k_1)^2}{(k_2^2-k_1^2)}\right) + \exp\left(-\frac{a^2}{2V}\frac{(k+k_1)^2}{(k_2^2-k_1^2)}\right)\right) \tag{3.116}$$

Finally the joint distribution of wave number and amplitudes is expressed as:

$$f(a,k) = f(a)f(k \mid a) = \frac{a^2}{\sqrt{k_2^2 - k_1^2}\sqrt{2\pi V^3}}\exp\left(-\frac{a^2}{2V}\right)\left(\exp\left(-\frac{a^2}{2V}\frac{(k-k_1)^2}{(k_2^2-k_1^2)}\right) + \exp\left(-\frac{a^2}{2V}\frac{(k+k_1)^2}{(k_2^2-k_1^2)}\right)\right) \tag{3.117}$$

3.3.7 Numerical Example

Sample calculations were performed to illustrate the distributions derived with Envelope Theory. A Bretschneider spectral density was used (Lewis 1989):

$$s(\omega) = A \cdot \omega^{-5} \exp\left(-B\omega^{-4}\right) \tag{3.118}$$

Here ω is wave frequency, while A and B are constants defined through the significant wave height H_S and the period corresponding to mean frequency T_1.

$$A = 173 \cdot \frac{H_S^2}{T_1^4}; \qquad B = 691 \cdot T_1^{-4} \tag{3.119}$$

The period corresponding to the mean frequency has the following relation with the mean zero-crossing period T_z and modal period of the spectrum T_m:

$$T_z = 0.71 \cdot T_m; \qquad T_1 = 0.773 \cdot T_m \tag{3.120}$$

The spectral density used for further sample calculations is shown in Figure 3.2.

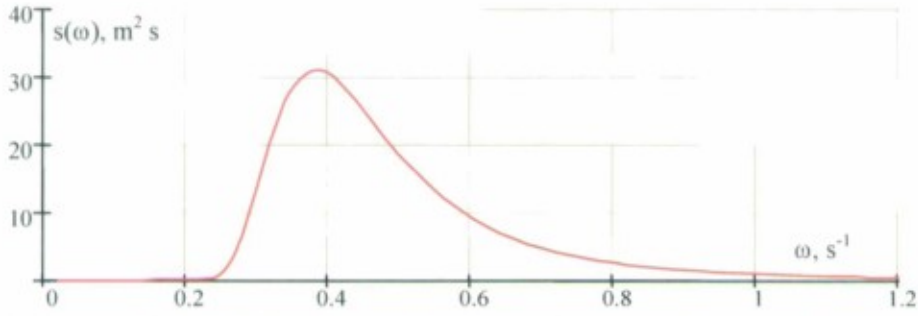

Figure 3.2 Temporal Spectral Density for Bretschneider Spectrum for Significant Wave Height= 11.5 m and Modal Wave Period= 16.4 s

Transition to the spatial spectral density is done through the dispersion relation (3.26). As the variance in space and time must be the same, the derivation of spatial spectral density is a substitution of variables from a mathematical point of view:

$$V = \int_0^\infty s(\omega)d\omega = \frac{1}{2}\int_0^\infty s\left(\sqrt{gk}\right)\sqrt{\frac{g}{k}}dk = \int_0^\infty S(k)dk \tag{3.121}$$

Here $S(k)$ stands for spatial spectral density:

$$S(k) = s\left(\sqrt{gk}\right)\sqrt{\frac{g}{k}} \tag{3.122}$$

The spatial spectral density for the numerical example is shown in Figure 3.3

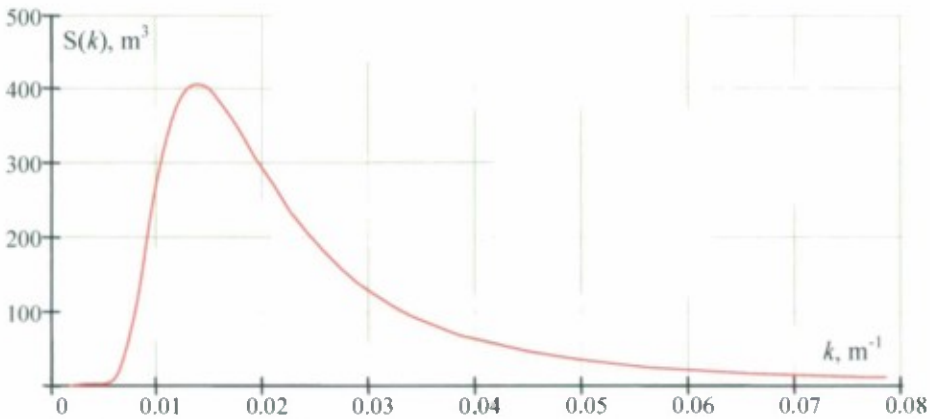

Figure 3.3 Spatial Spectral Density for Bretschneider Spectrum for Significant Wave Height= 11.5 m and Modal Wave Period= 16.4 s

Numerieal integration in formulae (3.95) and (3.96) eneounters convergenee diffieulties eaused by the empirieal nature of the Bretsehneider formula (3.118). To avoid this diffieulty, an upper limit is established for wave frequeney (Lewis 1989)

$$\omega_{\lim} = 5 \cdot \omega_m = 1.916\ s^{-1} \tag{3.123}$$

Here ω_m is a modal frequeney:

$$\omega_m = \frac{2\pi}{T_m} \tag{3.124}$$

The dispersion relation leads to the following expression for the upper limit of the wave number:

$$k_{\lim} = \frac{\omega_m^2}{g} \tag{3.125}$$

Then the mean value of wave number is expressed as:

$$k_1 = \frac{1}{V}\int_0^{k_{\lim}} S(k)k\,dk = \frac{1}{V}\int_0^{\omega_{\lim}} s(\omega)\frac{\omega^2}{g}d\omega = 0.028 \tag{3.126}$$

The value of k_2 (related to the seeond moment of the speetral area, normalized by the varianee):

$$k_2 = \sqrt{\frac{1}{V}\int_0^{k_{\lim}} S(k)k^2\,dk} = \sqrt{\frac{1}{V}\int_0^{\omega_{\lim}} s(\omega)\frac{\omega^4}{g^2}d\omega} = 0.0397 \tag{3.127}$$

The marginal distribution of the amplitude (envelope), defined by formula (3.51), does not differ for temporal or spatial eonsideration. It is shown in Figure 3.4. The marginal distribution of the derivative of phase ean be easily obtained from equation (3.101) by taking into aeeount that phase is distributed uniformly from 0 to 2π (see Figure 3.5a).

$$f(\Phi') = \frac{f(\Phi,\Phi')}{f(\Phi)} = \frac{k_2^2 - k_1^2}{2\sqrt{\left((\Phi' - k_1)^2 + \left(k_2^2 - k_1^2\right)\right)^3}} \tag{3.128}$$

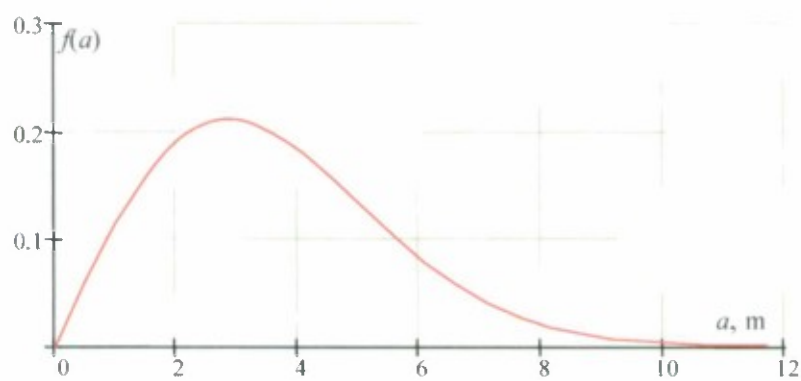

Figure 3.4 Marginal Distribution of the Amplitude / Envelope (Rayleigh Distribution)

The marginal distribution of the wave number can be evaluated using formulae (3.115) and (3.128). The distribution is shown in Figure 3.5b.

$$f(k)=\frac{k_2^2-k_1^2}{2\sqrt{\left((k-k_1)^2+\left(k_2^2-k_1^2\right)\right)^3}}+\frac{k_2^2-k_1^2}{2\sqrt{\left((k+k_1)^2+\left(k_2^2-k_1^2\right)\right)^3}} \tag{3.129}$$

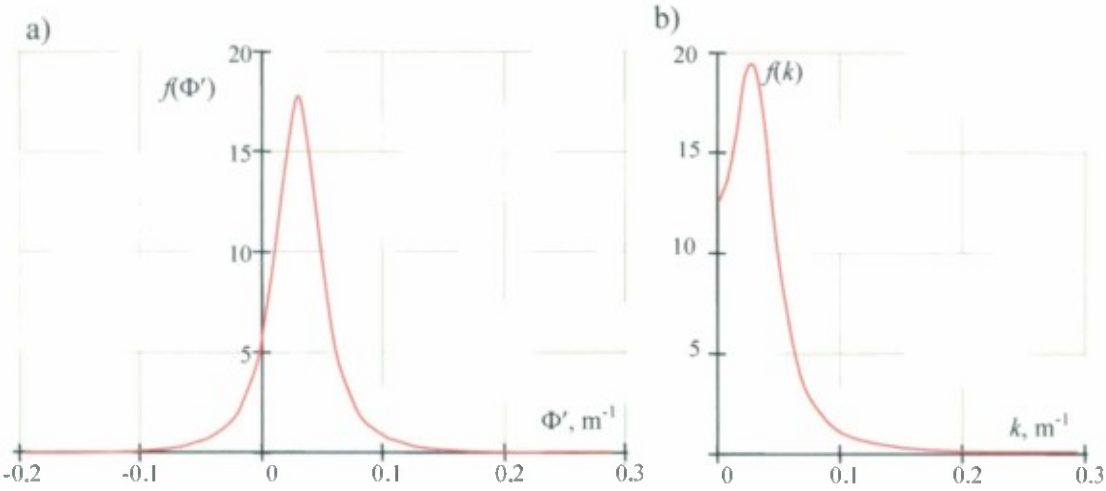

Figure 3.5 Marginal Distribution of (a) the Derivation of Phase and (b) the Wave Number

Figure 3.6 shows conditional distributions for the derivative of the phase (Figure 3.6a) and the wave number (Figure 3.6b) calculated for a series of sample amplitude value. With the increase of the amplitude, both distributions become "thinner," and the variance must be decreasing. At the same time, the conditional distribution of the derivative of the phase remains unchanged, while the distribution of wave number experiences some shift. The shape of the distribution of the derivative of the phase appears to be normal. A closer look at the formula (3.111) reveals a normal distribution for the conditional derivative of the phase, with the variance and mean value expressed as follows:

$$m(\Phi'\mid a)=k_1;\ \ V(\Phi'\mid a)=\frac{V(k_2^2-k_1^2)}{a^2} \tag{3.130}$$

The mean value and variance for the conditional distribution of the wave number cannot be expressed through elementary functions. At the same time, the distribution (3.116) is the distribution of the absolute value of a normal variable (folded normal distribution). The mean value and variance of the folded normal distribution are known and can be used to express the conditional mean value and the conditional variance of the wave number as function of amplitude. The conditional mean value is expressed as:

$$m_{k|a}(a) = \frac{1}{a}\sqrt{\frac{2V(k_2^2 - k_1^2)}{\pi}}\exp\left(-\frac{a^2 k_1^2}{2V(k_2^2 - k_1^2)}\right) + k_1\left(1 - 2F_N\left(-\frac{a k_1}{\sqrt{V(k_2^2 - k_1^2)}}\right)\right) \tag{3.131}$$

Where

$$F_N(x) = \int_{-\infty}^{x}\exp\left(-\frac{t^2}{2}\right)dt \tag{3.132}$$

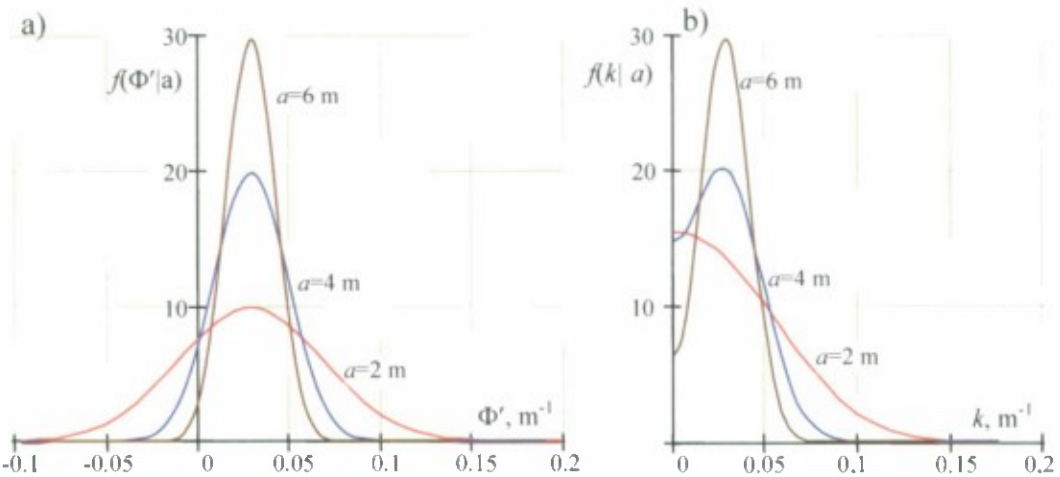

Figure 3.6 Conditional Distribution of the Derivative of the Phase (a) and the Wave Number (b), Calculated for Sample Values of the Amplitude

The conditional variance of the wave number is expressed as:

$$V_{k|a}(a) = k_1^2 + \frac{V(k_2^2 - k_1^2)}{a^2} - \left(\frac{1}{a}\sqrt{\frac{2V(k_2^2 - k_1^2)}{\pi}}\exp\left(-\frac{a^2 k_1^2}{2V(k_2^2 - k_1^2)}\right) + k_1\left(1 - 2F_N\left(-\frac{a k_1}{\sqrt{V(k_2^2 - k_1^2)}}\right)\right)\right)^2 \tag{3.133}$$

The graphs for these functions are given in Figure 3.7. For the considered example, the conditional mean value and variance of the derivative of the phase and the wave number converge starting at a value of wave amplitude of 5 m. This also means that the lengths of large waves are likely to have a length close to the mean, as the variance of the wave number deceases quickly with the growth of amplitude.

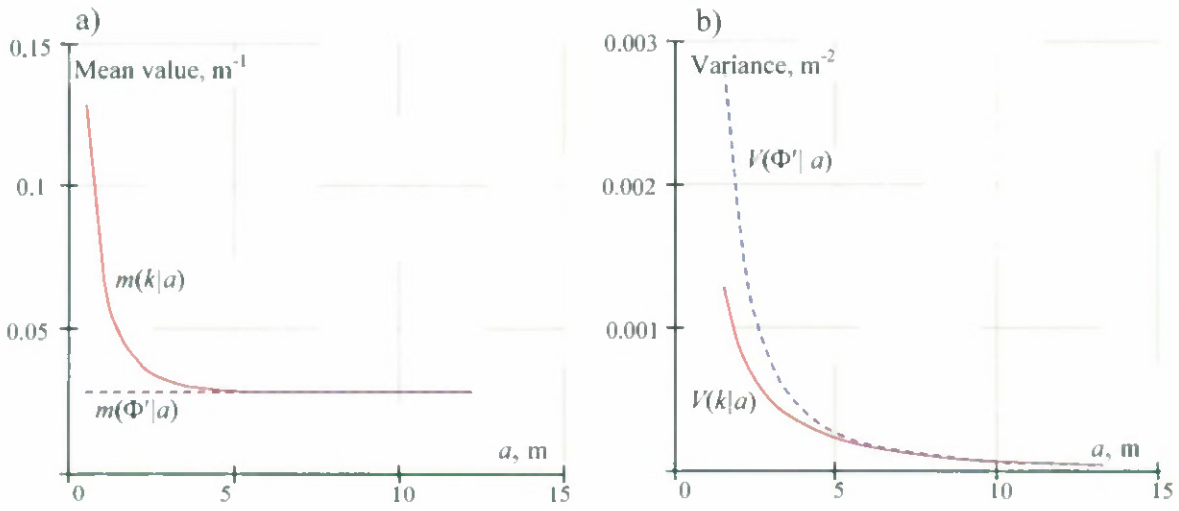

Figure 3.7 Conditional Mean Value (a) and Variance (b) of the Derivative of the Phase (Dashed) and the Wave Number (Solid), as Functions of Wave Amplitude

Finally, Figure 3.8 shows plots for the joint distributions of the amplitude and the derivative of phase (Figure 3.8a) and the wave number (Figure 3.8b). The latter represents the final result of this study, as it can be used to estimate the probability of encounter with the wave of a certain height and length.

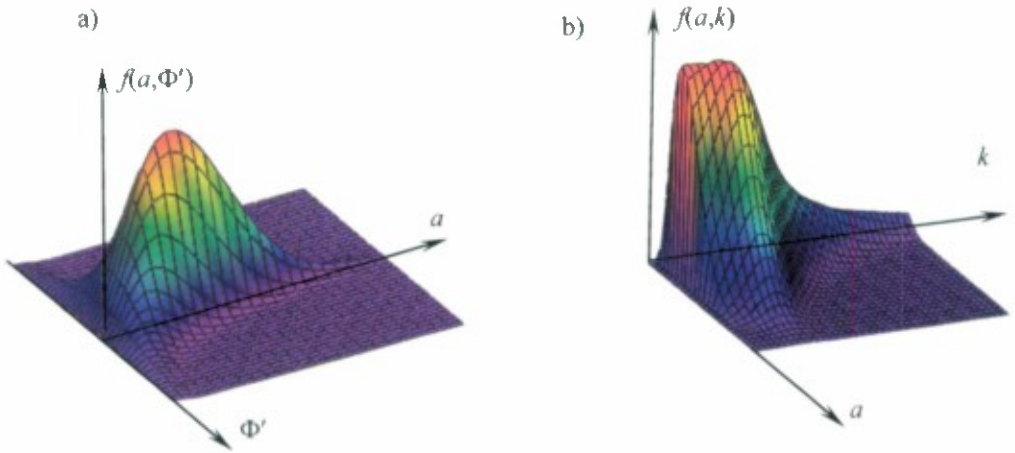

Figure 3.8 Joint Distributions of the Amplitude and the Derivative of the Phase (a) and the Amplitude and the Wave Number (b)

3.4 Level 1 Vulnerability Criteria

Both parametric roll and pure loss of stability are driven by stability variations in waves. As was discussed in subsection 2.1.1, certain features of the hull shape are "responsible" for stability. The level 1 criterion proposed here is focused on these geometric features. In principle, this criterion can be used as the level 1 criterion for both parametric roll and pure loss of stability.

Beeause both modes of intaet stability failure considered here, pure-loss and parametric roll, are fundamentally a result of the relation between variations in the area of the waterplane and the location of the wave erest along the hull, a eommon eriterion to assess level 1 vulnerability is proposed. However, this was not applied for level 1 parametric roll criteria, the reasons for whieh were diseussed in the previous seetion. Four prospective criteria are discussed, along with the results for the sample ships

A method to assess level 1 vulnerability to pure-loss of stability, based on static characteristics of the hull form, is proposed and four criteria were examined. The first criterion considered the value of the total coefficient for vertical "wall-sidedness," C_{VWS}, or the variability of hull shape from the maximum dimensions over the range of draft, $\max(A_{WP}(z)),\quad z \in [d-\Delta d; d+\Delta d]$, which is similar to the more traditional vertical prismatic coefficient, C_{VP}, taken from the calm waterplane. This provides an indication of the change of the shape of the hull from the volume projected using the maximum waterplane dimensions over the vertical height of the ship.

$$C_{VWS} = \frac{\int_{d-\Delta d}^{d+\Delta d} A_{WP}(z)dz}{\max(A_{WP}(z))\cdot 2\Delta d}; \quad \Delta d = \max\left(\frac{d}{2}, \frac{L}{20}, D-d\right) \tag{3.134}$$

The second criterion considered the average of the vertical wall-sidedness coefficients for the fore and aft quarter portions of the hull, both above and below the waterline (see Figure 3.9). For each of the four sections (fore, aft, above, and below), the C_{VWS} was computed as the fraction of the volume from the maximum waterplane projection for the given section. Then the average value for the four sections was used to provide an indication of the total relative changes for the bow and stern shapes, both above and below the waterline because these are the regions the form variations typically occur.

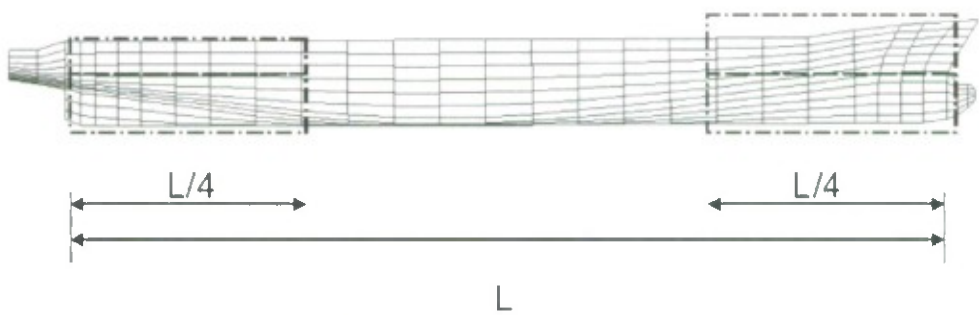

Figure 3.9 Notional Ship Profile With the Four Portions of the C_{VWS} Considered for the Level 1 Vulnerability Assessment

The third criterion considered the ratio of the transverse met centric radius to the height of the transverse metacenter above the keel.

$$C1_3 = \frac{BM}{KM} \tag{3.135}$$

The fourth eriterion eonsidered the ratio of the transverse metaeentrie radius to the beam.

$$C1_4 = \frac{BM}{B} \tag{3.136}$$

The first eriterion does not show any elear separation between the ships whieh are known to be vulnerable and the ships whieh are not (Figure 3.10). However, the seeond eriterion, the average of the vertieal wall-sidedness eoeffieient for the fore and aft quarters of the ship, seems to provide useful separation between the ships (Figure 3.11) for this sample population.

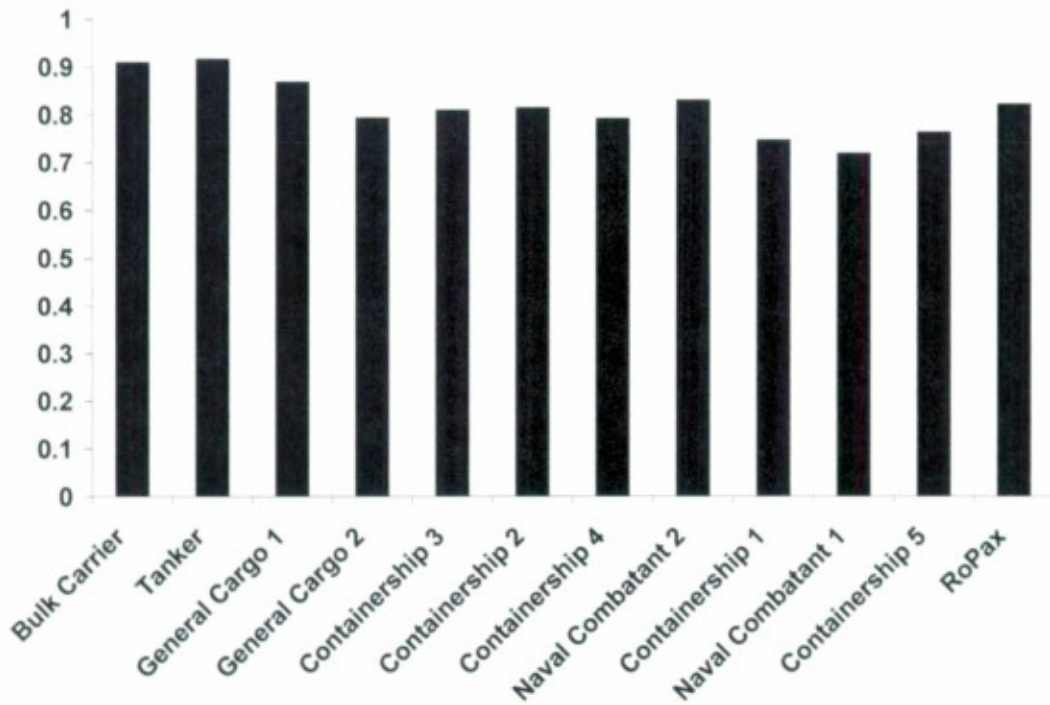

Figure 3.10 Total C_{WS}, Both Above and Below the Waterline, for the Sample Ship Population

Based on this sample population of ships, an initial estimate of the threshold for the standard eould be proposed around 0.75-0.80. Ships above this value, the Bulk Carrier, Tanker, and Series 60 are eonsidered to be eonventional vessels, not at risk for failures related to righting lever variations in waves. However, all of the other nine ships fall below this value, the highest being the General Cargo ship 2, or C4, with a value of 0.75. The ships with the lowest values are Containership 5 (the C-11 containership) and the RoPax, whieh have values of 0.69 and 0.67, respeetively

Of the four vertical wall-sidedness coefficients, fore and aft quarter, above and below the waterline, the aft coefficient above the waterline has the least variation for the ship population examined. However, in order to still account for ships outside this population, including ones with unconventional topside stern shapes, this effect should still be included.

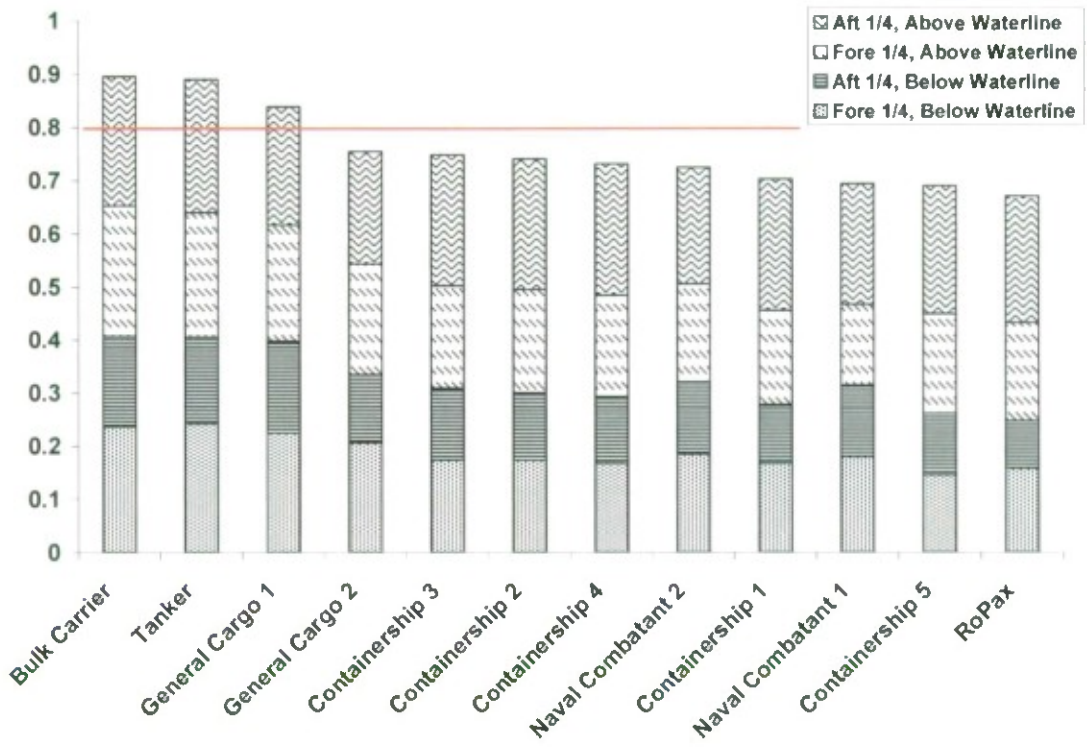

Figure 3.11 Total Average C_{VWS} for the Fore and Aft Quarters of the Ship, both Above and Below the Waterline, for the Sample Ship Population

The third and the fourth criteria, using ratios with the transverse metacentric radius, did not show any clear separation between the ships which are known to be vulnerable and the ships which are not.

The proposed method for level 1 vulnerability assessment does not consider the relative size of the ship and the waves. Typically, it is assumed that higher sea states are more likely to result in stability failure. However, waves of large height are more likely to have larger length and waves of large length may not greatly affect stability, depending on their comparison with ship length. This important consideration is included in further study, discussed below.

3.5 Level 2 Vulnerability Criteria

3.5.1 Formulation of the Criteria

As was discussed earlier in this section, pure loss of stability may be considered as a single wave event because of instantaneous changes in waterplane area. Typically, the worst-case wave length is close to the length of the ship, $\lambda/L = 0.75 \sim 2.0$. However, in order to account for the effect of ship size relative to the wave conditions, righting lever variations should be evaluated in irregular waves. To characterize an event of pure loss of stability, the distribution of random wave numbers and wave amplitudes, $f(a,k)$, is used to evaluate the statistical weight of a wave encounter:

$$W_{ij} = \int_{a_i-\Delta a}^{a_i+\Delta a} \int_{k_j-\Delta k}^{k_j+\Delta k} f(a,k)dkda \tag{3.137}$$

The GM value is calculated for each sinusoidal wave, with characteristics as defined above. These calculations are repeated for different positions of the wave crest along the ship length, so a complete wave pass is presented.

Calculation of the time while the stability is decreased can be easily performed when the GM is considered as a function of the wave crest. The critical GM was calculated in accordance with the 2008 IS Code (Figure 3.12).

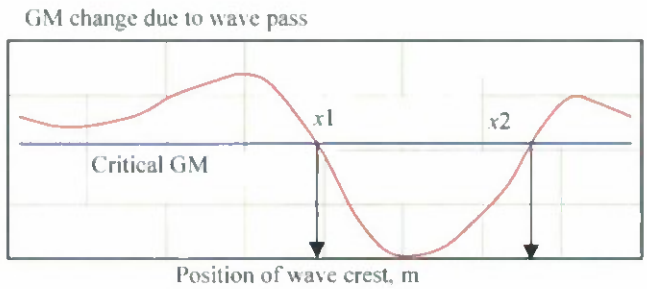

Figure 3.12 Calculation of "Time-Below-Critical-GM"

Points $x1$ and $x2$ (Figure 3.12) show the distance when the GM remains below the critical level (based on 2008 IS Code), while the wave passes the ship. The "time-duration-below-critical GM", tbc, can be calculated as:

$$tbc = \frac{x2 - x1}{c - V_S} \tag{3.138}$$

where c is wave celerity and V_s is ship speed. The time–below–critical GM is a random number in irregular waves. Its mean value is estimated as:

$$m(tbc) = \sum_i \sum_j tbc_{ij} W_{ij} \tag{3.139}$$

The criterion value, $Cr1$, is proposed as the following ratio:

$$Cr1 = \frac{m(tbc)}{T_\phi} \tag{3.140}$$

This criterion assesses the significance of stability changes in waves. If stability is degraded only for a short duration, the resulting ship response may not be significant. However, for longer durations of decreased stability below the critical level, the restoring moment may be degraded enough to result in a dangerously large heel angle.

The justification of assigning a critical level of GM can be done in a following way. As the GM variation due to the wave-pass takes care of waterplane changes, the critical GM has to take into account the features of hull form that can provide additional buoyancy at large heel angles. The influence of these features, such a flared bow, is reflected in the position of the maximum of the calm-water GZ curve. This can be illustrated by a comparison of the GZ curve of two notional ships from ONR topside series (Bishop, et al., 2005). These ships have exactly the same hull shape below the calm-water waterline, but differ in topside configuration, one with flare and one with tumblehome. To illustrate the effect of topside configuration, Figure 3.13 shows the GZ curve calculated for the same value of KG for each of the two topside configurations.

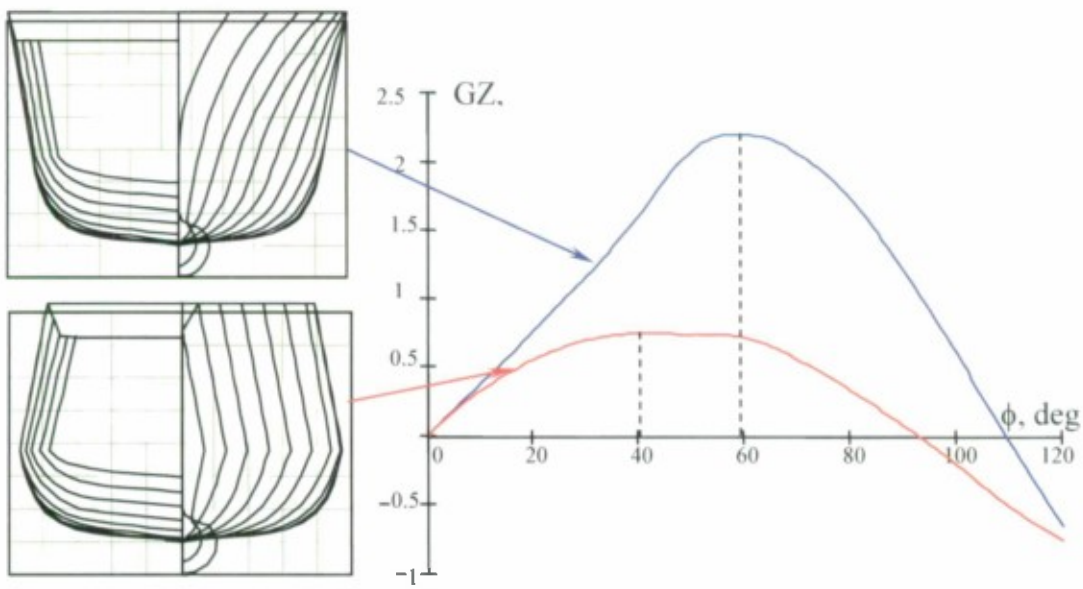

Figure 3.13 Geometries and the *GZ* Curves of the ONR Tumblehome (Naval Combatant 2) and Flared (Naval Combatant 1) Topside Configurations (KG=7.5 m in Both Cases)

As shown in Figure 3.13, the angle of maximum *GZ* of the flared topside configuration is much larger than that of the tumblehome topside configuration. The difference in the value of the maximum of the *GZ* curve is even more dramatic. However, the angle of the maximum of the *GZ* curve is a preferable measure. Stability failure near a wave crest is a phenomenon occurring at a very small encounter frequency, while the wave crest is slowly moving along the hull. As a result, heeling may occur almost statically; so in this case, the angle of maximum represents the actual stability range. All these parameters of the calm water *GZ* curve are related to the 2008 IS Code criteria in one way or another. Therefore, setting the level of critical *GM*, based on these criteria, seems to be reasonable, because it takes into account the influence of large volumes of buoyancy that may be used as a stability reserve.

The second criterion is set to detect significant durations of negative *GM* (see Figure 3.14). The appearance of an angle of roll may lead to the development of partial stability failure faster, as the upright equilibrium is no longer stable. It is quite possible that some ships may be more vulnerable for these types of failure than others.

The second criterion, *Cr2*, is based on characteristics of the time during which the angle of roll exceeds a certain limit angle, ϕ_{lim} (30 degrees was used in this example). For each position of the wave crest along the hull, the indicator value, z, is calculated:

$$z = \begin{cases} 0 & if \quad \phi_{roll} < \phi_{\lim} \\ 1 & if \quad \phi_{roll} \geq \phi_{\lim} \end{cases} \tag{3.141}$$

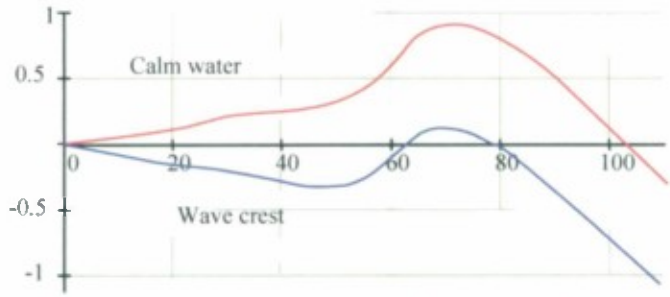

Figure 3.14 Deterioration of GZ Curve Near the Wave Crest (Illustration Only).

The angle of roll, ϕ_{roll}, can be obtained from the "true" instantaneous *GZ* curve in waves, or from its approximation using a calm water *GZ* curve and the instantaneous *GM* in waves:

The time while the angle of roll is too large during the wave pass is expressed as

$$tbz = \sum_k z_k \Delta t \tag{3.142}$$

where Δt is the time-step (providing at least seven steps per period) and index k corresponds to a particular time instant during the wave passing.

Formulation of the second criterion is similar to the first one:

$$Cr2 = \frac{m(tbz)}{T_\phi} \tag{3.143}$$

where $m(tbz)$ is the weighted average over the wave encounters:

$$m(tbz) = \sum_i \sum_j tbz_{ij} W_{ij} \tag{3.144}$$

Results of calculations using the sample population of ships are discussed further in subsection 3.5.3.

3.5.2 Evaluation of Stability in Waves

Details of the evaluation of the GM in waves for the assessment of pure loss of stability are presented in this subsection. The encounter frequency of waves in the situation where pure loss of stability is possible (following and stern-quartering seas) is low. Therefore, static balancing in trim and draft becomes relevant.

The area at each station and its moment relative to the vertical axis are expressed as function of the local draft, accounting for the sinkage and the trim:

$$A_i(z) = 2\int_0^z b_i(z)dz \qquad Mz_i(z) = 2\int_0^z z b_i(z)dz \tag{3.145}$$

i indicates the station number, $b_i(z)$ is the half-breadth at station i, at the local draft z. The volumetric displacement can be expressed as a function of the position of a wave crest an array of local drafts $\vec{z} = \{z_i\}, i = 1, N_s$:

$$V(x_c, \vec{z}) = 0.5 \sum_{i=1}^{N_{st}-1} \left(A_i(z_i) + A_{i+1}(z_{i+1})\right)(x_{i+1} - x_i) \tag{3.146}$$

x_i is the coordinate of the i-th station in the ship-fixed coordinate system.

The moments of the hull relative to vertical and longitudinal axes are expressed using a similar formulation:

$$MZ(x_C,\vec{z}) = 0.5\sum_{i=1}^{N_W-1}\left(Mz_i(z_i)+Mz_{i+1}(z_{i+1})\right)(x_{i+1}-x_i) \tag{3.147}$$

$$MX(x_C,\vec{z}) = 0.5\sum_{i=1}^{N_W-1}\left(x_iA_i(z_i)+x_{i+1}A_{i+1}(z_{i+1})\right)(x_{i+1}-x_i) \tag{3.148}$$

Formulae (3.146) through (3.148) can be used to express coordinates for the center of buoyancy:

$$LCB(x_C,\vec{z}) = \frac{MX(x_C,\vec{z})}{V(x_C,\vec{z})}; \qquad KB(x_C,\theta,z_S) = \frac{MZ(x_C,\vec{z})}{V(x_C,\vec{z})} \tag{3.149}$$

Consideration of the time for the change of stability in waves is redundant and the wave profile along the hull is considered as a function of wave crest position only. Therefore, the local draft at each station comes from the formula, describing wave elevations along the hull, and depends on sinkage and trim.

$$\zeta(x,x_C) = a\cos(k(x-x_c)) \tag{3.150}$$

To account for the trim on the wave profile, the following auxiliary function is introduced:

$$\Xi(x_i,z_i,\theta,x_C) = a\cos\left[k\left(x_i\cos\theta - z_i\sin\theta - x_C\right)\right] - \left(x_i\sin\theta + z_i\cos\theta\right) \tag{3.151}$$

This function equals zero when a point with coordinates x_i and z_i is exactly at the surface of the wave of amplitude a_W, rotated by the trim angle θ. Then the elevation of the wave profile at the i-th station is defined through the inverse of the function Ξ, calculated for each station located at x_i:

$$z_{WL}(\theta,z_S,x_i,x_C) = INV\left(\Xi(x_i,z_i,\theta,x_C)\right) + z_S \tag{3.152}$$

Where z_S is the value of parallel sinkage.

The wave profile along the ship hull is evaluated by satisfying equilibrium conditions through solving the following system of nonlinear algebraic equations, with trim and sinkage as unknowns

$$\begin{cases} V(x_C,z_{WL}(\theta,z_S,x_i,x_C)) = V_0 \\ LCB(x_C,z_{WL}(\theta,z_S,x_i,x_C)) = LCB_0 \end{cases} \tag{3.153}$$

Once sinkage and trim are found, the profile of the wave along the hull can be found as:

$$z_i = z_{WL}(\theta, z_S, x_i, x_{C\cdot}) \tag{3.154}$$

The moment of inertia of the waterplane made by the wave profile is:

$$I_X(x_{C\cdot}) = \frac{1}{3}\sum_{i=1}^{N_W-1}\left(b^3(z_i)+b^3(z_{i+1})\right)(x_{i+1}-x_i) \tag{3.155}$$

Other hydrostatic terms are also needed to determine GM

$$KB(x_{C\cdot}) = \frac{MZ(x_{C\cdot}, \vec{z})}{V_0}; \quad BM(x_{C\cdot}) = \frac{I_X(x_{C\cdot})}{V_0} \tag{3.156}$$

Finally the value of GM in waves is a function of the position of a wave crest

$$GM(x_{C\cdot}) = BM(x_{C\cdot}) - KG + KB(x_{C\cdot}) \tag{3.157}$$

It is known that balancing a ship (finding its equilibrium position) with sinkage and trim may significantly change the result for determining GZ in waves. To demonstrate this effect, the calculations described above can be complemented by partial balancing (sinkage/displacement only) or no balancing results. This demonstration is important, because balancing is the most intensive part of the calculation.

Partial balancing is implemented by setting $\theta = \theta_0$ (to the calm water value) in formula (3.152); this converts a system of equations (3.153) into a single equation:

$$V(x_{C\cdot}, z_{WL}(\theta = \theta_0, z_S, x_i, x_{C\cdot})) = V_0 \tag{3.158}$$

Results for the moment of inertia of the area of the waterplane are shown in Figure 3.15.

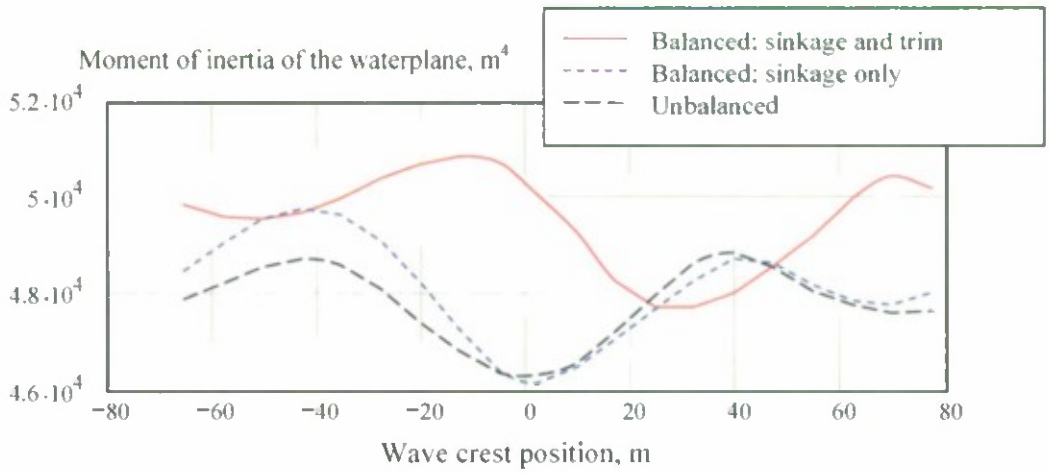

Figure 3.15 Change of the Moment of Inertia of the Area of the Waterline with Moving Wave Crest for Different Type of Balancing for ONR Tumblehome Topside Ship (Naval Combatant 2)

Figure 3.15 clearly shows that balancing both sinkage and trim results in a significant difference for the moment of inertia of the waterplane. It can also be seen from Figure 3.16, which shows the change of BM. The calculation of BM without balancing is done using the resulting volumetric displacement from the wave crest position.

$$BM(x_{C'}) = \frac{I_X(x_{C'})}{V(x_{C'}, \bar{z})} \tag{3.159}$$

A similar approach was used to calculate the unbalanced KB, which is shown in Figure 3.17.

$$KB(x_{C'}) = \frac{MZ(x_{C'}, \bar{z})}{V(x_{C'}, \bar{z})} \tag{3.160}$$

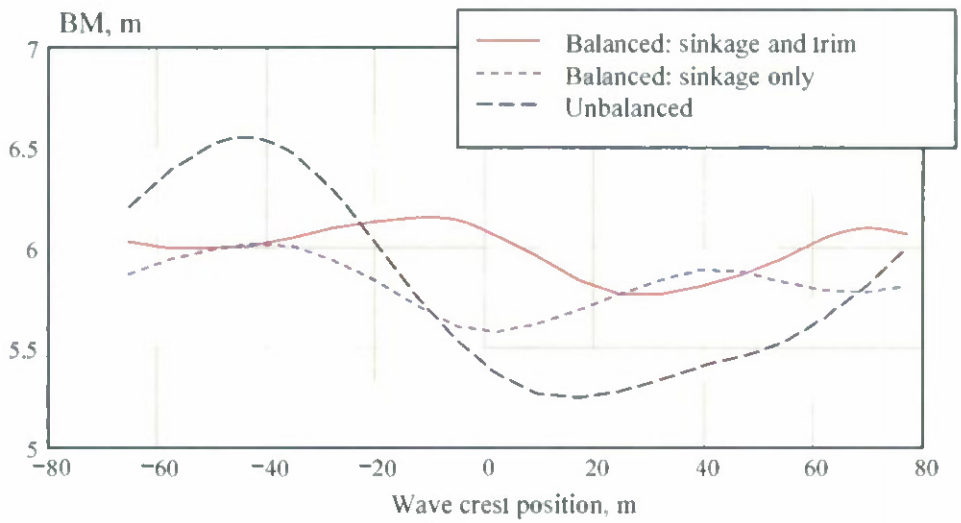

Figure 3.16 Change of the *BM* Value with Moving Wave Crest for Different Type of Balancing for ONR Tumblehome Topside Ship (Naval Combatant 2)

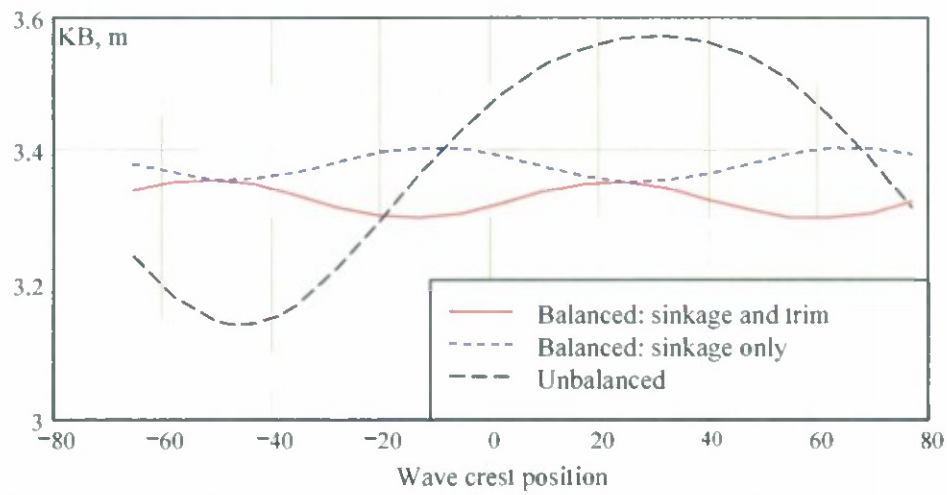

Figure 3.17 Change of the *KB* Value with Moving Wave Crest for Different Type of Balancing for ONR Tumblehome Topside Ship (Naval Combatant 2)

As seen in Figure 3.17, balancing with sinkage has the most influence for the *KB* value. Figure 3.18 shows *GM* in waves calculated with different balancing options. It is clear from Figure 3.18 that these balancing options have a significant influence on the initial stability in waves. Two features should also be noted. First, the magnitude of the change of stability is the largest for the unbalanced results. Second, the ONR tumblehome topside ship is an example of an unconventional vessel and, therefore, the observations of Figure 3.15 through Figure 3.18 may be generally applicable.

Stability changes in waves are not limited to *GM*; the entire *GZ* curve experiences changes. The main advantage of using *GM* is simplicity and to enable the possibility to perform spreadsheet style calculations. Using *GM* only for the evaluation of stability in waves also can be considered as an approximation, where the change of *GM* in waves is used to "modulate" the calm-water *GZ* curve.

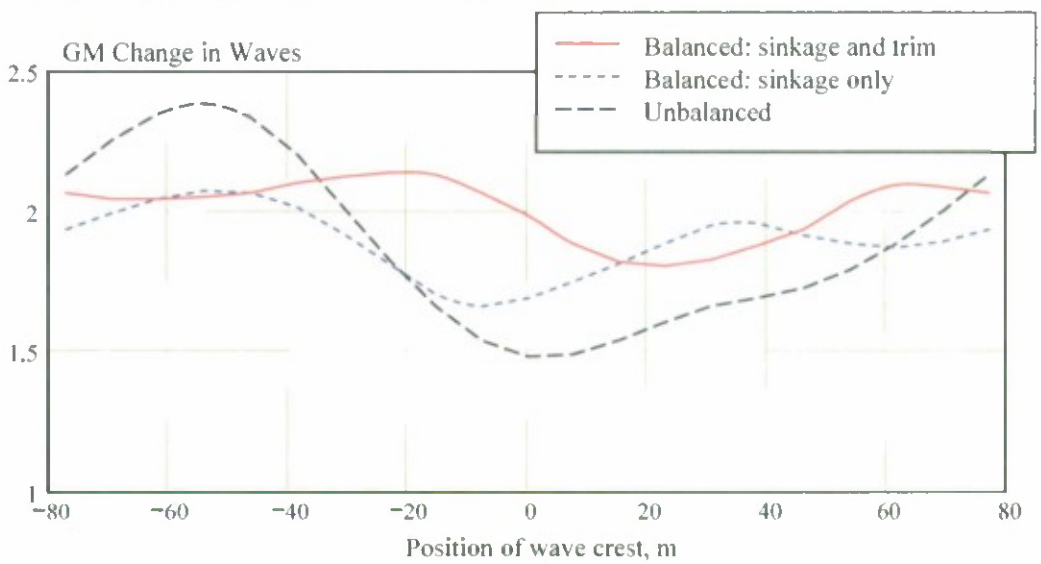

Figure 3.18 Change of GM in Waves with Moving Wave Crest for Different Type of Balancing for ONR Tumblehome Topside Ship (Naval Combatant 2)

$$GZ(\phi, x_c) = GZ_0(\phi) - (GM_0 - GM(x_c))\sin(\phi) \tag{3.161}$$

To evaluate the level of approximation introduced by "modulation" (3.161), the entire *GZ* curve was computed using a preprocessor, *PRELMP*, of the advanced panel code *LAMP* (Lin and Yue, 1990; 1993). The preprocessor uses a quasi-static wave and computes the righting moment by integrating pressures around the hull. Another tool capable of performing these calculations is *EUREKA* (Paulling, 1961). It was demonstrated that *PRELMP* calculations are identical to *EUREKA* (Belenky and Weems, 2008). The results of the direct calculation of the GZ curve in waves for the same conditions are shown in Figure 3.19, while Figure 3.20 shows the approximate "modulated" GZ curve.

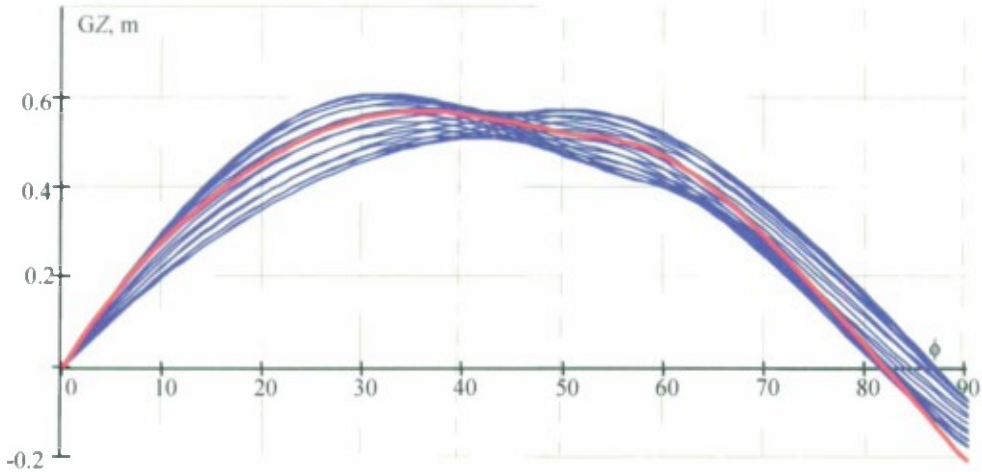

Figure 3.19 GZ Curve of the ONR Tumblehome Topside Ship in Wave Calculated with PRELMP

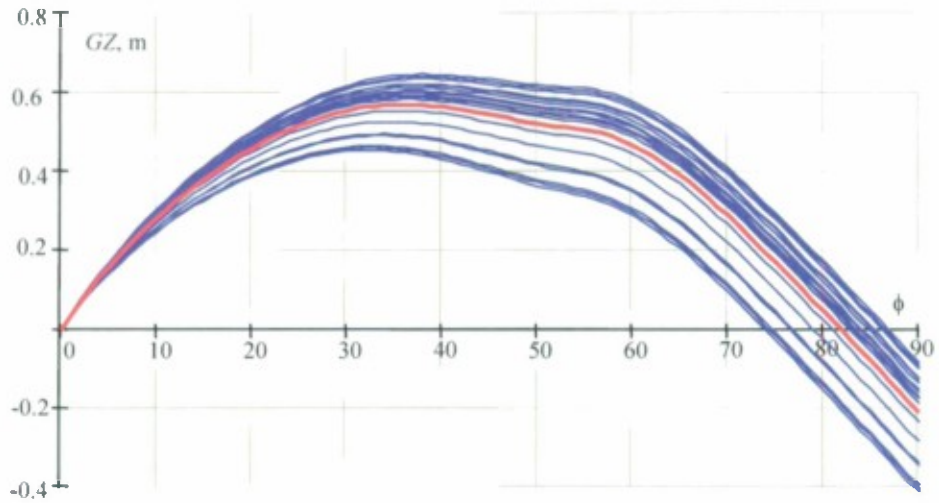

Figure 3.20 GZ Curve in Wave of the ONR Tumblehome Topside Ship Approximated with Formula (3.161)

The comparison between GZ curves in Figure 3.19 and Figure 3.20 shows the generally conservative character of approximation (3.161) as the influence of the wave, in general, is slightly exaggerated by the approximation (3.161). Despite the approximation, which is not capable of representing all the details of stability changes in waves, the approximation formula still seems to be a reasonable tool for vulnerability-level assessment.

3.5.3 Results for Sample Population

Results are shown for calculations using the two criteria ($Cr1$ and $Cr2$) for the sample ships (Figure 3.21, Figure 3.22 and Table 3). The results are given for Sea State 7 and an operational speed of 15 knots, with the critical KG based on the conditions obtained from compliance with the 2008 IS Code. Additional calculations were also made to examine

the criterion values as a function of the sea state. An example of this is presented in Belenky and Bassler (2010).

Comparing the sample calculations for the level 2 probabilistic criterion, *Cr*1, it can be observed that there is a great distinction between the Fishing Vessel 1 (ITTC-A2) and the Naval Combatant 2 (ONR tumblehome topside hull). Both known to be vulnerable to pure loss of stability (e.g. Spyrou, 1996; Umeda, *et al.*, 1999; Bishop, *et al.*, 2005; Umeda & Hashimoto, 2006; Bassler, *et al.*, 2007; Hashimoto, 2009), compared to other ships, which are not known to be vulnerable to this type of stability failure. The exception to this trend is the notional RoPax. Given these results, and the results of sample calculations with a notional naval fleet (Belenky and Bassler, 2010), a standard using the first criterion could be set at 1.0.

The second criterion indicates possible vulnerability for the notional RoPax vessel that is similar to one that attained large roll angles in stern waves (MNZ, 2007). This is due to the different specific mechanism of pure loss that was manifested for this ship type. A standard using the second criterion could be set notionally at 0.05. However, this should be examined with the results of additional sample ships which have increased vulnerability for this mechanism of pure loss of stability.

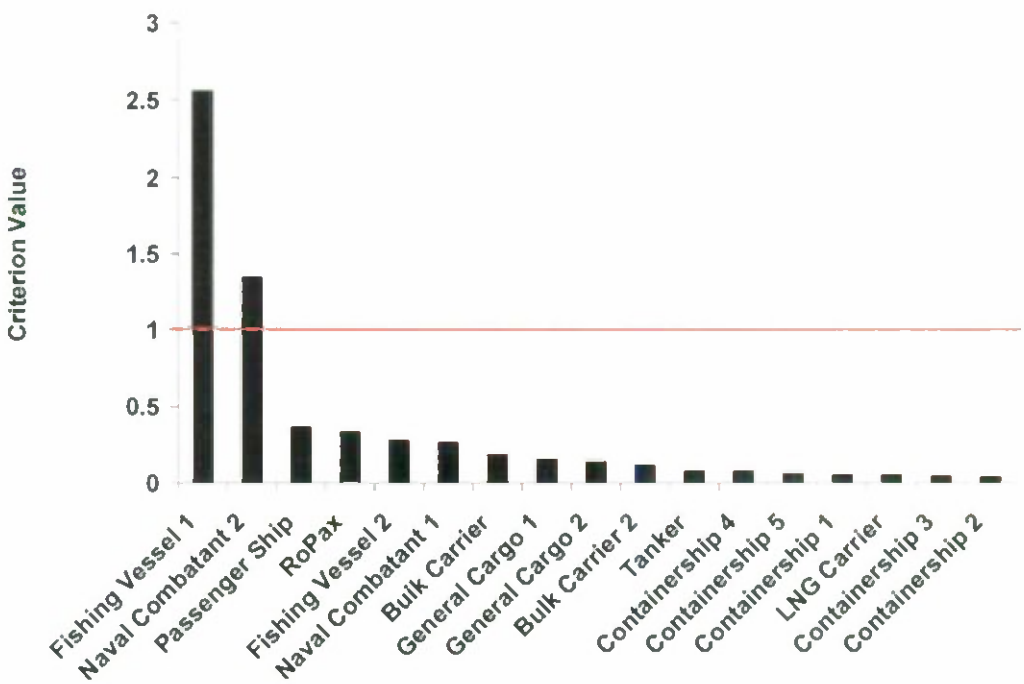

Figure 3.21 Calculation Results for the Level 2 Vulnerability Criterion Cr1 for Pure Loss of Stability for the Sample Ships, Ship Speed of 15 kts, in Sea State 7

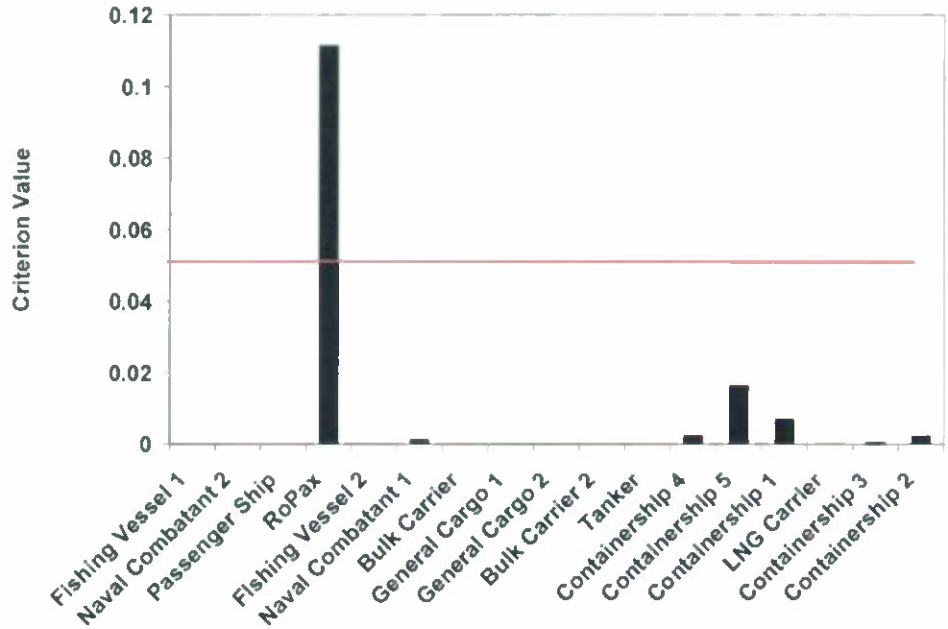

Figure 3.22 Calculation Results for the Level 2 Vulnerability Criterion Cr2 for Pure Loss of Stability for the Sample Ships, Ship Speed of 15 kts, in Sea State 7

Table 3 Results for Vulnerability Level 2 Pure Loss of Stability in Sea State 7

Type	L	GM	Vs	Cr1	Cr2
Fishing Vessel 1 (ITTC A2)	34.5	1.97	15	2.56	0.00
Naval Combatant 2 (ONR TH)	150	1.16	15	1.35	0.00
Passenger Ship	276.4	3.42	15	0.37	0.00
RoPax	137	0.36	15	0.34	0.11
Fishing Vessel 2	21.56	0.51	15	0.28	0.00
Naval Combatant 1 (ONR FL)	150	0.20	15	0.27	0.00
Bulk Carrier	275	4.19	15	0.19	0.00
General Cargo 1 (S60)	121.9	0.15	15	0.16	0.00
General Cargo 2 (C4)	161.2	0.15	15	0.14	0.00
Bulk Carrier 2	145	0.15	15	0.12	0.00
Tanker	320	1.72	15	0.08	0.00
Containership 4	283.2	0.15	15	0.08	0.00
Containership 5 (C11)	262	0.15	15	0.06	0.02
Containership 1	322.6	0.15	15	0.06	0.01
LNG Carrier	267.8	0.15	15	0.05	0.00
Containership 3	330	0.15	15	0.05	0.00
Containership 2	376	0.15	15	0.04	0.00

3.6 Summary

This section describes the development of vulnerability criteria for pure loss of stability. Subsection 3.1 describes the physical background for this mode of stability failure. The likelihood for this type of failure depends on the magnitude of the stability changes, as well as the probability of encountering a dangerous wave.

Taking into account the probabilistic character of pure loss of stability, subsection 3.2 reviews the basics of probability theory which are used for further development of vulnerability criteria. In particular, an emphasis is made on the differences between random variables and stochastic processes.

Because pure loss of stability is a single-wave event, the joint distribution of wave numbers and wave amplitudes is a key to relate pure loss with irregular waves, while also accounting for the relative size of the ship and the waves. Subsection 3.3 reviews a derivation of this joint distribution, based on envelope theory.

A proposal for the level 1 vulnerability criterion is considered in subsection 3.4. The proposal is based on the geometric characteristics of the hull, as these parameters reflect how significantly the waterline may change during a wave pass and therefore, are also related to possible stability deterioration on the wave crest.

Section 3.5 considers two level 2 vulnerability criteria. The first one is based on the average time that the ship's *GM* spends below the critical level during the wave pass. Specification of the critical level is also discussed. The second criterion is based on the likelihood of appearance of very large loll angles during the wave pass. Both criteria are based on the envelope presentation for irregular waves.

Sample calculations were performed using 17 ships.

4 Vulnerability Criteria for Broaching-to and Surf-Riding

This section describes the development of vulnerability criteria for broaching-to, including the physical background of this mode of stability failure. Surf-riding phenomenon usually precedes broaching-to, so determination of the vulnerability for broaching-to can be performed by evaluating a ship's propensity to surf-ride. Additionally, the mathematical background necessary for vulnerability criteria and two methods of calculating the speed, and the development of levels 1 and 2 vulnerability criteria, are presented. Sample calculations were performed using 17 ships.

4.1 Physical Background

Broaching-to is a violent uncontrollable turn, occurring despite maximum steering effort in the opposite direction. As with any other sharp turn event, broaching-to is frequently accompanied with a large heel angle, which may lead to partial or total stability failure. Broaching-to occurs in following and stern-quartering seas.

Broaching-to is usually preceded by surf-riding. Surf-riding occurs when a wave, approaching from the stern, captures a ship and accelerates its to the wave speed (wave celerity). While surf-riding, the wave profile does not vary relative to the ship. Most ships are directionally unstable in the surf-riding situation; this leads to the uncontrollable turn, defined as broaching-to (or often, just "broaching").

Therefore, the likelihood of surf-riding can be used to formulate vulnerability criteria for broaching-to. In order for surf-riding to occur, the wave length must be within the range of 0.75~2.0 of the ship length and the ship speed should be around 75% of the wave celerity (depending on wave steepness). Large ships are less likely to surf-ride, as waves of the necessary lengths usually are simply too fast compared to the ship speed. Also, long and steep waves are rare.

Consider an example of surf-riding. Assume a wave with a length comparable to ship length has a celerity of 30 kts, while the ship's engine is set at an rpm that provides a thrust corresponding to 20 kts in calm water (see Figure 4.1).

Sailing in calm water with a speed set at 20 kts means that the thrust (with account of the thrust reduction) produced by the propulsor equals the resistance at that speed (20 kts). When the wave overtakes the ship, axial wave forces push the ship back and forth, causing the ship to surge. During steady surf-riding, the ship's speed equals the speed of the wave. To move a ship with the speed of the wave (30 kts), the thrust provided by the ship is not sufficient, and there is a difference between the ship's thrust for 20 kts and the resistance of the ship at the (higher) wave speed.

As shown in Figure 4.1, the axial wave (surge) force is too small to compensate for this difference. Therefore, surf-riding is theoretically impossible at this speed condition. As a result, surging is the only possible mode of motion.

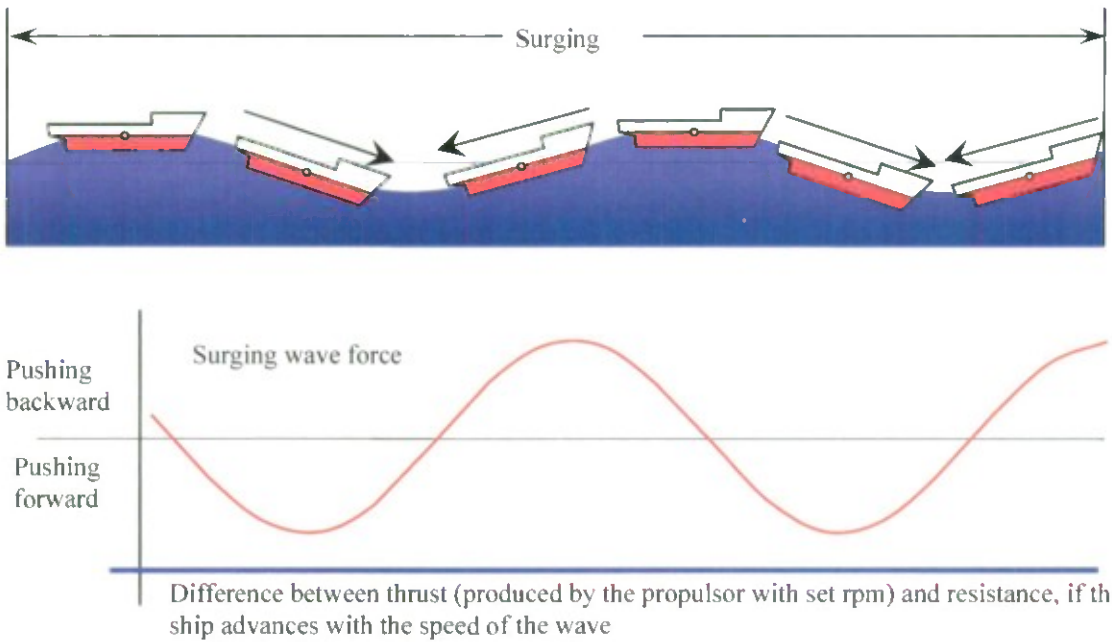

Figure 4.1 Surging in Following Waves. Surf-Riding is Impossible

Consider that the thrust setting has been increased to 22 knots, in calm water. Then the difference between the produced thrust and the resistance at the wave speed has decreased. At this speed, the axial (surge) wave force is enough to compensate for this difference and surf-riding becomes theoretically possible, but only if the ship is at a certain position on the front of the wave (see Figure 4.2).

Surf-riding is a stable equilibrium, achieved when a ship is located on the front slope of the wave close to the trough – shown here with a black dot in Figure 4.2 (another possible equilibrium is unstable – it is located near the wave crest, shown with a white dot in Figure 4.2).

Now, there are two possible modes of motions: surf-riding and surging. The result depends on the ship's location along the wave length and the ship's instantaneous speed. In order to observe surf-riding, the ship must be near the equilibrium and have sufficient instantaneous speed. The first threshold corresponds to a thrust that enables surf-riding to be possible under certain (generally ideal) conditions.

Consider a further increase of the ship's thrust up to 25 knots in calm water. The difference between the ship's thrust and the resistance at the wave speed has further decreased. Now, the axial (surge) force is sufficient enough to cause surf-riding for a ship located anywhere along the front of the wave. Therefore, surf-riding is the only mode of motion, and surging is no longer possible (Figure 4.3).

The 2nd threshold corresponds to the speed setting where the surging ceases to exist and the surf-riding becomes inevitable at every position along the wave and any instantaneous speed.

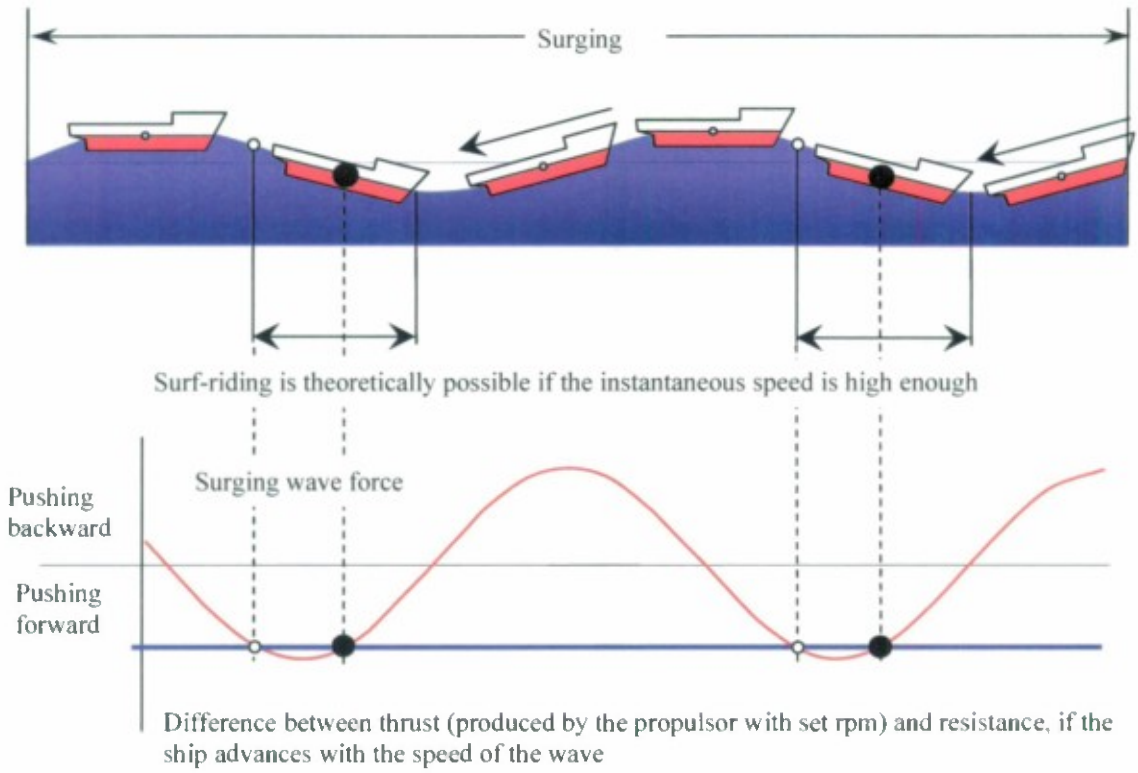

Figure 4.2 Both Surging and Surf-Riding Are Possible, Depending on Position of Wave and Instantaneous Speed

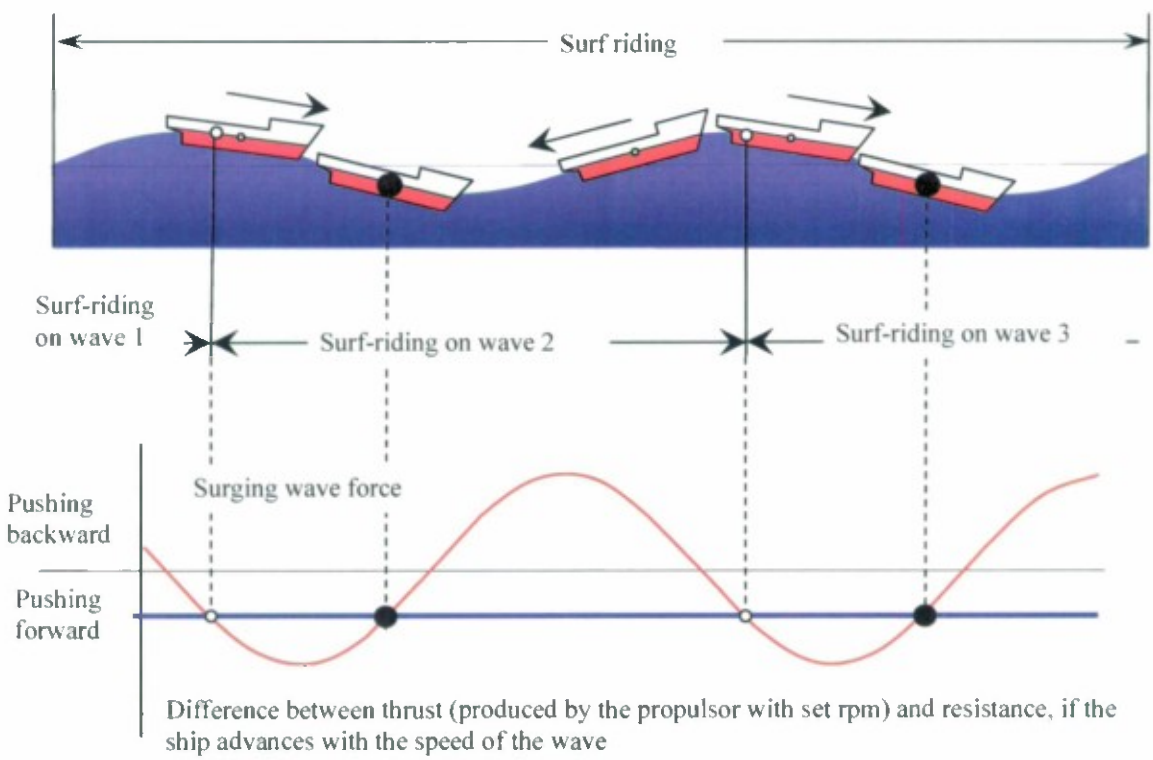

Figure 4.3 Surging is Not Possible - Surf-Riding is the Only Option

Both speed thresholds depend on the wave length and steepness. Therefore, in a realistic seaway they are random figures and the likelihood of exceeding one of these thresholds can be used for vulnerability criteria. The calculations show that the 1st threshold is easy to exceed, but in order to experience surf-riding, the instantaneous speed must be increased significantly when a ship is located at a particular position on a wave. The probability of such a coincidence is quite low. Therefore, to avoid excessive conservatism, the second threshold should be used for the criteria. Once it is exceeded, the surf-riding is guaranteed for this particular wave.

4.2 Mathematical Description of Surf-Riding in Following Seas

4.2.1 Review of Mathematical Tools – Phase Plane Analysis

Phase plane analysis is one of the main tools used in the development of vulnerability criteria for surf-riding. This subsection includes a brief overview of this tool.

A phase plane (sometimes the term "phase portrait" is also used) is a plot of velocity vs. motion. Each of the curves in the phase plane is called "phase trajectory". Each phase trajectory corresponds to a pair of initial conditions. For example, consider a pendulum (Figure 4.4a). The equation of small motions of a pendulum, without damping, is expressed as:

$$\ddot{x} + \omega_0^2 x = 0 \tag{4.1}$$

The two dots above the value x stands for the second derivative in time, i.e. acceleration, and ω_0 is the natural frequency of oscillations. A cosine (or sine) function is an obvious solution for the equation (4.1), as the second derivative of the cosine function turns it into itself, but with an opposite sign:

$$x = \cos \omega_0 t \tag{4.2}$$

$$\dot{x} = \frac{dx}{dt} = -\omega_0 \sin \omega_0 t \tag{4.3}$$

$$\ddot{x} = \frac{d\dot{x}}{dt} = -\omega_0^2 \cos \omega_0 t \tag{4.4}$$

Substitution of (4.2) and (4.4) into differential equation (4.1), turns this equation into a true equality; hence, the function (4.2) is the solution of the equation (4.1).

To reveal the form of the phase trajectory, the angular velocity (4.3) should be expressed through the angle (4.2) and the time should be excluded from the equation. If the angle (4.2) is multiplied by the natural frequency, then squared and added to the squared velocity (4.3), trigonometric functions disappear and the elliptic form of the phase trajectory becomes clear:

$$\omega_0^2 x^2 + \dot{x}^2 = \omega_0^2 \tag{4.5}$$

The phase trajectory described by formula (4.5) is shown in Figure 4.4b. For the solution (4.2), it starts at the point (1,0) of the phase plane. To see the initial conditions corresponding to the solution (4.2), it is enough to set t=0 in the formulae for angle and angular velocity:

$$\begin{aligned} x(t=0) &= \cos\omega_0 t = 1 \\ \dot{x}(t=0) &= \frac{dx}{dt} = -\omega_0 \sin\omega_0 t = 0 \end{aligned} \tag{4.6}$$

The phase trajectory (4.5) corresponds to other initial conditions as well. It can be seen if the sine function is used as the solution of equation (4.1) instead of cosine. Then the initial point will be (0,1). For this effect, a phase shift, ε, can be introduced in the solution (4.2):

$$x = \cos(\omega_0 t + \varepsilon) \tag{4.7}$$

This will move the initial point to (cos(ε), -sin(ε)), but will not change the phase trajectory (4.5), as shown in Figure 4.4b.

It is also easy to see that the introduction of amplitude (different than 1) into function (4.7) does not invalidate it as a solution of the equation (4.1):

$$x = A\cos(\omega_0 t + \varepsilon) \tag{4.8}$$

However, this solution leads to a phase trajectory different than (4.5):

$$\frac{\omega_0^2}{A^2} x^2 + \frac{1}{A^2}\dot{x}^2 = 1 \tag{4.9}$$

This trajectory is also an ellipse, but with different semi-axes, that is concentric to (4.5), see Figure 4.4c. These different ellipses correspond to different initial angles and therefore, show the different amplitude of oscillation of the pendulum.

In general, different initial conditions $(x_0; \dot{x}_0)$ lead to different values of amplitude, A, and phase, ε:

$$A = \sqrt{\omega_0^2 x_0^2 + \dot{x}_0^2}\ ; \quad \varepsilon = \arctan\frac{\dot{x}_0}{\omega_0 x_0} \tag{4.10}$$

The complete phase plane for the pendulum is a family of curves, showing how angular velocity changes with angle for different initial conditions. Figure 4.4c shows the complete phase plane for the small motions of the pendulum, without damping. This type of phase plane, being one of the basic forms, is called a "center" phase plane.

The introduction of damping makes the sinusoidal motions decay and turns the phase plane from a set of ellipses to a set of spirals, see Figure 4.4d. The special term for this type of the phase plane is the "stable focus."

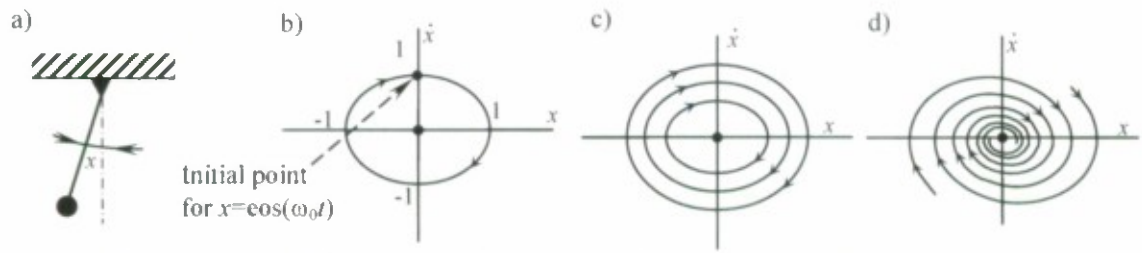

Figure 4.4 Example of an Oseillator – Pendulum (a), Phase Trajeetory without Damping for the Solution x=cos($\omega_0 t$) (b), Phase Plane without Damping (e) Phase Plane with Damping (d)

Equation (4.1) is only valid for small deviations of the equilibrium, where angles are so small that the value of the sine funetion ean be approximated by the value of the angle expressed in radians. Therefore, it does not describe all the features of motions of the pendulum. One of these features is an unstable equilibrium (shown in Figure 4.5a). The "straight-up" position is an equilibrium, as all of the forees are equal there, but it is not stable, as a small perturbation takes the pendulum back to the stable equilibrium. Motions in the vicinity of the unstable equilibrium (without damping) ean also be described by a linear differential equation:

$$\ddot{x} - \omega_0^2 x = 0 \qquad (4.11)$$

The phase plane of these motions is shown in Figure 4.5b. Depending on how the perturbation was delivered (only displacement, only velocity, or both) and how it was directed, the pendulum returns to the stable equilibrium through a right-hand or left-hand rotation. This is also one of the basic forms of the phase plane, called the "saddle."

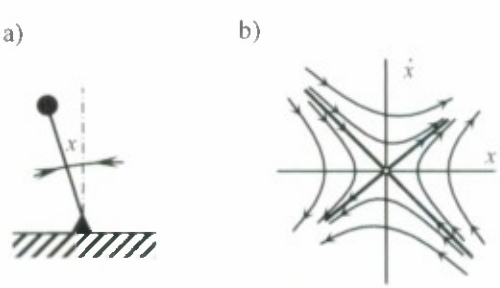

Figure 4.5 (a) Unstable Equilibrium and (b) Phase Plane of Motions in its Vieinity, "the Saddle Point"

To see the whole phase plane of possible motions without damping, one needs to combine the phase planes shown in Figure 4.4c (center) and in Figure 4.5b. (saddle), as there are only two equilibria for the pendulum: the stable one, "straight down," and the unstable one, "straight-up." Because the motion is rotational, the phase plane is expected to repeat after 180 degrees (due to the symmetry of the oscillator). Note, that all the trajectories in Figure 4.5b are curves, with exception of two straight lines (shown in bold). These straight lines connect to each other after 180 degrees, see Figure 4.6, making a boundary separating the ellipses (actually ovals) and sine-like trajectories above and below the thick lines. These sine-like curves correspond to a complete turn of the equilibrium. Because there is no damping, this rotation is infinite.

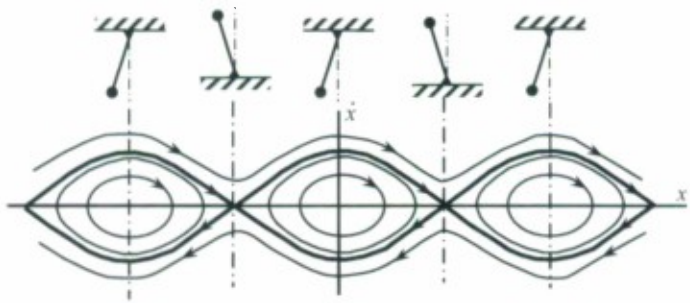

Figure 4.6 Complete Phase Plane for Pendulum without Damping

This boundary trajectory is called the "separatrix," for the cases when there are no external excitations, and an "invariant manifold" for the more general case, when the external excitation is present.

The introduction of damping will turn the ovals into spirals, but the separatrix still separates the initial conditions leading to the immediate attraction to the stable equilibrium from those that allow for at least one complete turn before the oscillator "moves down along the spiral" (see Figure 4.7).

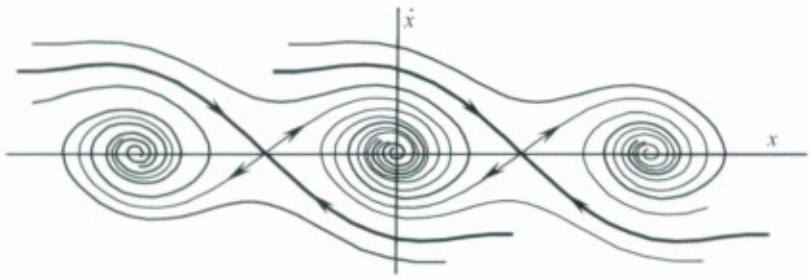

Figure 4.7 Complete Phase Plane for Pendulum with Damping

4.2.2 Mathematical Model of Surging and Surf-Riding

Following (Belenky, *et al.*, 2008), consider the simplest model for surf-riding of a relatively fast vessel in following regular waves. The origin of the coordinate system is located on the wave crest:

$$(m + m_x) \cdot \ddot{\xi}_G + R(c + \dot{\xi}_G) - T(c + \dot{\xi}_G, n) + F_W(\xi_G) = 0 \tag{4.12}$$

Here, m is the mass of the vessel, m_x is longitudinal added mass; R is resistance in calm water, T is the efficient thrust in calm water (with thrust deduction included), c is wave celerity, and F_W is Froude-Krylov wave force. The symbol ξ_G stands for the distance between the wave crest and the center of gravity of the vessel and $\dot{\xi}_G$ is the velocity of the ship relative to the wave celerity Finally, n is the commanded number of revolutions of the propeller— this is an independent parameter, related to the thrust delivered. This equation also uses the assumption that the encounter frequency ω_e is small (so the term containing time - $\omega_e t$ can be dropped from the equation of the wave force).

The Froude-Krylov force is a result of the integration of the incident wave pressure in the absence of the ship over the surface of the hull (a derivation is available from Belenky and Sevastianov, 2007):

$$F_W(\xi_G) = -\rho g k \zeta_A [A_S \sin(k\xi_G) - A_C \cos(k\xi_G)] \tag{4.13}$$

$$A_S = \int_{-0.5L}^{0.5L} A_0(x) \cdot \cos(kx) dx \; ; \quad A_C = \int_{-0.5L}^{0.5L} A_0(x) \cdot \sin(kx) dx \tag{4.14}$$

$$A_0(x) = 2 \int_{d(x)}^{0} y(x,z) \exp(kz) dz \tag{4.15}$$

Here, x, y and z are the coordinates of points on the surface of the hull, expressed in the ship-fixed coordinate system; $y(x, z)$ is the half-breadth on a station with coordinate x at the depth z; $d(x)$ is draft of a station at longitudinal position x; k is the wave number; ζ_A is the wave amplitude; and ρ is mass density of water. Calculation of the Froude-Krylov wave force is straightforward.

Surf-riding occurs as the equilibrium. Its position could be found from equation (4.12), assuming that $\dot{\xi}_G = \ddot{\xi}_G = 0$.

$$R(c) - T(c,n) + F_W(\xi_G) = 0 \tag{4.16}$$

Resistance $R(c)$ and thrust $T(c,n)$ are considered in the system of coordinates fixed to the wave. So the force, $R(c)$, is the resistance required to tow a vessel with a speed equal to wave celerity c. The value $T(c,n)$ is actually the efficient thrust that would be created if a vessel sails with speed c, while the number of revolutions has been set to n.

As can be seen from equation (4.16), the wave force compensates for some of the resistance, so the equilibrium can be achieved for an engine setting less than that which would be required to provide a speed, c, in calm water. That is why the balance between effective thrust and resistance $R(c) - T(c,n)$ is negative during the surf-riding.

Figure 4.8 shows the wave force as a function of the distance from the wave crest and the balance between resistance and thrust superimposed on the wave phase. An intersection of the wave force and the balance between resistance and thrust constitutes the solution of equation (4.16), which is the surf-riding equilibrium. It can be clearly seen that there are two equilibria on each wave: one closer to the wave crest and another one closer to the wave trough.

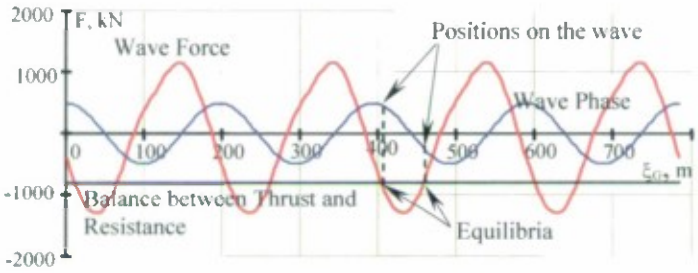

Figure 4.8 Surf-Riding Equilibria for a 100 m High-speed Vessel, Wave Height 6 m, Wave length 200 m, Speed Setting 24 kts (Belenky, *et al.*, 2008)

Engine-speed settings define how far the line of the resistance-thrust balance is from the origin. The line of the resistance –thrust balance is equal to the difference of the calm water resistance of the ship at the wave celerity and the thrust of the propulsor behind the ship i.e. with the thrust deduction included. If these settings are too low, the balance line will never intersect with the curve of the wave force, and equilibria and surf-riding itself are impossible in this case. An engine setting that makes the balance line barely touch the wave force curve is of special interest. Such a setting represents the boundary above which the surf-riding becomes possible for the given wave. The calm water speed corresponding to such a setting usually is referred to as the first critical speed (in this case, it equals 13.53 kts).

If the surf-riding equilibria exist, one of them must be unstable and the other one stable. Similar to the example with a pendulum considered in the subsection 4.2.1, unstable equilibrium must separate stable equilibria. Analysis of the stability of equilibria (a brief description is given in (Belenky and Sevatianov, 2007) shows that the equilibrium in vicinity of the wave crest is unstable and the equilibrium near the wave trough is stable.

The next step of the analysis is to determine what types of motions in waves are possible, using phase plane analyses. This result is shown in Figure 4.9. Four equilibria are shown in this figure. Two stable equilibria have stable-focus-type of the phase plane surrounding them. They can be recognized by the sets of spirals, pulling the dynamical system towards the stable equilibria, located at the points with coordinates (-150, 0) and (50, 0). The stable equilibria are separated by the unstable equilibria located at the points with coordinates (5,0) and (-195,0).

The phase plane in the vicinity of the unstable equilibria is a saddle point (Figure 4.5). As it was noted before, one should pay particular attention to the two straight lines of the saddle point, as they can be part of the boundary separating the initial conditions corresponding to the different types of motions. In the case of the pendulum without

damping (Figure 4.6), both these lines are part of the boundary between oscillatory motion and rotation. In case of the damped pendulum (Figure 4.7), one line (with the negative slope) belongs to the boundary.

The dynamical system describing surging and surf-riding is somewhat similar to the damped pendulum: compare Figure 4.7 and Figure 4.9. The straight line of the saddle point with the negative slope is a part of the boundary separating the initial conditions leading to surf-riding and surging. As the origin of the coordinate system is located at wave crest and moving with the wave celerity, the surging motion is shown as a sine-like curve in this phase plane. The point moves backwards along this curve with the time passed, because the average speed of the ship in surging mode is less than the wave celerity, so if the origin is moving with the wave, the ship in this coordinate system must be moving backwards.

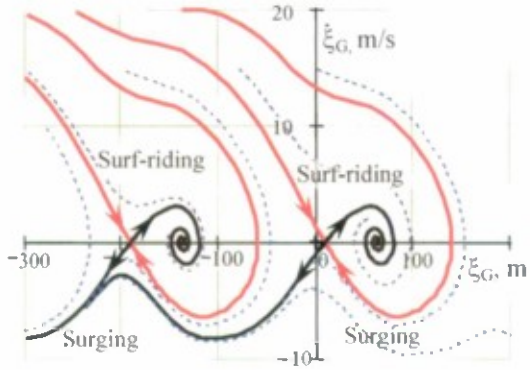

Figure 4.9 Phase Plane with Surging and Surf-Riding, Speed 22 Knots

Initial conditions corresponding to surging are located below and between the boundaries. The phase plane also helps to understand how surf-riding can occur when a ship is sailing with the speed of 22 knots (in the considered example). Assume that the ship is surging, therefore, the waves are overtaking her. The average speed is somewhere around -6.4 m/s in the coordinate system of the Figure 4.9, meaning that the wave celerity exceeds the ship speed at 6.4 m/s.

It can be also checked by a simple calculation, knowing that the wave length is 200 m and ship speed is 22 knots:

$$k = \frac{2\pi}{\lambda} = 0.031 m^{-1} \; ; \; \omega = \sqrt{kg} = 0.555 s^{-1} \; ; \; T = \frac{2\pi}{\omega} = 11.3 s$$
$$c = \frac{\lambda}{T} = 17.7 m/s \; ; \; V = 0.51444 \cdot 22 kn = 11.3 m/s \qquad (4.17)$$

So, in order to get into the surf-riding zone, the ship needs to be suddenly accelerated when she is at the particular spot on the wave. For example, if she is at the wave through (100 m in Figure 4.9), she may need another 3 m/s to surf-ride (visually from Figure 4.9). If she is around the wave crest, the speed addition is probably around 5 m/s, and so on.

Practically speaking, it is difficult to imagine how the ship can be accelerated with an additional of another 6 or 10 knots without changing speed settings. Therefore, in the considered example, the surf-riding at 22 knots setting, while theoretically possible, is not very likely.

Increasing the engine setting up to 24 knots in calm water leads to a dramatic change in the phase plane (see Figure 4.10). The boundaries between surging and surf-riding are unfolded. There is no longer any possibility of surging and the boundaries simply divide domains of attractions to the current or the next (or previous) wave.

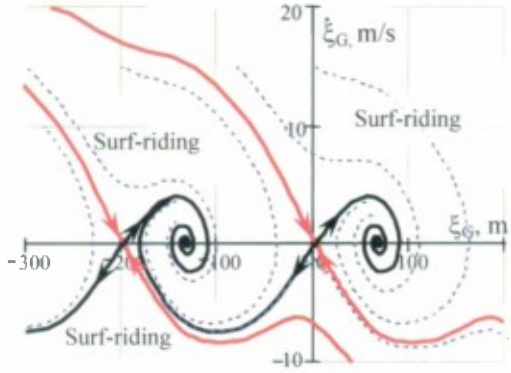

Figure 4.10 Phase Plane with Surf-Riding Only, Speed 24 knots

Somewhere between 22 and 24 knots, there is a speed that separates two distinct topologies of the phase planes: when surf-riding is only a possibility and when it coexists with surging. This speed (for the considered example, 23.3.knots) is commonly referred to as the second critical speed. In nonlinear dynamics, this is regarded as a type of global bifurcation, known as the heteroclinic saddle connection ("homoclinic" if one considers the cylindrical nature of system's phase space). The dynamics of surf-riding in quartering seas (as well as the consequence of broaching-to) due to this global bifurcation was identified and discussed in Spyrou (1996), on the basis of a surge-sway-yaw-roll model which produced the necessary connection between surf-riding and broaching-to behavior (see also Spyrou 2000).

To see the complete picture of development of this global bifurcation, it is more convenient to re-plot the phase plane in the cylindrical coordinate system, and the position on the wave is presented as:

$$\xi_G \rightarrow \cos\left(\frac{2\pi\xi_G}{\lambda}\right) \tag{4.18}$$

where λ is the length of the wave, while the velocity coordinate $\dot{\xi}_G$ remains the same. This transformation turns the sine-like trajectory of surging in Figure 4.9 into a closed oval-like curve, similar to the oscillatory mode of the pendulum without damping. The surf-riding equilibria still appear as points.

This picture is shown in Figure 4.11, as a set of changing phase planes, while the speed setting is changed. The first phase plane contains only surging, while surf-riding is

not possible. This is the situation shown in Figure 4.1, where surging force is insufficient to accelerate the ship to the wave celerity. The origin of the coordinate system is still located at the wave crest, but the periodic surging is seen as an oval due to the coordinate transformation (4.18).

The second phase plane in Figure 4.11 corresponds to the speed setting exactly at the first critical speed. The wave surging force just touches the balance between the thrust and resistance. This is a sort of degenerate case when the stable and unstable equilibria are located at the same point. The appearance of this point, however, disturbs the shape of the surging cycle: so it is no longer an oval.

The third phase plane in Figure 4.11 reflects the situation shown in Figure 4.2 and Figure 4.9. Surging and surf-riding co-exist, but the possibility of surf-riding is practically remote. The shape of the surging cycle, however is more disturbed as the unstable equilibrium gets closer; despite the equilibrium being unstable, it is still capable of accelerating the ship– note that the surging trajectory has a maximum near the saddle point in Figure 4.9.

The fourth phase plane describes the "surf-riding only" situation (shown in Figure 4.3 and Figure 4.10). All of the initial conditions lead to the surf-riding equilibria and the periodic surging cycle no longer exists.

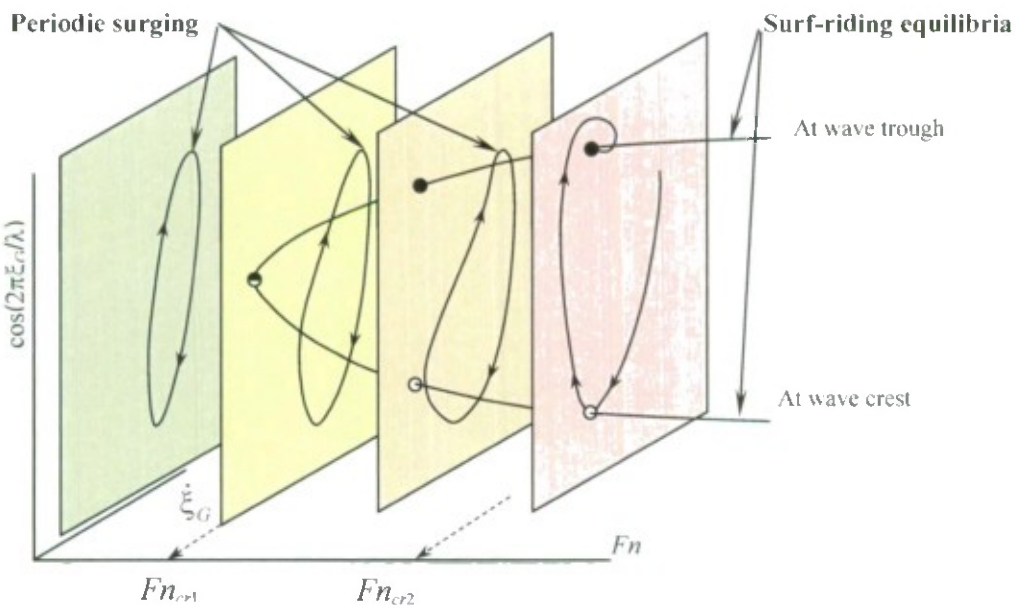

Figure 4.11 Changing of Surging and Surf-riding Behavior with Increasing Speed Settings - Nominal Froude Number (based on Spyrou 1996)

The examination of the dynamics of surging and surf-riding shows that the criteria for danger of surf-riding should be based on the second critical speed, or the second threshold. It truly separates the situations where surf-riding is inevitable.

4.2.3 Direct Numerical Method for the Second Threshold

Phase plane analysis allows one to find the second threshold by calculation of the boundaries and determining a speed when the boundary unfolds in the way shown in Figure 4.10.

One point of this boundary is known. It is the unstable equilibrium. Strictly speaking, the boundary consists of two phase trajectories, both of which take the system towards the unstable equilibrium. These trajectories also can be seen in Figure 4.5b as spanning through the II and IV quadrant.

Because the trajectories lead toward the equilibria, in order to find these trajectories, the equation (4.12) should be integrated backwards in time. Numerically it does not make any difference, as a mechanical problem expressed in an ordinary differential equation is completely reversible. Integration forward reveals the future, while integration backwards in time reveals the past of the motion. The phase trajectories found in such a way are unique. There are only two trajectories leading to the unstable equilibrium (see Figure 4.5b).

What happens if the integration of equation (4.12) starts with initial conditions which correspond exactly to the saddle point? The initial position on the wave corresponds to the unstable equilibrium and the speed is zero. Numerical integration of the equation forward in time takes the dynamical system from the equilibrium. As the equilibrium is unstable any disturbance takes the system away from it. The rounding error plays a role of this initial disturbance in the case of numerical integration of the equation (4.12). Depending on the sign of this error, the dynamical system ends up either with surf-riding or surging, as in the case of co-existence shown in Figure 4.9. In the case of surf-riding only, shown in Figure 4.10, the system goes to surf-riding either on this or the next wave.

If the integration is done backwards in time, the system will move along the boundary. Again, depending on the sign of the rounding error, the system "chooses" the boundary going through quadrant II or through quadrant IV. In order to avoid this uncertainty, it makes sense to introduce an initial small disturbance in the direction of the boundary, as shown in Figure 4.12.

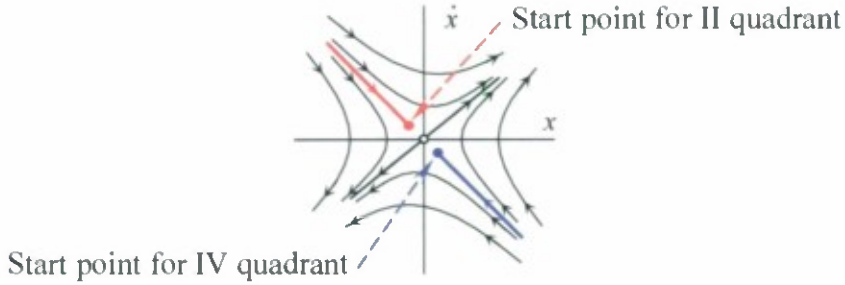

Figure 4.12 Initial Conditions for Calculation of the Boundary

To calculate the disturbance, equation (4.12) can be linearized. The linear differential equation has a solution that is expressed with elementary functions. This solution can be used to set the initial point of integration.

Linearization of the equation (4.12) involves linearization of the wave force at the unstable equilibrium (see Figure 4.13) and the balance between thrust and resistance.

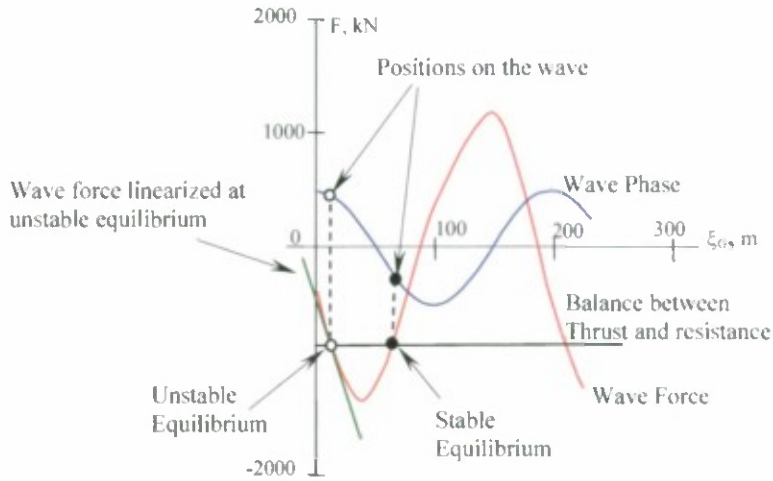

Figure 4.13 Linearization of Surging Wave Force at Unstable Surf-riding Equilibrium

The linearized wave surging force is expressed as

$$F_{WL}(\xi_G) = K_{WL}(\xi_G + \xi_{GU}) \tag{4.19}$$

Where ξ_{GU} is a location of unstable equilibrium, and K_{WL} is the slope coefficient:

$$K_{WL} = \left.\frac{dF_{WL}(\xi_G)}{d\xi_G}\right|_{\xi_G = \xi_{GU}} \tag{4.20}$$

The influence of the surging speed on thrust can be neglected in the first expansion. Also as the surging speed can be assumed small in comparison with wave celerity, resistance can be linearized:

$$R_L(c + \dot{\xi}_G) = K_{RL}(\dot{\xi}_G + c) \tag{4.21}$$

K_{RL} is the slope coefficient for the resistance

$$K_{RL} = \left.\frac{dR(\dot{\xi}_G)}{d\dot{\xi}_G}\right|_{\dot{\xi}_G = c} \tag{4.22}$$

Then, the surging equation, linearized near the unstable equilibrium, is expressed as:

$$(m+m_x)\cdot\ddot{\xi}_G + K_{RL}\dot{\xi}_G + K_{WL}\xi_G = T(c,n) - R(c) - K_{WL}\xi_{GU} \tag{4.23}$$

The value in the right hand side is a constant, depending on the wave characteristics and the thrust settings. Re-writing equation (4.23) into standard form yields:

$$\ddot{\xi}_G + 2\delta_x\dot{\xi}_G - k_{WL}\xi_G = b_U \tag{4.24}$$

Here b_U is a constant expressing that the equation has been linearized at the unstable equilibrium:

$$b_U = \frac{T(c,n) - R(c) - K_{WL}\xi_{GU}}{(m+m_x)} \tag{4.25}$$

The expression for the "repelling" coefficient k_{WL} accounts for its negative value (it is always the case for the unstable equilibrium):

$$k_{WL} = -\frac{K_{WL}}{(m+m_x)} \tag{4.26}$$

Finally δ_x plays a role of the damping coefficient:

$$\delta_x = \frac{K_{RL}}{2(m+m_x)} \tag{4.27}$$

The linearized equation (4.25) describes the motion near the unstable equilibrium. Its phase portrait is a saddle point. It is very similar to the equation (4.11); the only difference is that it contains a damping term and a constant.

The objective of all these derivations is to determine the position of the starting points for integration, as shown in Figure 4.12. Equations for the straight lines leading to and from the unstable equilibrium can be found using the characteristic equation of the linear differential equation

$$\lambda^2 + 2\delta_x\lambda - k_{WL} = 0 \tag{4.28}$$

Two solutions of the characteristic equation, the eigenvalues, are expressed as:

$$\lambda_{1,2} = -\delta_x \pm \sqrt{\delta_x^2 + k_{WL}} \tag{4.29}$$

As it is well known from the linear theory of oscillators (see, for example Andronov, *et al.* 1966), the straight line trajectories of the saddle point can be expressed using the eigenvalues, see Figure 4.14.

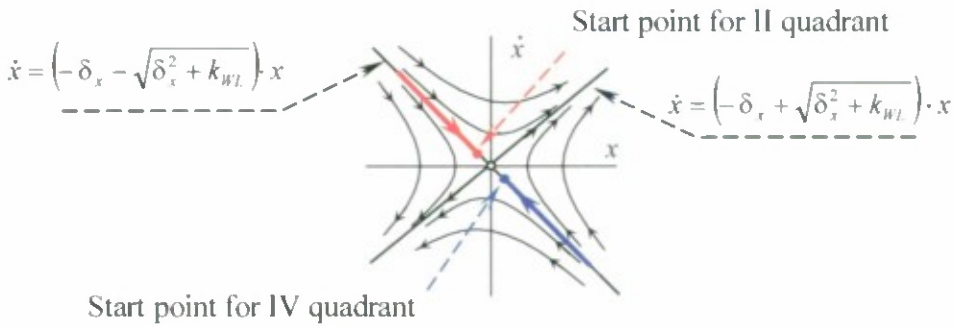

Figure 4.14 On the Calculation of the Initial Conditions for Calculation of the Boundary

Once the equation for the straight line trajectories of the saddle point have been defined, setting the initial points for the integration is trivial, as even a small disturbance from the unstable equilibrium (like 0.1 m) will serve the purpose. Integration of the equation (4.12) backwards in time does not produce any difficulties, with the exception of setting the end point.

Calculations of the boundary are repeated for a series of thrust settings, until a critical one, corresponding to unfolding of the boundary, is found. As it was shown above, the nominal Froude number corresponding to the unfolding of the boundary is the second threshold.

4.2.4 Approximate Method for the Second Threshold

The direct numerical method for calculation of the second threshold has a solid technical background, but may require calculations that may be too cumbersome, even for a second level of vulnerability check.

Instead, an approximate method, namely Melnikov's method, can present a practical solution (Spyrou 2006). The main idea is based on the fact that the boundaries touch each other when the speed/thrust settings correspond to the second threshold. While it is not possible to catch this exact instant, the tendency can be very clearly seen in Figure 4.15.

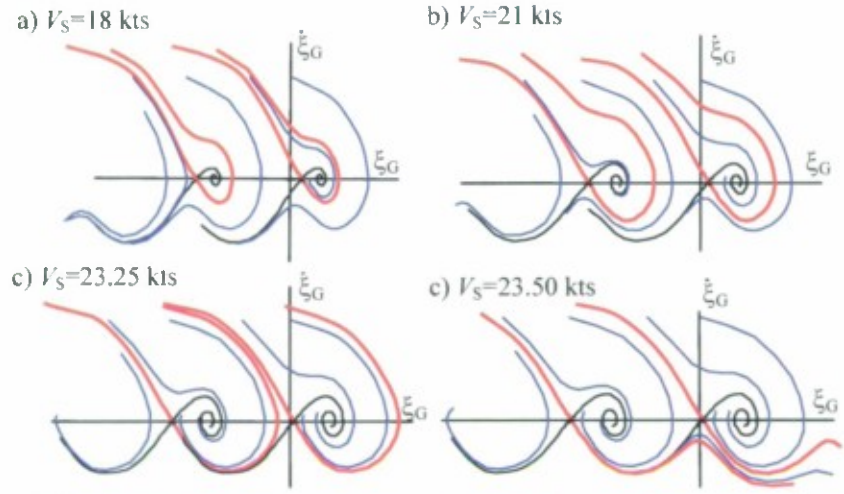

Figure 4.15 Change of Location of the Boundary while Approaching the 2nd Threshold

Melnikov's function is defined as the distance between the two boundaries. Therefore, the instant of achieving the second threshold corresponds to the zero-value of Melnikov's function.

A closed form expression of Melnikov's function is available for a dynamical system that can be approximated as a perturbation from the Hamiltonian system (here it mean autonomos dynamieal system e.g. pendulum without an external forcing). Praetieally, it means that the system should be lightly damped, as a Hamiltonian system includes nonlinearity in restoring. As a result, Melnikov's method, in eontrast with other perturbation methods, does require small nonlinearity in restoring to be applicable (Guckenheimer & Holms, 1983).

To apply Melnikov's method, thrust and resistance need to be expressed with elementary funetions. The solution available from Spyrou (2006) uses a polynomial approximation for thrust and resistance:

$$R(V_S) = r_1 V_S + r_2 V_S^2 + r_3 V_S^3 \tag{4.30}$$

$$T(V_S, n) = \tau_0 n^2 + \tau_1 V_S n + \tau_2 V_S^2 \tag{4.31}$$

Here r_1, r_2 , r_3 are polynomial eoefficients for resistance that ean be evaluated with standard regression methods.

The coefficients τ_0, τ_1 , τ_2 for thrust are defined as

$$\tau_0 = c_0(1-t_p)\rho D^4 \tag{4.32}$$

$$\tau_1 = c_1(1-t_p)(1-w_p)\rho D^3 \tag{4.33}$$

$$\tau_2 = c_2(1-t_p)(1-w_p)^2 \rho D^2 \tag{4.34}$$

Here t_p is the eoeffieient for thrust deduction, while w_p is the wake fraction eoefficient. Both coefficients are evaluated for calm water. D is the propeller diameter and ρ is mass

density of water. Coeffieients c_0, c_1, c_2 came from polynomial presentation of the coefficient of thrust K_T:

$$K_T = c_0 + c_1 J + c_2 J^2 \tag{4.35}$$

Where J is the advance ratio

$$J = \frac{V_S(1 - w_p)}{nD} \tag{4.36}$$

Then the balanee between the resistance and thrust in the equation (4.12) can be expressed as:

$$\begin{aligned} &R(c + \dot{\xi}_G) - T(c + \dot{\xi}_G, n) = \\ &\qquad A_1(c,n)\dot{\xi}_G + A_2(c)\dot{\xi}_G^2 + A_3\dot{\xi}_G^3 + R(c) - T(c,n) \end{aligned} \tag{4.37}$$

Here:

$$A_1(c,n) = 3r_3c^2 + 2(r_2 - \tau_2)c + r_1 - \tau_1 n \tag{4.38}$$

$$A_2(c) = 3r_3c + 2(r_2 - \tau_2) \tag{4.39}$$

$$A_3 = r_3 \tag{4.40}$$

To apply Melnikov's method, the equation (4.12) should be transformed into the non-dimensional form:

$$x'' + p_1x' + p_2x'^2 + p_3x'^3 + \sin x = \frac{r}{q} \tag{4.41}$$

Here:

$$x = k\xi_G \tag{4.42}$$

k is the wave number (spatial frequency)

$$q = \frac{k \cdot A_{Fw}}{m + m_x} \tag{4.43}$$

A_{Fw} is amplitude of surging wave foree:

$$A_{Fw} = \rho g k \zeta_A A_S \tag{4.44}$$

Note, that the eosine eomponent in formula (4.13) is negleeted, as it is small in eomparison with the sine eomponent, especially for long waves.

Coeffieients p_1, p_2, p_3 represent the ehange of resistanee and thrust:

$$p_1 = p_1(n) = \frac{A_1(c,n)}{\sqrt{kA_{Fw}(m + m_x)}} \tag{4.45}$$

$$p_2 = \frac{A_2(c)}{k(m + m_x)} \tag{4.46}$$

$$p_3 = \frac{A_3\sqrt{A_{Fw}}}{\left(\sqrt{k(m+m_x)}\right)^3} \tag{4.47}$$

The coefficient r (without any index) reflects the difference between resistance and thrust at the wave celerity

$$r(n) = \frac{k(T(c,n) - R(c))}{(m+m_x)} \tag{4.48}$$

Finally, equation (4.41) is written in the non-dimensional time, expressed as

$$\tau = \sqrt{q}\, t \tag{4.49}$$

The Melnikov's function for the equation (4.41) and given speed settings is expressed as (from Spyrou, 2006):

$$M(n) = -\frac{r(n)}{q} - \frac{4}{\pi} p_1(n) + 2p_2 - \frac{32}{3\pi} p_3 \tag{4.50}$$

Note that all the coefficients in the formula (4.50) are dependent of the elements of wave: amplitude, wave number, and wave celerity.

The number of revolutions corresponding to the second threshold n_{Tr2} can be found from (4.50), by satisfying the condition:

$$M(n_{tr2}) = 0 \tag{4.51}$$

The expression (4.51) is a nonlinear algebraic equation and can be solved with any appropriate numerical method.

4.2.5 Sample Calculations

This subsection presents sample calculations including the evaluation of the second threshold with the Melnikov's method, using equation (4.51) and the direct numerical method described in the subsection 4.2.3. The calculations were performed for the sample population of 17 ships.

Resistance in calm water was estimated using the method developed by Holtrop (1984). While this estimate may be not very accurate, nevertheless it seems to be acceptable for the sample vulnerability check; it is enough if the resistance estimate

captures just the principle features of the resistance curve. Then the resistance curve was approximated with the third-order polynomial (4.30). The result for the Fishing Vessel 1 (ITTC ship A2) is shown in Figure 4.16.

Thrust was modeled with the open-water propeller data by Oosterveld and van Oossanen (1975). The thrust coefficient curve was approximated with the second-order polynomial (4.31). The result for the Fishing Vessel 1 (ITTC Ship 2) is shown in Figure 4.17. The interaction between the propeller and the hull was estimated using data from Holtrop (1984)

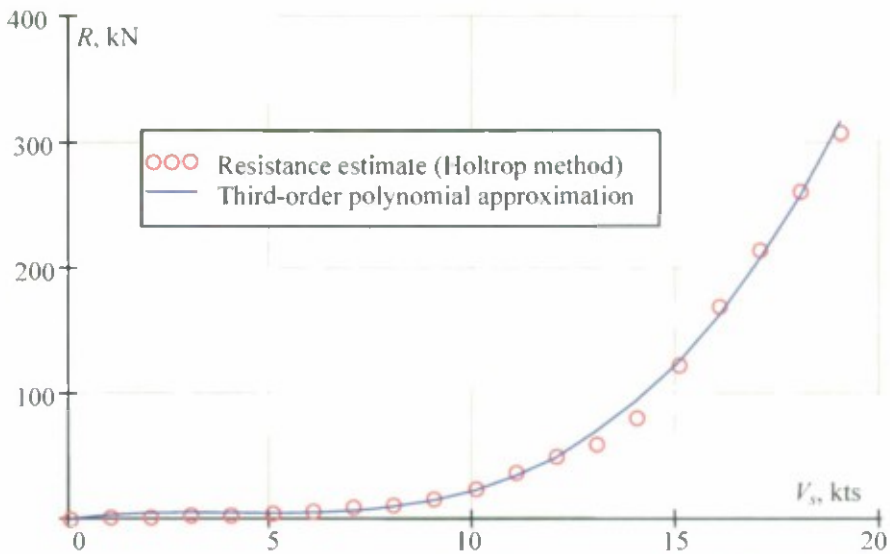

Figure 4.16 Approximation of Calm Water Resistance Curve with the Third-Order Polynomial for Fishing Vessel 1 (ITTC A2)

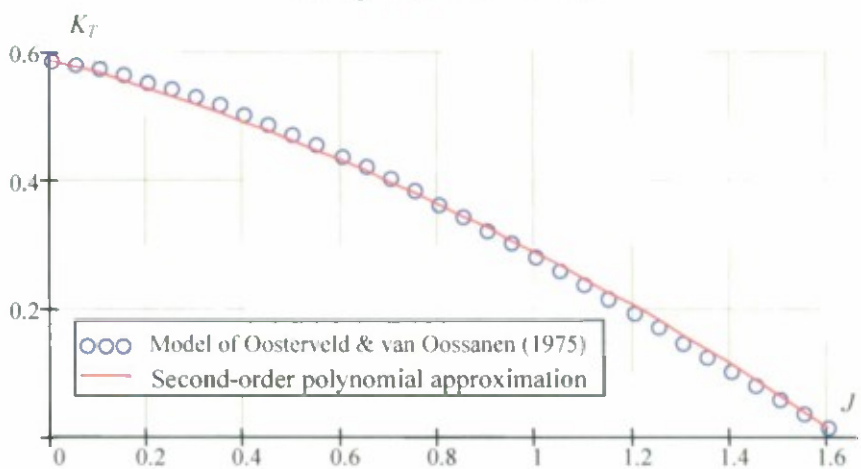

Figure 4.17 Approximation of Thrust Coefficient with the Second-Order Polynomial for Fishing Vessel 1 (ITTC A2)

For all the sample calculations, the surging added mass acted as 10% of the mass of the ship. The wave length was taken equal to the ship length while the steepness was taken as 1/15. Figure 4.18 shows Melnikov's function for the Fishing Vessel 1 (ITTC Ship A2).

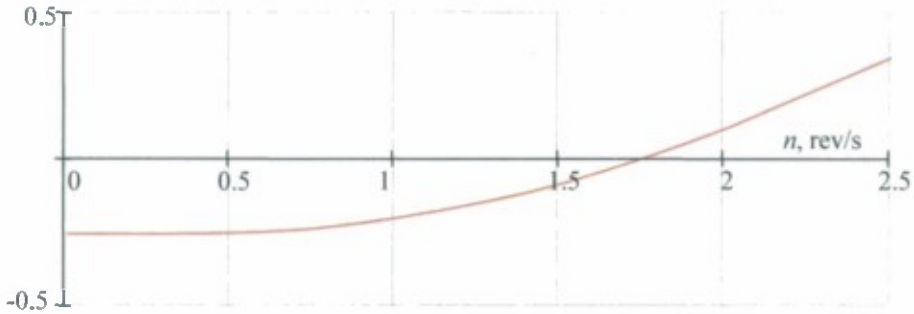

Figure 4.18 Melnikov's Function for Fishing Vessel 1 (ITTC A2)

The number of revolutions corresponding to the second threshold was calculated for each sample vessel using equation (4.51). Figure 4.19(a) shows boundaries of surf-riding mode (stable invariant manifold) calculated for this number of revolution (the sample ship is Fishing Vessel 1). The topology of the phase plane is similar to the one shown in Figure 4.15(c) and corresponds to co-existence of surging and surf-riding. However, the shape of the curve hints that the second threshold is near, as the flexion of the curve becomes sharp around 35 m in Figure 4.19(a).

A slight change of the number of revolutions leads to a dramatic change of the shape of the boundary shown in Figure 4.19(b). This is true for the second threshold (the calculation of the number of revolutions was performed up to the third significant digit). The results of these calculations for the entire sample population of ships are summarized in Table 4.

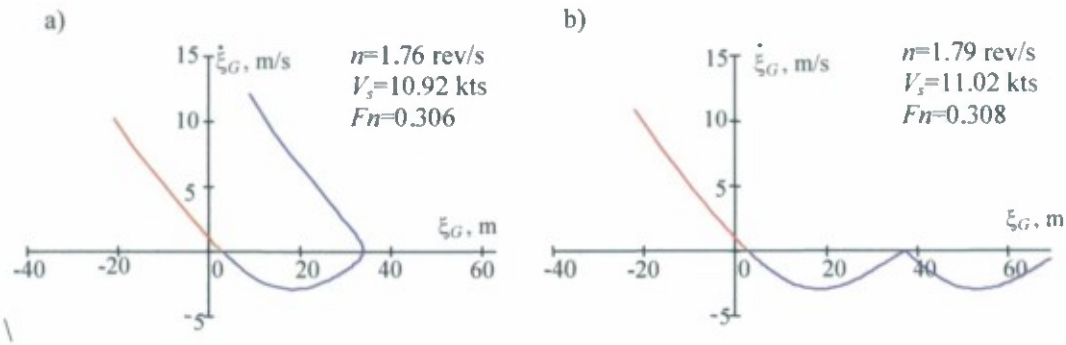

Figure 4.19 Stable Invariant Manifold (a) Corresponding to the Zero of Melnikov's Function (b) Corresponding to the Second Threshold to the Third Significant Digit

As can be seen from Table 4, the true values of the number of revolutions, as well as corresponding figures for the commanded speed and nominal Froude number, are slightly higher that the values estimated using Melnikov's method. These differences are also shown in Figure 4.20 and Figure 4.21.

The difference between the results of Melnikov's method and the direct numerical computation generally is small. Based on the sample population of ships, it can be concluded that Melnikov's method is slightly more conservative than the direct numerical

method, while being much simpler and less expensive in terms of the necessary calculations.

Table 4 Results of Sample Calculation for the Second Threshold

Ship Type	Wave		Melnikov's Method			Direct Calculations		
	λ, m	h, m	n 1/s	Vs, kts	Fn	n, 1/s	Vs, kts	Fn
Fishing Vessel 2	21.56	1.44	3.31	8.54	0.302	3.32	8.56	0.303
Fishing Vessel 1 (ITTC A2)	34.5	2.30	1.76	10.92	0.306	1.79	11.02	0.308
General Cargo 1 (S60)	121.9	8.13	3.35	19.91	0.296	3.37	19.98	0.297
RoPax	137	9.13	3.87	20.42	0.287	3.88	20.46	0.287
Naval Combatant 1 (ONR FL)	150	10.00	3.24	21.09	0.283	3.24	21.11	0.283
Naval Combatant 2 (ONR TH)	150	10.00	3.23	21.09	0.283	3.24	21.11	0.283
General Cargo 2 (C4)	161.2	10.75	3.91	21.33	0.276	3.93	21.42	0.277
Bulk Carrier 2	145	9.67	3.98	23.41	0.319	3.99	23.43	0.320
Containership 5 (C11)	262	17.47	1.82	27.99	0.284	1.83	28.07	0.285
Passenger Ship	276.4	18.43	3.42	28.10	0.278	3.43	28.17	0.278
Containership 4	283.2	18.88	2.15	29.20	0.285	2.16	29.33	0.286
LNG Carrier	267.8	17.86	2.77	30.17	0.303	2.78	30.22	0.303
Containership 1	322.6	21.50	2.00	30.59	0.280	2.01	30.64	0.280
Containership 3	330	22.00	2.07	32.13	0.291	2.08	32.20	0.291
Bulk Carrier	275	18.33	3.03	32.25	0.320	3.03	32.27	0.320
Containership 2	376	25.06	2.03	33.38	0.283	2.04	33.45	0.283
Tanker	320	21.34	4.45	34.40	0.316	4.47	34.54	0.317

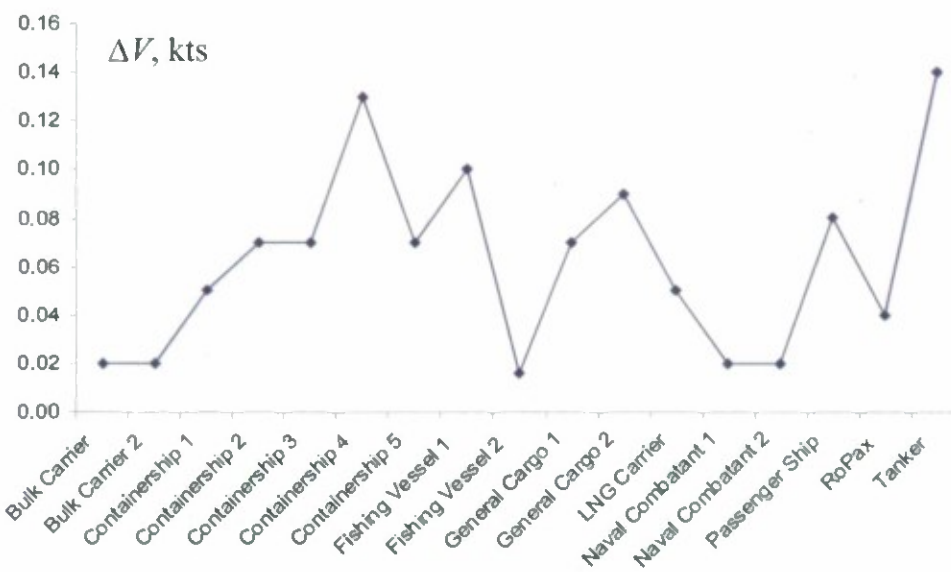

Figure 4.20 Difference in Terms of Nominal Speed (kts) between the Melnikov's Method and Direct Calculation for the Second Threshold

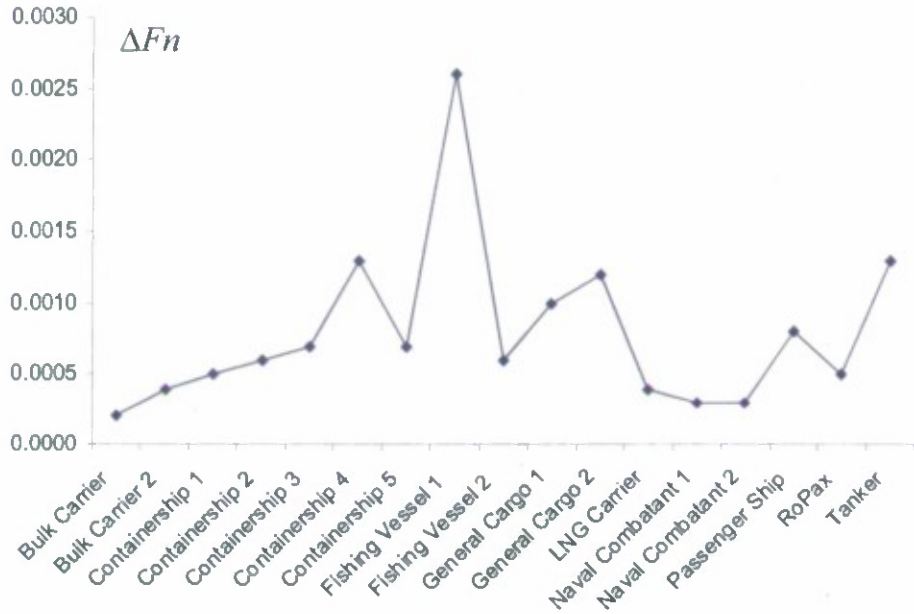

Figure 4.21 Difference in Terms of Nominal Froude Number between the Melnikov's Method and Direct Calculation for the Second Threshold

4.3 Level 1 Vulnerability Criteria

4.3.1 Second Threshold as a Background for the Level 1 Criterion

The document MCS.1/Circ. 1228 uses the following formula as an indicator of possible danger of surf-riding and following broaching-to.

$$V_S \geq \frac{1.8\sqrt{L}}{\cos(180-\alpha)}, \text{ kts} \tag{4.52}$$

Where L is length of the ship and α is a wave heading, 0 being head waves.

Assuming following waves (α =180°) and transforming (4.52) into the form of Froude number yields:

$$Fn \geq \frac{1.8 \cdot 0.51444}{\sqrt{g}} = 0.296 \approx 0.3 \tag{4.53}$$

Annex 3 of the document SLF 53/INF.10 states that this value is related with the nominal Froude number corresponding to the second threshold. As it can be seen from Table 4, values of the nominal Froude number are around 0.3. The average Froude number over the considered sample population equals 0.294.

Generally, it is a known fact and can be seen from Table 4, that the Froude number corresponding to the second threshold is varying in a relatively narrow range: from 0.277 to 0.320.

At the same time, all of the calculations in Table 4 were made for a wave with the length equal to ship length and wave steepness of 1/15. As the length of the ships in sample population varied significantly, the likelihood to encounter such a wave varies significantly from ship to ship. Therefore, the sample ships were not evaluated in equivalent conditions.

Surf-riding and broaching-to is caused by steep waves. The probability of encountering a long, steep wave is less than the probability of encountering a short and steep wave. Therefore, accepting Fn=0.3 as an "across-the-board" criterion and standard may unnecessarily penalize large ships. Thus, the size of a ship (at least its length) needs to be included in the criterion.

4.3.2 Relation between the Second Threshold and Steepness

To account for ship size, the irregularity of waves needs to be brought into consideration. Then the likelihood of encountering a wave capable of causing surf-riding can be quantified with a probability using a known distribution of wave characteristics.

A reference ship is then chosen. The reference probability of surf-riding can be evaluated for such a vessel. Then, a wave steepness can be found that leads to the probability of surf-riding that equals the reference probability. This will lead to the boundary for Froude number that depends on ship length.

The first step is to find the dependence of nominal Froude number corresponding to the second threshold on wave steepness. The most straightforward way to do this is to perform a calculation of the wave surging force, estimate resistance and thrust, and then apply Melnikov's method, as it was described in subsections 4.2.3 and 4.2.5. However, these calculations cannot be required for the first level of vulnerability check, as they are too complex for the first level. Therefore, the criterion should be based on pre-calculated data and approximations cannot be avoided.

Table 5 contains the results of the calculation of the nominal Froude number, corresponding to the second threshold, carried out for the sample ship population for a series of wave steepness. Melnikov's method was used. Figure 4.22 represents a graphical depiction of these results.

As it can be clearly seen from Figure 4.22, the values of Froude number change almost equidistantly with the wave steepness. Also the variation of the values of Froude numbers is not that significant, considering the diversity of the sample ship population.

Table 5 Second-Threshold Froude Number, as a Function of Wave Steepness

Fishing Vessel 2 L=21.56 m												
		Steepness λ/h										
λ/L	λ, m	40	30	24	22	20	18	16	14	12	10	8
0.750	16.170	0.330	0.327	0.325	0.324	0.323	0.322	0.321	0.319	0.317	0.314	0.311
1.000	21.560	0.338	0.329	0.321	0.318	0.314	0.310	0.305	0.299	0.292	0.283	0.271
1.250	26.950	0.356	0.344	0.333	0.328	0.323	0.317	0.310	0.302	0.293	0.281	0.266
1.500	32.340	0.377	0.361	0.348	0.343	0.337	0.330	0.322	0.313	0.301	0.288	0.270
1.750	37.730	0.398	0.381	0.366	0.360	0.353	0.346	0.337	0.326	0.313	0.298	0.279
2.000	43.120	0.419	0.400	0.383	0.377	0.369	0.361	0.352	0.341	0.328	0.313	0.290
Fishing Vessel 1 (ITTC A2) L=34.500 m												
		Steepness λ/h										
λ/L	λ, m	40	30	24	22	20	18	16	14	12	10	8
0.750	25.880	0.333	0.331	0.329	0.328	0.327	0.326	0.325	0.324	0.322	0.320	0.317
1.000	34.500	0.339	0.330	0.323	0.320	0.316	0.313	0.308	0.303	0.297	0.289	0.279
1.250	43.130	0.358	0.346	0.336	0.332	0.327	0.322	0.316	0.310	0.302	0.293	0.282
1.500	51.750	0.379	0.365	0.353	0.348	0.343	0.337	0.331	0.323	0.315	0.305	0.292
1.750	60.380	0.401	0.385	0.372	0.366	0.360	0.354	0.347	0.339	0.330	0.319	0.305
2.000	69.000	0.422	0.405	0.390	0.385	0.379	0.372	0.364	0.356	0.345	0.334	0.319
General Cargo 1 (S60) L=121.1 m												
		Steepness λ/h										
λ/L	λ, m	40	30	24	22	20	18	16	14	12	10	8
0.750	91.440	0.329	0.326	0.324	0.323	0.322	0.320	0.319	0.317	0.315	0.312	0.308
1.000	121.900	0.334	0.325	0.316	0.313	0.309	0.305	0.299	0.293	0.286	0.277	0.264
1.250	152.400	0.352	0.339	0.328	0.323	0.318	0.312	0.304	0.296	0.288	0.275	0.260
1.500	182.900	0.373	0.357	0.343	0.338	0.332	0.325	0.315	0.307	0.296	0.283	0.266
1.750	213.400	0.394	0.376	0.360	0.354	0.347	0.340	0.331	0.319	0.308	0.296	0.276
2.000	243.800	0.415	0.395	0.379	0.371	0.364	0.356	0.346	0.335	0.321	0.306	0.289
RoPax L=137 m												
		Steepness λ/h										
λ/L	λ, m	40	30	24	22	20	18	16	14	12	10	8
0.750	102.800	0.311	0.306	0.301	0.300	0.297	0.295	0.292	0.288	0.284	0.279	0.271
1.000	137.000	0.327	0.317	0.308	0.304	0.300	0.295	0.290	0.284	0.276	0.266	0.253
1.250	171.300	0.347	0.334	0.322	0.318	0.312	0.306	0.299	0.291	0.282	0.269	0.255
1.500	205.500	0.369	0.353	0.340	0.334	0.328	0.321	0.313	0.304	0.293	0.281	0.263
1.750	239.800	0.392	0.374	0.358	0.352	0.346	0.338	0.329	0.318	0.307	0.295	0.275
2.000	274.000	0.414	0.394	0.377	0.370	0.363	0.355	0.346	0.335	0.321	0.307	0.289
Naval Combatant 1 & 2 (ONR FL & TH) L=150 m												
		Steepness λ/h										
λ/L	λ, m	40	30	24	22	20	18	16	14	12	10	8
0.750	112.500	0.313	0.308	0.303	0.302	0.299	0.297	0.294	0.291	0.287	0.281	0.274
1.000	150.000	0.326	0.315	0.306	0.302	0.297	0.292	0.286	0.279	0.271	0.260	0.246
1.250	187.500	0.345	0.330	0.317	0.312	0.306	0.300	0.292	0.283	0.271	0.258	0.240
1.500	225.000	0.366	0.348	0.333	0.327	0.320	0.312	0.303	0.292	0.279	0.264	0.244
1.750	262.500	0.387	0.367	0.350	0.344	0.336	0.328	0.316	0.304	0.290	0.273	0.252
2.000	300.000	0.408	0.386	0.368	0.360	0.352	0.342	0.332	0.319	0.303	0.285	0.263

Table 5 Second-Threshold Froude Number, as a Function of Wave Steepness (Cont.)

General Cargo 2 (C4) L=161.2 m												
		Steepness λ/h										
λ/L	λ, m	40	30	24	22	20	18	16	14	12	10	8
0.750	120.900	0.304	0.297	0.292	0.289	0.287	0.284	0.280	0.276	0.270	0.264	0.255
1.000	161.200	0.321	0.310	0.300	0.296	0.292	0.286	0.279	0.272	0.264	0.254	0.239
1.250	201.600	0.343	0.327	0.315	0.310	0.304	0.298	0.290	0.280	0.269	0.258	0.239
1.500	241.900	0.365	0.348	0.332	0.326	0.320	0.312	0.303	0.293	0.280	0.265	0.247
1.750	282.200	0.387	0.368	0.351	0.345	0.336	0.328	0.318	0.307	0.292	0.277	0.259
2.000	322.500	0.409	0.388	0.370	0.363	0.354	0.344	0.334	0.322	0.308	0.289	0.273
Bulk Carrier 2 L=145 m												
		Steepness λ/h										
λ/L	λ, m	40	30	24	22	20	18	16	14	12	10	8
0.750	108.800	0.316	0.312	0.308	0.306	0.304	0.302	0.299	0.296	0.293	0.288	0.281
1.000	145.000	0.349	0.342	0.335	0.332	0.329	0.326	0.322	0.317	0.311	0.303	0.292
1.250	181.300	0.362	0.350	0.340	0.336	0.331	0.325	0.319	0.311	0.302	0.289	0.274
1.500	217.500	0.380	0.365	0.352	0.348	0.341	0.334	0.326	0.317	0.306	0.291	0.274
1.750	253.800	0.400	0.382	0.367	0.361	0.355	0.347	0.338	0.327	0.315	0.298	0.281
2.000	290.000	0.420	0.400	0.384	0.377	0.369	0.362	0.352	0.340	0.327	0.308	0.290
Containership 5 (C11) L=262 m												
		Steepness λ/h										
λ/L	λ, m	40	30	24	22	20	18	16	14	12	10	8
0.750	196.500	0.310	0.305	0.300	0.298	0.296	0.293	0.290	0.287	0.282	0.276	0.269
1.000	262.000	0.326	0.316	0.306	0.303	0.298	0.293	0.287	0.281	0.272	0.262	0.249
1.250	327.500	0.346	0.332	0.320	0.315	0.310	0.303	0.295	0.287	0.277	0.264	0.248
1.500	393.000	0.368	0.351	0.337	0.331	0.325	0.318	0.309	0.298	0.287	0.274	0.255
1.750	458.500	0.390	0.371	0.355	0.348	0.341	0.333	0.324	0.313	0.300	0.285	0.266
2.000	524.000	0.412	0.391	0.374	0.367	0.358	0.350	0.340	0.328	0.313	0.298	0.279
Passenger Ship L=276.4 m												
		Steepness λ/h										
λ/L	λ, m	40	30	24	22	20	18	16	14	12	10	8
0.750	207.300	0.307	0.301	0.296	0.293	0.291	0.288	0.285	0.281	0.276	0.270	0.262
1.000	276.400	0.322	0.311	0.301	0.297	0.293	0.287	0.281	0.274	0.266	0.255	0.241
1.250	345.500	0.342	0.327	0.315	0.310	0.304	0.296	0.289	0.281	0.272	0.257	0.241
1.500	414.600	0.364	0.346	0.332	0.326	0.320	0.312	0.302	0.292	0.281	0.267	0.248
1.750	483.800	0.386	0.367	0.350	0.344	0.336	0.328	0.318	0.306	0.294	0.278	0.260
2.000	552.900	0.408	0.387	0.369	0.361	0.353	0.344	0.334	0.322	0.307	0.292	0.274
LNG Carrier L=267.8 m												
		Steepness λ/h										
λ/L	λ, m	40	30	24	22	20	18	16	14	12	10	8
0.750	200.900	0.328	0.325	0.323	0.322	0.321	0.320	0.318	0.316	0.314	0.311	0.307
1.000	267.800	0.338	0.329	0.321	0.318	0.314	0.310	0.306	0.300	0.293	0.284	0.273
1.250	334.800	0.354	0.341	0.331	0.326	0.321	0.316	0.309	0.301	0.292	0.281	0.266
1.500	401.800	0.374	0.359	0.346	0.340	0.335	0.328	0.321	0.312	0.301	0.289	0.272
1.750	468.700	0.395	0.378	0.363	0.357	0.350	0.343	0.335	0.326	0.314	0.301	0.282
2.000	535.700	0.416	0.397	0.380	0.374	0.367	0.359	0.350	0.340	0.329	0.314	0.294

Table 5 Second-Threshold Froude Number, as a Function of Wave Steepness (Cont.)

Bulk Carrier 1 L=275 m												
		Steepness λ/h										
λ/L	λ, m	40	30	24	22	20	18	16	14	12	10	8
0.750	206.300	0.313	0.308	0.304	0.302	0.300	0.298	0.295	0.292	0.288	0.282	0.275
1.000	275.000	0.349	0.342	0.336	0.333	0.330	0.326	0.322	0.317	0.311	0.303	0.292
1.250	343.800	0.361	0.349	0.338	0.334	0.329	0.323	0.317	0.308	0.298	0.285	0.267
1.500	412.500	0.378	0.363	0.349	0.343	0.337	0.332	0.322	0.312	0.299	0.280	0.262
1.750	481.300	0.398	0.378	0.363	0.356	0.349	0.340	0.333	0.320	0.306	0.284	0.266
2.000	550.000	0.417	0.395	0.378	0.371	0.363	0.353	0.345	0.332	0.316	0.291	0.272
Containership 4 L=283.2 m												
		Steepness λ/h										
λ/L	λ, m	40	30	24	22	20	18	16	14	12	10	8
0.750	212.400	0.314	0.310	0.306	0.304	0.302	0.300	0.297	0.294	0.290	0.285	0.277
1.000	283.200	0.327	0.317	0.308	0.304	0.300	0.295	0.289	0.282	0.274	0.265	0.250
1.250	354.000	0.347	0.332	0.320	0.315	0.310	0.303	0.296	0.286	0.276	0.265	0.247
1.500	424.800	0.368	0.351	0.336	0.330	0.324	0.317	0.308	0.297	0.285	0.273	0.253
1.750	495.600	0.390	0.370	0.354	0.347	0.340	0.332	0.322	0.311	0.297	0.282	0.264
2.000	566.400	0.411	0.390	0.372	0.365	0.357	0.347	0.337	0.326	0.312	0.294	0.277
Tanker L=320 m												
		Steepness λ/h										
λ/L	λ, m	40	30	24	22	20	18	16	14	12	10	8
0.750	240.000	0.319	0.315	0.311	0.310	0.308	0.306	0.304	0.301	0.298	0.294	0.288
1.000	320.000	0.346	0.339	0.332	0.329	0.326	0.323	0.318	0.313	0.307	0.300	0.289
1.250	400.000	0.362	0.350	0.340	0.336	0.331	0.326	0.320	0.313	0.304	0.294	0.281
1.500	480.000	0.381	0.366	0.354	0.349	0.344	0.337	0.330	0.322	0.312	0.301	0.288
1.750	560.000	0.402	0.385	0.371	0.365	0.359	0.352	0.344	0.335	0.324	0.313	0.299
2.000	640.000	0.422	0.404	0.389	0.382	0.376	0.368	0.360	0.350	0.339	0.326	0.311
Containership 1 L=322.5 m												
		Steepness λ/h										
λ/L	λ, m	40	30	24	22	20	18	16	14	12	10	8
0.750	242.000	0.307	0.301	0.296	0.294	0.292	0.289	0.286	0.282	0.277	0.271	0.262
1.000	322.600	0.323	0.312	0.303	0.299	0.294	0.289	0.283	0.276	0.267	0.256	0.243
1.250	403.300	0.344	0.329	0.317	0.312	0.306	0.299	0.292	0.283	0.271	0.258	0.242
1.500	483.900	0.366	0.349	0.334	0.327	0.321	0.313	0.304	0.294	0.281	0.267	0.250
1.750	564.600	0.388	0.368	0.352	0.345	0.337	0.329	0.319	0.308	0.295	0.278	0.262
2.000	645.200	0.409	0.388	0.370	0.363	0.355	0.346	0.334	0.323	0.309	0.290	0.270
Containership 3 L=330 m												
		Steepnessλ/h										
λ/L	λ, m	40	30	24	22	20	18	16	14	12	10	8
0.750	247.500	0.320	0.316	0.313	0.311	0.309	0.308	0.305	0.303	0.299	0.295	0.289
1.000	330.000	0.330	0.320	0.312	0.308	0.304	0.299	0.294	0.287	0.279	0.269	0.256
1.250	412.500	0.349	0.335	0.324	0.318	0.313	0.307	0.300	0.291	0.281	0.268	0.255
1.500	495.000	0.370	0.354	0.340	0.334	0.327	0.320	0.311	0.302	0.290	0.275	0.259
1.750	577.500	0.391	0.373	0.357	0.351	0.344	0.335	0.325	0.315	0.303	0.286	0.268
2.000	660.000	0.412	0.392	0.375	0.368	0.360	0.352	0.342	0.329	0.316	0.300	0.279

Table 5 Second-Threshold Froude Number, as a Function of Wave Steepness (Cont.)

Containership 2 L=376 m												
		Steepness λ/h										
λ/L	λ, m	40	30	24	22	20	18	16	14	12	10	8
0.750	282.000	0.308	0.303	0.298	0.296	0.293	0.291	0.287	0.284	0.279	0.273	0.265
1.000	376.000	0.325	0.315	0.305	0.301	0.297	0.292	0.286	0.279	0.271	0.259	0.246
1.250	470.000	0.346	0.331	0.319	0.314	0.308	0.301	0.294	0.285	0.275	0.261	0.245
1.500	564.000	0.367	0.350	0.336	0.330	0.323	0.315	0.306	0.297	0.285	0.269	0.252
1.750	658.000	0.389	0.370	0.354	0.347	0.340	0.332	0.321	0.310	0.298	0.282	0.262
2.000	752.000	0.410	0.389	0.372	0.365	0.357	0.348	0.338	0.324	0.311	0.295	0.273

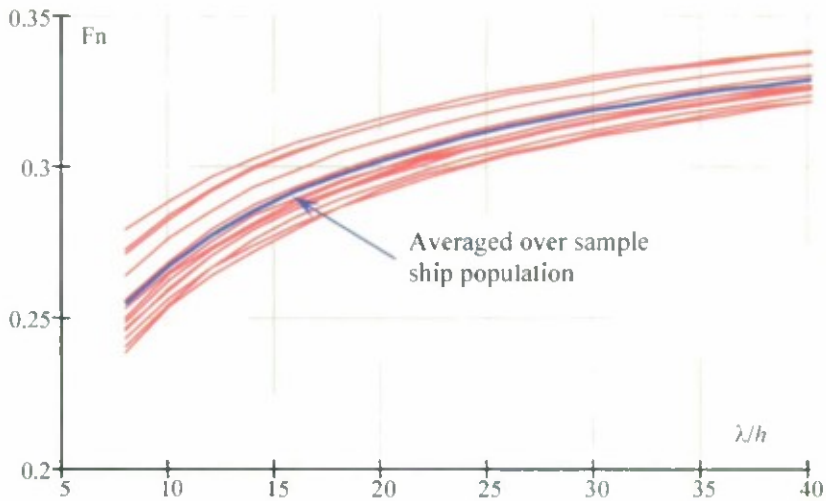

Figure 4.22 Second-Threshold Froude Number, as a Function of Wave Steepness

As it can be seen from Table 5, the lowest values and curves in Figure 4.22 do not necessarily belong to ships with known vulnerability for surf-riding and broaching-to. Therefore, it makes sense to use the average over the ship population for each steepness value rather than the lowest curve. The average curve is approximated as

$$Fn(\lambda/h) = 0.2324\ \sqrt[3]{\lambda/h} - 0.07364\ \sqrt{\lambda/h} \qquad (4.54)$$

where λ is wave length and h is the wave height. The approximate curve is plotted against the points in Figure 4.23.

For evaluation of probability, it is convenient to use the inverse function of (4.54). However, instead of transforming (4.54) into a cubic equation (4.53) and then solving it, it is easier to fit another approximation to the already inversed data:

$$h/\lambda = 0.0310\ Fn^{-3} + 0.06226 \qquad (4.55)$$

Note that the stiffness value is now expressed as h/λ. Points and the curve are shown in Figure 4.24.

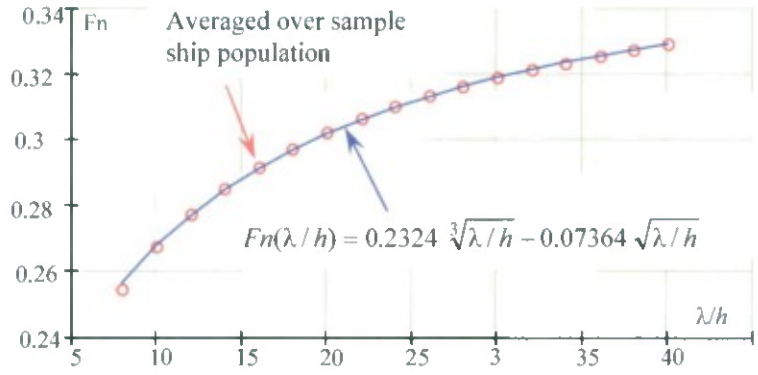

Figure 4.23 Approximation of Froude Number, as a Function of Steepness

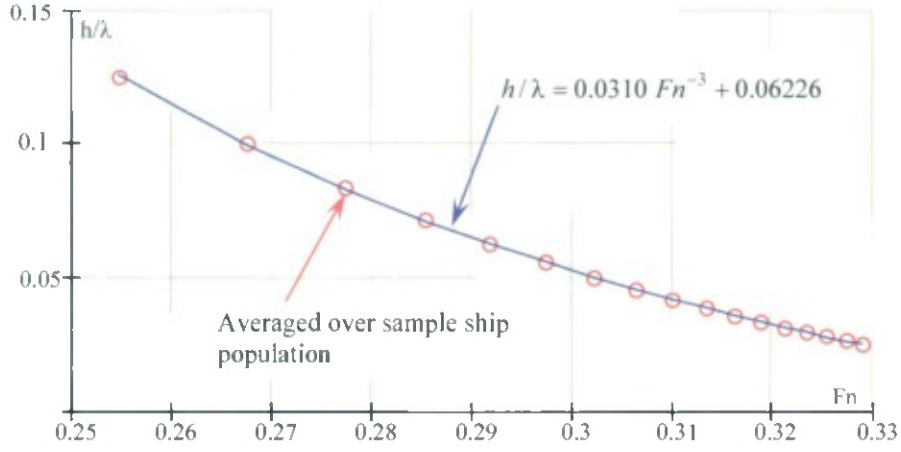

Figure 4.24 Approximation of Wave Steepness as a Function of the Nominal Froude Number, Corresponding to the Second Threshold (Averaged over the Sample Ship Population)

4.3.3 Criterion Accounting for Ship Length

The probability of encountering a wave equal to the ship length and capable of causing surf-riding becomes a function of Froude number

$$P(Fn) = \int_{a_{cr}(Fn)}^{L/7} f\left(a \mid k = \frac{2\pi}{L}\right) da \tag{4.56}$$

Here a_{cr} is critical amplitude that is determined from (4.55):

$$a_{cr} = 0.5L(0.0310\ Fn^{-3} + 0.06226) \tag{4.57}$$

The conditional distribution density $f(a|k)$ can be found using formulae (3.51) and (3.117):

$$f(a \mid k) = \frac{f(a,k)}{f(k)} \tag{4.58}$$

The formula (4.56) reflects the known fact that the increase of the speed leads to an increase of the probability of surf-riding. As it can be seen from Figure 4.24, increasing the Froude number reduces the steepness; this leads to a decrease of the critical amplitude (4.57) and to an increase of range of integration in (4.56). Since the conditional PDF (4.58) is always positive, the integral in (4.56) must increase with the increase of the Froude number.

To avoid any complexity unnecessary for the first level vulnerability check, N. Umeda proposed to limit the consideration of wave lengths to only those equal to the ship length. While changing the values of the probabilities, this assumption should not have much effect on the final results, as here the probabilities are only used for reference.

$$P(H_S, T_Z, L, Fn) = \int_{a_{cr}(Fn)}^{L/7} f\left(a \mid k = \frac{2\pi}{L}\right) da \tag{4.59}$$

Here, the probability is expressed as a function of significant wave height H_S and mean period of zero-crossing T_Z, as the conditional distribution (4.58) depends on the spectrum. A Bretshneider spectrum was assumed here, and it makes the reference probability dependent on these two parameters defining the spectrum.

N. Umeda also proposed to average the probability over a wave scatter diagram, like the one in IACS Recommendation 34. This is a very general approach, where the probability of encountering a certain weather condition is also considered.

$$P(L, Fn) = \frac{1}{N_{Tot}} \sum_{H_S} \sum_{T_Z} P_{Ref}(H_S, T_Z) N(H_S, T_Z) \tag{4.60}$$

Here $N(H_S,T_Z)$ is the number of observations of a sea state with significant wave height H_S and mean period of zero-crossing T_Z, while N_{Tot} is the total observations available.

Formula (4.60) expresses a probability (averaged over annual storm statistics) of encountering a wave that is equal to the length of the ship and capable of causing surf-riding to a ship heading with specified Froude number. While this value cannot be interpreted as the actual probability of surf-riding, it still can be used as a measure of danger of surf-riding, depending on speed and length. Figure 4.25 shows a graphical representation of formula (4.60).

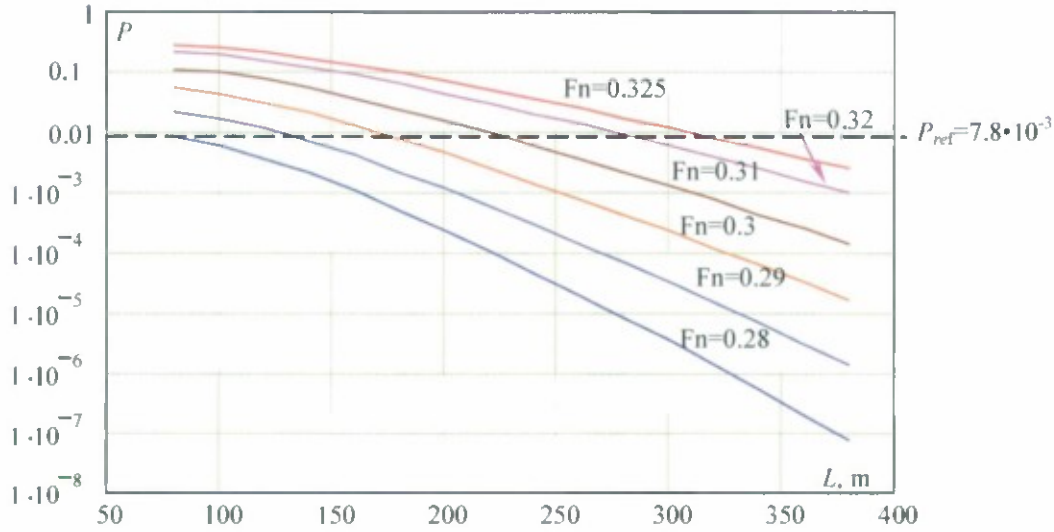

Figure 4.25 Probability of Encounter of a Wave Capable of Causing Surf-riding for as a Function of Ship Length for Different Nominal Froude Numbers

As can be seen from Figure 4.25, the probability deereases with an increase of the length and increases with the increase of Froude number. The observed tendency is consistent with operational experience. The danger of surf-riding is less for longer ships and inereases with inereasing speed. (For example, a ship with a length of 300 meters travelling at 35 knots has a Froude number of 0.332.)

To evaluate the reference probability, a reference ship length and Froude number should be assumed. Further calculations were performed for the referenee values L=80 m and Fn=0.28, subject for further scrutiny and additional discussions. The reference probability is calculated below and shown in Figure 4.25.

$$P_{ref} = P(L = 80, Fn = 0.27) = 7.8 \cdot 10^{-3} \tag{4.61}$$

Introduction of the reference probability allows for the expression of the Froude number as a function of length:

$$Fn(L) = Q(L, P = P_{ref}) \tag{4.62}$$

Here Q is an inverse function for probability (4.60).

Figure 4.26 presents the results of the calculation of the formula (4.62), depicted as circles, as well as the linear regression through these points:

$$Fn(L) = 0.0000181 \cdot L + 0.282 \tag{4.63}$$

The formula (4.63) relates Froude number with the ship length under the condition of encountering a wave with the length equal to ship length and steep enough to cause surf-riding. This line has a positive slope, meaning that a larger vessel would need to sail with higher speed, in order to keep the same probability of encounter with dangerous wave. This approach can be used to "give a credit" for larger ships, in terms of the likelihood of experiencing surf-riding and broaching-to.

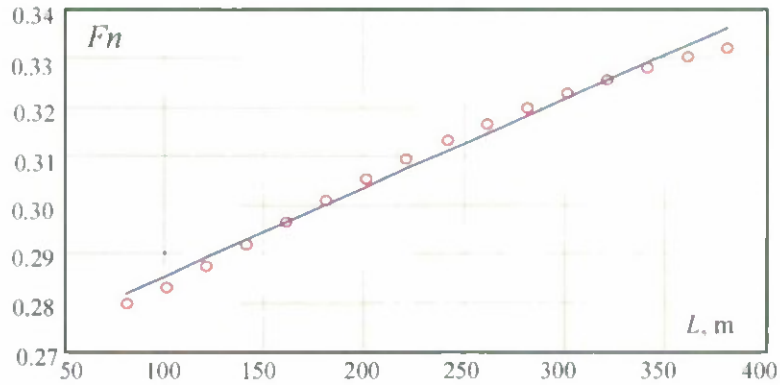

Figure 4.26 Fronde Number as a Function of Length, Under the Condition of the Eqnivalent Probability of Encountering a Wave Capable of Causing Surf-Riding

If one aeeepts Fn=0.28 as a standard for the level 1 vulnerability eriterion for a ship with length equal or less 80 m, then the entire eriterion ean be formulated as:

$$Fn > 0.28 \quad if \quad L \le 80\,m$$
$$Fn > 0.0000181 \cdot L + 0.282 \quad if \quad L > 80\,m \tag{4.64}$$

The obvious disadvantage of this eriterion is that it is based on an empiriеal relation between the Froude number eorresponding to the seeond threshold and the steepness of wave, expressed in formulae (4.54), (4.55) and (4.57). Beeause these formulae are based on a speeifie ship population, it may ehange if tried on another, or larger, population of ships. At the same time, the differenee between these ships, however noticeable, is not dramatic. The advantage of this approach is that it resulted in a simple formula and its safety level may be related with the referenee probability.

Alternatively, the doeument SLF-53/3/8 proposes an even simpler formula:

$$Fn \ge 0.3 \quad if \quad L \le 200\,m \tag{4.65}$$

This formula (4.65) expresses the same idea that the level 1 vulnerability criteria for surf-riding should inelude ship length as one of the parameters.

4.4 Level 2 Vulnerability Criteria

Similar to pure loss of stability, the phenomenon of surf-riding is a single-wave event. Despite the faet that the proeess of attraetion to a surf-riding equilibrium takes some time, the appearance of equilibria is instantaneous. The vulnerability to surf-riding ean be measured by the percentage of waves eapable of generating surf-riding equilibria. The irregular seaway is modeled as a sequenee of sinusoidal waves with random amplitude and length. The statistieal weight of eaeh wave is ealeulated with equation (3.137).

While direct application of Melnikov's method is considered to be too complex for the level 1 vulnerability criterion, the complexity of the the necessary calculations seems to be consistent with the requirements for the level 2 vulnerability criterion.

For each wave associated with a wave length and amplitude interval (i.e., a given λ_i and a_j) associated with a wave spectrum, the speed of the ship is compared with the speed corresponding to the second threshold for surf-riding, calculated with Melnikov's method (4.51). This comparison (using Froude number Fn) yields a factor $C2_{ij}$:

$$C2_{ij} = \begin{cases} 1 & if \quad Fn > Fn_{TR}(\lambda_i, a_j) \\ 0 & if \quad Fn \le Fn_{TR}(\lambda_i, a_j) \end{cases} \tag{4.66}$$

The weighted average of the factor $C2_{ij}$ over all of the values of λ_i and a_j represent the criterion:

$$C2(H_S, T_Z) = \sum_{i=1}^{N_\lambda} \sum_{j=1}^{N_a} W_{ij} C2_{ij} \tag{4.67}$$

Here, the criterion $C2$ is shown as a function of the significant wave height H_S and the mean zero-crossing period T_Z, since the distribution of wave numbers and amplitudes, used for the calculation of statistical weights, depends on the spectrum defined with these parameters.

The long-term version of the criterion can be formulated by averaging (4.67) over the values of significant wave heights and mean zero-crossing period using entries of scatter diagrams as weights:

$$C2_L = \frac{1}{N_{Tot}} \sum_{H_S} \sum_{T_Z} C2(H_S, T_Z) N(H_S, T_Z) \tag{4.68}$$

Here, $N(H_S,T_Z)$ is the number of observations of a sea state with significant wave height H_S and mean period of zero-crossing T_Z, while N_{Tot} is the total number of observations available.

4.5 Results of Sample Calculations

Calculations were performed for the sample population of ships and are presented in Table 6. The calculations included both versions of level 1 criterion (4.64) and (4.65) as well as the short-term version of the level 2 criterion. The sea state used for the level 2 criterion is characterized by the following values of significant wave height and the mean zero-crossing period:

$$H_S = 2.5\ m \qquad T_Z = 8.5\ s \tag{4.69}$$

As it can be seen from Table 6, all the criteria produced an essentially identical answers. Both the fishing vessels and the naval combatants were assessed to be vulnerable to surf-riding and broaching-to.

Fishing Vessel 1 (Purse seiner) is known for its vulnerability to surf-riding and broaching-to that was confirmed in numerous model tests (Umeda, 1999, Umeda *et al* 1999). Experimental data are also available for the Naval Combatant 2 (ONR tumblehome topside model), showing possibility of broaching-to (see Umeda, et al., 2008; Araki, et al., 2010).

The sample calculations show the consistency of the criteria, the level 1 criteria always show vulnerability, if it was indicated by the level 2 criteria.

Table 6 Sample Vulnerability Check for Surf-riding

Sample ship	L, m	Fn	V_s, kts	Level 1 (4.64)		Level 1 (4.65)		Level 2 (4.67)	
				Value	Outcome	Value	Outcome	Value	Outcome
Fishing Vessel 2	21.56	0.495	14	0.280	Fail	0.3	Fail	0.341	Fail
Fishing Vessel 1 (ITTC A2)	34.5	0.475	17	0.280	Fail	0.3	Fail	0.556	Fail
General Cargo 1(S60)	121.9	0.268	18	0.287	Pass	0.3	Pass	0.000	Pass
RoPax	137	0.267	19	0.290	Pass	0.3	Pass	0.000	Pass
Bulk Carrier 2	145	0.191	14	0.291	Pass	0.3	Pass	0.000	Pass
Naval Combatant 2 (ONR TH)	150	0.402	30	0.292	Fail	0.3	Fail	0.203	Fail
Naval Combatant 1 (ONR FL)	150	0.402	30	0.292	Fail	0.3	Fail	0.203	Fail
General Cargo 2 (C4)	161.2	0.233	18	0.294	Pass	0.3	Pass	0.000	Pass
Containership 5 (C11)	262	0.254	25	0.312	Pass	N/A	Pass	0.000	Pass
LNG Carrier	267.8	0.181	18	0.313	Pass	N/A	Pass	0.000	Pass
Bulk Carrier	275	0.159	16	0.314	Pass	N/A	Pass	0.000	Pass
Passenger Ship	276.4	0.247	25	0.315	Pass	N/A	Pass	0.000	Pass
Containership 4	283.2	0.244	25	0.316	Pass	N/A	Pass	0.000	Pass
Tanker	320.	0.129	14	0.322	Pass	N/A	Pass	0.000	Pass
Containership 1	322.6	0.229	25	0.323	Pass	N/A	Pass	0.000	Pass
Containership 3	330	0.226	25	0.324	Pass	N/A	Pass	0.000	Pass
Containership 2	376	0.212	25	0.332	Pass	N/A	Pass	0.000	Pass

4.6 Summary

This section describes the development of vulnerability criteria for broaching-to. Subsection 4.1 describes the physical background of this mode of stability failure; broaching-to is a violent uncontrollable turn occurring in steep stern quartering and following seas. Surf-riding is the capture of a ship by a wave when it is made to move with the wave celerity. The surf-riding phenomenon usually precedes broaching-to, so determining vulnerability for broaching-to can be performed by the evaluation of a ship's propensity to surf-ride.

There are two characteristic speeds, or Froude numbers, which are associated with surf-riding– typically called thresholds. The first threshold corresponds to the situation when the surf-riding becomes possible at a certain location on the wave and instantaneous speed. The second threshold is associated with the Froude number when

the surf-riding is inevitable for all possible crest locations and velocities. The second threshold is used for the development of criteria. Subsection 4.2 reviews the mathematical apparatus necessary for this purpose and describes two methods for calculation of the speed, corresponding to the second threshold: direct numerical integration and an approximate Melnikov's method.

The section 4.3 describes the development of level 1 vulnerability criteria. As the calculation of the second threshold is too complex for this level, dependence of the Froude number corresponding to the second threshold on the wave steepness is calculated and approximated with a regression formula. This allows for formulation of the level 1 criterion using the linear dependence of the Froude number on the ship length. An alternative level 1 criterion is also described.

Subsection 4.4 is focused on the level 2 vulnerability for surf-riding. It is also based on the second threshold evaluated with Melnikov's method. The criterion is formulated for irregular waves using envelope theory in a way similar to the level 2 vulnerability criteria for pure loss of stability.

Sample calculations were performed for 17 ships.

This page is intentionally left blank

5 Vulnerability Criteria for Dead Ship Conditions

This section is focused on the vulnerability of a ship to stability failure in dead ship conditions. The physical background of the phenomena is presented and the forces acting on a ship in dead ship conditions are briefly reviewed, including the influence of the freeboard on the ship dynamics in dead ship conditions. A proposal for using modified weather criterion as the level 1 vulnerability criterion is examined. An outlook for the level 1 and 2 vulnerability criteria is presented.

5.1 Physical Background

The danger to the stability of a ship in rough weather, when the ship loses power, was understood by naval architects as early as when the sail was abandoned as a source of power. Typical features of this generation of ship included a superstructure amidships, so the windage area was distributed approximately symmetrically. This resulted in the ship being vaned or reverting to a beam seas position in the dead ship condition, maximizing the adverse effect of wind and waves.

Dead ship condition was the first mode of stability failure addressed with physics-based severe wind-and-roll criterion, also known as the "weather criterion," which was adopted by IMO in 1985 (Res. A.562(14)) and is now embodied in section 2.3 of the 2008 IS Code, Part A. The scenario of the weather criterion is shown in Figure 5.1.

This scenario assumes that a ship has lost its power and has turned into beam seas, where it is rolling under the action of waves as well as heeling and drifting under the action of wind. Drift-related heel is a result of action of a pair of forces: wind aerodynamic force and hydrodynamic reaction caused by transverse motion of the ship.

Next a sudden and long gust of wind occurs. The worst possible instant for this is when the ship is rolled at the maximum windward angle; in this case, action of wind is added to the action of waves.

The strengthening wind increases drift velocity and this leads to an increase of the hydrodynamic drift reaction. The increase of the drift velocity leads to the increase of the hydrodynamic reaction and, therefore, to the increase of the heeling moment by the pair of aerodynamic and hydrodynamic forces.

The gust is assumed to last long enough so the ship can roll to the other side completely; the achieved leeward roll angle is the base of the criterion. If it too large, or some openings may be flooded, the stability of the ship is considered insufficient.

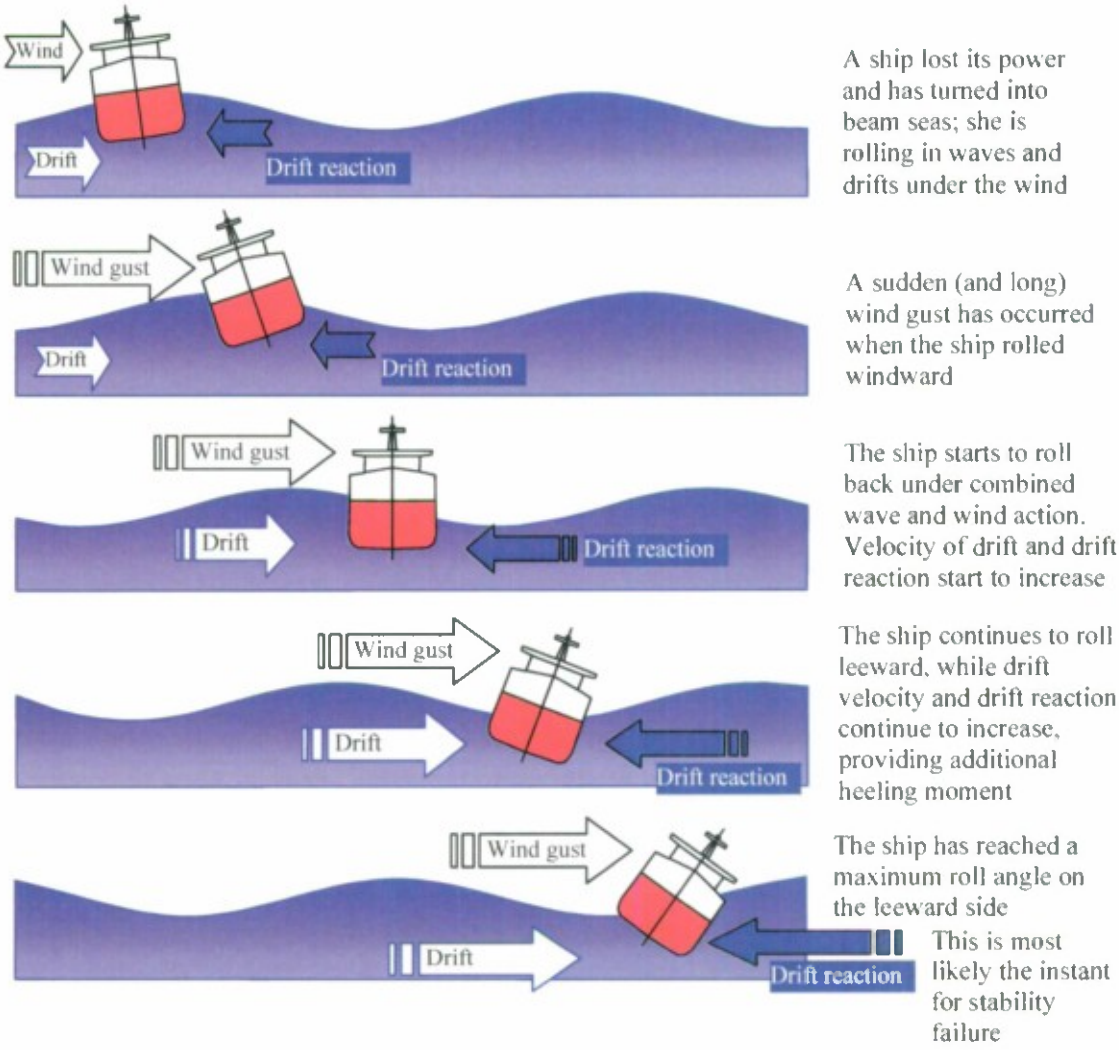

Figure 5.1 Scenario of Stability Failure in Dead Ship Conditions

5.2 On Dynamics of a Ship in Dead Ship Conditions

5.2.1 Description of Forces

The physics of the stability failure in dead ship conditions is not simple. Most modern ships do not have symmetrical windage area forward and aft, and as a result, such a ship will be located at a certain angle relative to wind and wave direction, which means that the consideration of motions may not be limited to just the transverse plane.

Even if beam seas are assumed (this is the first significant simplification), the problem still has be characterized by three degrees of freedom (sway/drift, heave and roll) and include forces of different characteristics. A brief discussion of these forces and the methods to estimate them is presented below, (excluding the forces related to entrance of deck into water, which are considered in the next subsection).

Hydrostatic and Froude-Krylov forces and moments are the result of the addition of normal pressures from the water onto the submerged portion of the hull. These forces include changes in pressure because of the waves, but do not include changes caused by diffraction and radiation of waves from the moving ship. The calculation of these types of forces is not difficult; well-established numerical procedures are available, although additional care may be necessary for large amplitude radiation and diffraction forces (Belknap, *et al.*, 2010). The problem associated with these forces is that the results, given for the general case Froude-Krylov forces, cannot be separated from the hydrostatic forces. In terms of ship dynamics, this means that both excitation and restoring are expressed in one term, and, as a result, the dynamical system cannot be expressed as an ordinary differential equation.

Diffraction and radiation forces take into account the presence of a ship and its influence on the local pressure field. Incoming waves are diffracting and reflecting from the ship's hull, as they would from any other body in the fluid. The ship is also moving and generates waves. The ship-generated waves interfere with the incoming waves, and distort them. As a result, the pressure field changes and the corresponding wave force is different from only the Froude-Krylov component. The introduction of diffraction and radiation forces covers this difference. The calculation of these types of forces is more involved, as a system of partial differential equations must be solved numerically. Nevertheless, because the viscosity of water does not have much of an influence for this scenario, the problem is still addressed within potential flow hydrodynamic theory. Computationally, this means that it is enough to consider the boundary rather than the entire volume. Also, the value of these forces is relatively small in comparison with the Froude-Krylov forces.

Damping forces are usually attributed to the oscillatory part of motions (keeping it separate from the hydrodynamic reaction to drift, which is not oscillatory). The damping forces are the result of the dispersion of kinetic energy of oscillatory ship motions and are applied to all three degrees of freedom. There are three distinct mechanisms of how the energy is lost. First, the energy is taken away with the waves that the ship makes. This component is calculated within the framework of potential flow hydrodynamics and it is dominant for heave motions. The second component is related with generating and shedding vortexes, while the third component is related to skin friction. The calculation of these two components leads to the consideration of fluid volume, as potential flow hydrodynamics is no longer applicable. This takes the problem into the realm of Computational Fluid Dynamics (CFD), and increases the computational cost by several orders of magnitude. As these components are important for roll motions, engineering solutions to approximate this energy loss includes the use of roll decay tests.

Inertial hydrodynamic forces, commonly presented as added masses, are calculated within the framework of potential flow hydrodynamic theory, and their evaluation is not difficult.

Aerodynamic forces also have a vortex nature. The common way to evaluate these forces is by means of a model test in a wind tunnel. This conventional way does not account for two circumstances that may be significant for stability assessment of dead ship conditions. When the waves are large, they influence the air pressure field: in a trough, the waves can shield the ship from wind and decrease aerodynamic forces. Also, when a ship is rolled, the decks also work as an aerodynamic surface and produce force.

Some experimental data has shown that deck-generated forces may exist for small angles as well, and that these forces may be significant (Belenky and Sevastianov 2007). Another possible deviation from the conventional scheme is the case of very large passenger vessels, where the spatial variability of the air flow may not be insignificant.

Hydrodynamic drift reaction forces are somewhat similar in nature to aerodynamic forces; generation and shedding vortices play an important role. However, there is no established mature technology for measurement of these forces. Again, some limited experiment-based information is available from (Belenky and Sevastianov 2007).

5.2.2 Influence of the Deck Entering the Water

If a ship has lower freeboard for a substantial part of its length, the forces related to the entrance of the deck into the water may play a significant role in the dynamics of a ship. A rather comprehensive review of this subject is available from Belenky and Sevastianov (2007), so only the key points are reported below.

Also, there is a difference between two situations: water on deck and deck in water. Water trapped on deck (without an interface of the green water with the outside fluid domain) acts like a moving mass when the ship rolls, while the deck-in-water situation (where the water on deck and outside the hull can be considered as one fluid domain) leads to the development of hydrodynamic forces on the deck surfaces, which dominates the dynamics. These effects were known since the late 1960s, and have been discussed previously at IMO (IMCO STAB/INF.27, 1966) and in succeeding sessions.

The influence of the deck entering water leads to drastically different dynamics between high and low freeboard ships, under the action of a similar sudden gust of wind, see Figure 5.2.

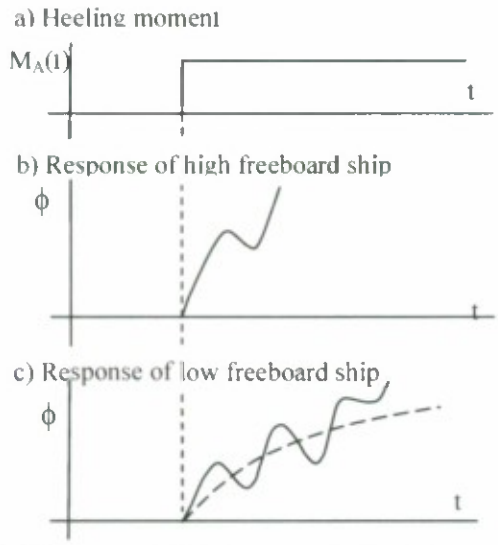

Figure 5.2 Difference in Response to a Sudden Wind Gust (Belenky and Sevastianov, 2007)

A trait of stability failure in the dead ship condition is that the forces of a different physical nature may dominate the dynamics, depending on geometry of the hull, as well as the geometry of its topside.

5.3 Vulnerability Criteria for Dead Ship Conditions

5.3.1 Level 1 Vulnerability Criterion

Any type of ship may be vulnerable in a dead ship condition, as synchronous roll resonance and large heeling moments due to wind may cause stability failure for a conventional ship, as well as an unconventional ship. Vulnerability to stability failure in dead ship conditions is determined by the weather criterion of the current IS code. Therefore, it may seem logical to use the modification of current weather criterion as the level one vulnerability criterion as it is proposed in Annex 1 of SLF 52/INF.2 and in SLF 53/3.

On the other hand SLF 53/3/6 states that modification of the weather criterion is not advisable, as it was not intended to be a module criterion; it only can be used "as is." The reason is that the parameters of the weather criterion were calibrated using a certain population of sample ships; as a result, these parameters are not independent, and may not be appropriate for unconventional ships.

The following discussion focuses on the assumptions that formed the background of the weather criterion and explains why modifications to it are not advisable.

Based on the formulation of the severe wind and rolling criteria in the 2008 Intact Stability Code (and its description in the explanatory notes), the roll motion can be given as:

$$(I_x + A_{44})\ddot{\phi} + M_D(\dot{\phi}) + \Delta \cdot GZ(\phi) = M_{FK}(t) + M_A(t) \qquad (5.1)$$

Here I_x is moment of inertia, A_{44} is added mass in roll, M_D is nonlinear roll damping, Δ is weight displacement, and M_{FK} is the Froude-Krylov excitation moment, while M_A is the wind heeling moment, including the influence of the gust.

It is assumed that coupling between heave and roll is small and coupling between sway and roll is cancelled out by not including the diffraction and radiation into the wave excitation – that is why the equation (5.1) only includes the Froude-Krylov component.

The energy balance method is used to solve the equation (5.1). The main idea is to re-write (5.1) in the form of the balance of energy and work for the different forces. Re-writing the equation of motion involves integration of the motion equation (5.1) from some initial state, characterized by the initial roll angle and rate, $\phi_0, \dot{\phi}_0$. See (Belenky and Sevastianov, 2007) for details of the derivation.

The integration of inertia yields the change of the kinetic energy of the dynamical system:

$$(I_x + A_{44}) \int_{\dot{\phi}_0}^{\dot{\phi}} \dot{\phi} d\dot{\phi} = K(\dot{\phi}_0, \dot{\phi}) = (I_x + A_{44}) \left[\frac{\dot{\phi}^2}{2} - \frac{\dot{\phi}_0^2}{2} \right] \tag{5.2}$$

The work of the damping moment is expressed as

$$\int_{\phi_0}^{\phi} M_D(\dot{\phi}) d\phi = A_D(\dot{\phi}_0, \dot{\phi}) = A_D(t_0, t) \tag{5.3}$$

A closed-form expression for (5.3) is only available when the solution and its derivatives are also expressed in closed-form. However, this is not the case for the restoring term:

$$\Delta \cdot \int_{\phi_0}^{\phi} GZ(\phi) d\phi = P(\phi_0, \phi) \tag{5.4}$$

The integral is the area under the *GZ* curve -- a traditional definition of ship "dynamic stability". This quantity is known. To express the work of Froude-Krylov forces, the time history of motion is required, similar to case of the work of the damping moment:

$$\int_{\phi_0}^{\phi} M_{FK}(t) d\phi = \int_{\phi_0}^{\phi} A_{FK} \sin(\omega t) d\phi = A_E(\phi_0, \phi, t_0, t) = A_E(t_0, t) \tag{5.5}$$

Here, A_{FK} is the amplitude of the Froude-Krylov forces. The expression of the Froude-Krylov forces only using a sine function is already an approximation and is only accurate when the ship breadth is small compared to the wave length. The introduction of the effective wave slope allows use of this approximation for the remainder of the cases.

The work of the aerodynamic heeling moment is expressed as:

$$\int_{\phi_0}^{\phi} M_A(t) d\phi = A_{MA}(\phi - \phi_0) = A_A(\phi_0, \phi) \tag{5.6}$$

Even for a constant wind heeling moment, with magnitude A_{MA}, the time history of the solution is required.

The energy/work balance equation is expressed as:

$$K(\dot{\phi}_0) + A_D(t_0, t) + P(\phi_0, \phi) = A_A(\phi_0, \phi) + A_E(t_0, t) \tag{5.7}$$

Only two of the five terms of the equation (5.7) can be evaluated without having the full solution of the motion equation (5.1). Therefore, a practical application of the energy balance method is impossible without additional assumptions.

To demonstrate how the energy balance method works and what the time history of each term looks like, consider a linear equation of roll:

$$(I_x + A_{44})\ddot{\phi} + B_{44}\dot{\phi} + \Delta \cdot GM \cdot \phi = M_{FK}(t) + M_A(t) \tag{5.8}$$

Another assumption is that the transition is over and roll motions are in the steady state mode:

$$\phi = \phi_a \sin(\omega t + \beta) + \phi_W \tag{5.9}$$

Here, ϕ_W is the static angle of heel caused by constant wind, while ϕ_a is the roll amplitude and β is the phase shift.

It is obvious that steady-state solution of the linear differential equation cannot describe large roll motion of a ship under a sudden gust of wind. Again, this model is considered only to clarify some concepts of the energy balance method. The closed-form solution (5.9) allows expression of the work due to damping, wave excitation, and wind heeling.

The work of the damping moment is expressed as:

$$\begin{aligned} A_D(t_0,t) &= B_{44}\int_{\phi_0}^{\phi}\dot{\phi}d\phi = 2\delta\int_{t_0}^{t}\phi_a^2\omega^2\cos^2(\omega t+\beta)dt = \\ &= B_{44}\phi_a^2\omega^2\left\{(t-t_0)+\frac{1}{2\omega}(\sin(2\omega t+2\beta)-\sin(2\omega t_0+2\beta))\right\} \end{aligned} \tag{5.10}$$

The work of wave excitation contains a term very similar to work of the damping moment:

$$\begin{aligned} A_E(t_0,t) &= \int_{\phi_0}^{\phi}A_{FK}\sin(\omega t)d\phi = \int_{t_0}^{t}A_{FK}\sin(\omega t)\dot{\phi}dt = \\ &= -\frac{1}{4}\phi_a A_{FK}\cos\beta(\cos(2\omega t+2\beta)-\cos(2\omega t_0+2\beta))- \\ &-\frac{1}{2}\phi_a A_{FK}\omega\sin\beta\left\{(t-t_0)+\frac{1}{2\omega}(\sin(2\omega t+2\beta)-\sin(2\omega t_0+2\beta))\right\} = \\ &= A_{ESync}(t_0,t)+A_{EAct}(t_0,t) \end{aligned} \tag{5.11}$$

Therefore, it makes sense to present this work as the sum of the two: the work of the active part of the excitation that is similar to the work of the damping moment:

$$\begin{aligned} A_{EAct}(t_0,t) &= -\frac{1}{2}\phi_a A_{FK}\omega\sin\beta \\ &\left\{(t-t_0)+\frac{1}{2\omega}(\sin(2\omega t+2\beta)-\sin(2\omega t_0+2\beta))\right\} \end{aligned} \tag{5.12}$$

The other part is the synchronization (or reactive) part of the work of the excitation:

$$A_{ESync}(t_0,t) = -\frac{1}{4}\phi_a A_{FK}\cos\beta(\cos(2\omega t+2\beta)-\cos(2\omega t_0+2\beta)) \tag{5.13}$$

The work of the aerodynamic heeling moments is expressed as:

$$A_A(t_0,t) = A_{MA}\phi_a\cos(\omega t+\beta) - A_{MA}\phi_a\cos(\omega t_0+\beta) \tag{5.14}$$

Expression for the change of kinetic and potential energy is trivial:

$$K(t_0,t) = (I_x + A_{44})\left[\frac{\dot{\phi}^2}{2} - \frac{\dot{\phi}_0^2}{2}\right] = \\ = \frac{(I_x + A_{44})}{4}\phi_a^2\omega^2\left(\cos(2\omega t + 2\beta) - \cos(2\omega t_0 + 2\beta)\right) \tag{5.15}$$

$$P(t_0,t) = \Delta \cdot GM \cdot \left[\frac{\phi^2}{2} - \frac{\phi_0^2}{2}\right] = \\ = -\frac{1}{2}\Delta \cdot GM \cdot \left(\frac{1}{2}\phi_a^2\cos(2\omega t + 2\beta) - 2\phi_a\phi_W\sin(\omega t + \beta)\right) + \\ + \frac{1}{2}\Delta \cdot GM \cdot \left(\frac{1}{2}\phi_a^2\cos(2\omega t_0 + 2\beta) - 2\phi_a\phi_W\sin(\omega t_0 + \beta)\right) \tag{5.16}$$

The time histories of all these components of work and changes of energy are shown in Figure 5.3. It is clear from this figure that the energy balance equation (5.7) can be separated into two independent balance equations:

$$A_D(t_0,t) = A_{EAct}(t_0,t) \tag{5.17}$$

$$K(\dot{\phi}_0,\dot{\phi}) + P(\phi_0,\phi) = A_A(\phi_0,\phi) + A_{ESync}(\phi_0,\phi) \tag{5.18}$$

This separation has a physical meaning. As is well known, the role of periodic excitation is two-fold: compensation of the damping losses and synchronization, i.e. forcing the dynamic system to oscillate with the excitation frequency, rather than with its own (natural) frequency.

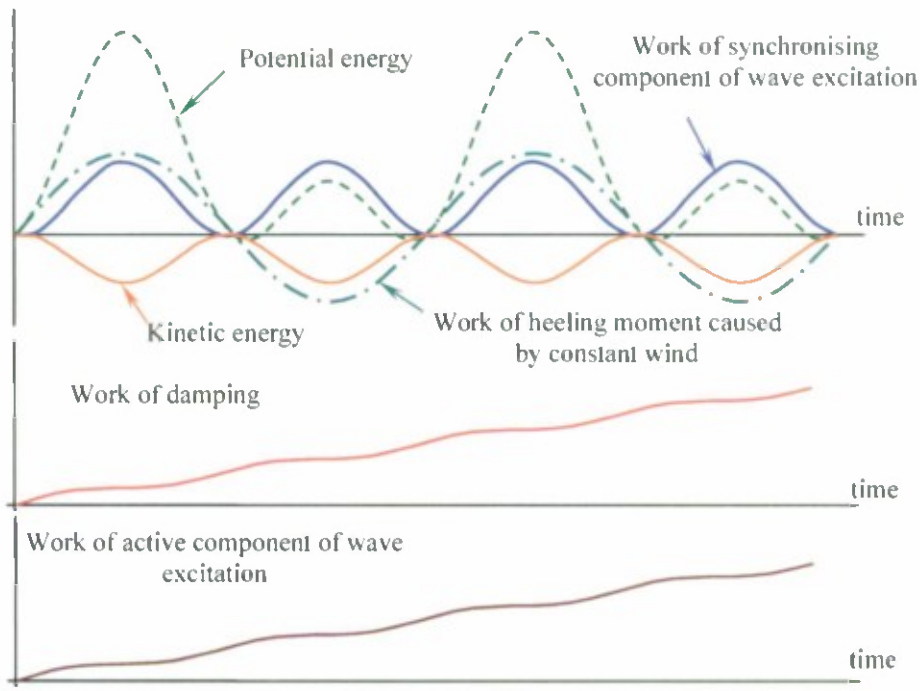

Figure 5.3 Time Histories of Work and Energy Changes Based on the Steady-State Solution of the Linear Equation of Roll (Belenky and Sevastianov, 2007)

This approach allows for examination of the phenomenon of the synchronous resonance from a different perspective. When a linear system is in resonance conditions, all the work of the periodic excitation is used for the compensation of losses due to damping, as the excitation frequency and natural frequency are equal. It also can be seen from equation (5.13) that at the resonance condition the phase shift, β, equals $\pi/2$; this makes the entire (5.13) equal to zero, so that only the active component of the excitation remains.

Then, in the case of the steady state resonance in a linear system, the balance equation can be re-written:

$$K(\dot{\phi}_0,\dot{\phi}) + P(\phi_0,\phi) = A_A(\phi_0,\phi) \tag{5.19}$$

Equation (5.19) is actually used in the weather criterion to find the angle of roll, and just the change of potential energy is defined using the area of the *GZ* curve. Figure 5.4 illustrates this procedure:

$$\frac{\dot{\phi}^2}{2} - \frac{\dot{\phi}_0^2}{2} = \frac{A_A(\phi_0,\phi) - P(\phi_0,\phi)}{(I_x + A_{44})} \tag{5.20}$$

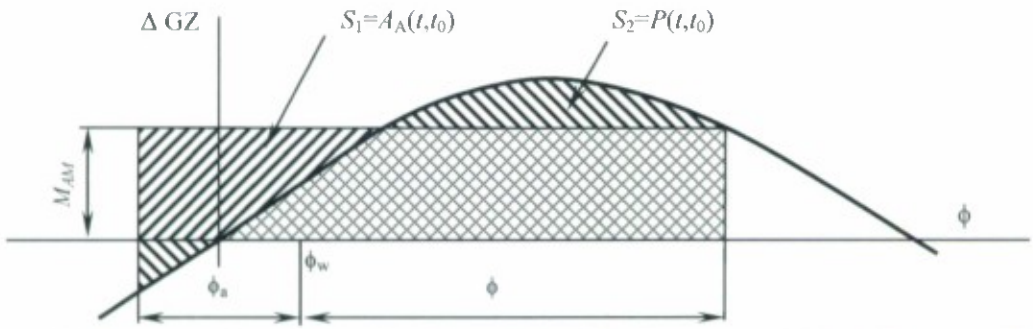

Figure 5.4 Evaluation of the Dynamic Angle under a Sudden Gust of Wind Using the Energy Balance Method (Belenky and Sevastianov, 2007)

The discussion above allows for summarizing the assumptions of the weather criterion:

- The energy balance of a nonlinear system at resonance behaves the same as the linear system in the steady-state mode. In reality, the synchronous resonance in a nonlinear system is quite different, as the natural frequency depends on the amplitude.
- The influence of the transition for energy balance is negligible. Even if the steady-state mode existed prior to the sudden gust of wind, the transition starts once the gust is applied.
- The hydrodynamic part of roll excitation cancels out with sway motion. This assumption may require long waves (in comparison with the ship size) to be accurate.
- The heave has no effect on roll. This assumption may work for relatively wall-sided ships; if the ship has a more complex geometry, the *GZ* curve may change significantly with large heave.

- Decks do not generate aerodynamic forces. Belenky and Sevastianov (2007) report on references showing they can generate aerodynamic forces.
- The heeling moment of drift hydrodynamic force is negligible. Model tests reviewed in Belenky and Sevastianov (2007) show that it may be of the same order as that of the aerodynamic moment.
- The deck never enters the water.

Obviously, all of these assumptions need to be valid to make the weather criterion practical. Taking into account the complexity of the physics associated with motions in dead ship conditions, the weather criterion definitely should be considered as a marvelous achievement in the development of stability regulations.

To compensate for the inaccuracies arising from these assumptions, all the parameters of the weather criterion were calibrated based on calculations on hundreds of sample ships[3]. That is why it is impossible to modify the weather criterion without re-calibrating its parameters and that is why it is so important to know the limits of application of the weather criterion.

The applicability of the current weather criterion is limited, as it was tuned to a certain population of ships which existed at the time of its development. Recognizing this fact, MSC.1/Circ.1200, "Interim guidelines for alternative assessment of the weather criterion," contains a specification of the limitations of applicability of the current weather criterion. In principle, the level 1 vulnerability criterion should be built around the applicability of the weather criterion.

5.3.2 Level 2 Vulnerability Criteria

Although the current weather criterion is mandatory, if it cannot be satisfied, and the parameters of a ship are outside of the specified limits, then model tests can be applied as an alternative assessment method. This means that MSC.1/Circ.1200 can be considered in terms of multi-layered approach, where the limitations of the current weather criterion itself play a role for the vulnerability criteria for dead ship conditions, and the model test is the direct stability assessment method.

The level 2 vulnerability criterion for dead ship condition should then be focused on double checking if a ship really has a problem with stability, since failing the level 1 criteria simply should mean that the weather criterion is not applicable. There are several factors that may need to be considered:

- The relation between the submerged hull form and drift forces;
- The freeboard and the interaction of the deck and water;
- The influence of the windage distribution on the actual position in dead ship conditions;
- The influence of the spatial variability of wind, including very large superstructures;
- The influence of irregularity of the waves and the stochastic character of the wind.

[3] According to Prof. L.K. Kobylinski, who was one of the developers of the weather criterion

Of these five factors only the last one was addressed in SLF 52/INF.2; so the consideration of other factors still remains for the development of level 2 vulnerability criteria for dead ship conditions.

5.4 Summary

This section focused on the vulnerability of a ship to stability failure in dead ship conditions. Subsection 5.1 describes the physical background of the phenomena, focusing on the scenario that is assumed for the current weather criterion. This scenario includes the ship's turn to beam seas after engine failure, resulting in resonant rolling and the sudden action of a gust of the wind.

Subsection 5.2 examines the forces acting on a ship in dead ship conditions and briefly reviews the influence of the freeboard on the dynamics of a ship in dead ship conditions.

Subsection 5.3 looks into a proposal of using modified weather criterion as the level 1 vulnerability criterion. The subsection contains the analysis of the assumptions of the current weather criterion and provides a justification to the statement that the modification of the current weather criterion is not advisable. An outlook for the future development of level 1 and 2 vulnerability criteria is presented.

This page is intentionally left blank

6 Framework for Direct Stability Assessment

This section contains an overview of the issues related with the direct assessment of dynamic stability for ships found to be vulnerable. This section considers the most general problem related to the direct assessment of dynamic stability, reviews three methods that are being developed for dynamic stability problems, and examines specifics of validation of tools of direct assessment, keeping in mind the extreme rarity of stability failures.

6.1 Formulation of the Problem

6.1.1 Introduction

Once vulnerability to a certain mode of stability failure has been established, a direct assessment of dynamic stability for that mode is expected to follow, as defined in the framework of the new generation of intact stability criteria.

The objective of direct stability assessment may be seen as two-fold: as a tool for detailed design analysis, and for the development of ship-specific operational guidance. At the core of the direct assessment lies a method capable of reproducing ship motions in severe seas, with a fidelity that is sufficient for sound technical decision-making.

Considering the current state-of-the art of computational ship hydrodynamics for these rare problems, general direct assessment options appear to be limited to model tests and fast simulations. These fast simulations use potential flow wave-body hydrodynamic codes, and are supplemented by empirical formulations for viscous and vortex forces, which are based on results from model tests. Due to the necessary computational speed requirements, the application of other numerical methods seems to be limited for specific tasks. Higher-fidelity numerical methods, such as computational fluid dynamics (CFD), may be used to evaluate coefficients for viscous and lifting force models. Ordinary differential equations (ODE) may be used for extreme nonlinearity, where application of physics-based codes may not be practical.

The validation of simulation tools for direct assessment represents a challenge and requires special attention (Reed, 2009). There are several aspects to this problem. First, it needs to be demonstrated that a tool is in fact capable of reproducing the considered mode of stability failure, and that the results of the simulation do not contradict the technical community's accepted knowledge of the physics of the problem (an example of this type of demonstration can be found in Spyrou, *et al.*, 2009). Because the simulation is expected to be performed in irregular waves, it is necessary to demonstrate that the model used for irregular waves is valid from probabilistic point of view (i.e. its autocorrelation function and distribution correspond to expected values). Quantitative validation may include comparisons with experimental measurements of forces acting on the ship and trajectories and motions for a ship maneuvering in waves.

6.1.2 Nonlinearities and the Problem of Rarity

Failures related to a ship's motions and loads in severe seas are characterized by both their rarity of occurrence and significant nonlinearity for each failure mode. Because of this, the accurate evaluation of the ship response in these conditions becomes difficult and impractical with the use of traditional "brute-force" direct assessment methods– Monte Carlo simulations and/or a large number of experimental realizations in the basin.

Assessing the dynamical response to these wave sequences constitutes the general problem of rarity – when the time between events is long, compared to a relative time-scale. The problem of rarity may be solved by separating the ship response into sub-problems, according to their time scale. For ship motions, the simplest example of an implementation using this approach is the piecewise-linear method for calculating capsizing probability (Belenky 1993; Paroka & Umeda, 2006; Paroka, *et al.*, 2006; Belenky, *et al.*, 2009). The same principle has also been applied to determine nonlinear response using numerical simulations (Belenky, *et al.*, 2010).

For example, large roll motion response (i.e. roll near, or beyond, the maximum of the GZ curve) appears when a dynamical system is characterized by significantly nonlinear stiffness. By its nature, the point of maximum is when the oscillator behavior changes from an attractor to a repeller. Additionally, large roll angles are typically the result of specific phenomena – nonlinear excitation, which may be exhibited in the form of fold bifurcation. Such phenomena are not limited to roll motion. Large yaw angles may also be the result of fold bifurcation (Spyrou 1997), such as in the case of direct broaching.

This nonlinearity makes it difficult to use traditional techniques to determine values associated with rare events, such as extreme value distributions. While the theory of extreme distributions is still applicable, the fitting of these distributions may be difficult, due to the insufficiency of the available data where these nonlinearities are significant. This situation can be resolved with the explicit modeling of nonlinear phenomena, but this would require consideration of the influence of random initial conditions and could be influenced by the occurrence of previous nonlinear events, depending on the time-scale. These considerations lead to the concept of a separation between the nonlinear phenomena resulting in a large response and the conditions which lead to the occurrence of such phenomena.

6.1.3 The Principle of Separation

This separation leads to a modeling of the ship response problem as a combination of two sub-problems: non-rare and rare. The non-rare problem is focused on determining the probability of occurrence of the precursor conditions which may lead to the nonlinear phenomena resulting in severe response, as well as determining the distribution of the appropriate initial conditions. The rare problem is focused on determining whether large responses occur for particular initial conditions.

In principle, if the failure is the result of a chain of events, there may be several rare problems involved. For example, in broaching due to surf-riding, the occurrence of surf-riding is required for the broaching event to manifest itself for the given environmental conditions. The non-rare problem would define the conditions where surf-riding is possible, while the rare problem represents the probability that surf-riding will occur, given the existence of the necessary conditions. The inception of broaching, given the occurrence of surf-riding (yaw repelling), is a function of the manifestation of instability in yaw after the occurrence of the surge equilibrium.

The main assumption behind the separation principle is that a mechanical system can be "restarted" at any moment of time, *if* the state variables at the instant of "restarting" are fully determined. For the case of a body moving in vacuum, this is an exact statement. However, for a ship on the free surface, this is an assumption because the hydrodynamic memory effect cannot be fully realized. In this sense, all of the necessary memory effects are contained within the initial conditions at the initialization of the rare problem.

6.1.4 Relation with Time

A failure event is assumed to follow the assumption of Poisson flow, so that the probability of at least one failure during time T is expressed as:

$$P(T) = 1 - \exp(-\lambda T) \tag{6.1}$$

Here, λ is the rate of events. The assumption of Poisson flow is only applicable if the failure events may be considered as independent events. By considering the rarity of a failure, this assumption seems to be reasonable and can be explicitly checked. The problem of determining the probability of a failure may be considered to be solved completely, if the rate of an event is found (Sevastianov 1994).

6.2 Addressing the Problem of Rarity

This subsection reviews three methods that are being developed for dynamic stability problems: the peaks-over-threshold method (using a fitted distribution of the peaks exceeding a fixed roll angle threshold), the split-time method (where the stability failure is associated with the upcrossing of a time-variant roll-angle-threshold, with roll rate exceeding the critical value), and the wave group method (where the ship response is evaluated) for a series of deterministic sequence of waves with random initial conditions.

6.2.1 Peaks over Threshold Method

Statistical extrapolation, as is obvious from the term itself, is focused on the use of observed statistics for the prediction of the statistical characteristics of an event which is too rare to observe directly. In principle, extreme value theory (Gumbel 1958) allows one to derive a distribution of the largest value observed during a given time. However, these derivations require exact knowledge of the distribution of the value and are quite

lengthy even for a normal distribution. At the same time, formulae for the distribution of an extreme itself are quite simple. Depending on the distribution of the value, it could be one of three extreme value distributions: Gumbel, Frechet, and Weibull. As a result, the practical solution is to fit one of these distribution using either experimental or simulation data. This approach has been used by McTaggart (2000, 2000a) and McTaggart & deKat (2000) to evaluate the probability of stability failure of an intact vessel.

The main difficulty with this approach is that collected motion data are statistically dominated by small motions, which may make a purely statistical prediction quite questionable. This difficulty can be avoided by applying the Principle of Separation. In terms of a statistical fit, this means that only the data above the threshold are used for extrapolation. The non-rare problem consists of a simple counting of the exceedances of a process over a given threshold. The threshold is chosen to separate regions where a linear solution is applicable from the regions where nonlinearity may be significant for the failure event of interest. The rare problem is solved by fitting an extreme value distribution to the data over the threshold. The method is generally known as the Peaks-Over-Threshold (POT) method. The application of the POT method for stability failures is considered by Campbell and Belenky (2010). The concept of the method is illustrated in Figure 6.1.

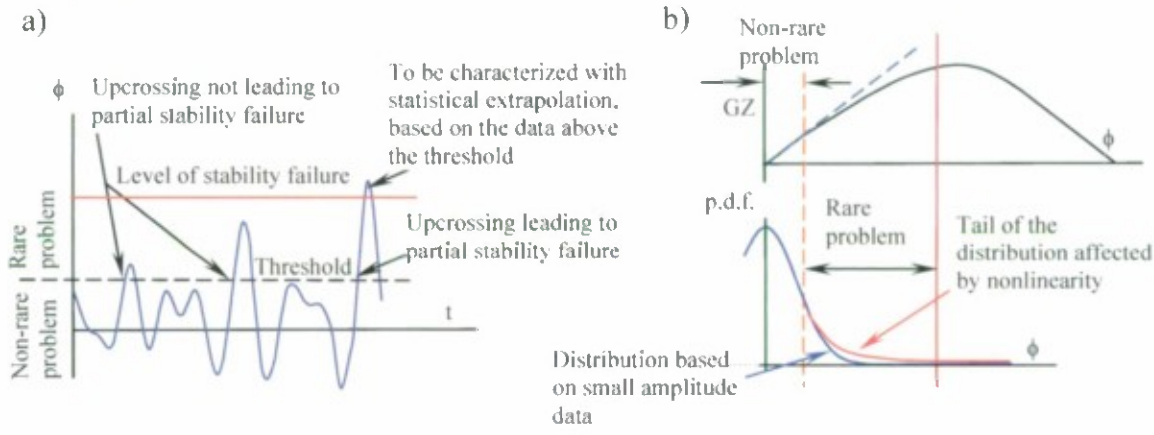

Figure 6.1 The Concept of the Peaks-Over-Threshold Method, (a) the General Scheme; (b) Influence of the Threshold

The POT method separates the solution based on a threshold. The rate of events is determined in the form:

$$\lambda = \xi \cdot P_C. \tag{6.2}$$

Here, ξ is exceedance rate of a threshold and P_C is a conditional probability of a given failure if the threshold has been crossed. It can also be considered as the fraction of upcrossings which lead to a failure. The evaluation of the upcrossing rate is the objective of the non-rare problem, while the conditional probability of failure is the objective of the rare problem.

The non-rare problem is well known from the theory of stochastic processes (e.g. Kramer and Leadbetter, 1967). If the distribution of a stationary process and its derivative are known, then the upcrossing rate can be expressed as:

$$\xi = f(\phi_{m0}) \int_0^{\infty} \dot{\phi} f(\dot{\phi}) d\dot{\phi} \tag{6.3}$$

The problem of modeling the distribution, based on the results of numerical simulations accounting for statistical uncertainty, is considered in Belenky and Weems (2008a). The non-rare-problem can be solved statistically by counting the number of observed upcrossings (upcrossing rate is the mean number of events per unit of time). Confidence intervals for the estimate can be evaluated using the binomial distribution of an auxiliary random variable (Campbell and Belenky, 2010, Belenky and Campbell 2011).

There are two possible formulations for the rare problem: using an extreme value distribution, or using a statistical fit of the peaks above the threshold. The formulation for the rate of events using extreme value distribution (Campbell and Belenky, 2010a) is given as:

$$\lambda = -\frac{1}{T_W} \ln\left(\exp(-\xi T_W) + (1 - \exp(-\xi T_W)) F_{EV}(\phi_{m2})\right) \tag{6.4}$$

Here, the level ϕ_{m2} is associated with stability failure and T_W is the observation time used to fit the extreme value distribution F_{EV}.

It is also possible to fit a distribution using a sample of the peaks that exceed the threshold. In this case, the formulation becomes very similar to the split-time method:

$$\lambda = \xi \cdot P_C; \quad P_C = \int_{\phi_{m2}}^{\infty} f_{POT}(\phi) d\phi = 1 - F_{POT}(\phi_{m2}) \tag{6.5}$$

Here, f_{POT} is a distribution fitted using the available data of peaks over the threshold and F_{POT} is the corresponding cumulative distribution function.

The application of the POT method is limited by relatively mild nonlinearity. Roughly, this means that the level ϕ_{m2} associated with stability failure should not exceed the maximum of GZ curve. The data used for the rare problem may not contain enough statistical information on the behavior of the system beyond that point. The range around the maximum of the GZ curve is characterized by severe nonlinearity, caused by the simultaneous influence of the attractor at upright equilibrium and the repeller at the angle of vanishing stability. This severe nonlinearity is manifested in a very significant sensitivity to initial conditions, resulting in tremendous physical uncertainty for data collected in this range.

As the intended use of the POT method is the evaluation of the probability of a partial stability failure, the method has been generalized to handle cases when the Poisson flow assumption may not be directly applicable. This includes cases with following and stern quartering seas, parametric roll resonance, and other cases when the response spectrum becomes narrow and the response itself becomes clustered. It also includes cases when the failure is defined as the crossing of a level on either side: port or starboard. As the Poisson flow requirements must be met to relate the probability of failure with the time of exposure, an envelope is used instead of the actual process.

As the proeess of motions is not neeessarily narrow banded, the uperossing of a theoretieal envelope may overestimate the rate of failures, therefore, a pieeewise linear approximation ean be used instead (see Figure 6.2).

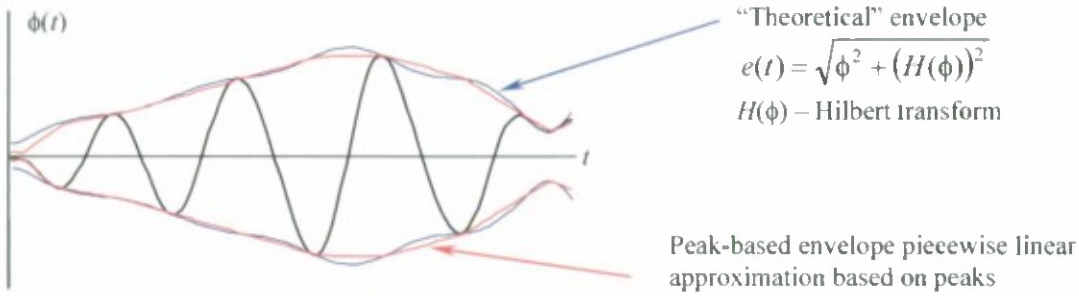

Figure 6.2 Approximation of the Envelope for a Non-Narrow Banded Process

All the ealeulations, ineluding the eounting of uperossings and the fitting of distributions, are performed on the peak-based envelope rather than the proeess itself. This version of the POT method is known as the Envelope Peaks-Over–Threshold, or EPOT, method (Campbell and Belenky, 2010a, Belenky and Campbell 2011).

The POT/EPOT method ean utilize data from numerieal simulation and/or physieal model tests, but may not be applieable to eonditions with severe nonlinearity, sueh as roll angles above the maximum of the GZ eurve, as it does not eontain an explieit model of extremely nonlinear motion.

6.2.2 Split-Time Method

The split-time method also separates the solution based on a threshold; however, the method is meant to be applieable for severe nonlinearity, up to eapsize. The rate of events is determined by formula (6.2), while the applieation of the split-time method for the evaluation of eapsizing probability is illustrated in Figure 6.3.

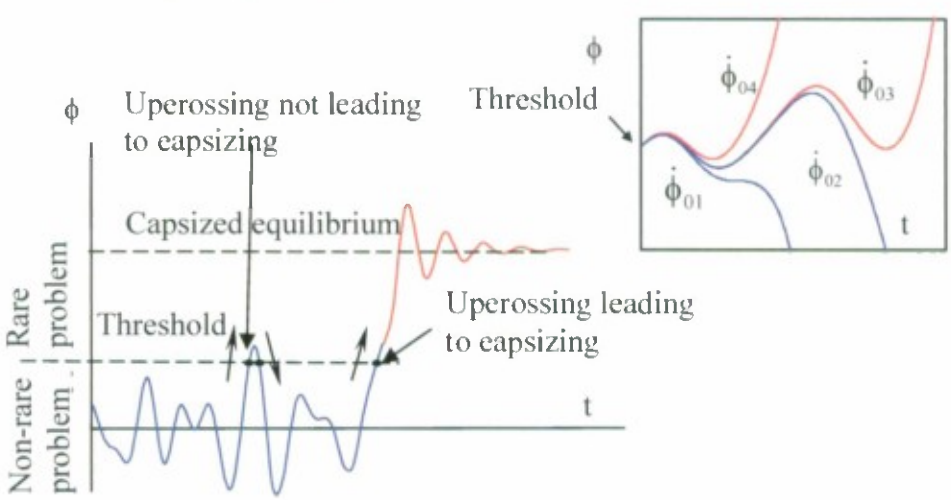

Figure 6.3 Applieation of the Split-Time Method for Evaluating Capsizing Prohability

The formulation of the non-rare problem is identical to that of the POT method. The solution of the rare problem is found by a set of short simulations, which are focused on finding the initial conditions at upcrossing which lead to a response event of interest (e.g. a large roll angle or slamming event). For example, when the capsizing problem is considered with just one degree of freedom, the only initial condition needed is the roll rate at the upcrossing of the specified threshold. A value of the roll rate at upcrossing that exceeds the rate that leads to capsizing is the critical roll rate. Its value can be determined by a bisection-line method, as illustrated in the insert to Figure 6.3. Once the critical roll rate is determined, the conditional probability of capsizing after upcrossing is expressed as:

$$P_C = \int_{\dot{\phi}_{cr}}^{\infty} f_u(\dot{\phi}) d\dot{\phi} \tag{6.6}$$

Here, $f_u(\dot{\phi})$ is the distribution of roll rate at upcrossing. It is not equal to the probability density function (PDF) of roll rates, as an instant of upcrossing is not just any occurrence. The distribution of roll rate at upcrossing can be expressed as follows (Belenky, *et al.*, 2008a; 2010)

$$f_u(\dot{\phi}) = \frac{\dot{\phi} f(\dot{\phi})}{\int_0^{\infty} \dot{\phi} f(\dot{\phi}) d\dot{\phi}} \tag{6.7}$$

This method can be applied for cases of extreme nonlinearity, as it contains an explicit model of very large motions. The method has been generalized for problems related to changing stability in waves, such as pure loss of stability, by tracking the change of the GZ curve in time (Belenky, *et al.*, 2009; 2010). An algorithm for these calculations was described by Belenky and Weems (2008) and has been implemented in Large Amplitude Motion Program (*LAMP*) ship motion simulation code (Lin and Yue 1990; 1993). An example of the GZ curve change for the ONR Topside Series, tumblehome configuration (ONRTH) (Bishop, *et al.*, 2005) is shown in Figure 6.4.

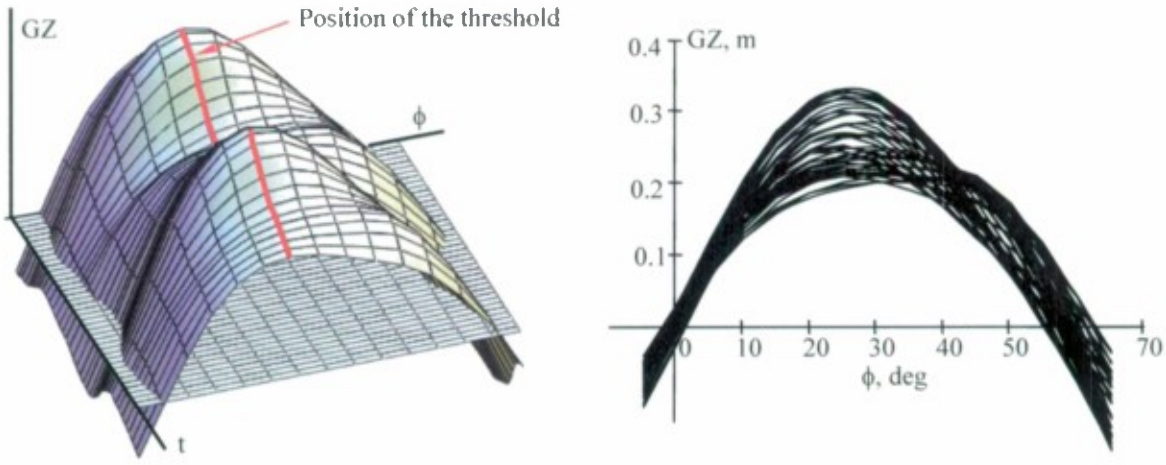

Figure 6.4 Change of the GZ Curve in Time, ONRTH in Stern Quartering Seas, Sea State 7, Speed 15 Knots

The random changes of the GZ curve in irregular waves result in the necessity of modeling the threshold roll angle as a stochastic process. In principle, this does not change the general scheme of application of the split-time method (see Figure 6.5). The critical roll rate also becomes a stochastic process. To express the probability of capsizing in this case, three stochastic processes must be introduced:

$$x(t) = \phi(t) - \phi_m(t) + \phi_{m0}\,; \quad y(t) = \dot{\phi}_{cr}(t) - \dot{\phi}(t)\,; \quad \dot{x}(t) = \dot{\phi}(t) - \dot{\phi}_m(t) \tag{6.8}$$

Here, $\phi_m(t)$ is the changing threshold, while ϕ_{m0} is a position of the threshold in calm water. The process $x(t)$ shows the distance to the moving thresholds, the process $\dot{x}(t)$ is its derivative, and the process $y(t)$ is the difference between the instantaneous and critical roll rate. Then, the rate of capsizing can be expressed as:

$$\lambda = \xi \cdot P_C\,; \quad \xi = f(\phi_{m0}) \int_0^\infty \dot{x} f(\dot{x}) d\dot{x}\,; \quad P_C = \int_{-\infty}^0 f_u(y) dy \tag{6.9}$$

Here, $f_u(y)$ is a distribution of process $y(t)$, at an instant when the process $x(t)$ upcrosses the threshold. It has been shown (Belenky, *et al.*, 2009) that this distribution can be expressed as:

$$f_u(y) = \frac{\int_0^\infty \dot{x} f(\phi_{m0}, \dot{x}, y) d\dot{x} dy}{f(\phi_{m0},) \int_0^\infty \dot{x} f(\dot{x}) d\dot{x}} \tag{6.10}$$

In this case, the capsizing event is considered as an upcrossing through the time-dependent threshold, where the instantaneous roll rate exceeds the critical roll rate (see Figure 6.6).

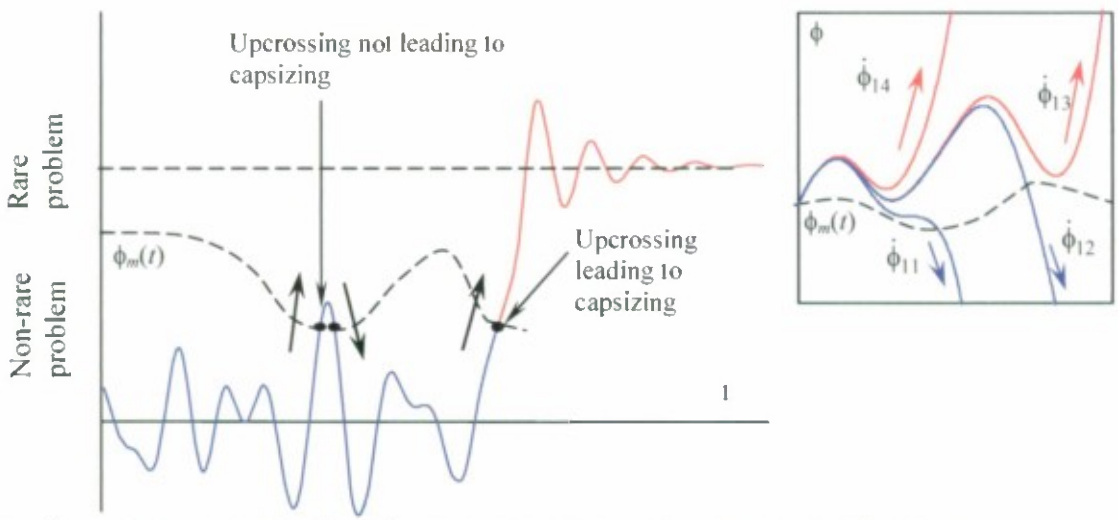

Figure 6.5 Application of Split-Time Method for the Case of Changing Stability in Waves

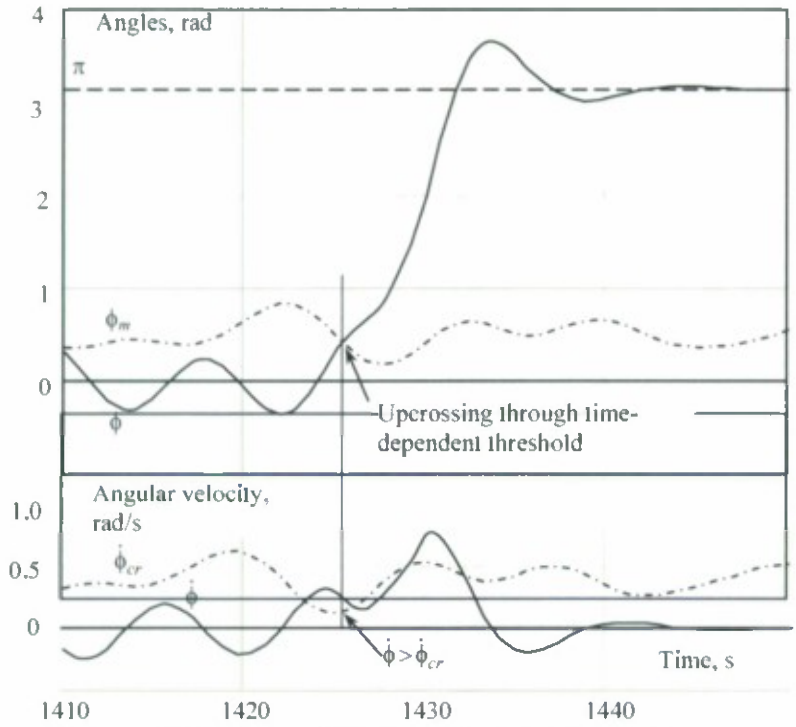

Figure 6.6 Definition of Capsizing With Critical Roll Rate

The testing of the concept of the split-time method with changing stability has been performed with a piecewise linear system, where the decreasing part of stiffness was random. A special formulation of a piecewise linear term for stiffness allows for the derivation of a closed form solution. The convergence of statistics to the theoretical solution has been demonstrated (Belenky, *et al.*, 2009).

It may be possible to extend the split time method for surf-riding by considering a spatial phase portrait described by Spyrou (1996) as a frozen frame in time. A similar approach was used by Vishnubhota *et al.*, (2000) for the definition of invariant manifolds for irregular waves.

In principle, the split-time method can be used with numerical simulations and/or model test data. The solution of the non-rare problem does not encounter any significant difficulties, although the experimental implementation of the rare problem may be challenging, as it requires full control of initial conditions. Some additional discussion on this topic occurs later in this section.

6.2.3 Method of Wave Groups

The wave group method separates the problem differently: the first part corresponds to ordinary oscillatory response of small amplitude; while the second represents the extreme behavior produced by the encounter of the wave group. The key concept associated with this method is to extract all those sequences of waves ("wave groups") that result in unacceptably large dynamic response with random (but near the upright state) initial conditions.

The occurrence and characteristics of wave groups has been studied extensively in oceanography (for a brief review see Bassler *et al.*, 2008; 2010). From the oceanographic point of view, there are two principal approaches to define wave groups: the envelope theory of Longuett-Higgins (1957); and the use of a Markov chain representation based on Kimura (1980). The formulations typically consider wave events that occur above a given threshold. However, from the ship response perspective, the important characteristics are different from those used typically in an oceanographic context. Here, both the amplitude and duration of the wave events must be considered. A definition of this wave sequence, or wave group, from the ship response perspective is proposed in Bassler *et al.* (2010a); this is briefly discussed below and illustrated in Figure 6.7

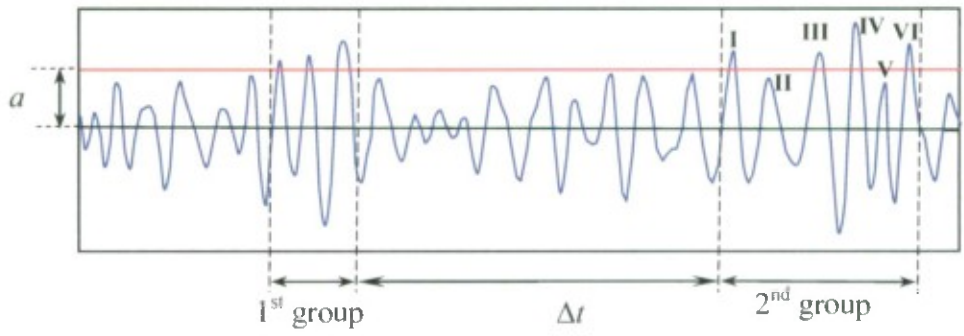

Figure 6.7 Definition of Wave Groups from the Ship Dynamics Perspective: Wave Events Must Occur Far Enough Apart in Time, So That the Autocorrelation Function of Ship Response Effectively Decays.

Groups of large waves, as well as single large waves, can be reproduced deterministically in an experimental basin (*e.g.* Davis and Zarnick 1964, Clauss 2000, Bassler *et al.*, 2008; 2009). Different aspects related to the application of assessing the response to wave groups and single large waves were discussed by Blocki (1980), Tikka and Paulling (1990), Boukhanovsky and Degrtyarev (1996), and Alford, *et al.* (2007). The first complete implementation of this type of approach with quantitative results was proposed during the SAFEDOR project (Spyrou and Themelis 2005; Themelis and Spyrou 2007; 2008). Similar approaches were followed more recently by Umeda *et al.* (2007) and Bassler *et al.* (2010, 2010a).

Intrinsic to Kimura's approach is the non-zero correlation between consecutive waves. This is accommodated by means of a correlation coefficient, γ_h, between successive wave heights that, in turn, determines the mean group length, $\bar{j}$.

A first order autoregressive model could be used for modeling the process of successive waves. As it's known, an autoregressive representation of a variable Y at time t depends on certain instants of its past, plus a random variable. For an autoregressive process of order r:

$$Y(t) = n_1 Y(t-1) + .. + n_r Y(t-r) + \varepsilon(t) \qquad (6.11)$$

where n_1,..., n_r are weights that can be related with correlation coefficients and $\varepsilon(t)$ is a zero mean Gaussian white noise process. A first-order autoregression process has the Markov chain property, meaning that the value of $Y(t)$ is completely determined by the

knowledge of $Y(t\text{-}1)$. Kimura had proposed the bivariate Rayleigh distribution as the joint PDF of successive wave heights H_1 and H_2 that depends on a correlation parameter κ; that in turn is a function of the correlation coefficient γ_h mentioned earlier (see Kimura 1980, and also Themelis and Spyrou 2008 for more details). The probability of a sequenee of high waves using the eonditional probability that a wavc height exceeds the threshold level H_{cr}, given that the previous wave also exceeds H_{cr} is eomputed from the following joint PDF:

$$p_{22} = P\left(H_{i+1} \geq H_{cr} \mid H_i \geq H_{cr}\right) = \frac{\int_{H_{cr}}^{\infty}\int_{H_{cr}}^{\infty} f(H_1, H_2)\,dH_1 dH_2}{\int_{H_{cr}}^{\infty}\int_{0}^{\infty} f(H_1, H_2)\,dH_1 dH_2} \tag{6.12}$$

The probability that a wave group has a run length, j, is then:

$$p(j) = (1 - p_{22})\,p_{22}^{j-1} \tag{6.13}$$

In Kimura's theory, group properties are not derived from the spectrum but they eome from the parameter γ_h, whose ealeulation is based on a series of wave heights. To improve Kimura's theory on this, Battjes and Van Vledder (1984) introduced a new correlation paramcter κ_s, determined from a spectrum:

$$\kappa_s^2 = \frac{1}{m_0}\left|\int_0^{\infty} S(\omega)\, e^{i\omega t}\, d\omega\right|, \quad t = T_{m2} \tag{6.14}$$

where $T_{m2} = 2\pi\sqrt{m_0/m_2}$ is thc average period between zero–uperossings. Then a new correlation coefficient, γ_s, can be produced. The parameter γ_s is, in reality, thc eorrelation coefficient between points of the wave envelope function, $\alpha(t)$, separated by a constant time interval, T_{m2}. Therefore, the correlation coeffieient between discrete waves is replaced (with certain assumptions that, in a strict sense, could only be satisfied in the limit of narrow spectra) by the correlation coefficient between points of the wave envelope. Stansell, *et al.* (2002) proposed calculating the correlation parameter, κ_s, not only for the mean zero upcrossing period, T_{m2}, but also for $T_m/2$ and $3T_m/2$, thus putting forward an improved (averaged) correlation eoeffieient.

An alternative viewpoint to modeling the wave group is discussed below: A failure ean be eaused by a single wave, or by a wave group, each resulting in different dynamical response characteristics for the ship. Therefore, the rate of failures could be expressed as a combination of both types of excitation events:

$$\lambda = \lambda_G \cdot P_{FEG} + \lambda_S \cdot P_{FES} \tag{6.15}$$

Here, λ_G is the rate of encounter for a wave group, and λ_S is the rate of eneounter for a single wave. P_{FEG} is the probability of failure if a wave group is encountered and P_{FES} is the probability of failurc if a single wave is encountered.

The usc of equation (6.1) for relating the probability of failure with thc timc of exposure implies the indcpendence of eneounters with either a wave group or single wave event. This leads to the definition in equation (6.15) of a wave group or a single wave, as

shown in Figure 6.7. In this case, from the ship dynamics perspective, all three waves in the first group must be considered as one excitation sequence event, or wave group event, while all six waves in the second group are considered as another event.

In order to use Poisson flow for modeling the relation with time, one may consider the response to a wave group encounter as a single random event; then the response to the current wave group should be independent from the response to the previous group. As a result, there should be enough time between these groups for the autocorrelation function of the response to effectively die out. Therefore, large waves that are close to each other in sequence could be considered as part of the same sequence, or group, even if they are intermittently separated by a few small waves. This approach is somewhat different from the mainstream wave group approach in the literature.

Two values are needed for this definition from the ship dynamics perspective: the threshold, a, and the time duration, Δt. Both of these values can be linked to ship-specific properties and enable ship-specific formulation of the characteristics of the wave sequence (or wave group) of interest. The threshold is defined as the amplitude of the excitation that leads to a significantly nonlinear response. One way to define this amplitude for roll motion is to use the roll response curve, see Figure 6.8a, where ϕ_a/ϕ_v is the ratio of the amplitude of response and the angle of vanishing stability. For this motion, significant nonlinearity can be characterized as the theoretical possibility of fold bifurcation; this requires the existence of at least one point on the response curve where the tangent is vertical. The smallest amplitude of excitation, α_1, which results in the appearance of such a point, can be used to determine the amplitude of wave steepness and to define the threshold. It may be observed that this threshold also corresponds to the onset of nonlinearity in the ship-specific roll stiffness (GZ curve).

The interval between the wave events, groups of large waves, or single large wave can be evaluated using the autocorrelation function, $R_\phi(\tau)$, of the linear or linearized response, from the non-rare problem, see Figure 6.8b. The use of the linear or linearized response is fully justified, as the large amplitude response is only expected as a result of a single or small group of large waves. As a result, a linear, or linearized, model can be used to determine the response between the excitation events of interest. The same method is also a source of data for initial condition at the instant of group encounter.

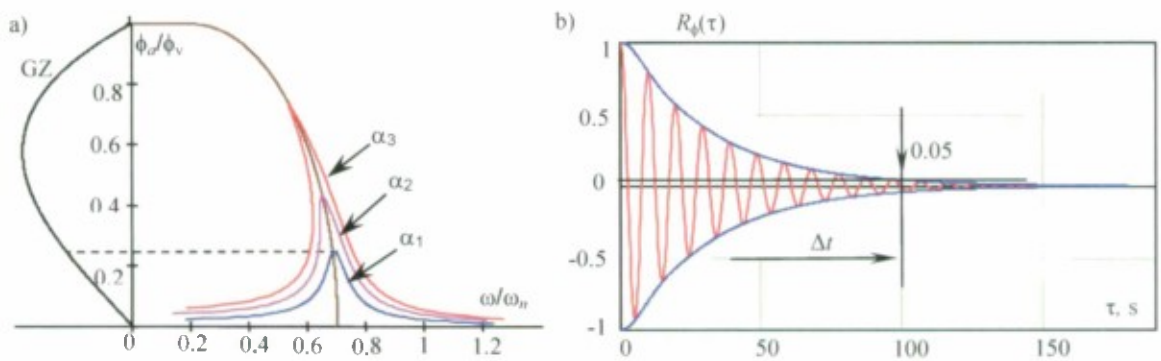

Figure 6.8 The Definition of Wave Groups: (a) Determining the Threshold and (b) Time Duration

The non-rare problem is simply evaluating the response of the linear, or linearized, system in the frequency domain. This produces the autocorrelation function that is used for defining the wave groups and characterizes the initial conditions for an encounter with the wave group or a single large wave. The rare problem consists of evaluating the response of a nonlinear dynamical system to a deterministic group of waves or to a single large deterministic wave. The initial conditions of the dynamical system at the moment of encounter with the wave event are random and have a normal distribution. The variance and mean, if any, are known from the non-rare problem.

Bassler, *et al.* (2010) described statistical testing of the concept using simulated wave elevation data. It was shown that a random event of encountering a wave group and a single large wave follows Poisson flow, as the time between these events has an exponential distribution, see Figure 6.9a. A method to estimate rates of encounter for a group and a single wave was also proposed. This can be performed using the distribution of the number of waves in a group, or the probability mass function (pmf), where the first bin corresponds to the single large wave events (see Figure 6.9b).

A series of wave parameter distributions were also studied, including amplitude, period, and steepness of the first, second, and third waves in a group. These data may be useful to help formulate a model of a wave group based on ship-specific characteristics with consideration of the different dynamical response mechanisms associated with single wave and multiple wave encounters.

The wave group method can be applied to model tests and/or numerical simulations. Using either technique, the probability of failure due to encounter, P_{FEG} and P_{FES}, as given in equation (6.15), can be determined. However, because of the formulation of the principle of separation in this method, precise control of initial conditions is necessary. This is the subject of ongoing work. For numerical simulations, one realization for each set of initial conditions can be used to determine the probability of failure due to the deterministic wave sequence. For model tests, because of inherent experimental uncertainties, a set of runs for each initial condition can be used to determine the probability of failure. The number of necessary experimental realizations is determined by the precision of the control of initial conditions that is possible in a basin with deterministic wave generation capability.

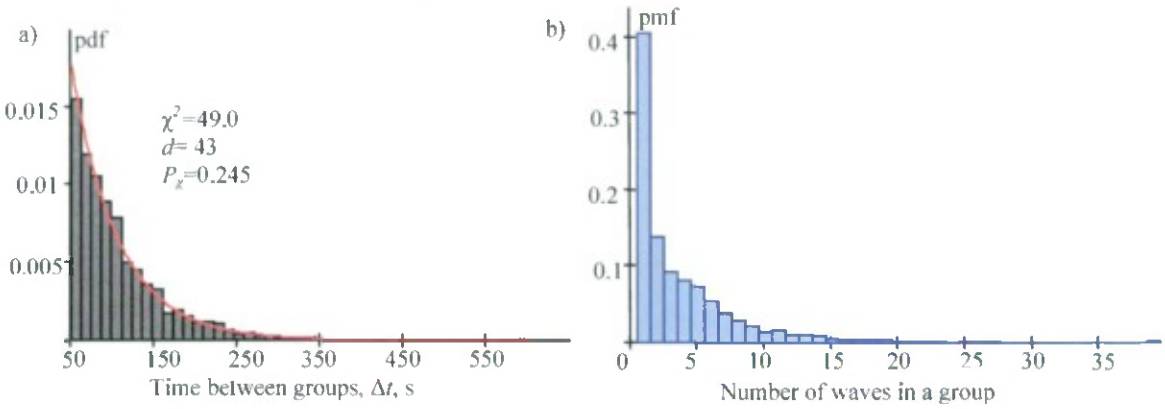

Figure 6.9 Distribution of the Time Duration Between Groups (a), and the Number of Waves in a Group (b); Statistics Estimated Based on 200 Simulated Records of Wave Elevation, 30 min Each; Threshold was a = 5 m, Time Between Groups Δt = 50 s

6.3 Specifics of Validation of Solution of the Problem of Rarity

6.3.1 General

The validation of numerical tools intended to characterize rare events is more than just a challenging task. Some considerations of how the principle of separation can be used to assist with this task are discussed below. However, the practical implementation of these ideas remains the subject of future work.

Reed (2009) reviewed different aspects related to the validation of simulation tools in context with two related processes: verification and accreditation. As emphasized by Reed, bifurcation analysis is important as it allows a demonstration that the theoretical basis of a simulation tool correctly reproduces the qualitative behavior of the nonlinear dynamical system. Quantitative validation may include comparisons with experimental measurements of the forces acting on ship and the resulting motions, including trajectories for maneuvering in steep waves.

The validation of simulation tools for large motions in irregular waves presents significant additional challenges related to the stochastic nature of the processes and the rarity of events, and also the problems related with nonlinear behaviors. An application of the principle of separation can simplify the required validation by allowing separate validation of the non-rare and rare problems.

6.3.2 Validation of Wave Model

Initial consideration is given to the validation of the wave model. The usual procedure is to compare spectra for the environmental conditions of interest. However, this may be insufficient for the simulation of rare events.

The wave model used in a simulation tool must provide a reasonable representation of the statistical characteristics of real waves, taking into account unavoidable uncertainties caused by the finite volume of experimental and simulated sample data. The first issue is related to the reliable comparison of two variance estimates, while both of them are random numbers.

A comparison of the distribution of wave elevation with the theoretical normal distribution may also prove useful. Because a wave-maker is also a nonlinear system, it may disturb the normality of the distribution. If an experiment is carried out in natural (irregular) waves, such as in a large-scale or full-scale environment) the normality of the distribution can be disturbed by influences due to current, the shoreline, bottom effects, etc. If this is the case, the expectations for the accuracy of validation may need to be adjusted.

Because the interest is in simulation of the nonlinear ship response, consideration of the wave effects on the instantaneously submerged portion of the hull is necessary. Particularly for large, steep waves, the fluid pressures and orbital velocities below the free-surface may vary significantly, and not be adequately captured by lower-order models (Minnick, *et al.*, 2011a). The wave model used in the simulation must have

sufficient accuracy to represent the fluid behavior for the wave conditions of interest. Although difficult, model experiments may be performed to determine the velocity-field characteristics for these types of events (Minnick, *et al.* 2010; 2011; 2011a) and then used to validate the selected wave model.

Another aspect to be addressed is the stationarity of experimental wave data. While it is not considered to be a problem for an experiment in a controlled environment, the stationarity of natural waves in large-scale testing may be an issue. A metric used to assess the degree of stationarity in these conditions could be very useful for validation. One possible metric could be the use of the "run test" to evaluate the duration of stationarity, as discussed by Bendat and Piersol (2010).

If wave elevations are determined with the traditional inverse Fourier transform of the wave spectrum, the resulting time history is valid as a model of a stochastic process for a limited time. This time depends on the number of frequencies considered in the model. In the case of an insufficient number of frequencies, the restored time history of wave elevations may suffer from self-repeating effects (Belenky and Sevastianov, 2007). The presence of the self-repeating effect can be revealed by calculation of the autocorrelation function, using the cosine Fourier transform from the given spectrum, with an accepted frequency set.

6.3.3 Validation of Non-Rare Solutions

Validation of the solution for the non-rare problem has a mostly statistical character and may be different for each method.

The split-time method was originally developed to evaluate the probability of capsizing. However, it can be used to calculate the probability of partial stability failure (e.g. a large roll or yaw angle) as well. The threshold used in this method is fairly high, relative to the degree of nonlinearity of the system, and is a random value. The threshold is located on randomly changing *GZ* curve and therefore, depends on the method used to calculate the *GZ* curve in waves.

A direct validation of the calculated *GZ* curve in waves may not be simple. However, several key points can be checked experimentally. In one key stability condition of interest, a ship model travels with the wave celerity, close to the wave crest. The position of the ship model relative to the wave crest can be estimated from a video record. The model has an asymmetric load and, therefore, is heeled. The angle of heel depends on the instantaneous righting arm in waves and can be compared with calculated value. Such an experiment could also reveal how much influence the local waterplane distortion has on the stability in waves and how accurate quasi-static calculations of the instantaneous *GZ* curve (Belenky and Weems, 2008) really are.

Nevertheless, it may be possible to compare experimental and numerical solutions of the non-rare problem using a so-called "equivalent" threshold. This threshold is defined as follows: the same number of upcrossings of roll motion through an equivalent threshold exists as the roll process has through the random threshold. Then the rate of upcrossing through the equivalent threshold can be compared with experimental data. A similar approach may be taken towards the distribution of roll rates at upcrossing.

Another aspect of the validation of the non-rare solution is the direct comparison of the statistical characteristics of motions between an experiment and numerical simulation. As the threshold is relatively high, the motion response may be influenced by nonlinearity, including practical non-ergodicity (Belenky and Sevastianov, 2007). The effect of practical non-ergodicity may be observed as the increased difference between the statistical characteristics of different records belonging to the same ensemble. It is desirable to quantify the effect of non-ergodicity, as it is unrealistic to expect that the difference between the experiment and simulation can be smaller than the one caused by practical non-ergodicity.

In contrast to the split-time method, the non-rare solution of the peaks-over-threshold method is expected to be within the linear range. However, the tail of the distribution remains above the threshold. Therefore, the distribution of motions is, in fact, truncated. This must be accounted for when making a comparison of the variance estimate of the motion. The expected accuracy of the statistical estimate below the threshold is higher than the estimates of the whole process. The same can be observed about the distributions – a comparison of the distribution of values below the threshold is expected to yield a more definitive answer since the influence on nonlinearity and the associated uncertainties are minimal. The distribution of both motions and velocities are expected to be close to normal.

In the case of the POT method, the distribution of the peak-based envelope values is expected to be close to Rayleigh. In the case of a narrow banded process, the derivatives of a peak-based envelope are expected to be close to normal. In both cases, the statistical comparison of the estimates of upcrossing rates is meant to be a very important validation parameter.

In principle, the validation of the non-rare problem for the wave group method is similar to the peaks-over-threshold. The difference is that the threshold is defined in terms of excitation, rather than the motion displacement. For this method, the distribution of motion and its derivative at upcrossing of the excitation process are the focus for validation.

6.3.4 Validation of Rare Solutions

To validate the solution of the rare problem in the split-time method, one should demonstrate that a ship capsizes if a critical roll rate is exceeded. As it is very difficult to control initial roll rate, it may be attempted backwards by checking the roll rate at the instant of threshold crossing for a time-series where capsizing was actually observed. This experiment can be done in steep regular waves, where observing capsizing is not so difficult, and the instantaneous waterline is relatively easy to estimate– reducing the uncertainty of the calculations of the *GZ* curve in waves and the critical roll rate.

Validation of the rare solution for the POT method appears to be rather straight forward. Two distributions of peaks (or envelope peaks) above the threshold can be compared using the Pierson chi-square goodness-of-fit test. Additionally, statistical frequencies which exceed a certain level above the threshold can be compared. A

significant difference between them can be evaluated to determine if such a difference is caused by random factors.

Validation of the rare solution for the wave group method has two components. First, it must be demonstrated that the proposed model of wave groups is a true representation, supported by statistical data from the realistic seaway conditions of interest. Second, the numerical response of a ship being excited by the wave group agrees well with the behavior obtained with experimental realizations of the deterministic wave group. This can be achieved by direct comparison with experimental results in a basin capable of reproducing deterministic wave groups (Bassler, *et al.*, 2008; 2009). However, as mentioned previously, the precise control of initial conditions is an essential component to this experimental validation and is currently being pursued.

6.4 Summary

This section contains an overview of the issues related with the direct assessment of dynamic stability for ship found to be vulnerable.

Subsection 6.1 considers the most general problem related to the direct assessment of dynamic stability. Failures related to large ship responses (motions and/or loads) in waves are rare, and large-amplitude ship motions are significantly influenced by the nonlinearity of the dynamical system. The necessity of modeling these significant nonlinearities results in only one option for simulation – the Monte-Carlo method in the time-domain, while the rarity of occurrence of the failure events makes direct "brute-force" approaches computationally cost prohibitive. The principle of separation seems to provide an alternative to overcome this difficulty. The concept is to consider, separately, the nonlinear phenomena resulting in a large response and the conditions which result in the occurrence of such phenomena. This can be achieved by introducing an intermediate threshold, the crossing of which is frequent enough to be observable. The probabilistic characteristics of the conditions leading to a failure are considered at the instant of the crossing of the threshold. As a result, the problem is separated into two sub-problems: non-rare (crossing of the threshold) and rare (evaluation of conditions at the threshold which result in a failure).

Subsection 6.2 reviews three methods that are being developed for dynamic stability problems: the peaks-over-threshold method (using a fitted distribution of the peaks exceeding a fixed roll angle threshold), the split-time method (where the stability failure is associated with the upcrossing of a time-variant roll-angle-threshold, with roll rate exceeding the critical value), and the wave group method (where the ship response is evaluated) for a series of deterministic sequence of waves with random initial conditions.

Subsection 6.3 examines specifics of validation of tools of direct assessment keeping in mind extreme rarity of stability failures. It is shown that the principle of separation is also applicable for validation. The advantage of applying the principle of separation is the ability to perform validation separately for the non-rare and rare sub-problems. This separation allows both the physical and statistical uncertainty to be reduced, while also providing a robust validation technique for nonlinear phenomena.

This page is intentionally left blank

7 Sample Ship Population

A sample population of 17 ships was used for testing and evaluation of vulnerability criteria for three of the identified intact stability failure modes (pure loss of stability, parametric roll, and surf-riding). The general characteristics of these ships are given in Table 7.

Table 7 Ship Types and General Characteristics

Type	Note	L (m)	L/B	B/d	D/d
Bulk Carrier		275	5.85	2.67	1.36
Bulk Carrier 2		145	6.34	2.21	1.45
Containership 1	Post-panamax	322.6	7.07	3.05	1.65
Containership 2	Post-panamax	376	6.53	3.57	2.36
Containership 3	Post-panamax	330	7.24	3.55	2.26
Containership 4	Panamax	283.2	8.80	2.51	1.70
Containership 5	Post panamax C11-type	262	6.55	3.12	1.93
Fishing Vessel 1	Japanese purse seiner –ITTC Ship A2	34.5	4.53	2.87	1.16
Fishing Vessel 2		21.56	3.40	2.53	1.21
General Cargo 1	Series 60 CB=0.7 (S60)	121.9	7.50	2.51	1.60
General Cargo 2	C-4 type	161.2	7.05	2.73	1.61
LNG Carrier		267.8	6.39	3.57	2.29
Naval Combatant 1	ONR topside series –flared (FL)	150	8.19	3.42	3.09
Naval Combatant 2	ONR topside series –tumblehome (TH)	150	8.19	3.42	3.09
Passenger Ship		276.4	8.04	4.03	1.75
RoPax		137	6.76	3.64	3.24
Tanker		320	5.52	2.76	1.48

Twelve of these ships were previously considered in Peters, *et al.* (2010) for the assessment of stability failures related to righting lever variation (levels 1 and 2 pure loss and parametrie roll). Histograms of the distribution of the ratio of different hull form parameters (length-to-beam, beam-to-draft, depth-to-draft) for this sample ship population are given in Figure 7.1, Figure 7.2 and Figure 7.3.

Containership 5 is the C11-class containership. General Cargo Ship 1 is Series 60 hull form, C_B=0.7 variant (Todd, 1953). General Cargo Ship 2 is the C4 type, similar to the one used in Paulling, *et al.* (1972). Naval Combatants 1 and 2 are the ONR Topsides Series, flared and tumblehome configurations, respectively (Bishop, *et al.*, 2005). The RoPax is a notional vessel, similar to the one from a reported stability accident (MNZ, 2007). Fishing Vessel 1 is the ITTC Ship A2 (a Japanese purse seiner type hull form).

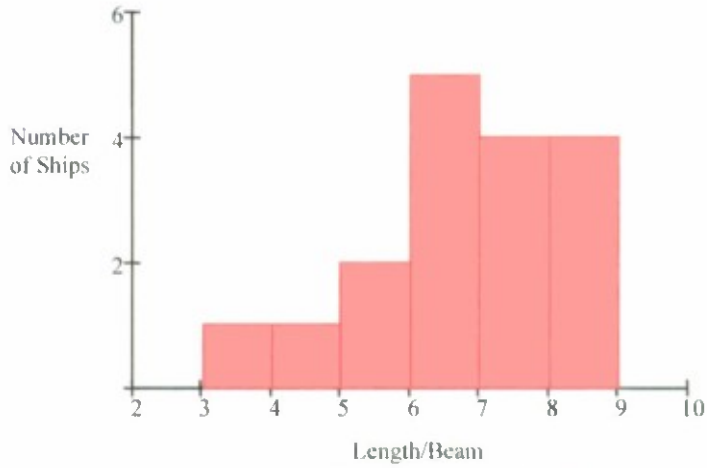

Figure 7.1 Length to Beam Ratio Distribution for the Population of 17 Sample Ships

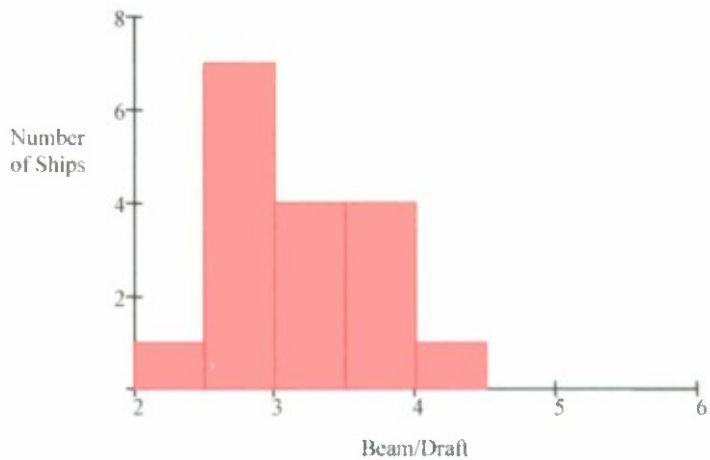

Figure 7.2 Beam to Draft Ratio Distribution for the Population of 17 Sample Ships

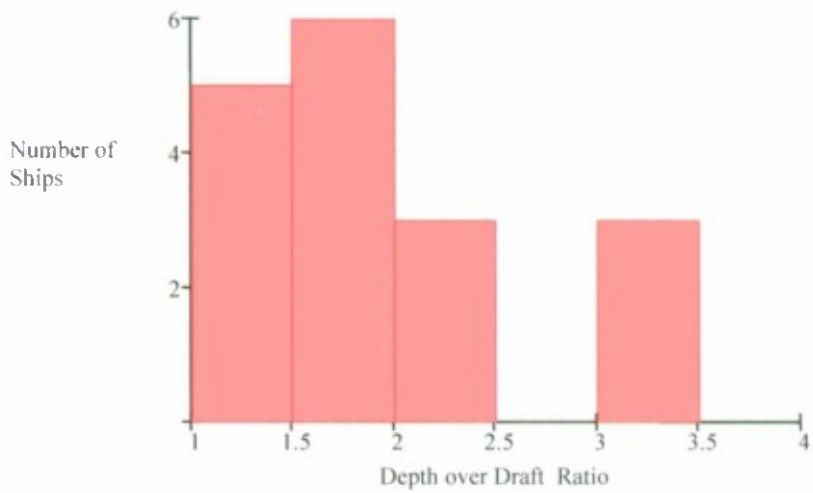

Figure 7.3 Depth to Draft Ratio Distribution for the Population of 17 Sample Ships

8 Conclusions

The main objectives of this project were to develop vulnerability criteria, test them, and prepare initial information on methods for direct stability assessment. The following summarizes the achievements and gives a brief outlook on future work.

The level 1 vulnerability criteria for parametric roll is built upon the transition solution of Mathieu equation. The proposed criteria consist of two conditions. The first condition examines if a ship is capable of achieving speeds that provide dangerous frequencies of encounter, while the second condition examines if the magnitude of stability changes may result in an increase in roll angle during a certain number of cycles.

The level 2 vulnerability criterion for parametric roll is based on numerical integration of roll equation using instantaneous GM or GZ. The mathematical model used is more sophisticated, in order to avoid possible excessive conservatism. The method accounts for irregular waves by limiting the number of waves, using a typical wave group with properties of a specified sea state. The criteria also includes the influence of heave and pitch (through attitude of the wave), and the nonlinearity of the GZ curve.

The level 1 vulnerability criterion for pure loss of stability is based on geometric characteristics of the hull, as these parameters reflect how significantly the waterline may change during a wave pass and therefore, are also related with possible stability deterioration of a ship on the wave crest.

The level 2 vulnerability criteria for pure loss of stability consist of two conditions. The first one is based on the average time that the ship's GM spends below the critical level during the wave pass. Specification of the critical level is also discussed. The second criterion is based on the likelihood of appearance of very large loll angles during the wave pass. Both criteria are based on the envelope presentation of irregular waves. A sea state is presented as a population of regular waves associated with a statistical weight, calculated with appropriate probability distributions.

Two alternative proposals for the level 1 vulnerability criteria for surf-riding are considered, but both of them are based on the second speed threshold– above this threshold surf-riding is inevitable in regular waves. Since the calculation of the second threshold is too complex for this level, the dependence of the Froude number corresponding to the second threshold on the wave steepness is calculated and approximated with a regression formula. This allows formulating the level 1 criterion as the linear dependence of the Froude number on the ship length. An alternative level 1 criterion is based on the same idea of the dependence on length; it simply limits the length of vulnerable ships to a value of 200 m.

The level 2 vulnerability criterion for surf-riding is also based on the second threshold, which is evaluated with Melnikov's method. The criterion is formulated for irregular waves using envelope theory, in a way similar to the level 2 vulnerability criteria for pure loss of stability.

All six of the vulnerability criteria were tested on the sample population of 17 ships including 5 container carriers, 2 fishing vessels, 2 bulk carriers, 2 general cargo vessels, 2 naval vessels, a passenger RoPax ferry, a passenger cruise vessel, an LNG carrier, and a tanker. Several of those ships had known vulnerability to parametric roll,

pure loss of stability, or surf-riding / broaching-to. The essenee of the testing was to see if the proposed eriteria would be able to distinguish ships with known vulnerabilities from ships that are known to be safe from the partieular mode of stability failure. All of the proposed eriteria were tested sueeessfully. Also, all of the proposed criteria were consistent between the levels. In other words, if a ship fails the level 2 eriterion, it always fails the level 1 eriterion.

The modified weather criterion was considered as a candidate for the level 1 vulnerability eriterion for dead ship eonditions. An analysis of the assumptions of the weather eriterion was earried out. However, due to the eomplex physieal nature of ship response in dead ship eonditions, the parameters of the eurrent weather eriterion underwent signifieant ealibration. This was done using a certain population of ships, whieh was typical at the time of the development of current weather criterion. As a result, the modification of the current weather eriterion may have limited applieability, and is not advisable.

The report also ineludes an overview of the methods for direet stability assessment. These are methods of numerieal simulation of model testing that are eapable of addressing the extreme rarity of stability failures, without ineurring impraetical expenses. It was shown that the applieation of the prineiple of separation allows for a praetieal solution.

Three methods whieh are being developed for dynamie stability problems were reviewed: the peaks-over-threshold method (using a fitted distribution of the peaks exeeeding a fixed roll angle threshold), the split-time method (where the stability failure is assoeiated with the uperossing of a time-variant roll-angle-threshold, with roll rate exeeeding the eritieal value) and the wave group method (where the ship response is evaluated for a series of deterministie sequenee of waves with random initial eonditions).

The problems related to validation of these methods and tools are very ehallenging. However, it was shown that the prineiple of separation is also applieable for validation. The advantage of applying the principle of separation is the ability to perform validation separately for both the non-rare and rare sub-problems. This separation allows both the physieal and statistieal uneertainty to be redueed, while also providing a robust validation technique for nonlinear phenomena.

9 References

ABS (2004) *Guide for the Assessment of Parametric Roll Resonanee in the Design of Container Carriers*, American Bureau of Shipping, Houston, Texas.

Alford, L.K., M.S. Khalid, D. Kim, K. Maki, and A.W. Troesch (2007) "A Methodology for Creating Design Ship Responses," *Proe. 10th Int. Symp. on Praetieal Design of Ships and Other Floating Struetures (PRADS 2007)*, Houston, Texas.

Andronov, A. A., A.A. Vitt and S. E. Khaikin, (1966) *Theory of Oseillators*, Pergamon Press, Oxford, New York.

Araki, M., N. Umeda, H. Hashimoto and A. Matsuda (2010) "Broaching Prediction Using an Improved System-Based Approach," *Proe. 28thth ONR Symp on Naval Hydrodynamics*. Pasadena, California.

Bassler, C, B. Campbell, W. Belknap, and L. McCue (2007) "Dynamic Stability of Flared and Tumblehome Hull Forms in Waves," *Proe. 9th Intl. Ship Stability Workshop*, Hamburg, Germany.

Bassler, C. (2008) "Application of Parametric Roll Criteria to Naval Vessels," *Proe. 10th Int. Ship Stability Workshop*, Daejeon, Korea.

Bassler, C. C., G. E. Lang, S. S. Lee, J. B. Carneal, J. T. Park, and M. J. Dipper (2008) *Formation of Large-Amplitude Wave Groups in an Experimental Model Basin*, Hydromechanics Dept. Report, NSWCCD-50-TR-2008/025.

Bassler, C.C., M.J. Dipper, and G.E. Lang (2009) "Formation of Large-Amplitude Wave Groups in an Experimental Basin in *Proe. 10th Int. Conf. on Stability of Ships and Oeean Vehieles*, St. Petersburg, Russia.

Bassler, C.C., V. Belenky, G. Bulian, A. Francescutto, K. Spyrou, and N. Umeda (2009) "A Review of Available Methods for Application to Second Level Vulnerability Criteria," *Proe. of the 10th Int. Conferenee on Stability of Ships and Ocean Vehicles*, St. Petersburg, Russia.

Bassler, C.C., V. Belenky, and M. J. Dipper (2010) "Characteristics of Wave Groups for the Evaluation of Ship Response in Irregular Seas," *Proe. 29th Int. Conf. on Ocean, Offshore and Aretie Engineering*, Shanghai, China.

Bassler, C.C., V. Belenky, and M. J. Dipper (2010a) "Application of Wave Groups to Assess Ship Response in Irregular Seas," *Proe. 11th Int. Ship Stability Workshop*, Wageningen, the Netherlands.

Battjes, J.A and G.Ph. van Vledder (1984) "Verification of Kimura's Theory for Wave Group Statistics," *Proe. 10th Int. Coastal Engineering Conferenee*, pp. 642-648.

Belenky, V.L. (1993) "A capsizing Probability Computation Method," *J. Ship Research*, Vol. 37, pp. 200- 207.

Belenky, V. L. and N. B. Sevastianov (2007) *Stability and Safety of Ships: Risk of Capsizing.* (2nd ed) SNAME, Jersey City, ISBN 0-939773-61-9.

Belenky, V. and K. M. Weems, (2008) "Probabilistic Qualities of Stability Change in Waves," *Proc. 10th Intl. Ship Stability Workshop,* Daejeon, Korea.

Belenky, V., and K.M. Weems (2008a) "Procedure for probabilistic evaluation of large amplitude roll motions," *Proc. of the Osaka Colloquium on Seakeeping and Stability of Ships*, Osaka, Japan.

Belenky, V. J.O. de Kat, and N. Umeda (2008), "Towards Performance-Based Criteria for Intact Stability," *Marine Technology*, Vol. 45, No 2, pp.101-123.

Belenky, V., Weems, K., M. and W.-M. Lin (2008a), "Numerical Procedure for Evaluation of Capsizing Probability with Split Time Method," *Proc. 27th Symposium on Naval Hydrodynamics,* Seoul, Korea.

Belenky, V., A.M. Reed, and K.M. Weems (2009) "Probability of Capsizing in Beam Seas with Piecewise Linear Stochastic GZ Curve," *Proc. 10th Intl. Conf. on Stability of Ships and Ocean Vehicles*, St. Petersburg, Russia.

Belenky, V., C. Bassler, and K. Spyrou (2009a) "Dynamic Stability Assessment in Early-Stage Ship Design," *Proc. of the 10th Int. Conference on Stability of Ships and Ocean Vehicles*, St. Petersburg, Russia.

Belenky, V. and C. Bassler (2010) "Procedures for Early-Stage Naval Ship Design Evaluation of Dynamic Stability: Influence of the Wave Crest," *Naval Engineers J.* ASNE, Vol. 122, No. 2, pp. 93-106.

Belenky, V.L., K.M. Weems, W.M. Lin. and K.J. Spyrou (2010) "Numerical Evaluation of Capsizing Probability in Quartering Seas with Split Time Method," *Proc. 28th Symp. Naval Hydrodynamics*, Pasadena, California.

Belenky, V., K.M. Weems, C.C. Bassler, M.J. Dipper, B. Campbell, and K. Spyrou (2010a), "Approaches to Rare Events in Stochastic Dynamics of Ships," *Proc. of 6th Int. Conf. Computational Stochastic Mech.* Rhodes, Greece.

Belenky, V., C.C. Bassler, M.J. Dipper, B. Campbell, K.M. Weems, K. Spyrou (2010b) "Direct Assessment Methods for Nonlinear Ship Response in Severe Seas," *Proc. of ITTC Workshop on Seakeeping,* Seoul, Korea.

Belenky, V. and B. Campbell (2011) *Evaluation of the Exceedance Rate of a Stationary Stochastic Process by Statistical Extrapolation Using the Envelope Peaks over Threshold (EPOT) Method*, Report NSWCCD-50-TR-2011/032.

Belknap, W., C. Bassler, M. Hughes, P. Bandyk, K. Maki, D. H. Kim, R. Beck, and A. Troesch (2010) "Comparisons of Body-Exact Force Computations in Large Amplitude Motion," *Proc. 28th Symp. on Naval Hydrodynamics*, Pasadena, California.

Bendat, J.S. and A. G. Piersol (2010) *Random Data: Analysis and Measurement Procedures* (4th Ed.), John Wiley & Sons, Inc., Hoboken.

Bishop, R. C., W. Belknap, C. Turner, B. Simon, and J. H. Kim (2005) *Parametric Investigation on the Influence of GM, Roll damping, and Above-Water Form on the Roll Response of Model 5613*. Report NSWCCD-50-TR-2005/027.

Blocki, W. (1980) "Ship Safety in Connection with Parametric Resonance of the Roll," *Int. Shipbuilding Progress*, Vol. 27, No. 306, pp. 36-53.

Boukhanovsky, A. V. and A. B. Degtyarev (1996) "Nonlinear Stochastic Ship Motion Stability in Different Wave Regime," *Proc. 3rd Intl. Conf. in Commemoration of the 300th Anniversary of Creating Russian Fleet by Peter the Great*, St. Petersburg, Russia.

Campbell, B. and V. Belenky (2010) "Assessment of Short-Term Risk with Monte-Carlo Method," *Proc. 11th Intl. Ship Stability Workshop*, Wageningin, the Netherlands.

Campbell, B and V. Belenky (2010a), "Statistical Extrapolation for Evaluation of Probability of Large Roll," *Proc. PRADS 2010*, Rio de Janeiro, Brazil.

Clauss, G.F. (2000) "Tailor-made Transient Wave Groups for Capsizing Tests," *Proc. 7th Int. Conf. on Stability of Ships and Ocean Vehicles*, Launceston, Australia.

Davis, M.C. and E. E. Zarnick (1964) "Testing Ship Models in Transient Waves," *Proc. 5th Symp. on Naval Hydrodynamics*, Bergen, Norway.

Hayashi, C. (1985) *Nonlinear Oscillations in Physical Systems*, Princeton University press, ISBN 0-691-08383-5, Princeton, New Jersey.

IMO International Code on Intact Stability, 2008, IMO, London, 2009.

IMO MSC.1/Circ.1200 *Interim Guidelines for Alternative Assessment of the Weather Criterion*, London, 2006.

IMO MSC.1/Circ. 1228 *Revised Guidance for Avoiding Dangerous Situations in Adverse Weather and Sea Conditions*, London, 2007.

IMO MSC.267(85) Adoption of the International Code on Intact Stability, 2008 (2008 IS Code), London, 2008.

IMCO STAB/INF.27 On Dynamic Stability of a Ship with Water on Deck, Submitted by USSR, IMCO London, 1966.

IMO SLF 48/4/12, On the Development of Performance-Based Criteria for Ship Stability in Longitudinal Waves, Submitted by Italy, IMO, London, 2005.

IMO SLF 49/5/2, Proposal of a Probabilistic Intact Stability Criterion, Submitted by Germany, IMO London, 2006.

IMO SLF 49/INF.3, Benchmarking for a Proposal of a Probabilistic Inact Stability Criterion, Submitted by Germany, IMO, London, 2006.

IMO SLF 50/4/4, Framework for the Development of New Generation Criteria for Intact Stability, submitted by Japan, the Netherlands and the United States, London, 2007.

IMO SLF 50/WP.2, Report of the Working Group (Part 1), London, 2007.

IMO SLF 51/4/1, Report of the Intersessional Correspondence Group on Intact Stability, Submitted by Germany, London, 2008.

IMO SLF 51/INF.4, Development of Performance-Based Intact Stability Criteria, Submitted by the United States, London, 2008.

IMO SLF 51/WP.2, Report of the Working Group (Part 1), London, 2008.

IMO SLF 52/3/1, Report of the Intersessional Correspondence Group on Intact Stability, Submitted by Japan, London, 2009.

IMO SLF 52/INF.2, Information Collected by the Intersessional Correspondence Group on Intact Stability, Submitted by Japan, London 2009.

IMO SLF 52/WP.1, Report of the Working Group (Part 1), London, 2010.

IMO SLF 53/3, Report of the Working Group at SLF 52 (Part 2), Submitted by the Chairman of the Working Group, London 2010.

IMO SLF 53/3/3 Activities of the Dynamic Stability Task Group of the Society of Naval Architects and marine Engineers, Submitted by the Royal Institution of Naval Architects (RINA), London, 2010.

IMO SLF 53/3/5 Comments On the Structure of New Generation Intact Stability Criteria (Report of the Correspondence Group), Submitted by Poland, London, 2010.

IMO SLF 53/3/6, Comments on the Report of the Working Group at SLF 52 (Part 2), Submitted by Poland, London 2010.

IMO SLF 53/3/7, Comments on Level 1 Vulnerability Criteria for Parametric Rolling," Submitted by the United Stats, London 2010.

IMO SLF 53/3/8, Comments on Proposed Criteria for Surf-riding and Broaching, Submitted by Japan and the United States, London 2010.

IMO SLF 53/INF.8, Sample Calculations on the Level 2 Vulnerability Criteria for Parametric Roll, Submitted by Sweden, London 2010.

IMO SLF 53/INF.10, Information Collected by the Correspondence Group on Intact Stability, Submitted by Japan, London 2010.

IMO SLF 53/WP. 4, Report of the Working Group (Part 1), London, 2011.

Ikeda, Y., M. Kashiwagi & N. Umeda, *eds*. (2008) *Proc. 6th Osaka Colloquium on Seakeeping and Stability of Ships*, Osaka, Japan.

Goodman, J. W. (1985) *Statistical Optics*, ISBN 0 471-01502-4 188, Wiley-Interscience, New York,

Guckenheimer, J. and P. Holmes (1983) *Nonlinear Oscillations, Dynamical System and Bifurcation of Vector Fields*, Springer-Verlag, New York, Berlin and Heidelberg.

Gumbel, E.J. (1958) *Statistics of Extremes,* Colombia University Press, New York.

France, W.M, M. Levadou, T.W. Treakle, J. R. Paulling, K. Michel, and C. Moore (2003) "An Investigation of Head-Sea Parametric Rolling and its Influence on Container Lashing Systems," *Marine Technology,* Vol. 40, No. 1, pp. 1-19.

Francescutto, A. (2004) "Intact Ship Stability– The Way Ahead," *Marine Technology*, Vol. 41, pp. 31-37.

Franeeseutto, A. (2007) "Intaet Stability of Ships– Reeent Developments and Trends," *Proc. 10th Int. Symp. on Practical Design of Ships and Other Floating Structures (PRADS 2007)*, Houston, Texas.

Hashimoto, H. (2009) "Pure Loss of Stability of a Tumblehome Hull in Following Seas," *Proc. of the 19th Intl. Offshore and Polar Engineering Conf.*, Osaka, Japan.

Hashimoto, H. and A. Matsuda (2009) "Parametrie Roll of a Tumblehome Hull in Head Seas," *Proc. 19th Intl. Offshore and Polar Engineering Conf.*, Osaka, Japan.

Holtrop, J. (1984) "A Statistieal Re-analysis of Resistanee and Propulsion Data" *Intl. Shipbuilding Progress*. Vol. 31, No 363, pp 272-276.

Kimura, A., (1980) "Statistieal Properties of Random Wave Groups" *Proc. 17th Coastal Engineering Conf.*, Sydney, Australia.

Kobylinski, L. K. and S. Kastner (2003), *Stability and Safety of Ships: Regnlation and Operation,* Vol. 9 of Elsevier Engineering Book Series, Elsevier, Amsterdam.

Kobylinski, L.K. (2009) "Future Generation Stability Criteria – Prospeets and Possibilities", *Proc. of the 10th Int. Conference on Stability of Ships and Ocean Vehicles*, St. Petersburg, Russia.

Kobylinski, L.K. editor (2009a) *Proceedings of International Workshop on Dynamic Stability Consideration in Ship Design*, Foundation for Safety of Navigation and Environment Proteetion, Ilawa, Poland.

Kramer, H., and M.R. Leadbetter, (1967) *Stationary and Related Stochastic Processes*, John Wiley, New York.

Lewis, E. (Ed.) (1989) *Principles of Naval Architecture* Vol. 3 SNAME, Jersey City.

Lin, W. M. and D. K. P. Yue (1990) "Numerieal Solutions for Large Amplitude Ship Motions in the Time-Domain," *Proc. of 18th Symp. of Naval Hydrodynamics*, Ann Arbor, Miehiagn.

Lin, W. M. and D. K. P. Yue, (1993) "Time-Domain Analysis for Floating Bodies in Mild Slope Waves of Large Amplitude," *Proc. of 8th Intl Workshop on Water Waves and Floating Bodies*, Newfoundland, Canada.

Longuet-Higgins, M. S. (1957) "The Statistieal Analysis of a Random, Moving Surfaee," *Philosophical Transactions A*, 249.

Longuet-Higgins, M. S., (1976) "On the Nonlinear Transfer of Energy in the Peak of a Gravity-Wave Speetrum: A Simplified Model," *Proc. Royal Society of London A*, 347, pp. 311-328.

Longuet-Higgins, M. S. (1984) "Statistieal Properties of Wave Groups in a Random Sea State," *Philosophical Transactions A*, 312.

Maritime New Zealand (2007) "Ineident Report Heavy Weather/Cargo Shift *Aratere* 3 Mareh 2006," Maritime New Zealand Investigation Report, 23 August.

McTaggart, K.A. (2000) "Ship Capsize Risk in a Seaway Using Fitted Distributions to Roll Maxima," *J. Offshore Mechanics and Arctic Engineering*, Vol. 122 No 2, pp. 141-146.

McTaggart, K.A. (2000a.) "Ongoing Work Examining Capsize Risk of Intact Frigates Using Time Domain Simulation," In *Contemporary Ideas of Ship Stability*, D. Vassalos, M. Hamamoto, A. Papanikolaou and D. Moulyneux (Eds.), Elsevier Science, pp. 587–595,

McTaggart, K.A. and J.O. de Kat (2000) "Capsize Risk of Intact Frigates in Irregular Seas," *Trans. SNAME*, Vol. 108, pp. 147–177.

Minnick, L., C. Bassler, S. Percival, and L. Hanyok, (2010) "Large-Scale Wave Kinematics Measurements of Regular Waves and Large-Amplitude Wave Groups," *Proc. 29th Intl. Conf. on Ocean, Offshore and Arctic Engineering*, Shanghai, China.

Minnick, L. M., C. C. Bassler, S. Percival, and L. W. Hanyok (2011), *Characterization of Regular Wave, Irregular Waves, and Large-Amplitude Wave Group Kinematics in an Experimental Basin* Hydromechanics Dept. Report, NSWCCD-50-TR-2011/001.

Minnick, L, C. Kent, C. Bassler, S. Percival, and L. Hanyok (2011a), "Kinematics of Experimentally Generated Severe Wave Conditions and Implications for Numerical Models," *Proc. 30th Intl. Conf. on Offshore Mechanics and Arctic Engineering*, Rotterdam, the Netherlands.

Olivieri, A., A. Francescutto, E. F. Campana, and F. Stern (2008), "Parametric Roll: Highly Controlled Experiments for an Innovative Ship Design," *Proc 27th Intl. Conf on Offshore Mechanics and Arctic Engineering*, Estoril, Portugal.

Oosterveld, M. W. C. and P. van Oossanen (1975), "Further Computer-Analyzed Data of the Wageningen B-Screw Series," *Intl. Shipbuilding Progress*, pp 251-262.

Paroka, D., Y. Okura, and N. Umeda, (2006) "Analytical Prediction of Capsizing Probability of a Ship in Beam Wind and Waves," *J. Ship Research*, Vol. 50, No. 2, pp. 187-195.

Paroka, D. and N. Umeda, (2006) "Capsizing Probability Prediction of the Large Passenger Ship in Irregular Beam Wind and Waves: Comparison of Analytical and Numerical Methods," *J. Ship Research*, Vol. 50, No. 4, pp. 371-377.

Paulling, J. R., (1961), "The Transverse Stability of a Ship in a Longitudinal Seaway," *J. Ship Research*, Vol. 4, No. 4, pp. 37-49.

Paulling, J. R., S. Kastner, and S. Schaffran (1972), "Experimental Studies of Capsizing of Intact Ships in Heavy Seas," U.S. Coast Guard Technical Report (also IMO Doc. STAB/7, 1973).

Peters, W. S., V. Belenky and C. Bassler (2010), "On Vulnerability Criteria for Righting Lever Variations in Waves," *Proc. 11th Intl. Ship Stability Workshop*, Wageningen, the Netherlands.

Rahola, J. (1939), *The Judging of the Stability of Ships and the Determination of the Minimum Amount of Stability*, Ph.D. Thesis, Helsinki, Finland.

Reed, A. M. (2009), "A Naval Perspective on Ship Stability," *Proc. 10th Intl. Conf. on Stability of Ships and Ocean Vehicles*, St. Petersburg, Russia.

Rice, S.O. (1944), "Mathematical Analysis of Random Noise". *Bell System Techn J.*

Vol. 23, No. 3, pp. 282–332.

Rice, S.O. (1945), "Mathematical Analysis of Random Noise". *Bell System Techn J.* 24(1):46–156.

Sevastianov, N. B. (1994), "An Algorithm of Probabilistic Stability Assessment and Standards". *Proc. of 5th International Conference on Stability of Ships and Ocean Vehicles*, Vol. 5, Melbourne, Florida.

Shin, Y.S., V. L. Belenky, J. R. Paulling, J.R., K. M. Weems and W.M. Lin (2004) "Criteria for Parametric Roll of Large Containerships in Longitudinal Seas," *SNAME Trans.* Vol. 112, pp. 14-47.

Shigunov, V., O. El Moctar and H. Rathje (2009) "Conditions of Parametric Rolling," *Proc. of the 10th Int. Conference on Stability of Ships and Ocean Vehicles*, St. Petersburg, Russia.

Spyrou, K.J. (1996) "Dynamic Instability in Quartering Seas: The Behavior of a Ship During Broaching," *J. Ship Res.*, Vol. 40, No. 1.

Spyrou, K.J., (1997) "Dynamic Instabilities in Quartering Seas – Part III: Nonlinear Effects on Periodic Motions," *J Ship Research*, Vol. 41, No 3, pp. 210-223.

Spyrou K.J. (2000) "The Nonlinear Dynamics of Ships in Broaching," *The Annals of Marie-Curie Fellowships, Publisher European Commission*, Vol. 1, pp. 62-69, http://www.mariecurie.org/annals/volume1/spyrou.pdf.

Spyrou, K. J. (2004) "Criteria for Parametric Rolling?," *Proc. 7th Intl. Ship Stability Workshop*, Shanghai, China.

Spyrou, K.J. (2005) "Design Criteria for Parametric Rolling," *Oceanic Engineering International*, Vol. 9, No. 1, pp. 11-27.

Spyrou, K. J. and N. Themelis (2005) "Probabilistic Assessment of Intact Stability," *Proc. 8th Intl. Ship Stability Workshop*, Istanbul, Turkey.

Spyrou, K.J. (2006) "Asymmetric Surging of Ships in Following Seas and its Repercussions for Safety," *Nonlinear Dynamics*, Vol. 43, pp. 149-172.

Spyrou, K.J., K.M.Weems and V. Belenky (2009) "Patterns of Surf-Riding and Broaching-to Captured by Advanced Hydrodynamic Code," *Proc. 10th Intl. Conf. on Stability of Ships and Ocean Vehicles*, St. Petersburg, Russia.

Stansell, P., J. Wolfram, and B. Linfoot (2002) "Statistics of Wave Groups Measured in the Northern North Sea; Comparisons Between Time Series and Spectral Predictions," *Applied Ocean Research*, 24:91–106.

Todd, F. H. (1953) "Some Further Experiments on Single-Screw Merchant Ship Forms," *Trans. SNAME*, Vol. 61, pp. 516-589.

Themelis, N.I. (2008) *Probabilistic Assessment of Ship Dynamic Stability in Waves*, Doctoral Thesis, National Technical University of Athens, Greece.

Themelis, N. and K.J. Spyrou (2007) "Probabilistic Assessment of Ship Stability," *SNAME Trans.* Vol. 115. pp. 181-206.

Themelis, N. and K.J. Spyrou (2008) "Probabilistic Assessment of Ship Stability Based on the Concept of Critical Wave Groups," *Proc. 10th Intl. Ship Stability Workshop*, Daejeon, Korea.

Tikka, K.K. and J.R. Paulling (1990) "Predictions of Critical Wave Conditions for Extreme Vessel Response in Random Seas," *Proc. 4th Intl. Conf. on Stability of Ships and Ocean Vehicles*, Naples, Italy.

Umeda, N. (1999), "Nonlinear Dynamics of Ship Capsizing due to Broaching in Following / Quartering Seas," *J. Mar. Sci. Tech.*, 4, pp. 16-26.

Umeda, N. A. Matsuda, M. Hamamoto, and S. Suzuki (1999), "Stability Assessment for Intact Ships in the Light of Model Experiments," *J. Mar. Sci. Tech.*, 4, pp. 45-57.

Umeda, N. and H. Hashimoto (2006) "Recent Developments of Capsizing Prediction Techniques of Intact Ship Running in Waves," *Proc. 26thth ONR Symposium on Naval Hydrodynamics*, Rome, Italy.

Umeda, N., M. Shuto, and A. Maki (2007) "Theoretical Prediction of Broaching Probability for a Ship in Irregular Astern Seas," *Proc. 9th Intl. Ship Stability Workshop*, Hamburg, Germany.

Umeda N., S. Yamamura, A. Matsuda, A. Maki and H. Hashimoto (2008) "Extreme Motions of a Tumblehome Hull in Following and Quartering Waves," *Proc of the 6th Osaka Colloquium on Seakeeping and Stability of Ships*, Osaka, Japan, pp.392-398.

Umeda N., A. Maki, S. Izawa, H. Sano, Y. Sogawa, E. Maeda and I. Tsukamoto (2009) "New Generation Intact Stability Criteria: A Step Forward," *Proc. of the 10th Int. Conference on Stability of Ships and Ocean Vehicles*, St. Petersburg, Russia

Vishnubhota, S., J. Falzarano, and A. Vakakis (2000) "A New Method to Predict Vessel/Platform Critical Dynamics in a Realistic Seaway," *Phil. Trans. R. Soc.*, 358:1967-1981, London.

Womack, J. and B. Johnson (2005) "A Systematic Study of Wave Phasing on Righting Arm Curves for Fishing Vessels", *SNAME Trans.*, Vol. 113.

Initial Report Distribution

Hard Copies	PDF Copies	Agency	Individual
1	1	USCG Headquareters (CG 521) 2100 Second st, SW Washinton DC 20593	Jaideep Sirkar
2	2	USCG Headquareters (CG 521) 2100 Second st, SW Washinton DC 20593	William S. Peters
1	1	USCG Headquareters (CG 9122) 2100 Second st, SW Washinton DC 20593	Tracy Marcinowski
0	1	NAVSEA 05D	J. Webster
0	1	NAVSEA 05P	R. Waters
0	1	NAVSEA 05P	D. Cimino
0	1	NAVSEA 05P	T. Mazumdar
0	1	NAVSEA 05P	P. Alman
0	1	NAVSEA 05T	N. Doerry
1	1	ONR 331	L. P. Purtell
1	1	DTIC	

NSWCCD Internal Distribution

0	1	2440	J. Rosborough
0	1	3452	TIC
0	1	50	J. Etxegoien
0	1	501 (w/o enclosure)	D. Intolubbe
1	1	504	A. Reed
0	1	505	T. Fu
0	1	508	J. Brown
1	1	55	M. Dipper
1	1	551	T. Smith
2	2	551	C. Bassler
3	3	551	V. Belenky
1	1	551	W. Belknap
1	1	551	B. Campbell
1	1	551	M. Hughes
1	1	552	D. Hayden
0	1	553	T. Carrico
0	1	58	R. Hurwitz